

Investigation of the High Frequency Dynamic-Mechanical Properties of Polymer Systems Using Ultrasonic Longitudinal Waves

Der Naturwissenschaftlichen Fakultät
der Gottfried-Wilhelm-Leibniz-Universität Hannover
zur Erlangung des Grades
Doktor der Naturwissenschaften
Dr. rer. nat.
genehmigte Dissertation
von

Ingenier Diplomat Cristian Alexandru Oprisoni

geboren am 23.08.1981 in Timisoara, Rumänien

2011

Referent: Prof. Dr. R. H. Schuster
Korreferent: Prof. Dr. J.-Ch. Buhl
Drittprüfer: Prof. Dr. P. Behrens

Tag der Promotion: 20.07.2011

*These earthly godfathers of Heaven's lights,
That give a name to every fixed star,
Have no more profit of their shining nights
Than those that walk and know not what they are.*

William Shakespeare

Acknowledgement

The scientific work presented in this dissertation was carried out, under the supervision of Prof. Dr. Robert H. Schuster, at the Deutsches Institut für Kautschuktechnologie e. V. (DIK), Hannover, between the years 2006 and 2011.

I would like to use this opportunity to express my gratitude for the invaluable help and support I have received in the years I worked on this topic:

I am grateful to Prof. Dr. Robert Schuster for the supervision of this dissertation, for giving me the opportunity to walk on a path very few tried before in this interesting scientific field, for his constant encouragement and motivational discussions.

I thank Dr. Thomas Alshuth for the constant helpful discussions and for always keeping the door open to us.

To Dr. Jochen Kroll I am grateful for introducing me to Ultrasonics and for his patience during the first part of the experimental work.

I thank the colleagues in the Physical Testing Lab especially Mr. Peter Erren, Mr. Joachim Heier, Mr. Jürgen Hamann, Mr. Manfred Backhaus and Mrs. Gundula Pardey for their help and for the friendly working environment. To John, Steve, Jarek, Heike, Marcus, Stefan, Mircea and Ramona I am grateful for the fruitful discussions during the scientific breaks.

Last but not least I thank my family and Sabrina for their understanding and helpful words during the last years.

Kurzfassung

Im Rahmen der vorliegenden Arbeit wurden die Ultraschallspektrometrie (US) sowie die Dynamisch - Mechanische Analyse (DMA) als Methoden zur Untersuchung der dynamisch - mechanischen Eigenschaften von ungefüllten und gefüllten Kompositen vorgestellt.

Beobachtet man das dynamische Verhalten diverser ungefüllter Homo- und Copolymere bei 1 Hz und 0.5 MHz, so zeigen sich je nach Messfrequenz bekanntermaßen unterschiedliche Glasumwandlungstemperaturen. Dieser Effekt wird nun um die Abhängigkeit des ΔT_g - Werts von der Makro- und Mikrostruktur der Polymere ergänzt. Hierbei weisen Polymere mit einfacher linearer Struktur (BR, NR) den höchsten ΔT_g - Wert auf, während dieser bei steigender Anzahl von Nebengruppen (wie bei SBR und NBR) zunehmend reduziert wurde.

Das Zeit - Temperatur - Superpositions - Prinzip das, nach der Williams - Landel - Ferry (WLF)-Theorie, benutzt wird um die dynamischen Eigenschaften bei Hochfrequenzen von Niedrigfrequenz-DMA-Daten abzuleiten, führte bei gleicher Frequenz sowohl für BR als auch für NR zu Abweichungen von den US-Daten.

Es wurden Komposite untersucht, die mit konventionellen Nanofüllstoffen wie Ruß oder Silica gefüllt wurden, aber auch solche mit weniger verwendeten Stoffen wie Zellulose, Montmorillonit und CNTs. Es stellte sich heraus, dass die Verstärkung der Komposite am Glasumwandlungspunkt sich durch die Eigenschaften des Rußes wie Oberflächenaktivität oder Struktur nicht verändert. Sowohl Ruß als auch Silica erhöhen allerdings bei zunehmendem Volumenanteil die Temperatur der Glasumwandlung bei 0.5 MHz. CNT und MMT führten bei gleicher Konzentration zu einer noch größeren Verstärkung.

Schlagworte: Ultraschall, Hochfrequenz, Verstärkung

Abstract

The work presented in this dissertation describes the use of Ultrasonic Spectrometry (US) and Dynamic Mechanical Analysis (DMA) to analyze the dynamic-mechanical properties of unfilled and filled rubber composites.

On observing the dynamic behavior of several unfilled homopolymers and copolymers at 1 Hz and at 0.5 MHz a variation of the glass transition temperature with the measurement frequency was noticed. This known effect was also followed by a dependence of the glass transition temperature difference (ΔT_g) on the macro and micro structure of the polymer. The ΔT_g was found to be largest for the polymers with simple and linear structure (BR, NR) and it decreased with increasing number of side-groups. The time-temperature superposition principle, as described by the Williams-Landel-Ferry (WLF) theory, used to estimate the high frequency dynamic properties from low frequency DMA data, lead to results that differed from the US data at the same frequency, for NR and BR.

Filled composites prepared with conventional nano fillers, such as carbon black and silica and also less used cellulose, montmorillonite (MMT) and carbon nano tubes (CNTs) were investigated. The reinforcing characteristics induced by the carbon blacks were found not to vary with their surface area or structure at the glass transition temperature. Both silica and carbon black were found to shift the high frequency T_g to higher temperatures with increasing volume fraction. CNT and MMT were found to induce a stronger reinforcement compared to carbon black and silica for the same concentration.

Keywords: ultrasound, high frequency, reinforcement

Contents

Acknowledgement	v
Kurzfassung	vii
Abstract	viii
1 Introduction	3
2 Objectives	7
3 State of the art	9
3.1 Rubber elasticity	9
3.1.1 Thermodynamic description	9
3.1.2 Mechanical stresses and deformations	13
3.1.3 The Maxwell model	17
3.1.4 The Kelvin-Voigt model	19
3.1.5 The α -transition process	20
3.1.6 Entanglements and the reptation model	28
3.2 Dynamic mechanical behavior	31
3.2.1 Low frequency DMA	32
3.2.2 Wave propagation in viscoelastic media	34
4 Materials	43
4.1 Synthetic rubbers	44
4.1.1 Emulsion polymerization	44
4.1.2 Ionic polymerization	47
4.1.3 Hydrogenation of polymers	52
4.2 Natural Rubber (NR)	53
4.3 Blending of polymers	54

4.4	Fillers	56
4.4.1	Reinforcement of elastomers	58
4.4.2	Carbon Black	59
4.4.3	Silica	62
4.4.4	Layered silicates	64
4.4.5	Carbon nanotubes	66
4.4.6	Dispersion and distribution of fillers	67
4.5	Vulcanization of elastomers	69
5	Results and Discussion	73
5.1	Method development	74
5.1.1	Apparatus and procedure	74
5.1.2	Requirements	76
5.1.3	Data treatment	77
5.1.4	Determination of the longitudinal wave attenuation, velocity and modulus	78
5.1.5	Error sources in ultrasonic measurements	80
5.2	Investigation of homopolymers	82
5.2.1	Butadiene Rubber (BR)	84
5.2.2	Natural Rubber (NR)	86
5.2.3	Butyl Rubber (IIR)	87
5.3	Investigation of copolymers	89
5.3.1	Influence of vinyl groups	90
5.3.2	Effect of styrene groups	94
5.3.3	Influence of SBR hydrogenation	95
5.3.4	Effect of acrylonitrile groups	97
5.4	Frequency effects on the glass transition temperature	101
5.5	Broad range frequency analysis - WLF	105
5.6	Compression modulus	110
5.7	Influence of processing parameters	113
5.7.1	Molar mass	114
5.7.2	Plasticizer	115
5.7.3	Crosslinking density	117
5.8	Polymer blends	119
5.9	Influence of inactive fillers	129
5.10	Investigation of carbon black filled compounds	131

5.10.1	Variation of the volume fraction	133
5.10.2	Influence of the polymer structure	135
5.10.3	Apparent activation energy of the CB network.	137
5.10.4	Investigation of filler networking	138
5.10.5	Filler influence on Tg	141
5.10.6	Effect of the carbon black surface and structure	142
5.10.7	Influence of the filler dispersion on ultrasonic wave velocity.	145
5.10.8	Broad range frequency analysis - WLF	147
5.11	Investigation of silica filled compounds	150
5.11.1	Variation of the volume fraction	150
5.11.2	Influence of the polymer structure in silica filled compounds	152
5.11.3	Broad range frequency analysis - WLF	153
5.11.4	Influence of silica surface treatment	154
5.12	Investigation of novel fillers	156
6	Conclusions	161
7	Experimental	164
7.1	Sample preparation	164
7.1.1	Unfilled samples	164
7.1.2	Filled samples	164
7.1.3	Vulcanization	165
7.2	Testing methods	165
7.2.1	Ultrasonic spectrometry	165
7.2.2	Dynamic Mechanical Analyzer	166
7.2.3	Transmission Electron Microscopy	169
7.3	Polymers and chemical aids	169
	References	171
	Glossary	184

1

Introduction

Elastomers or crosslinked rubbers represent a group of polymer materials without which modern technology is unthinkable. The annual consumption of rubber at present amounts to more than 20mio. tons rising by a 4% every year. More than half of the global production of rubber, natural and synthetic, is used in tires whilst the remainder fulfills the needs for other industrial and consumer products ranging from motor mounts and fuel hoses to window profiles and heavy conveyor belts.

The predominant characteristic of elastomers is the highly elastic behavior after deformation in tension or compression and the almost complete recovery of the original dimensions when the external force is released. As an example it is possible to stretch an elastomer ten times its original length and after removal of the tension it will return, under ideal conditions, to its original shape and length. Moreover, elastomers are characterized by great toughness under static or dynamic stress, abrasion resistance higher than that of steel, a fair impermeability to air and gases, and resistance to solvents and chemicals from case to case. These properties are exhibited from temperatures above the glass transition up to temperatures above room temperature and are retained under most climatic conditions.

The property profile which can be attained with elastomers depends mainly on the choice of the particular polymer, the compound composition, the production process and the shape and design of the product. Remarkable properties can only be obtained by proper compounding with chemicals and other additives and subsequent vulcanization. Depending on the type and amount of rubber chemicals and additives in the compound and depending on the degree of vulcanization, a given rubber can yield vulcanizates with considerably different properties with respect to hardness, elasticity or strength. Natural and synthetic rubbers are rarely applied in their pure form. They are too "weak" to fulfill practical requirements because of their lack of hardness, strength properties and wear resistance. Nanoscaled Fillers are used in order to improve the

properties of rubber compounds.

The large volume utilization of rubber is ascribed to its quieting, cushioning, vibration energy absorbing and isolating characteristics. Applications such as tires, belts, engine mounts employ rubber under conditions of rapidly repeated deformations which are relatively small compared to ultimate breaking values. Although ultimate values and fatigue tests are relevant as criteria of quality, they are of a lesser use for anticipating the response of their products to the forces experienced in service. These repeated deformations occur over a broad frequency spectrum and an understanding of the behavior of rubber parts in service necessitates devices and methods that can evaluate the stored and dissipated energy over the entire frequency range. To fill this need scientific methods, data and principles has been developed, usually referred to as the field of dynamic properties [1].

The term dynamic-mechanical properties when applied to elastomers refers to vibrations displayed in response to sinusoidal forces¹. It has been demonstrated that the most relevant material characteristics to be investigated are the storage modulus and the loss modulus. The field known as dynamic properties of elastomers comprises the properties exhibited in response to periodic or transient forces for all types of deformation small enough not to induce appreciable fatigue or failure during the investigation, with no limitation as to frequency ranges and having temperature as most important variable.

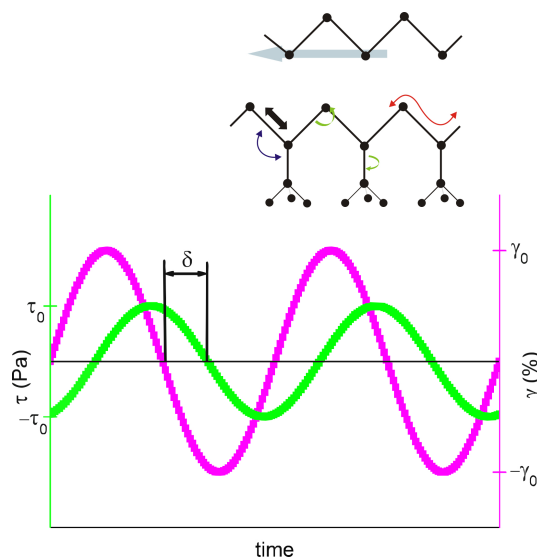


Figure 1.1: Influence of the polymer structure on dynamic mechanical properties

Dynamic mechanical properties assumed increasing technological significance in the

¹In principle, both theory and experiment can be extended to more complex force patterns such as square (see the ultrasonic measurements in this work) or saw tooth waves, if necessary.

development of synthetic rubbers. Examination with dynamic test procedures gave judgments of the essential rubber elastic character of the elastomers, their ability to respond to rapid deformations of low amplitude in a rubberlike way. Furthermore, the results provided an evaluation of energy losses and relative heat generation which turned out to be properties of paramount importance for the use of rubber in tires, engine mounts, belts, etc. as discussed also in [2]. As the understanding of the frequency dependence of the dynamic mechanical properties developed so the measuring systems diversified (based on forced oscillation or on free oscillations). The measurement frequencies were increased up to 1000 Hz. This value was also topped by mechanical devices capable of oscillating up to 10 kHz. However, the motors used to drive the oscillator came to their limits above this frequency. Consequently the MHz frequency region, also proven to be relevant to understanding, for example, the friction that occurs when sliding rubber on a surface, was unreachable to direct dynamic-mechanical measurements which can simulate real deformations.

The relevance of such measurements becomes manifest when the reaction of the macromolecular chains to sinusoidal deformations is considered in relation to deformation frequency and amplitude of the respective polymer. The amount of short side groups along the chain backbone, the type of filler, its loading and degree of dispersion, the state of crosslinking play a decisive role in influencing the dynamic response of the backbone (see figure 1.1).

To fill this gap several techniques which exploit high frequency have been employed. Characterization of high frequency dynamic-mechanical properties of polymer compounds using ultrasonic wave propagation dates back to the late 1940's when Nolle [3, 4] was one of the pioneers that discussed the propagation of acoustic waves in elastomer materials and also provided a solution to the wave equation taking into consideration damping of waves in polymers. These early studies were mainly concerned with demonstrating the feasibility of the various acoustic techniques for characterizing the viscoelastic properties of polymers and were unsuited to practical implementation. It has been well documented, also by Ferry [5, 6] among others, that by using longitudinal and shear wave propagation techniques the corresponding complex dynamic moduli of polymers may be determined [7].

The advances in the last years, concerning sensors, hardware and software evaluation technologies, brought about a renewed interest in this field. Several theoretical methods have also been developed, which can, to a certain extent, predict the dynamic behavior at almost any technologically relevant frequency, i.e. the time - temperature superposition principle, Williams Landel Ferry and Vogel Fulcher Tamann equations, but they also are of no use in the case of thermorheologically complex materials such as multi - phase rubber blends.

Despite the work mentioned above there are still many questions which need be answered. In the use of theoretical approaches to estimate high frequency dynamic mechanical properties the glass transition temperature change is considered to be polymer independent. An increase of the frequency is expected to induce an increase of T_g of $6 - 7^\circ\text{C}$.

There is also much debate on whether the glass transition temperature of a polymer depends at all on the amount of active filler.

As mentioned before, polymer blends are at the moment impossible to characterize using theoretical models. The work done in this region is rather scarce despite their absence in every rubber part being unthinkable.

In the use of ultrasonic wave propagation to investigate high frequency dynamics of polymers the investigations were mostly performed on one or two polymers with few variations of important parameters such as polymer structure, filler content, processing parameters, etc.

A comprehensive investigation on the use of ultrasonics in the dynamic-mechanical characterization of rubber composites is necessary in order to understand its full capabilities and restrictions.

2

Objectives

It is the aim of this work to investigate the dynamic-mechanical properties of unfilled and filled rubbers over a wide frequency range in order to better understand their behavior at frequencies in the MHz region. In order to pursue this goal it was necessary to further develop an Ultrasonic Spectrometer, which functions in the MHz region of the acoustic spectrum and can deliver more precise and reliable data for the sound velocity and the attenuation coefficient. Only with this prerequisite deeper insight into the high frequency polymer dynamics was possible. The theoretical aspects regarding traveling waves in different media as well as error sources and correction are delineated.

The principal part of the work is consecrated to testing different model elastomer formulations prepared with a systematic variation of polymer type, micro structure and filler content. It should be demonstrated, by performing measurements on several polymers - NR, IIR, BR (with different vinyl content), SBR (with different styrene and vinyl content), NBR (with different acrylonitrile content) - that the changes that occur in the dynamic response of macromolecular chains by increasing the measuring frequency depend on the polymer structure. The glass transition temperature, T_g , shift will be investigated as a function of the polymer macro and micro structure at 1 Hz and 0.5 MHz.

For the first time it will be possible to check the validity of the time-temperature superposition principle which allows a more or less accurate extrapolation of data obtained at low frequencies to the MHz region for thermorheologically simple materials.

The high sensitivity of the ultrasonic method will be tested in investigations of the crystallinity effect in BR and the detection of side group motions which are expected to determine the appearance of characteristic peaks at the respective temperatures.

Processing relevant parameters such as the molar mass, crosslinking density and plasticizer effects will be analyzed by comparing the 1 Hz measurements with the 0.5 MHz

ones, with the purpose of better understanding their influence on the chain dynamics.

Polymer blends are present in most rubber applications. There is at the moment no theoretical model that can reliably predict their dynamic-mechanical behavior in the MHz regime. Ultrasonic spectrometry enables for the first time a temperature dependent characterization of the energy dissipation at 0.5 MHz in blends of SBR:NR, SBR:NBR and SBR:BR. It is expected that the increase of the frequency determines unification of the peaks also in the absence of miscibility. As BR is known to crystallize, the effects induced by the possible presence of the crystallites will also be described.

It will be shown that inactive fillers of certain sizes, depending on the measurement frequency, induce scattering effects which prevent the correct characterization of the dynamics of the polymer matrix. It is demonstrated that for active, reinforcing fillers such as carbon black and silica, scattering does not occur ascribed to the formation of a layer of intermediate density between the matrix and the filler particles.

The investigation of composites filled with different amounts of carbon black and silica at 1 Hz and at 0.5 MHz should demonstrate whether there is any variation of the glass transition temperature of the composite with the filler content. It will be investigated whether the measurements at 0.5 MHz are more sensitive to the influence of the rubber-filler interface than their 1 Hz counterparts. The dependence of the ultrasound velocity on the filler content will be analyzed and a connection between the state of dispersion of the filler in the matrix and the reduced ultrasound velocity should be seen.

Novel fillers such as cellulose, montmorillonite and carbon nanotubes are investigated as possible replacement fillers. The high frequency characterization of their reinforcing properties should show whether they display improved properties by comparison with carbon black and silica.

3

State of the art

3.1 Rubber elasticity

The study of polymer (visco)elasticity treats the relationships among elasticity, flow, and molecular motion. In reality, no liquid exhibits pure Newtonian viscosity, and no solid exhibits pure elastic behavior, although it is convenient to assume so for some simple problems. Rather, all deformation of real bodies includes some elements of both flow and elasticity. Because of the long-chain nature of polymeric materials, their viscoelastic characteristics come to the forefront [8].

In order to acquire a better understanding of the dynamic viscoelastic properties of elastomers and their dependence on the polymer architecture and filler type/content, it is of great significance to summarize some basic ideas and the most important concepts of polymer physics. Besides this, the measurement methodology and devices as well as the theories behind dynamic mechanical measurements will be briefly reviewed.

3.1.1 Thermodynamic description

The deformation behavior of elastomers is of a high complexity and, to this day, still far from being fully understood and characterized. Ascribed to the large amount of research that has been carried out over the years, a complete physical description of rubber-elastic behavior exists. This is due to the almost fully reversible deformation behavior of elastomer networks, which constitutes the basis for a rigorous thermodynamic description [9].

The thermodynamic treatment of the deformation behavior starts with the first law of thermodynamics:

$$dU = \partial Q + \partial A \tag{3.1}$$

The internal energy change, dU , of a closed system is equal to the sum of the heat that is introduced and the work done on the system:

$$\begin{aligned}\partial Q &= TdS \\ \partial A &= -pdV \\ dU &= TdS - pdV\end{aligned}\tag{3.2}$$

The equation $\sigma = ma$ follows.

The entropy, $S(J/K)$, is a thermodynamic variable that characterizes the system's state of order.

The second law of thermodynamics states that it is not possible for the order of a closed system to increase ($dS \geq 0$) and thus dictates the direction in which a process runs. In thermodynamics, the description of equilibrium is done using state functions which describe the instantaneous state of a system as a function of additional state variables.

If the pressure p and the temperature T are kept constant in a system then this is referred to as isothermal, isobaric system and use is made of the Gibbs energy \tilde{G} , i.e. free energy, as a state function for describing the state of equilibrium. A detailed example of the use of the free energy is given in the description of the glass process as second order phase transition in [10–12]. If a system of macromolecules is observed with a constant volume and a constant temperature then the free energy ($F = U - dS$) can be regarded as the relevant state function. If mechanical work is performed on the system the free energy will undergo a change. Transposed to a strain experiment this means that work $\partial A = fdl$ must be performed in order to stretch a sample by dl with a force f . At constant temperature, the change in the free energy is:

$$dF = dU - TdS = \partial A = fdl\tag{3.3}$$

Then the force required to deform the sample is:

$$f = \left(\frac{\partial F}{\partial l}\right)_{T,V} = \left(\frac{\partial U}{\partial l}\right)_{T,V} - T \left(\frac{\partial S}{\partial l}\right)_{T,V}\tag{3.4}$$

According to Eq. 3.4 the force is made up of two components - an energy component $f_e = \left(\frac{\partial U}{\partial l}\right)_{T,V}$ and an entropy component $f_s = -T \left(\frac{\partial S}{\partial l}\right)_{T,V}$.

The energy component characterizes the change in internal energy that comes about with deformation. This component predominates in typical solids, since the internal

energy undergoes a dramatic increase if molecules or atoms are displaced from their equilibrium positions within the crystal structures. The flexible long chain nature of polymer molecules enables them to respond to mechanical deformation in a way that is fundamentally different from the response given by rigid materials such as metals or ceramics. In such materials the entropy term dominates the deformation behavior. Entropy elasticity demonstrates itself in easily observed thermodynamic behavior such as the contraction of a stretched rubber band as described by Gough in 1805:

If one end of a slip of Caoutchouc be fastened to a rod of metal or wood, and a weight be fixed to the other extremity, in order to keep it in a vertical position; the thong will be found to become shorter with heat and longer with cold.

Gough, 1805

Entropy elasticity is characterized by the fact that the lengths of the bonds between segments of the chain do not change with strain. The only consequence of the deformation is the smaller number of potential chain configurations that are possible with an increasing strain and the higher order that results. A fully extended chain, in the shape of a rod, has only one conformation, and its conformational entropy is zero [8].

Another characteristic of materials that exhibit entropy-elastic behavior is the influence of the temperature on their deformation behavior. It is clear from Eq. 3.4 that the entropy term is directly proportional to the temperature, while the energy elastic term is independent of temperature. The typical example that can be given is that of a rubber band stretched under a constant weight. The force acting as a result of the weight causes the rubber thread to stretch by dl . At high temperature the deformation can only be kept constant if the force is increased by the entropy elastic component which increases with temperature. If this is not the case, the initial deformation will be reduced and the rubber will contract.

A simple method of characterizing entropy elastic and energy elastic deformation behavior was developed by Flory and involves determining the temperature dependent force, $f(T)$, necessary for the constant strain of a specimen dl (see Figure 3.1) [13]. The correlation between the parameters shown in this figure and Eq. 3.4 is obvious if the free energy is derived as below. The change in free energy works out at

$$dF = -SdT - pdV + fdl \quad (3.5)$$

The free energy is a state function dependent only on the temperature, volume and length of the specimen and can be written as a total differential.

$$dF = \left(\frac{\partial F}{\partial T} \right)_{V,l} dT + \left(\frac{\partial F}{\partial V} \right)_{T,l} dV + \left(\frac{\partial F}{\partial l} \right)_{T,V} dl \quad (3.6)$$

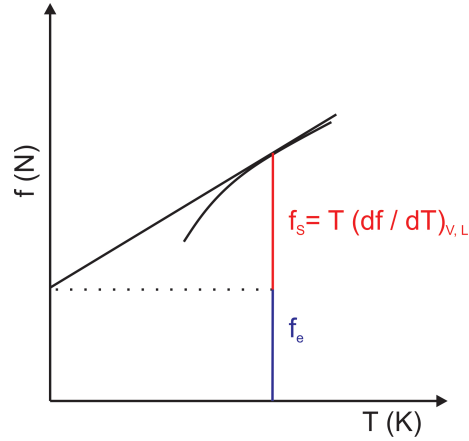


Figure 3.1: Temperature dependence of entropy elastic and energy elastic deformations

The last two equations yield

$$\left(\frac{\partial F}{\partial T}\right)_{V,l} = -S \quad \text{and} \quad \left(\frac{\partial F}{\partial l}\right)_{T,V} = f \quad (3.7)$$

Since a variable specifies the instantaneous state of a system and is independent of the route by which this state is attained the following applies:

$$\frac{\partial \left(\frac{\partial F}{\partial T}\right)}{\partial l} = \frac{\partial \left(\frac{\partial F}{\partial l}\right)}{\partial T} \quad (3.8)$$

Again, combining the last two equations one obtains:

$$-\left(\frac{\partial S}{\partial l}\right)_{T,V} = \left(\frac{\partial f}{\partial T}\right)_{V,l} \quad (3.9)$$

The entropy elastic component can be determined both from the change in entropy with a change in specimen length and by measuring the change in force df for a temperature change of dT which is easier to establish in experimental terms.

$$f_s = -T \left(\frac{\partial S}{\partial l}\right)_{T,V} = T \left(\frac{\partial f}{\partial T}\right)_{V,l} \quad (3.10)$$

A review of experimentally determined energy elastic contributions for several elastomers performed by Treloar [14] shows that for virtually all elastomers the entropy component of the force is several times greater than the energy component. This means that the deformation behavior of elastomers (according to Flory [13]) can be described in a good approximation by pure entropy-elastic behavior. The force required to deform a system of macromolecules is then a direct consequence of the entropy that has

been modified as a result of the deformation [9].

$$f = f_S + \underbrace{f_e}_{\approx 0} = -T \left(\frac{\partial S}{\partial l} \right)_{T,V} \quad (3.11)$$

3.1.2 Mechanical stresses and deformations

The evaluation of the effects deforming forces have on a structure requires the introduction of stresses and deformations. Stress is commonly depicted by the Greek letter τ and it is defined as the force f divided by the area A to which it is applied and it is measured in $Pa = \left[\frac{N}{m^2} \right]$.

$$\tau = \frac{f}{A} \quad (3.12)$$

If the force is applied perpendicularly on the area, or if say a perpendicular i on the area is parallel to the direction of the force, the stress is called normal stress and is denoted σ instead of τ . The definition of the resulting deformation γ - value given in % - comes from the ratio between the deformation ΔL and the original length L .

$$\gamma = \frac{\Delta L}{L} \quad (3.13)$$

Again, if the direction of the deformation is parallel to that of the body one speaks of the normal deformation ϵ . Generally, material properties can be located between two limiting extremes, namely the limits of elastic or Hookean behavior [15] and viscous or Newtonian behavior. Hooke's law for the ideal elastic body represents a linear relation between stress and strain (see Eq. 3.14)

$$\bar{\tau} = \bar{\bar{c}} \cdot \bar{\gamma} \quad (3.14)$$

Due to the complexity that comes with the spatial propagation of forces, it is necessary to use tensors to describe Hooke's law. In equation 3.14 $\bar{\tau}$ represents the stress tensor, $\bar{\gamma}$ the deformation tensor and $\bar{\bar{c}}$ depicts the tensor of the elastic constant.

The tensorial representation is usually envisaged by applying the stress-strain relationships to a cubic volume element as the one shown in Figure 3.2. If a stress acts in a direction, for example perpendicular to a surface of the cube, it becomes deformed. This deformation, however, will not restrict itself to the direction of the stress but will have contributions in all spatial directions¹.

¹In Figure 3.2 and in equation 3.15, therefore, the indices 1, 2, 3 stand for the directions ox , oy and oz

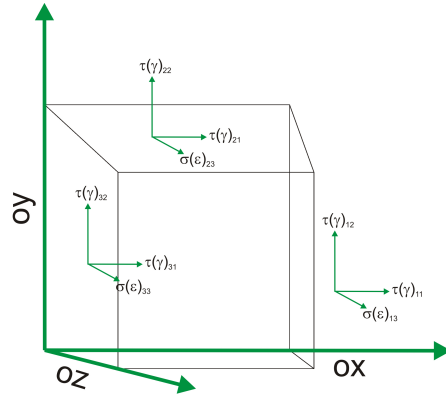


Figure 3.2: Stress(τ) and strain (γ) components

In this case Eq. 3.14 must be rewritten to account for the spatial effects as follows:

$$\begin{aligned}
 \tau &= \sum_{l=1}^3 \sum_{m=1}^3 c_{lm} \cdot \gamma_{lm} \\
 &= c_{11} \cdot \epsilon_{11} + c_{12} \cdot \gamma_{12} + c_{13} \cdot \gamma_{13} \\
 &\quad + c_{21} \cdot \gamma_{21} + c_{22} \cdot \epsilon_{22} + c_{23} \cdot \gamma_{23} \\
 &\quad + c_{31} \cdot \gamma_{31} + c_{32} \cdot \gamma_{32} + c_{33} \cdot \epsilon_{33}
 \end{aligned} \tag{3.15}$$

So there are nine different stress components linked to deformation components via nine elastic constants c_{lm} which yields a total of 81 constants which must be determined in order to describe the stress and strain state of the cubic element.

The number of necessary elastic constants can be reduced in most cases, according to the symmetry characteristics of the material. Due to polymers being mostly amorphous and homogeneous they can be regarded as isotropic (all physical properties are independent of direction) the number of independent constants being reduced to two.

In case of a dynamic mechanical experiment a polymer sample, a viscoelastic body is subjected to a periodic stress. For a sinusoidal stress the body typically responds, in the linear range, i.e. as long as the relationship between stress and deformation is linear, with a reproducible sinusoidal signal of the same frequency but shifted in phase.

If the sample is deformed sinusoidally in shear the deformation at any given time t is determined by the shear amplitude γ_0 and by the angular frequency $\omega = 2\pi f = \frac{2\pi}{T}$ of the excitation.

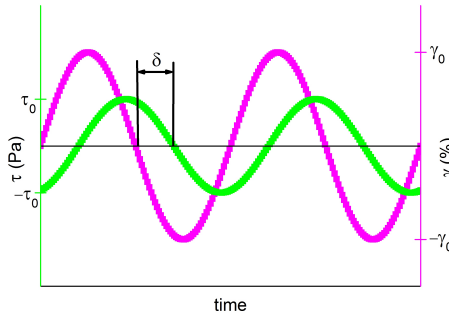


Figure 3.3: Sinusoidal periodic oscillations

Related to time, the shear deformation can be described by the following equation:

$$\gamma(t) = \gamma_0 \cdot \sin(\omega t) \quad (3.16)$$

The response to this deformation is a time delayed, periodic stress signal (Figure 3.3) described by Eq. 3.17.

$$\tau(t) = \tau_0 \cdot \sin(\omega t + \delta) \quad (3.17)$$

The displacement δ between deformation and stress is ascribed to the fact that the response to deformation occurs with a delay. The broad range of values that the phase displacement can take is best observed for the extreme cases of the ideal viscous fluid and the ideal solid [9, 16]. In case of an incompressible, isotropic solid Hooke's Law assumes the form $\sigma = E \cdot \epsilon$. In this case, the proportionality constant E is named the elasticity modulus, or Young's modulus - a material specific value measured in $[Pa]$. For a simple shear deformation of an isotropic solid one obtains $\tau = G \cdot \gamma$. In this case, the proportionality constant G is named the shear modulus, also a material constant with the same measurement unit as E . The description of the mechanical properties of solids often affords the usage of other elastic constants such as the longitudinal wave modulus M , the compression modulus K and Poisson's ratio ν . These can all be calculated from the elastic and the shear modulus (see Table in [17]). The longitudinal wave modulus M is characteristic for the propagation of longitudinal waves. It is calculated from the sonic attenuation and velocity in case of sonic waves or directly $M = K + \frac{4}{3}G$. It includes along side G and E the compression modulus K a constant that indicates the extent to which the volume of a body changes under pressure from all sides $\Delta p = -K \cdot \frac{\Delta V}{V}$. Poisson's ratio can be determined from the ratio between transverse elongation and longitudinal elongation $\nu = -\frac{\epsilon_Q}{\epsilon_L}$. However, since rubber is known to be a viscoelastic medium, it will show both fluid and solid characteristics, therefore the phase difference between deformation and stress can take any value between $0^\circ C$ and $90^\circ C$ (i.e. $0 \leq \delta \leq \frac{\pi}{2}$). This implies that a part of the energy introduced in the deformation cycle is dissipated in another way. The phase angle gives an indication of

the proportion of stored to lost energy. The conversion of Eq. 3.17 yields the stored and lost components of the energy.

$$\begin{aligned}
 \tau(t) &= \tau_0 \cdot \sin(\omega t + \delta) \\
 &= \tau_0 \cdot \cos(\delta) \cdot \sin(\omega t) + \tau_0 \cdot \sin(\delta) \cdot \cos(\omega t) \\
 &= \underbrace{\tau_0 \cdot \cos(\delta) \cdot \sin(\omega t)}_{\text{storage component}} + \underbrace{\tau_0 \cdot \sin(\delta) \cdot \sin(\omega t + \frac{\pi}{2})}_{\text{loss component}}
 \end{aligned} \tag{3.18}$$

Thusly, the stress response is divided into two components, one in phase ($\delta = 0$) with the deformation and another part displaced by 90° ($\delta = \frac{\pi}{2}$). Converting this to the modulus level, the part in which stress and deformation are in phase is termed storage modulus G' .

$$G' = \frac{\tau_0 \cdot \cos(\delta) \cdot \sin(\omega t)}{\gamma_0 \cdot \sin(\omega t)} = \frac{\tau_0}{\gamma_0} \cdot \cos(\delta) \tag{3.19}$$

The remaining part, where stress and deformation are displaced by 90° is called the loss modulus G'' .

$$G'' = \frac{\tau_0 \cdot \sin(\delta) \cdot \sin(\omega t)}{\gamma_0 \cdot \sin(\omega t)} = \frac{\tau_0}{\gamma_0} \cdot \sin(\delta) \tag{3.20}$$

The dual component nature of the shear modulus G reflects the proportion of stored and dissipated energy during an oscillation. It can therefore be displayed as a bidimensional vector. Mathematically, the modulus is represented as a complex figure composed of the real part (the storage modulus G') and the imaginary part (the loss modulus G'') always multiplied by the imaginary number i where $i^2 = -1$.

$$G^* = G' + iG'' \tag{3.21}$$

The loss modulus G'' is proportional to the energy dissipated into heat during the deformation whereas the storage modulus G' is proportional to the stored energy. The work performed in each cycle by a material that undergoes sinusoidal shear deformation $\epsilon^* = \epsilon_0 \text{Im}e^{i\omega t}$ is given by:

$$\begin{aligned}
 W &= \oint \sigma^* d\epsilon^* = \oint [G'(\omega) + iG''(\omega)] \epsilon^* d\epsilon^* \\
 &= \frac{1}{2} G'(\omega) \oint d\epsilon^{*2} + \frac{G''(\omega)}{\omega} \oint \dot{\epsilon}^* d\epsilon^*
 \end{aligned} \tag{3.22}$$

where it has been considered that $i\epsilon^* = (1/\omega)d\epsilon^*/dt$. In the integral containing $G'(\omega)$, the work done during one part of the cycle is recovered during the other part of the cycle and the integral of the entire cycle is null. The total work in a complete cycle

represents the dissipated energy given by:

$$W = \frac{G''(\omega)}{\omega} \oint \dot{\epsilon}^* d\epsilon^* = \frac{G''(\omega)}{\omega} \oint \dot{\epsilon}^{*2} dt \quad (3.23)$$

where $d\epsilon^* = \frac{\dot{\epsilon}^*}{dt}$. According to this equation the energy dissipated in a material under a sinusoidal deformation is proportional to the loss modulus and the reciprocal of the frequency. Taking for the last integral in Eq. 3.23 limits from 0 to $T = 2\pi/\omega$ one gets:

$$W = G''(\omega) \epsilon_0^2 \omega \int_0^{2\pi/\omega} \cos^2 \omega t dt = \pi \epsilon_0^2 G''(\omega) \quad (3.24)$$

Finally, this equation shows the proportionality between the dissipated energy and both the square of the deformation amplitude and the loss modulus [18].

The determination of the range for which the dynamic properties are linear is made using so called ‘‘amplitude sweeps’’.

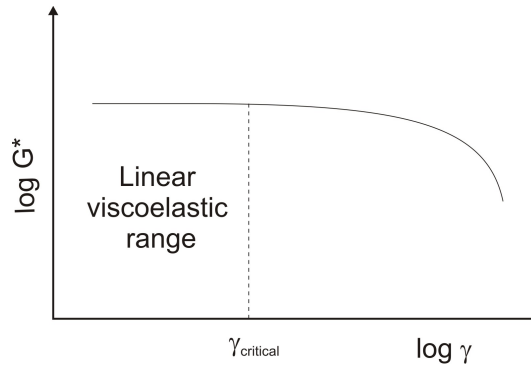


Figure 3.4: Linear deformation range

This will imply measuring the value of the complex shear modulus G^* with different deformation amplitudes, γ , at constant angular frequency. As long as no amplitude dependence of the modulus is noticed, i.e. up to $\gamma_{critical}$, the material is in the linear deformation range (see Figure 3.4).

At amplitudes higher than $\gamma_{critical}$, nonlinear effects become an ever greater importance and most considerations made above lose their validity. This renders results from dynamic mechanical measurements irreproducible.

3.1.3 The Maxwell model

Several mathematical models exist which attempt to describe the viscoelastic behavior of rubber. Most of them rely on the mechanical properties of the ideal solid and the

ideal fluid. In these models the ideal solid is envisaged as a spring whereas the ideal fluid is viewed as a dashpot. Through various combinations of the two a mechanical behavioral model can be set up which gives a quantitative description of the polymer viscoelasticity.

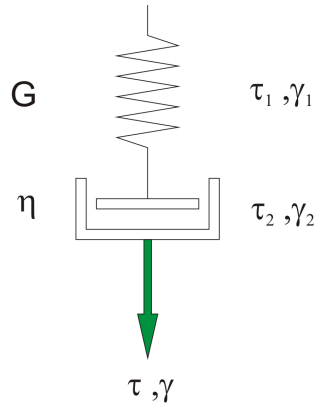


Figure 3.5: The Maxwell element

The Maxwell model is composed of one spring and one dashpot connected in series. The premises for this model are:

$$\begin{aligned}\tau(t) &= \tau_1(t) = \tau_2(t) \\ \gamma(t) &= \gamma_1(t) + \gamma_2(t)\end{aligned}\quad (3.25)$$

When the dashpot and the spring are connected in series, the stresses $\tau_1(t)$ and $\tau_2(t)$ are identical and equal to the resultant stress $\tau(t)$, whereas the total deformation $\gamma(t)$ is comprised of the sum of the individual deformations $\gamma_1(t)$ and $\gamma_2(t)$. The time dependent deformation $\dot{\gamma}(t)$ of a Maxwell model is obtained by inserting into Eq. 3.25 the basic equation for a spring $\tau_2(t) = G \cdot \gamma_2(t)$ and a dashpot $\tau(t) = \eta \cdot \dot{\gamma}_1(t)$.

$$\dot{\gamma}_1(t) = \frac{\tau(t)}{\eta} + \frac{\dot{\tau}(t)}{G}\quad (3.26)$$

Equation 3.26 allows the calculation of the reaction the Maxwell model has to any time dependent excitation.

In a dynamic mechanical experiment the Maxwell element is deformed by a sinusoidal periodic excitation. In a complex representation stress and strain become:

$$\begin{aligned}\gamma^*(t, \omega) &= \gamma_0 \cdot e^{i\omega t} \\ \tau^*(t, \omega) &= \tau_0 \cdot e^{i(\omega t + \delta)}\end{aligned}$$

The derivation as a function of time yields:

$$\begin{aligned}\dot{\tau}^*(t, \omega) &= \frac{d}{dt} \{ \tau_0 \cdot e^{i(\omega t + \delta)} \} = \tau_0 \cdot i\omega \cdot e^{i(\omega t + \delta)} = i\omega \cdot \tau^*(t, \omega) \\ \dot{\gamma}^*(t, \omega) &= \frac{d}{dt} \{ \gamma_0 \cdot e^{i\omega t} \} = \gamma_0 \cdot i\omega \cdot e^{i\omega t} = i\omega \cdot \gamma^*(t, \omega)\end{aligned}$$

Inserting this into the basic Maxwell equation (3.26) and performing some transformations the frequency dependent complex modulus $G^*(\omega)$ of the Maxwell model can be obtained.

$$G'(\omega) = G \cdot \frac{\omega^2 \tau_R^2}{1 + \omega^2 \tau_R^2} \quad G''(\omega) = G \cdot \frac{\omega \tau_R}{1 + \omega^2 \tau_R^2} \quad (3.27)$$

Here τ_R represents the Maxwell model relaxation time. It is calculated from the ratio of the dashpot' viscosity to the modulus of the spring G $\tau_R = \frac{\eta}{G}$. If the time in which a mechanical load is applied is much shorter than the relaxation time or the frequency is much higher than the reciprocal of the relaxation time then the elastic properties of the spring will dominate the Maxwell element so it will behave like an ideal solid.

If the time in which a mechanical load is applied is much longer than the relaxation time or the frequency is much lower than the reciprocal of the relaxation time than the dashpot will dominate and the Maxwell element will behave like an ideal fluid.

If both the times and the frequencies of the load application are similar both viscous and elastic behaviors are observed.

3.1.4 The Kelvin-Voigt model

Similar to the Maxwell element, the Kelvin-Voigt element is composed of a spring and a dashpot, but this time they are connected in parallel. For this model the mechanical

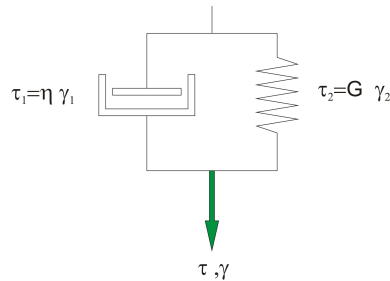


Figure 3.6: The Kelvin-Voigt element

properties can be again fully described by the modulus of the spring G and the viscosity

of the dashpot η . The equations for the spring - dashpot parallel connection are:

$$\begin{aligned}\tau(t) &= \tau_1(t) + \tau_2(t) \\ \gamma(t) &= \gamma_1(t) = \gamma_2(t)\end{aligned}\tag{3.28}$$

Therefore the total stress in this case consists of the sum of the stresses acting on the elements of the Kelvin-Voigt model whereas the deformations are identical for each element and equal the total deformation $\gamma(t)$.

The time dependent stress $\tau(t)$ of a Maxwell model is obtained by inserting into Eq. 3.28 the basic equation for a spring $\tau_2(t) = G \cdot \gamma_2(t)$ and a dashpot $\tau_1(t) = \eta \cdot \dot{\gamma}_1(t)$.

$$\tau(t) = \eta \cdot \dot{\gamma}(t) + G \cdot \gamma(t)\tag{3.29}$$

This equation allows the calculation of the response of the Kelvin-Voigt element to any time-dependent excitation.

The response of the Kelvin-Voigt element to a sinusoidal, periodical load is calculated by introducing the equations for time dependent deformation and stress, as done for the Maxwell element, into Eq. 3.29 and doing the necessary transformations.

$$\begin{aligned}G'(\omega) &= G \\ G''(\omega) &= \omega\eta \\ G^*(\omega) &= \frac{\tau^*(t, \omega)}{\gamma^*(t, \omega)} = G \cdot (1 + i\omega\tau_R)\end{aligned}\tag{3.30}$$

If the duration of the loading is much longer than the relaxation time or if the frequency is much lower than the inverse of the relaxation time then the spring dominates the dynamic mechanical response of the Kelvin Voigt element, i.e. it behaves like an ideal solid.

In the other extreme case, if the duration of the loading is much shorter than the relaxation time or the frequency is much larger than the reciprocal of the relax time then the dashpot dominates and the Kelvin-Voigt element behaves as an ideal fluid. Since the loss modulus of an ideal fluid is inversely proportional to the duration of the loading (or proportional to the frequency), in case of infinitely short times it can assume any values, i.e. the Kelvin-Voigt is mechanically blocked.

3.1.5 The α -transition process

The state of a polymer depends on the temperature and on the time allotted to the experiment. At low enough temperatures all polymers are stiff and brittle finding

themselves in what is called the *glassy state*, i.e. the movements of the chain segments are vibrations around fixed positions. If the temperature increases, the amplitude of the vibrations also rises transmitting an increase in tension to the intermolecular interactions. If the temperature continues to rise a growing fraction of chain segments acquire enough energy to overcome these intermolecular interactions. Stronger modes of movement also occur that involve the rotation and translation of chain terminals and chain segments or loops incorporating about 10 bonds. As for most polymers these movements can be detected as a separate peak in a dynamic mechanical measurement. A convention was reached to assign to each of the transitions a Greek letter. According to this nomenclature, first used by Deutsch et al. [19], the transition that occurs at the highest temperature in a constant frequency measurement or at the lowest frequency in a constant temperature measurement is coined the α -transition.

For crystalline polymers the first transition, or α -transition is the melting of the crystallites. The occurrence of crystallinity in polymers depends on the regularity of structure of the main chain. Thus, isotactic and syndiotactic polymers usually crystallize, whereas atactic polymers, with a few exceptions (where the side groups are small or highly polar), do not. Several types of polybutadiene rubbers are known to crystallize and this phenomenon could pose some difficulties to the dynamic mechanical ultrasonic measurements if their size grew over the Rayleigh scattering limit. Furthermore, such polymers are most of the times of a thermorheologically complex nature meaning that their behavior cannot be evaluated at high frequency using the time-temperature superposition principle.

For amorphous polymers this transition is represented by the glass to rubber change. Considering the temperature axis of a dynamic-mechanical experiment starting at the lower temperatures and heating up, the region where movements of a more global nature, affecting the whole chain and depending on the polymer nature, start to be detected is coined the glass transition temperature [20, 21]. The glass transition is named after the softening of ordinary glass. On a molecular basis, the glass transition involves the onset of long-range coordinated molecular motion, the beginning of reptation.

Polymers with a glass transition temperature above room temperature are termed thermoplastics while polymers whose glass transition temperature lies well below room temperature are called elastomers.

The transformation is caused by a continuous increase in the liquid relaxation time up to an experimental time, usually of order 100 seconds. For a given pressure and composition the glass transition is characterized by the glass transition temperature, T_g [22].

3.1.5.1 Thermodynamic concepts

Thermodynamic theories work on the assumption based on the Kauzmann paradox [23] that the glass transition conceals a true phase. If the entropy of a supercooled liquid is measured and extrapolated to lower temperatures, the extrapolation intersects the entropy curve of the crystalline phase at a critical temperature T_K , i.e. at temperatures lower than T_K the entropy of the supercooled liquid must be lower than that of the crystal, which is of course a contradiction. For this reason the thermodynamic theories assume the existence of a concealed transition at or above T_K and approximately 50 K below the measured glass transition temperature.

A very important aspect of the thermodynamic theories is the concept of regions in which molecules react cooperatively. The reason for cooperativity is the understanding that local molecular motion is not sufficient to maintain molecular mobility for very low free volume. The molecules do not relax independently of one another. The motion of a particular molecule depends to some degree on that of its neighbors therefore the rearrangement movement of one particle if a certain number of nearby particles are also moved.

The size of these regions increases with decreasing temperatures (the number of molecules in a region increases while the number of regions drops) until they become infinitely large at a certain critical temperature. This interpretation is mainly based on the work of Gibbs [10–12]. According to him the solidification of polymers can be described by a second order phase transition¹. In such a transition the volume-temperature dependence undergoes a change in slope, and only the derivative of the expansion coefficient, dV/dT , undergoes a discontinuity. There is no heat of transition at T_g , but rather a change in the heat capacity, ΔC_p . A first-order transition normally has a discontinuity in the volume-temperature dependence, as well as a heat of transition, ΔH_f , also called the enthalpy of fusion or melting [8]. However, describing the glass transition process in this way requires the phases both above and below the transition point to be in a thermodynamic equilibrium, i.e. in case of polymers the occurrence of an equilibrium glass. This and the existence of the aforementioned critical temperature have yet to be proven for polymeric materials.

3.1.5.2 Kinetic description - the free volume theory

The glass transition process is also a process of a distinctly kinetic character because

- the temperature of the transition can be changed by changing the time scale of experiment, slower measurements resulting in lower T_g s

¹A review of the Ehrenfest phase transitions can be found in [24].

- the measured relaxation time near the transition approach the time scale of the experiment

Therefore, thermodynamically it can be viewed as a non equilibrium state. In this case, besides the thermodynamic variables another order parameter is necessary to properly describe it, i.e. the free volume [25].

Within this theory it is assumed that the free volume changes with temperature. At high temperatures it is so large that any movement within the chain is possible and the polymer therefore has the properties of a viscous melt. If the temperature is reduced the free volume decreases proportionally, consequently the mobility of the chain is reduced. As of a certain temperature the free volume is so small that no movements (besides vibration) can be observed in the time frame of the measurement. The free

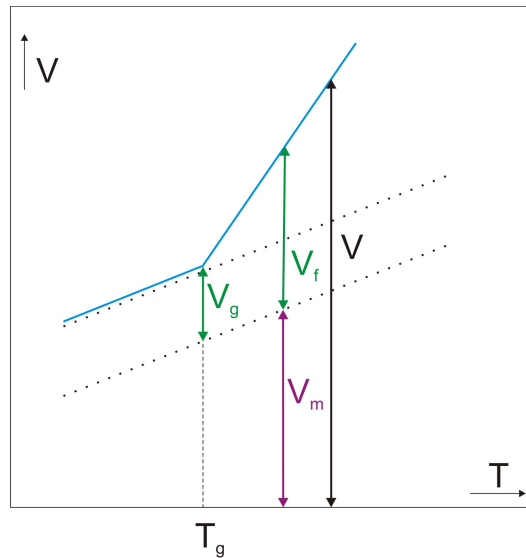


Figure 3.7: The free volume temperature dependence

V - total volume

V_f - free volume

V_g - free volume at T_g

V_m - specific volume of the molecules

volume can be calculated (see Figure 3.7) from the difference between the total volume V and the molecular volume V_m where the latter represents a sum of a hypothetical volume in a melt free of voids at absolute 0 and a volume expanded due to thermal vibrations:

$$V_f = V_g + V_m \Delta\alpha (T - T_g) \quad (3.31)$$

$\Delta\alpha$ represents the difference between the coefficients of thermal expansion of the melt and the glassy region $\Delta\alpha = \alpha_{melt} - \alpha_{glass}$. The probability that at a given temperature

T there will be sufficient free volume for a so called *site exchange* process¹ can be expressed by the term $e^{V^*/V_f(T)}$ where V^* is the minimum volume necessary for such a process. The activation energy will then be:

$$Q(T) = Q^* + RT \frac{V^*}{V_f(T)} \quad (3.32)$$

where Q^* is the temperature dependent amount of energy necessary to overcome the intramolecular potential. As the temperature rises the probability that enough free volume will be available also increases, consequently, the activation energy of such a process decreases until the limiting lower value Q^* - corresponding to the intramolecular potential threshold - is reached.

The glass transition of copolymers Ascribed to their technological relevance, a large amount of work has been directed at derivation of the glass transition temperature of copolymers from the ratio of the individual homopolymers. Based on the additive properties of the free volumes of two homopolymers analytical equations have been derived by different authors to estimate the T_g of copolymers. These formulae, derived by Gordon and Taylor [26]

$$T_g = \sum_i \phi_i T_{gi} \quad (3.33)$$

or Fox and Flory [25]

$$T_g = \frac{1}{\sum_i \frac{\phi_i}{T_{gi}}} \quad (3.34)$$

allow an analytical calculation of the glass transition temperature. The equations can only be applied if all the components of the copolymer are amorphous. The crystallinity of one of the components means the free volume theory cannot be used to calculate the T_g anymore. A great disadvantage of these equations is that they depend only on the volume fraction of the monomer and show no dependence on the frequency. As is shown later in section 5.4 only the Gordon-Taylor equation correlates to experimental data and only to those obtained at 1 Hz.

3.1.5.3 The WLF equation

A quantitative description of the glass process done by Doolittle [27] was examined and extended by Williams, Landel and Ferry [28] and has since been termed the WLF equation.

The starting point for deriving the WLF equation is the viscosity depiction in relation

¹see [9] on page 68

to the free volume mentioned by Doolittle.

$$\ln \eta = B \left(\frac{V}{V_f} \right) + \ln A \quad (3.35)$$

where A and B are constants, V is the occupied volume and V_f is the free volume. The Doolittle equation can be derived by considering the molecular transport of a liquid consisting of hard spheres [29–31].

One derivation of the WLF equation begins with a consideration of the need of free volume necessary for the rotation of chain segments, and the hindrance to such rotation caused by neighboring molecules.

P is henceforth defined as the probability of the barriers to rotation or cooperative motion per unit time being overcome [32]. An Arrhenius type relationship is assumed, where ΔE_a is the activation energy of the process:

$$P = e^{-\frac{\Delta E_a}{kT}} \quad (3.36)$$

In what the time (t) frame of the experiment is concerned, long times imply a greater probability of the required motion therefore P increases. It is assumed that tP must reach a certain value for the onset of the motion:

$$\ln tP = \text{constant} = -\frac{\Delta E_a}{kT} + \ln t \implies \ln t = \text{constant} + \frac{\Delta E_a}{kT} \quad (3.37)$$

The differential of the above equation gives:

$$\Delta \ln t = -\frac{\Delta E_a}{kT} \Delta T \quad (3.38)$$

An increase in the logarithm of time is therefore equivalent to a decrease in the absolute temperature.

The quantity ΔE_a is associated with free volume and qualitatively would be expected to decrease as the fractional free volume increases.

$$\frac{\Delta E_a}{kT} = \frac{B}{f_f} \quad (3.39)$$

where f_f is the fractional free volume. Substituting in Eq. 3.36 yields:

$$P = e^{-\frac{B}{f_f}} \quad (3.40)$$

tP remains constant and the substitutions and subsequent differentiation yields:

$$\ln t = B\Delta \left(\frac{1}{f_f} \right) \quad (3.41)$$

which states that a change in the fractional free volume is equivalent to a change in the logarithm of the time scale of the event to be observed.

The expansion in the glassy state occurs at constant free volume. (Actually, free volume must increase slowly with temperature, even in the glassy state.) The coefficient of expansion increases at T_g , allowing for a steady increase in free volume above T_g . Considering α_f the expansion coefficient of the free volume, and f_0 as the fractional free volume at T_g or other point of interest, the dependence of the fractional free volume on temperature is written:

$$f = f_0 + \alpha_f (T - T_0) \quad (3.42)$$

where T_0 is a transition temperature. Now Eq. 3.41 can be differentiated as:

$$\Delta \ln t = B \left(\frac{1}{f} - \frac{1}{f_0} \right) \quad (3.43)$$

and by inserting 3.42:

$$\Delta \ln t = B \left[\frac{1}{f_0 + \alpha_f (T - T_0)} - \frac{1}{f_0} \right] \quad (3.44)$$

then cross multiplying yields:

$$\Delta \ln t = B \left\{ \frac{f_0 - [f_0 + \alpha_f (T - T_0)]}{f_0 [f_0 + \alpha_f (T - T_0)]} - \frac{1}{f_0} \right\} \quad (3.45)$$

$$\Delta \ln t = - \frac{\frac{B\alpha_f(T-T_0)}{f_0}}{f_0 + \alpha_f (T - T_0)} \quad (3.46)$$

Dividing by α_f yields:

$$\Delta \ln t = - \frac{\frac{B}{f_0} (T - T_0)}{\frac{f_0}{\alpha_f} + (T - T_0)} \quad (3.47)$$

Finally, considering the meaning of $\Delta \ln t$:

$$\Delta \ln t = \ln t - \ln t_0 = \ln \left(\frac{t}{t_0} \right) = \ln a_T \quad (3.48)$$

According to [6, 33] a_T is termed the reduced variables shift factor. The quantity a_T relates not only to the transition time but also to other time dependent quantities at the transition temperature and other temperatures. The theoretical form of the WLF equation can be written as:

$$\log a_T = -\frac{B}{2,303f_0} \left[\frac{T - T_0}{\frac{f_0}{\alpha_f} + (T - T_0)} \right] \quad (3.49)$$

This equation shows that a shift in the logarithmic time scale will produce the same change in molecular motion as will the change in temperature.

Conveniently, $\frac{B}{2,303f_0} = C_1$ and $\frac{f_0}{\alpha_f} = C_2$ which turns Eq. 3.49 into its known form:

$$\log a_T = -\frac{C_1 \cdot (T - T_0)}{C_2 + (T - T_0)} \quad (3.50)$$

In the original equation derived by Ferry et al. the term T_0 , representing an arbitrarily chosen reference temperature, was substituted by T_g connecting the relation to a unambiguous determination of the T_g which is an experimentally challenging task. The parameters C_1 and C_2 have only an empirical character, not being related to the glass transition.

The general form of the WLF equation is mainly used in the creation of master curves. If the frequency dependent modulus of a polymer is measured at different temperatures, a master curve can be created by shifting the individual curves along the frequency axis. The WLF equation gives then an analytical relationship between the shift factors $\log a_T$ and the measuring temperature. Furthermore, if the WLF parameters for a specific reference temperature are determined the frequency dependent behavior can be calculated for any desired temperature as long as the deformations are in the linear range and the materials are single phase and unfilled.

The WLF equation assumes that T_g will change 6°C to 7°C per decade of frequency. Obviously this depends on the apparent energy of activation of the individual polymer, but many of the common carbon-backbone polymers have similar energies of activation. The limitations that come from this assumption are illustrated by typical examples in section 5.5.

The equivalence of time and temperature A key point in the glass process' kinetics is the equivalence of temperature and frequency. Temperature is a measure of molecular motion. At higher temperatures, time moves faster for the molecules. The WLF equation, derived above, expresses a logarithmic relationship between time and temperature. Starting from this, the time-temperature superposition principle states that with viscoelastic materials, time and temperature are equivalent to the extent that data at one temperature can be superimposed on data at another temperature by shifting the curves along the log time axis [6]. This means that temperature dependent measurements of the complex modulus at constant frequency and frequency dependent measurements of the complex modulus at constant temperature lead to the same conclusions. The explanation for this is that both measurements reflect the same elementary relaxation processes taking place on a molecular level.

In multicomponent polymeric systems such as polymer blends or blocks (also termed *thermorheologically complex* materials), each phase stress relaxes independently [34–36]. Thus each phase will show a glass-rubber transition relaxation. While each phase follows the simple superposition rules illustrated above, combining them in a single equation must take into account the continuity of each phase in space. Attempts to do so have been made using the Takayanagi models [36, 37], but the interpretation of the results is not trivial.

3.1.6 Entanglements and the reptation model

The mechanical behavior of high molecular polymer melts was interpreted by Treloar, back in the 1940s [14], based on the influence of entanglements¹. He assumed that the entanglements would form a temporary network which would be rather stable mechanically, under short time or high frequent stress, ascribed to the high number of conformational changes a chain would have to make to come out of an entanglement. After extended exposure to mechanical loading entanglements can come undone through changes in chain conformation. The viscous flow of polymer melts is, therefore, not dependent only on the length of the chain but also, to a high extent, on the dynamics of chain entanglements. This approach was extended by Doi, Edwards and de Gennes [39–41] and they were able to describe the dynamics of the macromolecular chain. The snake like creep of the chains between entanglements was termed *reptation* by de Gennes.

The basic idea is best explained for polymer diffusion through a gel that is swollen by some solvent. The gel consists of polymer strands that are chemically linked together to form a three dimensional network. In the solvent filled space between the strands

¹Entanglements are ascribed to several topological restrictions induced to one another by neighbouring chains [38]

some free chain, not chemically linked to the gel, may exert a Brownian motion. The strong interaction with the strands of the gel constrains this motion to a “tube” that is defined by the strands surrounding the instantaneous chain configuration. Due to crosslinking, these ‘topological constraints’, i.e. entanglements, are essentially fixed. (The thermal motion of the gel is neglected.) The array of entanglements forming a tube around the instantaneous chain configuration is one important ingredient of reptation (see Figure 3.8). The second important ingredient of this theory is the specific mechanism of microscopic chain motion within the tube. Since the chain is highly flexible, it cannot move as a whole like a rigid body, but it moves through thermal displacements of individual segments. It also does not lie stretched in its tube, but, as a consequence of flexibility and entropy, there will be a finite density of small wiggles or side loops of “spared length”. These loops, called “defects” by de Gennes, exert a diffusive motion along the chain and thus along the tube. This is taken as the basic dynamical mechanism. If a defect reaches a chain end, it can be destroyed, thus prolonging the tube by its spared length in some random direction. A chain end can also contract into the tube, thus creating a defect and destroying the end of the previous tube over a distance of its spared length. This mechanism results in a thermal motion of the chain ends, which gradually destroys the original tube until finally the chain has found a completely new configuration.

For branched, star, and cyclic polymers to diffuse the following possibilities exist for translational motion. First, one end may move forward, pulling the other end and the branch into the same tube. This process is strongly resisted by the chains as it requires a considerable decrease in entropy to cause a substantial portion of a branch to lie parallel to the main chain in an adjacent tube [42]. Instead, it is energetically cheaper for an entangled branched-chain polymer to renew its conformation by retracting a branch so that it retraces its path along the confining tube to the position of the center. Then it may extend outward again, adopting a new conformation at random. The basic requirement is that the branch not loop around another chain in the process, or it must drag it along also. De Gennes [43] calculated the probability P_1 of an arm of n -mers folding back on itself as where n_c is the critical number of mers between physical entanglements and a is a constant. More detailed discussions on rubber elasticity based on this idea are given in the literature [44–47].

$$P_1 = \exp\left(\frac{-\alpha n}{n_c}\right) \quad (3.51)$$

The result is that diffusion in branched-chain polymers is much slower than in linear chains. For rings, diffusion is even more sluggish, because the ring is forced to collapse into a quasilinear conformation in order to have center-of-mass motion. Since many commercial polymers are branched or star-shaped, the self-diffusion of the polymer is

correspondingly decreased, and the melt viscosity increased.

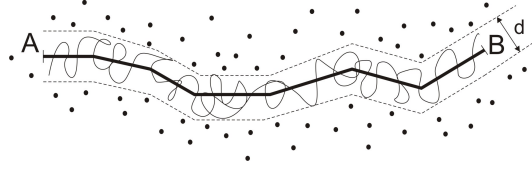


Figure 3.8: The reptation model. The points A and B denote the cross-linked points, and the dots represent other chains assumed to be perpendicular to the paper. Entanglements confine the chain to the tube-like region marked by the broken line. The bold line shows the primitive path [48].

The reptation model assumes that the polymer chain can move, reptate, by diffusion only through a tube due to the hindrances induced by the presence of neighboring chains. The size of the tube can be estimated from the number of entanglements. For an average of N_e segments of chain between two entanglements, the diameter of the tube, d_{rep} , will be equal to the end-to-end distance of a chain with N_e segments. For this ideal chain it holds:

$$d_{rep} = a_l \cdot \sqrt{N_e} \quad (3.52)$$

with a_l being the length of a chain segment. In the case of diffusion the square of covered distance is proportional to time. The time τ_{rep} a chain needs to diffuse - reptate out of the tube is proportional to the square of its contour length L .

$$\tau_{rep} \approx \frac{L^2}{D} \quad (3.53)$$

where the Einstein diffusion coefficient is:

$$D = \frac{kT}{N_S \zeta_0} \quad (3.54)$$

This gives a correlation between reptation time τ_{rep} and the contour length of the chain as a function of temperature T , friction coefficient ζ and the number of segments in the chain N_S , namely:

$$\tau_{rep} \approx L^2 \cdot \frac{N^S \zeta_0}{kT} \quad (3.55)$$

The contour length is calculated by multiplying the diameter of the tube by the number of entanglements ($\frac{N_S}{N_e}$ where N_e is the number of segments between two entanglements)

$$L = \frac{N_S}{N_e} \cdot d_{rep} \quad \xrightarrow{d_{rep}=a \cdot \sqrt{N_e}} \quad L = \frac{1}{\sqrt{N_e}} \cdot a \cdot N_S \quad (3.56)$$

The time, or frequency dependent modulus is proportional to the portion of the chain

that is still inside the tube. Through complex mathematical derivations, Doi and Edwards [48–51] obtained the characteristic spectrum of relaxation processes:

$$\begin{aligned} G(t) &= \frac{8G_e}{\pi^2} \sum_{\text{odd}}^{\infty} \frac{1}{q^2} \cdot e^{-q^2 \frac{t}{\tau_{rep}}} \\ G^*(\omega) &= \frac{8G_e}{\pi^2} \sum_{\text{odd}}^{\infty} \frac{1}{q^2} \cdot \frac{i\omega\tau_{rep}}{q^2 + i\omega\tau_{rep}} \end{aligned} \quad (3.57)$$

G_e is termed the plateau modulus. It is indirectly proportional to the mean molecular weight, M_e , of a chain located in between two entanglements, therefore, it is a measure of the crosslink density.

$$G_e = \frac{\rho RT}{M_e} \quad (3.58)$$

The molecular weight of the chain between two entanglements is a material specific parameter, independent of the main chains' length or its molecular weight. A chain with a high flexibility will form more entanglements with neighboring chains, hence displaying a lower molecular weight between the chains than one with a more rigid structure, i.e. the higher the plateau modulus, the more flexible the polymer will be.

Nonlinear behavior

The reptation model described above is valid in the linear viscoelastic range, i.e. at small deformations. For nonlinear dynamics of polymers there are other models that describe the phenomena occurring in that case. Such partly empirical considerations and calculations are thoroughly described in [52–55]. For the present work they are, however, of a lesser relevance.

3.2 Dynamic mechanical behavior

Dynamic mechanical analysis (DMA) is a technique of applying an oscillatory or pulsing force to a sample. It supplies information about major transitions as well as secondary and tertiary transitions not readily identifiable by other methods. It also allows characterization of bulk properties directly affecting material performance. The method is also called, besides DMA, DMTA - dynamic mechanical thermal analysis, dynamic thermo mechanical analysis or dynamic rheology.

This section is divided into two parts, the first concerned with the low frequency dynamic mechanical analysis where the most common devices are described. The second part discusses the high frequency DMA achieved through ultrasonic measurements.

3.2.1 Low frequency DMA

First attempts at measuring elastic properties via oscillatory measurements are traced back to Poynting [56] who, in 1909, performs theoretical and experimental analysis of steel wires. During the 1930s Lessig [57] developed the Goodrich flexometer in Akron, device which became an ASTM standard (*D623*) for tire rubbers and was modernized in the 1990s to operate from 5 Hz to 40 Hz and from room temperature to 120°C.

In Germany, during the 1940s, Roelig [58] did some dynamic mechanical work on rubbers at a constant temperature.

Takayanagi published dynamic-mechanical data on crystalline polymers in 1965 and developed the Rheovibron apparatus [59]. The modern period of DMA debuted in 1966 when Gillham developed the torsional braid analyzer [60]. In 1971 Macosko and Starita built a DMA that measured normal forces using torsional geometry and this step represented the advent of the Rheometrics corporation [61]. In 1976 the first Gabo Eplexor was built by the local Rheovibron agent as a larger Rheo unit for the tire industry.

The breadth of the dispersion regions for elastomers, regions where the dynamic properties change with frequency, makes a large range of frequencies desirable for many investigations. For such wide frequency range nonresonant methods are usually preferred. Experimentally it is easier to secure a wide range of low frequencies than of high frequencies. Nolle [4, 62–64] used six methods-amongst which low frequency DMA to cover a range of 0.05 Hz to 10^5 Hz in studying the dynamic properties of NR, NBR, IIR, SBR and neoprene over a temperature range from about -60°C to 100°C . One of the most interesting observations he made at that time was that at very low frequency and sufficiently high temperatures (0°C for NR) the modulus increased in proportion to the absolute temperature, the same relation as the kinetic theory of rubber elasticity gives for the equilibrium static modulus. At higher frequencies the modulus decreased with increasing temperature, the transition occurring at approximately 100 Hz for NR and 1 Hz for IIR. Philippoff [65] performed DMA measurements below 10 Hz with a single mechanically driven forced vibrator managed to secure the same frequency ratio as Nolle. The load and deflection of the test piece were indicated by signals from linear differential transformers. The output from the transducers was fed into a cathode ray oscilloscope and the hysteresis loops recorded photographically. Blizard [66] used an electromagnetic drive and small shear strains and worked over a frequency range from 0.0124 Hz to 750 Hz, a ratio of 1 to 50000. When it is kept in mind that such frequency ranges as the above can be extended based the time/temperature equivalence principle it is apparent that forced vibrations methods are characterized by enormous frequency ranges.

Currently, dynamic testing is covered by ISO 2856 which separates it into two broad classes, free vibration methods and forced vibration methods.

3.2.1.1 Free resonance analyzers

The free oscillating torsion pendulum is a classical instrument in rubber research and technology. Its operating principle involves the decay of the initial oscillation amplitude with successive swings and this decay provides an indication of the energy loss. The oscillation frequency gives information for calculating the dynamic modulus. There is always a dependence of the frequency on the particular sample used and usually a limitation to two or three decades of frequency, achieved by varying the oscillating mass, the sample size and shape or by the use of an auxiliary stiff torsion wire [67]. Periods are usually of the order of 0.02 to 30 seconds. Since the apparatus is compact at the sample, temperature control is relatively convenient and the effective temperature range can be very large if the principle of the equivalence of temperature and frequency changes is established and used for the materials being investigated.

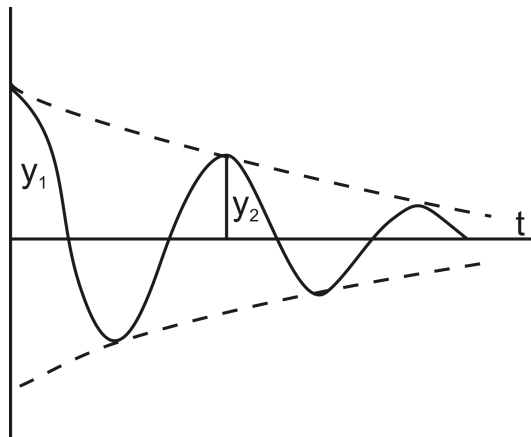


Figure 3.9: Trace of a damped free vibration

More information regarding this type of DMA can be found in [1, 18, 68, 69].

Free oscillation methods such as the torsion pendulum are covered by ISO 4663 and are limited to very low strains and frequencies, hence, much less used nowadays than the forced vibrations nonresonant systems.

3.2.1.2 Forced resonance analyzers

Forced oscillations in torsion are used in the most versatile and accurate technique for measuring the viscoelastic functions, in the frequency domain, of melts and concentration solutions [70].

These methods involve direct measurement of the force on the specimen and the corresponding deformation. To evaluate the losses, the phase angle between force and deformation may be measured. It should be noted that free vibration methods have greater sensitivity with low loss materials. Thus in a forced vibration method $\tan\delta$ might be determined but in a free vibration method the measured quantity is the logarithmic decrement which is $\pi\tan\delta$. The Dynamic Mechanical Analyzer (DMA) functions on this principle and can be used to measure dimensional and viscoelastic changes as a function of temperature or time. The DMA is capable of measuring the viscoelastic changes as a function of periodic changes in the stress applied to the sample. The DMA primarily consists of three components: the Linear Variable Differential Transformer (LVDT), a furnace and a linear motor for probe loading. The LVDT measures displacement by detecting a change in voltage caused by movement of the probe through a magnetic core. The change in voltage is related to the displacement of the probe. The top section of the LVDT is the linear motor which provides the load for the static force used during the runs. The DMA apparatus can be fitted with various geometries, the most relevant ones for the current work are shown in figure 3.10 whereas other possible assemblies can be reviewed in [69].

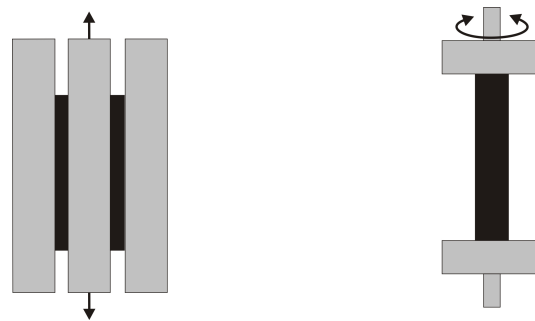


Figure 3.10: Geometries used in DMA measurements
left - double shear sandwich
right - torsion rectangle

3.2.2 Wave propagation in viscoelastic media

Ultrasonic testing is based on the propagation of waves in materials. Wave propagation is the result of an applied disturbance in a medium. When the applied disturbance is of mechanical origin, stress waves are produced. Strictly speaking, a wave in a continuous medium is a propagating surface of discontinuity.

Wave motion is the mechanism by which energy is conveyed from one place to another in mechanically propagated waves without the transference of matter 3.11. At any point along the path of transmission a periodic displacement, or oscillation, occurs

about a neutral position. The oscillation may be of air molecules, as in the case of sound traveling through the atmosphere; of water molecules, as in waves occurring on the surface of the ocean; or of portions of a rope or a wire spring. In each of these cases the particles of matter oscillate about their own equilibrium position and only the energy moves continuously in one direction. Such waves are called mechanical because the energy is transmitted through a material medium, without a mass movement of the medium itself¹.

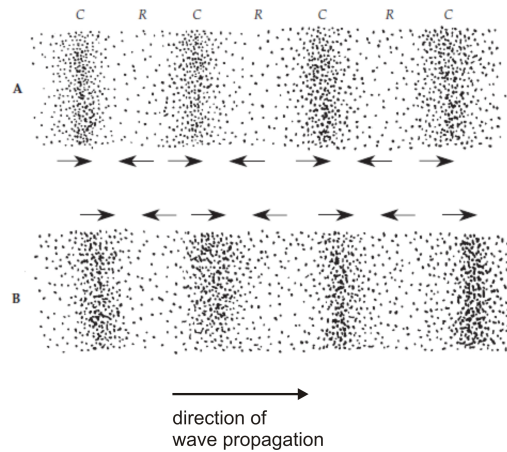


Figure 3.11: Sound waves traveling through a medium change localized air particle density.

(A) The sound wave causes the air particles to be pressed together (compression) in some regions and spread out (rarefaction) in others.

(B) An instant later the sound wave has moved slightly to the right.

Waves are divided into types according to the direction of the displacements in relation to the direction of the motion of the wave itself. If the vibration is parallel to the direction of motion, the wave is known as a longitudinal wave (see Figure 3.11). The longitudinal wave is always mechanical because it results from successive compressions (state of maximum density and pressure) and rarefactions (state of minimum density and pressure) of the medium.

Both ultrasonic and dynamic mechanical analysis are governed by laws based on harmonic oscillations, i.e. on an applied force that varies sinusoidally with time. Motion equations are defined using a sine or cosine wave of singular frequency or wavelength. As the visualization of ultrasound behaving like a mechanical wave from which viscoelastic material constants can be calculated tends to be rather abstract, the following passage is focused on the derivation of the ultrasound modulus from the wave equation. The derivation of the wave equation through an elastic model applied to polymeric materials can be found in several books [71–73].

¹The only form of wave motion that requires no material medium for transmission is the electromagnetic wave; in this case the displacement is of electric and magnetic force fields in space.

The wave equation of motion is derived by considering transverse motion of a wave on a string. A section of the string will perform vertical simple harmonic motions, i.e. a simple oscillator with displacement y is used to represent the variable which changes as the wave propagates through the material - displacement of an element in the direction x at a time t . Therefore, $y = f(x, t)$. The wave equation of a string will relate the displacement y of a single oscillator to distance x and time t . This can be expressed by Newton's second law $f = m \cdot a$ where f is the force, m is the mass and a is the acceleration, in a derivative form [73]:

$$\tilde{\tau} \frac{\partial^2 y}{\partial x^2} = \rho \frac{\partial^2 y}{\partial t^2} \quad (3.59)$$

The term on the right side represents the linear density ρ of the elementary segment of the string times the acceleration of that segment. The required restoring tension, $\tilde{\tau}$, is proportional to the curvature of the string. For practical reasons the above wave equation can be expressed in terms of sound velocity. The term $\tilde{\tau}/\rho$ has the same units as c^2 .

$$\begin{aligned} \frac{\partial^2 y}{\partial x^2} &= \frac{\rho}{\tilde{\tau}} \frac{\partial^2 y}{\partial t^2} & \text{where} & & c^2 &= \frac{\tilde{\tau}}{\rho} \\ \frac{\partial^2 y}{\partial x^2} &= \frac{1}{c^2} \frac{\partial^2 y}{\partial t^2} \end{aligned} \quad (3.60)$$

The simple harmonic motion of an oscillator y of amplitude a at position x and time t can be expressed using the typical formulation for harmonic oscillations:

$$y = a \sin(\omega t - \theta) \quad (3.61)$$

where θ represents the phase lag with respect to the oscillator at position x_0 . Two points are in phase if they are a multiple of wavelength apart, hence, θ will have values between 0 and 2π . As the measured parameters in acoustic measurements are sound velocity and attenuation the equation for a harmonic oscillation needs to be rewritten accordingly:

$$\begin{aligned} \theta &= \frac{2\pi x}{\lambda} & \text{and} & & \omega &= \frac{2\pi c}{\lambda} = 2\pi f & \text{and} & & k &= \frac{2\pi}{\lambda} \\ y(x, t) &= a \sin(\omega t - \theta) \\ &= a \sin k(ct - x) \\ &= a \sin \frac{2\pi}{\lambda}(ct - x) \end{aligned} \quad (3.62)$$

To convert the factor $(ct - x)$ to radians, it must be multiplied by the wave number k .

$$\begin{aligned} y(x, t) &= a \sin \frac{2\pi}{\lambda} (ct - x) \\ &= a \sin (\omega t - kx) \end{aligned} \quad (3.63)$$

This equation is used, in turn, to get from Eq. 3.59 the wave parameters in terms of an elastic modulus:

$$y = a (\sin (\omega t - kx) + i \cos (\omega t - kx)) = ae^{i(\omega t - kx)} \quad (3.64)$$

For viscoelastic materials the modulus is represented in a complex form, i.e. $M^* = M' + iM''$. The terms M' and M'' represent the real and imaginary parts of this complex modulus and they have to be integrated into the wave Eq. 3.59 which gives:

$$\begin{aligned} \rho \frac{\partial^2 y}{\partial t^2} &= M^* \frac{\partial^2 y}{\partial x^2} \\ \rho \frac{\partial^2 y}{\partial t^2} &= M' \frac{\partial^2 y}{\partial x^2} + iM'' \frac{\partial^2 y}{\partial x^2} \end{aligned} \quad (3.65)$$

The decay of the oscillation amplitude is described by an exponential factor, $e^{-\alpha x}$, to express the rate at which the amplitude in the material is reduced. The larger the material damping coefficient or attenuation α the faster the wave amplitude decays. The term α is measured directly from the rate of the emitted wave amplitude to the received amplitude after passing through the sample, see equation 5.6. By integrating α into Eq. 3.64 the wave equation for viscoelastic materials becomes:

$$y = a (\sin (\omega t - kx) + i \cos (\omega t - kx)) e^{-\alpha x} \quad (3.66)$$

This conclusion is also presented in [74] albeit using different notations. By substituting in Eq. 3.65, evaluating the terms M' and M'' it is possible to form two similar equations which can then be solved by real and imaginary parts depending on the four measured parameters ρ , c , α and ω .

$$M' = \rho c^2 \frac{1 - \beta^2}{(1 + \beta)^2} \quad (3.67)$$

$$M' = \rho c^2 \quad \text{when} \quad \beta \ll 1 \quad (3.68)$$

$$M'' = \rho c^2 \frac{\beta}{(1 + \beta)^2} \quad (3.69)$$

$$M'' = \frac{\rho c^3 \alpha}{\omega} \quad \text{when} \quad \beta \ll 1 \quad (3.70)$$

where $\beta = \frac{\alpha c}{\omega}$.

Relations between dynamic moduli The velocity of a longitudinal wave propagating in a solid depends to a great extent on the dimensions of the specimen in which the waves are traveling. For a bar shaped specimen (lateral dimensions are small compared to the wavelength) under tensile loading then the dynamic properties are characterized by Young's modulus E . On the other hand, a longitudinal wave in a medium compresses and distorts it laterally which in a solid body is always accompanied by the development of shear forces. However, in bulk solids longitudinal and shear (transversal) waves can be considered separately.

For samples whose dimensions are large compared to the wavelength, the complex modulus describing the material is the longitudinal wave modulus, in case of longitudinal wave propagation. In this work the dimension of the thinnest sample was at least three times the wavelength, therefore the following formulations are valid and can be derived from the wave equation as shown.

The various moduli are interrelated by the Poisson's ratio, ν , which describes the relationship between the changes in length per unit length and the changes in width per unit length.

$$E^* = \frac{9G^*K^*}{G^* + 3K^*} \quad \text{and} \quad \nu^* = \frac{E^*}{2G^*} - 1 \quad (3.71)$$

then the equation relating all four basic mechanical properties is:

$$E^* = 3K^*(1 - 2\nu^*) = 2(1 + \nu^*)G^* \quad (3.72)$$

Any of these properties can be varied independently and the knowledge of any two of them enables one to calculate the remaining ones. The modulus of the longitudinal waves is given by Love's mathematical theory of elasticity [75].

$$M^* = K^* + \frac{4}{3}G^* \quad (3.73)$$

Such formulations are particularly useful as one can relate terms evaluated from experimental measurements (M' and M'') to the other moduli. Obviously, K' and K'' can only be evaluated when the attenuation and sound velocity are known both for the longitudinal waves as well as for the shear waves. In liquids, where shear waves do not propagate, $M^* = K^*$, i.e. the longitudinal wave modulus in liquids is equal to the bulk compression modulus. For the ultrasonic characterization of materials, the interrelation of the moduli is of high interest especially if results given by different methods are to be compared.

$$L^* = G^* \frac{E^* - 4G^*}{E^* - 3G^*} = \frac{4G^* - E^*}{3 - \frac{E^*}{G^*}} \quad (3.74)$$

The complex moduli in Eq. 3.74 may be replaced by either the storage or the loss

components. In material science, however, the longitudinal wave modulus is a rather uncommon term and Young's or shear modulus are more familiar. Young's modulus could be determined by longitudinal propagation in thin strips or rods but the method ceases to function when the wavelength becomes comparable to the cross sectional dimensions at high frequencies. In this case the longitudinal waves do not yield E' but the longitudinal modulus M' . The shear modulus could also be determined by propagating transverse waves in the material but the great disadvantage comes from the fact that shear waves do not propagate in liquids or in soft polymers (above T_g).

Acoustic impedance Sound travels through materials under the influence of sound pressure. Because molecules or atoms of a solid are bound elastically to one another, the excess pressure results in a wave propagating through the solid.

Ultrasonic waves are reflected at boundaries where there is a difference in acoustic impedances¹ (Z) of the materials on each side of the boundary. The impedance is expressed as the product of longitudinal wave velocity and density of the medium and can be expressed in either its constituent units (pressure per velocity per area) or in *rayls*.

$$Z = c \cdot \rho \quad (3.75)$$

This difference in Z is commonly referred to as the impedance mismatch. The greater the impedance mismatch, the greater the percentage of energy that will be reflected at the interface or boundary between one medium and another.

The fraction of the incident wave intensity that is refracted can be derived because particle velocity and local particle pressures must be continuous across the boundary. When the acoustic impedances of the materials on both sides of the boundary are known, the fraction of the incident wave intensity that is reflected can be calculated with equation

$$R^2 = \left(\frac{Z_2 - Z_1}{Z_2 + Z_1} \right)^2 \quad (3.76)$$

The value produced is known as the reflection coefficient. Multiplying the reflection coefficient by 100 yields the amount of energy reflected as a percentage of the original energy. Since the amount of reflected energy plus the transmitted energy must equal the total amount of incident energy, the transmission coefficient is calculated by simply subtracting the reflection coefficient from one.

In order to measure the dynamic-mechanical properties of polymers using ultrasound a coupling medium must be used for the transmission of the longitudinal waves to occur with minor losses. In a simple example, not using a couplant would yield a reflection

¹Here the characteristic acoustic impedance is referred to.

coefficient of 99.94% of the incident wave (for an SBR air interface) so there will be as good as nothing passing through to the receiving transducer. For an SBR propanol system the reflection coefficient will be around 10%.

Wave scattering The principal cause of loss of energy in ultrasonic testing of materials is *scattering* by inhomogeneities in the material. The inhomogeneities may consist of different particle orientation in a polycrystalline substance since each individual particle is anisotropic for the propagation of ultrasound; they may also be inclusions of different materials or even pores as in the case of foamed materials [76].

Each inhomogeneity will scatter the incoming wave and so the reflected and transmitted acoustic fields will be the result of many wave-scatterer interactions. The precise nature of these interactions is governed by the ratio of the wavelength to the size of scatterers. If the wavelength of the incident ultrasonic wave is large compared to the size of the inhomogeneities (which, in turn, must be over a hundredth of the wavelength in size) then *Rayleigh scattering* occurs. This is perhaps the simplest regime to work in as many factors become insignificant at long wavelengths and in particular, spring approximations apply [77, 78]. As the wavelength is large compared to the length of the grains and the wave falls over many grains it is no longer necessary to consider the individual effects of the gaps. This type of scattering increases as the third power of the particle size and the fourth power of the frequency as long as the wavelength remains greater than the grain size.

3.2.2.1 Dynamic-mechanical experiments

Ultrasound as a non-destructive testing technique is usually associated with the detection and evaluation of defects, cracks or pores in solid parts. Also, a wide number of applications can be found in medicine, mostly based on the different densities of tissues which enables specially designed software programs to show exact reproductions of internal organs.

Ultrasonic techniques are also well suited for determining the values of different elastic and viscous coefficients for polymeric composites. Wave propagation is the result of an applied disturbance in a medium. When the applied disturbance is of mechanical origin, stress waves are produced. Strictly speaking, a wave in a continuous medium is a propagating surface of discontinuity. The simplest relation describing elastic recovery of crystalline materials is $M = \rho c^2$ where M is a modulus and c is the velocity of the propagating wave. Rubbers have a viscous component which induces energy dissipation, therefore they are usually described by complex numbers.

The wave theory combined with experimental evidence for bulk waves propagation in polymers was mainly developed by [3, 79–82].

Ivey et al. [81] made early ultrasonic measurements where they investigated the longitudinal wave velocity and damping using the pulse transmission technique on IIR, SBR and NR at frequencies between 0.04 and 10 MHz in a temperature range from -60°C to 40°C . The rotating plate method was employed by Kono [83] to measure transverse and longitudinal wave propagation on polystyrene and polymethyl methacrylate (PMMA) at frequencies of 0.5 MHz, 1 MHz and 2.25 MHz in a temperature range from 20°C to 210°C and drew some conclusions with regard to the effect of large side groups on the positions of the longitudinal and shear maxima on the temperature scale and the effect of frequency on the maxima shift. Also Yee and Takemori [84] calculated the dynamic compression modulus and the shear modulus from the simultaneous measurement of the dynamic Young's modulus and Poisson's ratio on PMMA at frequencies of 0.01 Hz, 0.1 Hz, 1 Hz and 11 Hz between 0°C and 40°C .

The acoustic parameters related to viscoelastic polymer properties are obtained from transmission times, t , and amplitudes or intensities, I , through the sample. When the sample thickness is known the sound velocity, c , and attenuation, α , can easily be calculated (see equations 5.6 and 5.7) providing the basis for the calculation of the complex longitudinal wave modulus, M^{ast} . There are no generally agreed parameters employed to describe material properties using ultrasound. Several authors, for example Ferry [6] use sound velocity and attenuation to describe viscoelastic properties whereas others prefer the longitudinal modulus, real part of the complex Poisson's ratio [85–87], attenuation per wavelength [80, 81] real and imaginary part of the complex longitudinal wave modulus [88, 89]. As can be seen the wide distribution in choice of measuring parameters has been maintained over the years since this technique is used. Most authors have been largely satisfied with empirical correlations when it came to comparing results from different measuring techniques.

Over the time there have been different attempts at correlating such different methods. For example Chalis [90] chose to formulate the results in terms of relaxation times to facilitate a comparison with dielectric measurements. Lionetto [91], on the other side, compared results from low frequency dynamic mechanical analysis, dielectric analysis and ultrasound to investigate post cure characteristics of unsaturated polyester resins. Using the Williams Landel Ferry equation (see [6]) he shows a plot of six experimentally determined points which takes him to the conclusion that all three methods are sensitive to the α relaxation process.

More detailed investigations were carried out by Maeda [92] who employed a both ultrasound and dielectric analysis in a similar frequency range to study PVC - plasticizer compounds. His work shows results that are pretty much the opposite of Lionetto's

as he revealed that the main relaxation peak appears at a 40K difference in the two methods independent of frequency. His conclusion was that ultrasonic measurements are based on mechanical principles and directly related to dynamic modulus and loss whereas dielectric measurements are based on electrical properties and mainly related to dipole mobility, hence, only indirectly related to the mechanical properties. Results yielded by this method will therefore not only depend on the physical properties but also on dipole content. Ferry [5] also confirms discrepancies between dynamic mechanical and dielectric analysis on two PVC compounds.

Theoretical considerations and experimental results performed in our laboratory on the high frequency properties of elastomers (NR, NBR, BR) and their interactions with reinforcing fillers were published by J. Kroll [88] and S. Eckert-Kastner [93].

High frequency dynamic analysis has been used by several authors to study the compatibility behavior in several rubber blends. Singh et al. [94–96] described the use of ultrasonic velocity measurements for compatibility determination. Their results showed a non linear dependence of the compressional sound velocity on blend composition for incompatible polymers and a linear correlation in compatible blend systems. Using the same method, Abd El-All et al. [97] conducted experiments on NR-SBR, NR-CR, NBR-CR and NBR-SBR. Similar to Singh, they concluded that NR-SBR and NBR-CR were compatible blends due to the linearity of the dependence of sound velocity with mole percent of the blend. Sidkey et al. [98, 99] performed sound attenuation and velocity measurements on several polyurethane-rubber blends at 4 MHz and concluded such tests were sufficient to provide a clue to the compatibility of the aforementioned polymers, however neither of the authors made any comments on how the ability of the ultrasonic method to distinguish between different phases is affected by the measuring frequency. This aspect is discussed in the results part of this work.

As noticed from the reviewed literature above, the two main measuring techniques are wave reflection and wave transmission. For the current work the latter was used. The advantages over the reflexion technique reside in the lower damping of the ultrasonic wave ascribed to its traveling only one time through the measuring chamber before being received and analyzed whereas in the reflection technique, the waves pass once through the medium, are reflected and have to pass once more so the losses will be twice as high.

4

Materials

The term *elastomer* is actually used to depict crosslinked polymers whose glass transition temperature is usually found below 0°C. These compounds are hard below their glass transition temperature and display rubber-elastic properties above it up to their decomposition point.

The initial polymers, which are crosslinked to form the aforementioned elastomers, are known under the name of *rubber*. It's characteristic trait is viscoelastic flow at room temperature ascribed to which it can be easily processed under fitting conditions. The process through which a *rubber* is transformed, through a change in its structure and by so doing conferring the material elastic properties, into an *elastomer* is termed *vulcanization* [100]. Rubber can be obtained either from natural sources, i.e. natural rubber,

Year	Production			Consumption		
	Natural Rubber	Synthetic Rubber	Total Rubber	Natural Rubber	Synthetic Rubber	Total Rubber
1998	6,634	9,880	16,514	6,570	9,870	16,440
1999	6,577	10,390	16,967	6,650	10,280	16,390
2000	6,762	10,870	17,632	7,340	10,830	18,170
2001	7,332	10,483	17,815	7,333	10,253	17,586
2002	7,337	10,877	18,214	7,552	10,687	18,239
2003	8,033	11,379	19,412	7,944	11,369	19,313
2004	8,758	11,999	20,757	8,701	11,851	20,552
2005	8,906	12,136	21,042	9,069	11,904	20,973
2006	9,698	12,690	22,388	9,329	12,481	21,810
2007	9,707	13,442	23,149	9,884	13,161	23,045
2008	9,876	12,819	22,695	9,726	12,573	22,299
2009	9,093	2,754	4,847	2,044	2,574	4,618

Figure 4.1: World rubber production according to the International Rubber Study Group (IRSG) Vol. 63, No. 10-12, April-June 2009 (data for 2009 for the first quarter only)

Table 4.1: Synthetic rubber: chemical mechanisms and process characteristics

Chemical mechanism	Process features				
	Emulsion	Solution	Dispersion	Bulk	Gas phase
Radical polymerization	E-SBR; CR; NBR; E-BR; ACM; FPM; EVM	EVM	EVM	AEM; EVM; ENM	
Ziegler-Natta polymerization		BR; EPM; EPDR	EPM; EPDM	EPM; EPDM; EPDM(BR)	EPM; EPDM
Anionic polymerization		BR; S-SBR; IR		Q	
Cationic polymerization		ECO; CO	IIR	Q	
Polyaddition and polycondensation		AU; EU	EU	AU; Q	
Polymer modification		CIIR; BIIR; CM; CSM; HNBR; FZ	CM; CSM;		

or by specially developed synthesis processes. An overview of the rubber production and consumption over the last decade is shown in Figure 4.1.

4.1 Synthetic rubbers

The production of synthetic rubbers, i.e. SBR, NBR, IIR, encompasses a wide array of different methods and processes, which have been developed as a response to the ever increasing demand for elastomers with with good heat and mineral oil resistance, both of which natural rubber cannot offer. The great variety of production solutions can be classified from a chemical as well as from an engineering point of view. The chemical side is concerned with the mechanism by which the polymerization takes place while to the chemical engineering the relevant aspects are the process and the series of process steps involved in the production (see Table 4.1).

Concerning nowadays polymers, it is worth mentioning that a great percentage is manufactured via emulsion and solution polymerization.

4.1.1 Emulsion polymerization

4.1.1.1 Poly(acrylonitrile-co-butadiene) (NBR)

One of the most versatile techniques in polymer production, emulsion polymerization can be applied to many monomers in batch or continuous processes.

An emulsion consists of a discontinuous liquid phase dispersed throughout a different,

continuous liquid phase. Most emulsion polymerizations are free-radical reactions. Characteristic of an emulsion polymerization is that the reaction takes place within the dispersed micelles, which act as discrete micro-reactors. One advantage is the relatively constant viscosity of the emulsion during the reaction and the excellent heat transfer due to the water matrix. The emulsion process uses water as a heat sink. The polymerization reaction is easier to control in this process than in bulk or solution systems because stirring is easier and removal of the exothermic heat of polymerization is facilitated.

The main difference compared to alternative free-radical polymerizations, such as those in bulk, solution and suspension systems, is that the propagating macro radicals in emulsion reactions are isolated from each other. Encounters between macro radicals are hindered as a consequence and termination reactions are less frequent than in comparable systems in which the reaction mixture is not subdivided. This type of polymerization often yields high-molecular-weight products at fast rates when suspension or bulk reactions of the same monomers are inefficient.

The essential ingredients in an emulsion polymerization are water, a monomer that is not miscible with water, an oil-in-water emulsifier (either anionic surfactants, including salts of fatty acids or alkane sulfonic acids, or non-ionics based on polyether groupings or sugar derivatives) and a compound or compounds which release free radicals in the aqueous phase. Typical proportions (by weight) are monomers 100, water 150, emulsifier 2-5 and initiator 0.5 although these ratios may vary over a wide range [101].

It is generally accepted that in the case of the emulsion polymerization the process takes place in the monomer containing emulsifier micelles. The free radicals, produced by the decomposition of the initiator, are formed in the aqueous phase and move into the micelles by passing through the separation surface between the two phases. The dual character of the emulsifier, which contains both hydrophilic and hydrophobic groups, eases this passage. During this process the micelles transform into a particle that contains both monomer and polymer protected by a layer of emulsifier. However, this process does not take place in all the micelles, therefore the ones in which the polymerization occurs are known as "active" and the others as "inactive".

This polymerization process is divided, according to [102] and [103], into four stages (see also Figure 4.2):

- Until a conversion of 10-20% is achieved, (a), the micelles containing no monomer disappear, the emulsifier they were made of moving to the micelles containing monomer and polymer. The inactive micelles also disappear and the monomer they contained participates at the growth of the active micelles. At this level of conversion the number of monomer-polymer particles becomes constant.

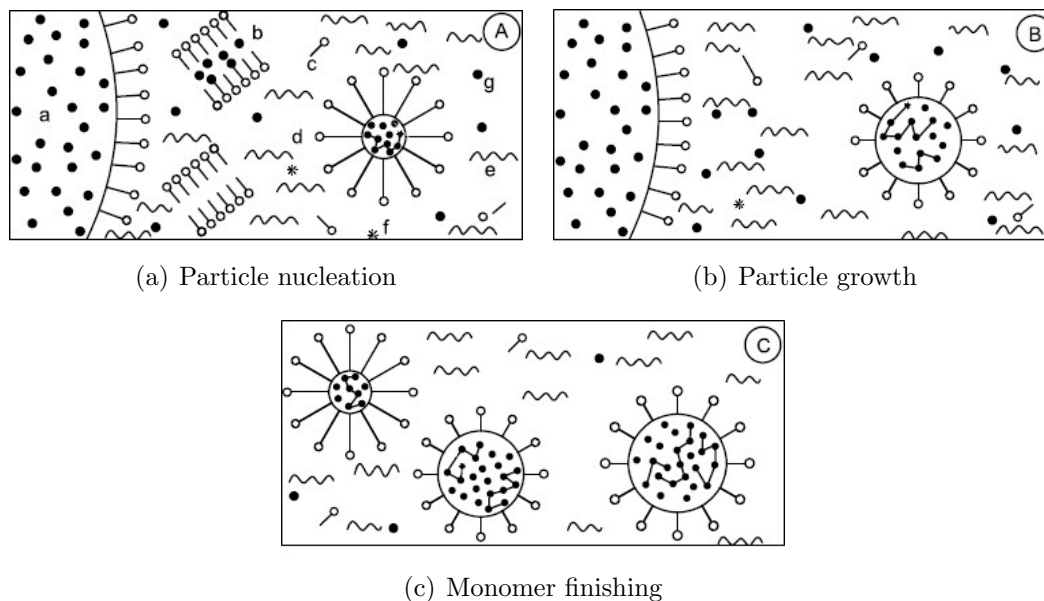


Figure 4.2: Schematic display of an ideal emulsion polymerization reaction

a-monomer droplet
 b-micelle
 c-emulsifier molecule
 d-latex particle
 e-water
 f-radical
 g-monomer molecule

- With the advance of the process to higher conversions (20-60%) (b) the monomer inside the particles is transformed to polymer. The free drops of monomer come now into play by alimenting the growing polymer particle, protected by the emulsifier layer, threw diffusion, constantly increasing their volume.
- Up to a conversion of 60% the reaction rate remains almost constant. Beyond this point, (c), the reaction rate decreases because the free monomer particles are now exhausted. At this stage chain transfer reactions occur with a higher frequency and lead to long chain branching and finally to formation of undesired rubber-gel.
- In the final stage, (d), the particle dimensions have shrunk, after growing continuously after stage (a) due to volume contraction and are approximately 400-1500Å.

One of the most eloquent examples of valuable copolymer is obtained by the free radical emulsion polymerization of acrylonitrile and butadiene. NBR was produced on an industrial scale for the first time by IG Farbenindustrie Leverkusen in 1934.

The production of NBR includes several stages amongst which polymerization, de

gassing, precipitation, washing, drying and finishing. All producers use the same temperature range for the process.

The reaction takes place at a pressure between 2 and 7 bar. The monomers are emulsified in water using rosin acids, arylalkylsulfonic acids, long chain fatty acids, alkyl sulfates as emulsifiers or dispersion agents.

The polymerization is initiated mainly by redox systems, i.e. organic peroxides, hydroperoxides, persulfates, which allow polymerization temperatures between 0°C and 30°C, and metal salts are used as cocatalysts. The molar mass is controlled using mercaptanes as modifiers.

The reaction is stopped at 70-80% conversion by using a shortstopping agent in the form of a reducing agent (sodium dithionite, diethylhydroxyl amine, hydroquinone, etc.) that destroys the initiator [104].

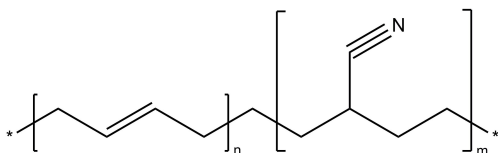


Figure 4.3: polyacrylonitrile-co-butadiene

NBR (Figure 4.3) vulcanizates show good hot air and abrasion resistance combined with resistance to swelling in oils, fats and fuels determined mainly by the acrylonitrile content in the polymer ascribed to the polarity it induces. The presence of the nitrile group also favors the interaction with polar fillers, e.g. silica or silicates.

4.1.2 Ionic polymerization

The International Union of Pure and Applied Chemistry (IUPAC) defines ionic polymerization as a type of chain polymerization in which the kinetic chain carriers (the chain ends) are ions or ion pairs [105]. The main advantage of ionic polymerization over radical polymerization is the very low activation energy of the initiation stage which basically means that this type of polymerization is relatively insensitive to temperature and can be carried out at temperatures as low as -70°C. The intermediates produced during polymerization cannot react with each other therefore the reaction stops only when impurities are encountered or special reagents are introduced conferring, thusly, a certain amount of control over the final molecular weight of the compound.

The energy required to form a pair of ions from a neutral molecule is large, and therefore these very unstable ions must be stabilized by solvation at low temperature before polymerization will occur. Polar solvents cannot be used to solvate ions because they

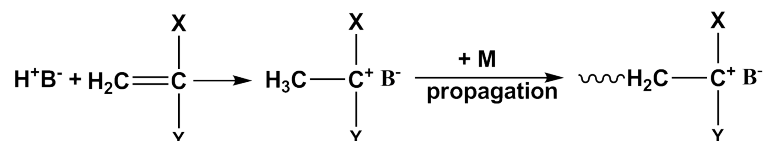
are overly reactive and destroy the ionic initiators. Ionic polymerizations are usually carried out at low temperature in solvents of low polarity. These solvents may give ion pairs as well as free ions. Thus, a propagating ionic chain may have a counterion close to the active center during its growth. The proximity of the ion on the growing chain to its counterion depends on the type of counterion, which is determined by the initiator type, and the solvation power of the solvent. Therefore, unlike free-radical polymerization the type of initiator and the nature of the solvent have a large effect on monomer addition during chain growth. The propagation rate depends not only on temperature but also on the type of initiator and the type and amount of solvent [106].

Unlike radical polymerization, termination of an active center of a polymer chain occurs by reaction with the counterion, solvent, monomer, or other species. Often, the initiation reactions are very fast, and the initiator is consumed in the early stages of polymerization before the polymer chains have grown much beyond oligomeric size. In the absence of unimolecular termination a population of polymer chains having the same molecular mass can grow. The concentration of ionic reactive centers is usually much larger than that of radical centers. Ionic polymerization kinetics are not as well understood as those radical-based polymerizations because of the requirements of extreme purity for the components of the reacting mixture.

Ascribed to the duality of ions and to the differences in the project course, there are three subtypes of ionic polymerization illustrated in the following by relevant examples: cationic polymerization and anionic polymerization and Ziegler-Natta polymerization.

4.1.2.1 Cationic polymerization - Poly(Isobutylene-co-Isoprene) (IIR)

Cationic polymerization proceeds through attack on the monomer by an electrophilic species, resulting in heterolytic splitting of the double bond to produce a carbenium ion [107, 108]. The most important commercial polymers produced by cationic poly-



merization are polyisobutylenes and butyl rubber. IIR or butyl rubber is a copolymer of 2-methylpropene (isobutene) and about 1-3 mol% of 2-methylbuta-1,3-diene (isoprene). The small amount of isoprene introduces unsaturations in the main chain therefore enabling sulfur vulcanization. This was also the first time in history when extra functionality was deliberately introduced in a saturated polymer [109].

The copolymerization of isobutylene and isoprene follows a cationic process. A typical polymerization is carried out at about 100°C in chlorinated solvents such as

chloromethane and is initiated by AlCl_3 . The polymerization is very fast. In the copolymer the isobutylene units are linked exclusively head to tail while the randomly distributed isoprene units display a trans-1,4 configuration [110]. The reaction is initiated by a species resulting from a Lewis acid such as $\text{AlX}_n\text{R}_{3-n}$ where X is usually Cl, $n = 1 - 3$ and R = *Et*. This Lewis acid is activated by proton donor species i.e. water, hydrochloric acid, organic acids or alkyl halides.

The isobutylene monomer reacts with the Lewis acid catalyst to yield a positively charged carbocation (i.e. a carbenium ion) during the initiation. Units of monomer are continuously added in the propagation step until chain transfer occurs or the reaction is terminated. During the chain transfer step that terminates propagation the carbenium ion of the polymer chain reacts with the isobutylene or isoprene to halt the growth of the current macromolecule and form a new propagating chain. By using reaction temperature as low as -100°C the chain transfer is delayed leading to higher molecular weight polymers. More than 90% of the isoprene is copolymerized by trans-1,4 addition. Termination can also be achieved through the destruction of the carbenium ion by hydrogen abstraction from the comonomer, formation of stable allylic carbenium ions or by reaction with nucleophilic species such as alcohols or amines. Termination is critical after polymerization in order to control the molecular weight [111].

The main application of IIR is the production of halobutyl rubber with the rest finding use in tire applications including but not restricted to inner tubes, tire curing bladders and inner liners. Another less relevant use is as food component, especially in chewing gum and in sealing cements [110].

4.1.2.2 Anionic polymerization - Solution Poly(Styrene-co-Butadiene) (SSBR)

Anionic polymerizations show many of the same characteristics as cationic polymerizations. However, since the nature of carbanions is different from carbenium ions, there are distinct differences. In contrast to cationic polymerization, neither termination nor chain transfer occur in many anionic polymerizations (living polymerization) especially when polar substances are absent. Anionic active centers are usually much more stable than cationic active centers. Although anionic polymerizations proceed rapidly at low temperatures, they are not usually as temperature sensitive as cationic polymerizations, and polymerizations usually proceed well at ambient temperature and higher.

Copolymers of 1,3-butadiene and styrene are elastomers highly sought after and their primary application is car tires [112]. The process that can yield the most different forms of SBR with regard to the microstructure of the butadiene moieties and the styrene sequence distribution takes place in solution through anionic polymerization

[113–115].

This type of polymerization is concerned with reactions in which the reactive species present at the end of the growing polymer chain is an anion. The anionic polymerization of a monomer to polymer involves the three main processes found in most polymerization reactions: initiation, propagation and termination.

The first stage of a polymerization reaction, i.e. initiation, requires the presence of the active species that will add molecules of monomer and form the desired polymer. A variety of basic initiators have been used to initiate anionic polymerizations [114, 116]. The initiation involves the addition of an anion (base) to the double bond of the monomer. Alkyl lithium initiators have been most widely used in the polymerization of butadiene and isoprene, since they are easy to prepare and are soluble in hydrocarbon solvents. There are several different mechanisms that produce the required anions but the most relevant to the present work are alkali metal alkyls of which, the most used is *n*-butyl lithium.

It is worth mentioning that *n*-butyl lithium produces a living polymer chain which grows only at one end, the other one being locked by the butyl group.

The initiation ends with the formation of the first carbanion. Further, another monomer is attacked and another carbanion is formed and so on until there are several chains growing at the same time. The rate of growth is always the same for all chains and this continues until all the monomer is consumed. At this stage the polymer molecules are still active and, since carbanions are relatively stable, anionic polymerization with carefully purified reagents may lead to systems in which chain termination is absent, i.e. they still bear the reactive anion, so should more monomer be added the reaction will continue consumed by the free ion. Such polymers are referred to as living polymers [117, 118]. The only way to stop the reaction is to remove the anion thus rendering the chain incapable of further growth [119].

Propagation occurs by the successive insertion of monomers into the partial bond between the propagating anion and its cationic counterion.

Termination is accomplished by the reaction of the living polymer with an electrophile. Out of the vast array of species that can be used to terminate the reaction the most relevant for SBR are amine- and tin-containing electrophiles which provide the best interaction with carbon black while epoxy compounds and alkoxysilanes are most beneficial for silica filled compounds [111]. It must also be noted that any impurities present in the polymerization reactor can interact with the active center destroying the living ion.

The production of SSBR is usually carried out by batch and continuous anionic solution process. The different stages of this process are: polymerization, monomer and solvent

recycling, product recovery. The reaction takes place at a temperature between 50°C and 100°C, at a pressure of 1-5 bar in a batch reactor or in a reactor train of two to four stirred tank reactors. The polymerization is complete in 1 to 4 hours depending on the temperature, catalyst, monomer concentration and modifier content. After purging the reactor the conversion is stopped with a polar liquid (i.e. alcohol). The addition of stabilizers, extender oils followed by a treatment with steam and hot water to remove unreacted monomer and solvent mark the end of the process [104].

At present, sequential addition of monomers to a living anionic polymerization system is the most useful method for synthesizing well defined block copolymers [106].

4.1.2.3 Ziegler-Natta polymerization - Polybutadiene (BR)

Due to the interactions between the propagating chain end, counterion, and incoming monomer molecule, ionic polymerizations tend to give stereospecific polymers. Polar monomers such as methacrylates and vinyl ethers undergo stereospecific polymerization initiated by conventional ionic initiators under certain conditions. However, the coordinating power of the Ziegler – Natta initiators is much stronger than the usual ionic initiators, so it is appropriate to treat Ziegler – Natta (ZN) systems separately. The use of ZN initiators for diene polymerization has yielded remarkable results that far surpass the stereospecificity exhibited by organolithium initiators [106].

With butadiene, four different stereospecific polymer structures, namely, *cis*-1,4, *trans*-1,4, syndiotactic-1,2, and isotactic-1,2 can each separately be obtained to almost total exclusion of the others by an appropriate choice of initiator system [120].

The ZN initiators consist of a combination of alkyls or hydrides of group 1 – 3 metals (e.g. Na, Be, Al) with salts of group 4 – 8 metals (e.g. Ti, V, Cr, Mn). The Ti-Al initiator systems, especially $(C_2H_5)_3Al-TiCl_3$, have been most thoroughly studied. Many important ZN initiators are solids and during polymerization are suspended in liquid or gaseous media. Discussions on the mechanism of ZN polymerization can be found elsewhere [108, 120, 121]. However, at present, none of the proposed mechanisms have been comprehensively verified and the observed kinetics are quite complex.

Ziegler–Natta polybutadiene was first produced by Phillips Petroleum in 1956 using titanium catalysts. This was followed very rapidly by development of cobalt and nickel systems [104].

Polybutadiene rubber is the second largest synthetic rubber product after SBR: In 1995, 1,402,000t were produced, exclusive of Eastern Europe and the socialist countries of Asia. Worldwide annual BR capacities were about 23,280,000t at the end of 1996, as estimated by the International Institute of Synthetic Rubber. This figure is, however, difficult to interpret, because most of the capacity can be used to produce BR, SBR,

and block copolymers. Special BR types – e.g., polymers with special end groups, liquid polymers, high-vinyl polymers – are produced only in small amounts. Ziegler–Natta

Table 4.2: Dependence of microstructure of Ziegler–Natta polybutadiene on catalyst used.

	% cis	% trans	% vinyl	Molar mass distribution	$T_g(^{\circ}C)$
Cobalt	97	1	2	moderate	–106
Titanium	93	3	4	moderate	–103
Nickel	97	2	1	broad	–107
Neodymium	98	1	1	very broad	–109

polybutadienes are produced by solution processes using a variety of solvents. The neodymium-catalyzed process, can be carried out only in aliphatic or cycloaliphatic solvents. The raw monomer and solvent are usually dried by azeotropic distillation and fed to a series of polymerization reactors. Ziegler–Natta catalysts are, commonly, three-component systems, and both the order of addition and the mixing conditions can be important. The catalyst components may be added directly into the first reactor or some components may be added into a premix vessel ahead of the reactor or into the feed line. Various methods are used to control the molar mass of the products. Molar mass modifiers specific to the catalyst system are used where necessary. The final conversion of ca. 70–99% is achieved in a polymerization time of 2–3h. After polymerization a short stop is added. Water, fatty acids, or alcohols, can be used to terminate the reaction. Antioxidants are added, and steam and water are brought into contact with the polymer solution to strip off the solvent and any residual monomer. This coagulation and stripping operation leaves the rubber in the form of small particles floating in water. The water is drained off through a screen, and the material is dewatered, usually in an extruder.

In extenso reviews of the technology can be found in publications by Burford and Bhowmick [122, 123] as it does not make the subject of this work.

4.1.3 Hydrogenation of polymers

Hydrogenation of polymers has attracted attention ever since the work of Staudinger, Harries and Pummerer in the early 1900s [124–126]. Most of the hydrogenation reactions carried out by early workers were accompanied by a considerable amount of chain scission leading to the formation of oils, liquids, and gases (destructive hydrogenation). The objective of these early works was to prepare lubricating oils, motor fuels, and products suitable for insulation and coatings. Cowley and King described the hydrogen-cracking process which converts natural rubber to motor fuel or to a

mixture of hydrocarbons boiling over a wide range [127]. Later the attention shifted to the study of selective hydrogenation of synthetic unsaturated polymers.

4.2 Natural Rubber (NR)

More than 2000 years before the natural rubber was introduced in Europe, the tribes of Central America developed several ways of collecting it and forming it into a wide range of objects ranging from toys to medicinal devices and items relating to ritual sacrifices or tribute payments [128]. The Europeans first became aware of the odd material in the 15th century when Christopher Columbus brought samples from the Americas [129].

The French and German words for it (*caoutchouc* and *kautschuk*) are inspired by the writings of Charles Marie de la Condamine, a member of the Academie Royale des Sciences, who in 1736 sent a package with rubber samples and a letter describing them in which he mentioned several times the words *Heve* as the name of the tree from which the milk or *latex* flowed and *cahuchu* or *caoutchouc* the name given to the material by the Maninas Indians, which basically stands for *weeping tree*.

Nowadays more than 99% of the natural rubber latex is extracted from the *Hevea Brasiliensis* tree. Most plantations are in Southeast Asia with Malaysia and Indonesia responsible for 24% (each) of the world production and Thailand for 25%.

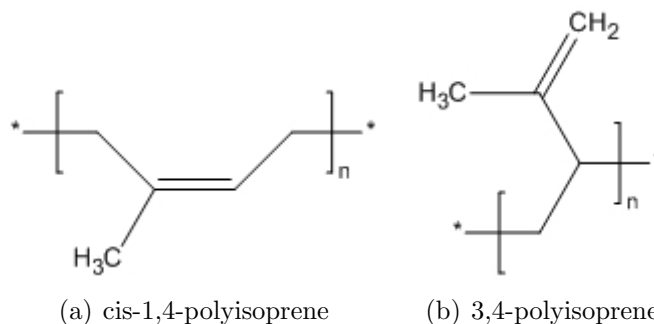


Figure 4.4: Natural rubber structure

NR latex is a dispersion of 98% *cis*-1,4-polyisoprene (and about 2% 3,4-polyisoprene) -see Figure 4.4- in water with an average particle size between 0.15 and 0.3 μ m and a rather broad particle distribution. The solids contained by the aqueous dispersion amount to 30-30% depending on the time of the year and the age of the tree. Other components that occur in a rather low concentration are proteins, resins, fatty acids and inorganic salts.

The synthesis of the NR latex in the plant occurs through a polycondensation reaction starting from a basic unit comprised of five carbons, i.e. isopentenyl pyrophosphate with the entire reaction being controlled by enzymes[130].

About 44% of the natural rubber production is used up by the general rubber goods (GRG) sector. The remaining is used in the production of tires, particularly for trucks where its property profile (namely low heat buildup) makes it more suitable than synthetic rubber. In the car tires it is used mainly blended with SBR. Due to the high elasticity that accompanies the low hysteresis NR is also used for vibration and shock damping in spring elements and buffers.

4.3 Blending of polymers

In order to fulfill the diverse requirements of the industry with regard to new elastomeric compounds two different strategies can be followed: The first would involve the improvement of the polymer synthesis methods or the elaboration of completely new ones. Elastomers with tailor made properties could, therefore, be produced by synthesizing new monomers or by using better catalysts/initiator systems and improved polymerization conditions. This elegant solution is, however, hindered by economical reasons which prevent the availability of large quantities of monomers as well as difficulties that appear in the synthesis of polymers with sufficient chain mobility therefore the expected number of new rubbers ($T_g < 0$) that will be available in the future is quite low. Moreover, no single rubber available on the market at the moment is able to fulfill the complex requirements regarding operation under extreme conditions that nowadays compounds are expected to comply with [131].

The second strategy, that has been employed for several years in the industry, involves the use of blends. Polymer blends, by definition, are physical mixtures of structurally different homo and copolymers [132]. The blending procedure involves the mechanical mixing of two, three or more rubbers in the required volume fractions almost exclusively on the two roll mill or in the internal mixer resulting into a mix that retains the properties of the individual rubbers. This way in the development of compounds for tire treads, the requirements for high abrasion resistance and good grip are fulfilled by combining the high chain flexibility of the cis-BR with the high T_g SBR. Additionally, the reduction of the rolling resistance is achieved through a good dispersion and distribution of reinforcing fillers.

If two polymers are mixed the most frequent result is a system that exhibits near to total phase separation. Qualitatively, this can be explained in terms of the reduced

combinatorial entropy of mixing two types of polymer chains.

$$\Delta G_{mix} = \Delta H_{mix} - T\Delta S_{mix} \quad (4.1)$$

Single-phase systems, i.e. complete miscibility, are obtained for negative values of ΔG_{mix} and two phase systems, i.e. incompatibility, for positive values of ΔG_{mix} [133].

The early literature on polymer blends, based also on the experimental work of Scott [134] and Bohn [135], was dominated by the idea that polymer-polymer miscibility would be the rare exception due to the usual endothermic heat of mixing and the very small combinatorial mixing entropy which would make it unlikely to realize the necessary negative free energy of mixing.

When two polymers do mutually dissolve, they are generally found to phase separate at some higher temperature rather than at some lower temperature, this being called a lower critical solution temperature (*LCST*) see figure 4.5.

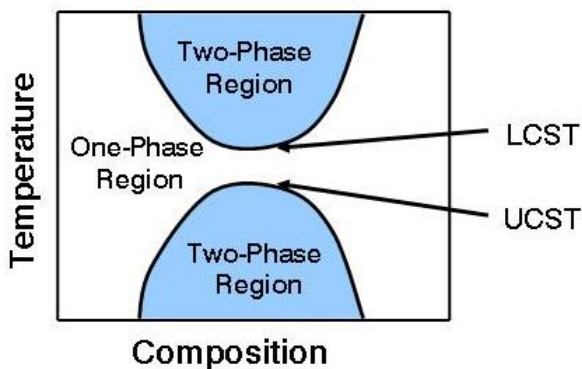


Figure 4.5: Phase diagram for a polymer blend displaying an upper and a lower critical solution temperature (UCST and LCST).

This unusual result can be interpreted by considering that at the critical point in the mixing process the heat of mixing must balance the entropy of mixing times the absolute temperature. The latter is known to be unusually small so that the free energy of mixing, according to the Flory - Huggins theory, is the difference between two small quantities. The aforementioned theory does not permit volume change on mixing and it doesn't take into account the equation of state properties of the pure components. It also does not properly consider the important size differences between solvent and polymer.

The continuous growth of the global request for polymer blends drove the development of the theory into two new directions: the first was the Flory equation of state [136] and the second was Sanchez's lattice fluid theory [137, 138]. These theories were expressed

in terms of the reduced temperature $T = T/T^*$, reduced pressure $P = P/P^*$, reduced volume $\tilde{V} = V/V^*$ and reduced density $\tilde{\rho} = 1/\tilde{V}$. The starred quantities represent characteristic values for particular polymers, usually referred to as "close-packed" values, i.e. with no free volume [8].

These theories point out that LCST behavior is characteristic of exothermic mixing and negative entropy caused by the densification of the polymers on mixing. The usually small (compared to other quantities) value of the volume change entropy comes to the fore in polymer-polymer blends.

The ultimate goal of polymer blending is a practical one of achieving products that are commercially viable either through their unique properties or through a lower cost [139].

4.4 Fillers

In most general terms, fillers are finely divided solids that are used to modify the mechanical, electrical and/or optical properties of a material in which it is dispersed. From the very beginning of the rubber industry the importance of fillers in providing performance and durability has been recognized.

At the beginning of the 20th century, materials that were used to reduce the tack, increase the hardness or reduce the cost of natural rubber compounds were predominantly finely ground naturally occurring products such as mica and clay or flour of wood, wheat and bone, manufacturing by-products such as factory dusts and zinc oxide. As the industry expanded, materials of finer particle size, such as precipitated calcium carbonate and titanium dioxide, were added to the non-black fillers while carbon black became the principal filler in the rubber industry.

The filler loading of a rubber compound is usually between 50 and 80 parts per 100 parts of rubber (phr) and of all the ingredients added to the rubber products it has the most important property changing/adjusting role [140].

The main characteristics which determine the properties a filler will confer the rubber compound are the size of the filler particles, the surface area, the structure and the surface activity.

- **Particle size** - The inclusion of particles exceeding 10.000 nm into the rubber matrix can cause chain rupture by introducing an area of localized stress, since they are much bigger than the interchain distance. Such fillers are therefore generally avoided. Fillers with particle sizes between 1000 and 10000 nm are used as diluents and have an insignificant effect on polymer properties. The ones

belonging to the size group of 100 to 1000 nm are called semi-reinforcing and they bring about an improvement in modulus and strength properties. Reinforcing fillers have a particle size between 10 nm and 100 nm and they bring a significant improvement to the overall properties.

- **Surface area** - The contact between the filler and the polymer must be as close as possible for a good reinforcement to occur. The surface area is the opposite of the particle size, therefore small particles have a large surface area which they can use to interact with the polymer chains providing reinforcement. The shape of the particles is also relevant - particles with a planar shape have more surface available than spherical particles with the same size. Carbon blacks used in rubbers have a surface varying from 6 m²/g to 250 m²/g whereas precipitated silicas range from 125 m²/g to 200 m²/g.
- **Structure** - The shape of any individual filler particle is of lesser relevance, after the filler is incorporated in the rubber matrix, then the effective shape. Carbon blacks and silicas have round shaped particles but they function as anisometric aggregates once they're mixed. The aggregate properties, i.e. size, shape, density, define their structure. The more an aggregate deviates from a spherical shape the higher is its structure and the higher its structure the greater the reinforcement it will incur. It should be noted that mixing has a strong effect on the structure destroying the aggregates and it is possible, in the case of silica, to reduce the aggregates to primary particles. This situation is not encountered in the case of carbon black.
- **Surface activity** - This property plays an important role in reinforcement since it is very much possible that a filler with high surface area and structure has poor reinforcing properties ascribed to low interaction with the rubber matrix. For the fillers that have a low surface activity several surface treatments have been developed (for example silans for silica and silicates) which help improve filler-polymer interactions.

The aforementioned properties of rubber fillers are interdependent in improving rubber properties. The effect of a filler on the physical properties of rubber can be related to how many macromolecular chains are attached to the filler surface and how strongly they are attached.

The nanofillers used in polymer nanotechnology are mostly of different shapes and can be categorized into the following classes [141]:

- Spherical/Cubical e.g., silica, carbon black, polyhedral oligomeric silsesquioxanes (POSS), nano CaCO₃, metal oxides etc.
- Rod/fibre e.g., synthetic whiskers, carbon nanotubes, carbon nanofibers, boehmite,

sepiolite, nano CaCO_3 , etc.

- Sheet/platelet e.g., layered silicates such as smectite group clays, synthetic mica etc.

The details about the nanofillers used in elastomers are discussed below.

4.4.1 Reinforcement of elastomers

From a technological point of view, a distinction is made between active or reinforcing fillers¹ and inactive or extender fillers². The former are used to achieve particular vulcanizate properties; the latter, to make the compound cheaper (to extend it).

The term *reinforcement* refers to all polymer-filler interactions that improve the dynamic-mechanical and physical properties of a rubber. The term itself was first used by Wiegand [142] in 1920. In his work the criterion used to characterize reinforcing effects was the tearing energy obtained by integrating the surface of a stress-strain curve. In case of reinforcing fillers he noticed an increase of the tearing energy up to a maximum value.

The influences of reinforcing and inactive fillers on some elastomer properties are summarized in Figure 4.6 (adapted from [129]). According to it, a linear increase with the inactive filler concentration is noticed for the viscosity, hardness and abrasion resistance whereas the tear resistance shows a linear decrease. In the case of reinforcing fillers the viscosity and hardness show a clear increase while the tearing and abrasion resistance display an optimum for a certain concentration of filler.

Another trait of reinforcing fillers is the formation of an interphase with the rubber matrix. If a filler – rubber mixture is extracted with a suitable solvent, after drying of the the extraction residue, a hard, brittle gel is obtained, which contains all the filler. The rubber content of this gel is known as bound rubber. The quantity of bound rubber formed on mixing depends on many factors, such as type of filler, degree of filling, polymer type, mixing technique and extraction conditions. In the case of carbon blacks, bound rubber is a measure of filler activity, but it is not used for assessment, unlike other physical properties such as surface area and structure, whose dependence on the compound and vulcanizate properties are known.

¹With usual particle sizes between 10 and 100 nm

²With usual particle sizes between 500 and 1000 nm

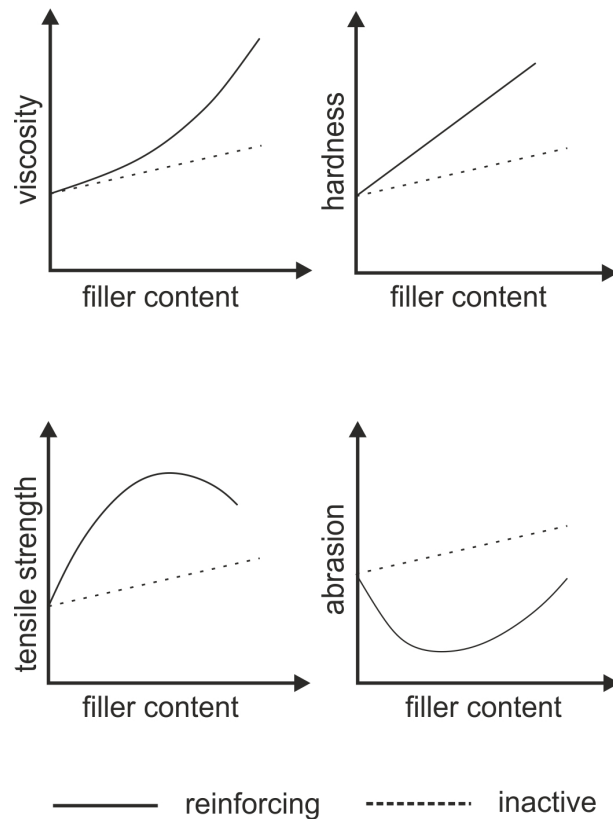


Figure 4.6: Effects of reinforcing and inactive fillers.

4.4.2 Carbon Black

Carbon black is a form of highly dispersed elemental carbon with nanosized primary particles. Depending on the production process and the raw materials, carbon black also contains chemically bound hydrogen, oxygen, nitrogen, and sulfur [143, 144].

Carbon black is formed either by pyrolysis or by partial combustion of vapors containing carbon. Besides carbon black, also hydrogen, CO, CO₂ result in the process. During the production process liquid carbon drops are formed which subsequently come together to form the stratified spherical primary particle¹.

There are several procedures through which carbon black is produced:

- *the lamp black process* is the oldest and simplest method of obtaining carbon black [145]. It involves the burning of aromatic oil in deficit of oxygen and the subsequent deposit of carbon black on a cold surface. The resultant blacks have a rather large particle size and a broad size distribution.
- *the channel black and gas black processes* involves the burning of natural gas in

¹Its size varies depending on the carbon black type between 10 and 80 nm

the presence of an excess of oxygen. Carbon black condenses subsequently on contact with water cooled channels where it is scraped off and collected. This procedure results in very fine-particle blacks but its use has been abandoned since 1976 [146]. An improvement (in terms of yield) of this process was undergone by Degussa in 1930 by substituting natural gas with vaporised oil. The particle size was again around 10 nm [147].

- *the thermal black process* is not based, as the above mentioned procedures, on incomplete combustion of hydrocarbons but on the thermal decomposition of lower gaseous hydrocarbons in the absence of air at 2600°C. This leads to blacks with particle sizes of 300-500 nm [148].
- *the acetylene black process* is also based on thermal decomposition, this time of the thermally labile acetylene at 800°C in carbon black, hydrogen and other products.
- *the furnace black process* is today's most used method for the manufacturing of carbon blacks. It involves the injection of the feedstock, usually as an atomized spray, into a high-temperature zone of high energy density which is achieved by burning a fuel (natural gas or oil) with air. The oxygen, which is in excess with respect to the fuel, is not sufficient for complete combustion of the feedstock, the majority of which is therefore pyrolyzed to form carbon black at 1200–1900°C. The whole process takes place in a furnace. The reaction mixture is then quenched with water and further cooled in heat exchangers, and the carbon black is collected from the tail gas by a filter system.

During the transition from liquid to solid phase the primary particles combine to form primary aggregates. According to the number of primary particles one can distinguish between very branched (100-300 primary particles) and less branched (30-100 primary particles) primary aggregates. The word *structure* is used to characterize the constitution of the primary aggregates (see figure 4.7).

Since 1957 carbon blacks are divided and named by the ASTM according to their influence on vulcanization kinetics and processing properties. Letter N therefore, stands for normal vulcanizing systems, letter S for slow vulcanizing. The first number gives the size class of the primary particle diameter; the last 2 numbers are arbitrarily chosen. They give information on the structure of the respective black.

The size of the specific surface is usually characterized according to the BET-Theory by the adsorption of nitrogen on the surface of the carbon black. The specific surface is given in terms of BET-SA or $N_2 - SA^1$.

The structure of a filler is characterized by the absorption of dibutylphthalate (DBP)

¹SA stands for Surface Area

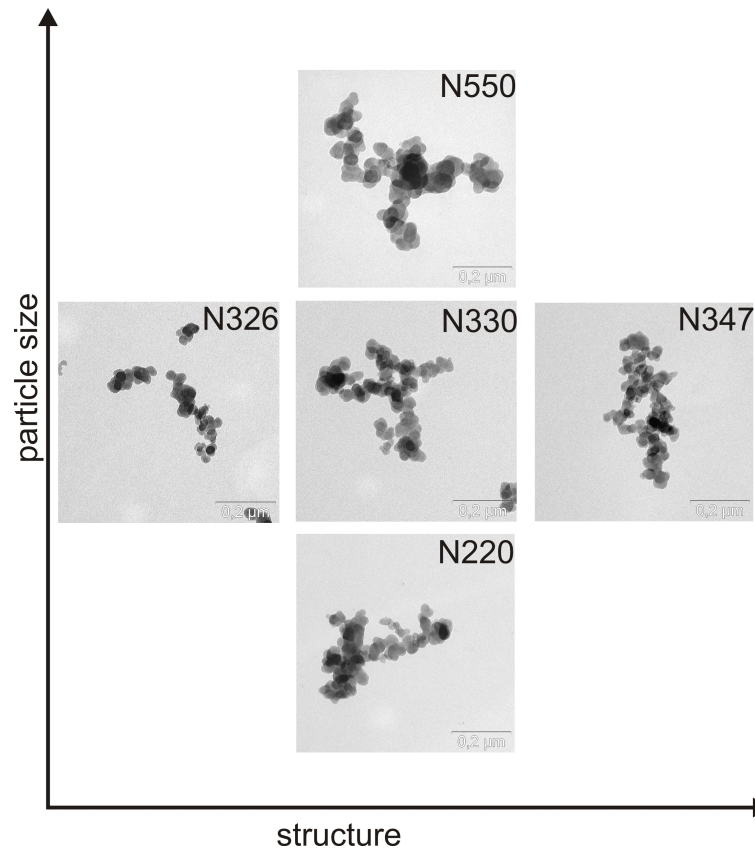


Figure 4.7: Carbon black as a function of particle size and structure - TEM

according to ASTM 4656/1 – 78¹. Thereby a certain amount of DBP is applied. Above a certain critical volume percent of DBP the flow properties of the carbon black change drastically ascribed to the formation of liquid bonds between the filler particles. The change of the flow characteristics above a critical DBP concentration is signaled in a mixer by the sudden increase of the torque. The critical volume of DBP correlated with the filler mass is termed DBP number.

Due to Van der Waals bonds that occur between primary aggregates, they combine with neighboring aggregates and form secondary aggregates and agglomerates. The latter grow to sizes of approximately 10 microns and are therefore accessible for microscopical evaluation.

Alongside the specific surface and the structure of the primary aggregates and agglomerates, the activity and the chemical structure of the carbon black surface are of great importance due to their decisive influence in the interactions with the polymeric matrix. A characterization of the activity and chemical structure of the carbon black surface is rather complex and subject of many current investigations. Carbon

¹ASTM 4656/1 – 78 Carbon black for use in the rubber industry-Determination of dibutylphthalate absorption number-Part I. Method using absorptometer.

blacks usually contain 90 – 99% elemental carbon with oxygen and hydrogen as other major constituents. Generally channel blacks contain the largest amount of oxygen, i.e. 3 – 8% and hydrogen (less than 1%) and the furnace blacks contain the smallest amounts of both hydrogen (0.2 – 0.4%) and oxygen (0.2 – 1.2%). Any sulfur present on the surface results from the feedstock and contents of 0.6% are common in furnace blacks while thermal blacks are virtually free of it. Functional groups likely to occur on the carbon black surface include phenol, carboxyl, quinone, lactone, ketone, lactole, pyrone, etc.

4.4.3 Silica

The importance of synthetic silicas in rubber technology has grown into importance with especially with the introduction of the silica tire technology. The breakthrough in the use of silica was attained with the introduction of the chemical treatment of its surface (the silanol groups) using a coupling agent termed Silan either during vulcanization or in another stage beforehand. This chemical link between silica and the rubber matrix induced a drastic increase of filler reinforcing properties and, subsequently, an improvement of the tire properties such as rolling resistance, wet grip properties and abrasion.

There exist two types of synthetic silicas, relevant for tires, e.g. fumed or pyrogenic silicas and precipitated silicas. The former offer the smallest particle size, therefore the highest degree of reinforcement.

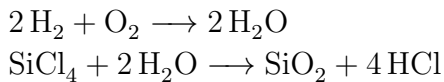
4.4.3.1 Pyrogenic Silica

This procedure was developed in the late 1930s and patented in 1942 by Degussa under the name Aerosil-Process. The idea was the production of white carbon black as reinforcing filler for the rubber industry.

The term pyrogenic silica refers to highly dispersed silicas formed from the gas phase at high temperature. Nowadays, the most important production process is flame hydrolysis¹. The electric-arc process is of little and the plasma process of no economic significance.

Silicon tetrachloride is the usual raw material for flame hydrolysis. It is continually vaporized, mixed with dry air and then with hydrogen, fed to a burner, and hydrolyzed. The gases leaving the reaction chamber contain all of the silica in the form of an aerosol. The properties of pyrogenic silica can be controlled by varying reaction parameters such as flame composition and flame temperature [149].

¹100,000 t worldwide in 1991



4.4.3.2 Precipitated Silica

Precipitated silicas have only been produced commercially since the 1940s but were quick to become the most important group of silica products on the basis of the amounts produced¹.

Figure 4.8 displays a TEM micrograph of silica 7000GR. Raw materials for the produc-

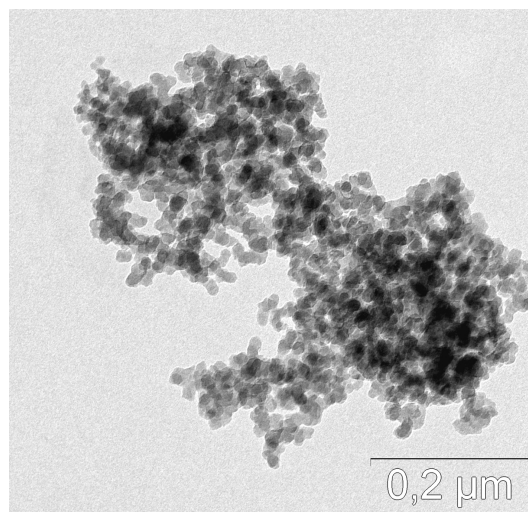
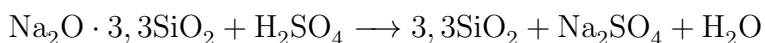


Figure 4.8: Silica 7000GR

tion of precipitated silicas are aqueous alkali metal silicate solutions (e.g., water glass) and acids, usually sulfuric acid. Precipitation with hydrochloric acid, organohalosilanes, carbon dioxide, or a combination of the latter with mineral acids are of minor economic importance. In the reaction of alkali metal silicate solution with mineral acid, the silica precipitates according to the following equation:



In contrast to silica gels, which are produced under acidic conditions, in this case precipitation is carried out in neutral or alkaline media. The properties of the precipitated silicas can be influenced by the design of the plant equipment and by varying the process parameters (i.e. pH, temperature, electrolyte concentration, reaction time). The production process consists of the following steps: precipitation, filtration, drying, grinding, and, in some cases, compacting and granulation.

¹1,100,000 t in 1999

The mean particle size of precipitated silicas is between 10 and 20 nm similar to that of carbon blacks. An interesting difference to carbon black is the property termed structure. Black structure can be regarded as the formation of branched or chained configurations during manufacture. These features are permanent, cannot be changed during mixing and are the basis for classifying blacks as low or high structured. Silica structure refers, in contrast, to the hydrogen bonding of individual particles to form clusters not chains. This structure can be easily modified or removed during mixing and by the use of additives. It is responsible for the stiff nature of some silica reinforced compounds [149].

Regarding the characterization of the specific surface and structure the same considerations are valid as related for carbon black. $N_2 - SA$ is used for the specific surface and the DBP number for the structure.

4.4.4 Layered silicates

Silicates one of the most interesting class of minerals. Approximately 30% of all minerals are silicates and geologists estimate that 90% of the Earth's crust is made up of silicates. The basic chemical unit of silicates is the SiO_4^{4-} tetrahedron with a negative charge (-4). They can form as single units, double units, chains, sheets, rings and framework structures.

The silicates are divided into the following subclasses, not by their chemistries, but by their structures:

- Nesosilicates (single tetrahedrons)
- Sorosilicates (double tetrahedrons)
- Inosilicates (single and double chains)
- Cyclosilicates (rings)
- Phyllosilicates (sheets)
- Tectosilicates (frameworks)

The layered silicates mostly belong to the phyllosilicate subclass. In this subclass, tetrahedrons are linked by shared oxygens to other tetrahedrons in a two dimensional plane that produces a sheet-like structure. The typical crystal habit of this subclass is flat, platy, book-like and display good basal cleavage. Some members of this subclass have the sheets rolled into tubes that produce fibers as in asbestos serpentine.

This phyllosilicate subclass contains the clay group. The Clay Group consists of four subgroups:

- Kaolinite
- Smectite
- Illite
- Chlorite

Of these, the most relevant for this work is the Smectite Group. This group is composed of several minerals including pyrophyllite, talc, vermiculite, saponite, hectorite (H), **bentonite**, nontronite, beidellite, volkonskoite, sepiolite (SP), stevensite, sauconite, sobockite, vinfordite, kenyaite and most importantly of them all **montmorillonite** (MMT). They differ mostly in chemical content. The general formula is $(\text{CaNaH})(\text{AlMgFeZn})_2(\text{SiAl})_4\text{O}_{10}(\text{OH})_2-x\text{H}_2\text{O}$, where x represents the variable amount of water that members of this group could contain. The structure of this group is composed of silicate layers sandwiching a gibbsite (or brucite) layer in between, in a silicate-gibbsite-silicate (s-g-s) stacking sequence. The variable amounts of water molecules would lie between the s-g-s sandwiches. Until now smectite group clays are the most used nanofillers in elastomers. MMT is the most common smectite clay [150].

In order to render MMT compatible with hydrophobic polymers, it is required to replace the alkali ions with ω -amino acid hydrochloride salt and organic surfactants such as alkylammonium and arylphosphonium ion. The surfactant provides a hydrophobic nature to the silicate surface and also increase the layer distance improving the compatibility with the polymer. This causes the layers to become organophilic and such clay is known as organoclay [151, 152]. In order to enable each layer to be coated with the surfactant the layers should be accessible for the surfactant molecules from the solution, and for this reason the clay layers need to swell to exfoliate in a solvent.

It may be pointed out that intercalation is based on ionic interactions and exothermic heats of mixing, whereas exfoliation is prompted by a mutual interaction of the hydrophobic groups of the surfactant with the hydrophobic polymer chains. This is essentially parallel to the compatibilization process in a polymer blend. Processing of nanoclay-based composites has been accomplished in three different modes [153]:

- Intercalation of difunctional monomers with interactive groups that are capable of exfoliating the clay layers followed by polymerizing a monomer in the exfoliated clay matrix
- Intercalation of a surfactant with a long hydrophobic chain that exfoliates the silicate galleries and helps the distribution of the filler in the polymer matrix
- In situ generation of nanofiller particles in a matrix that subsequently polymerizes to provide a nanocomposite

4.4.5 Carbon nanotubes

Another class of nanofiller, carbon nanotubes (CNT), is being widely used in plastic and rubber composites. Exceptional mechanical strength, combined with high electrical conductivity and corrosion resistance provides tremendous opportunities for their application in making high strength and highly conducting polymeric nanocomposites [153].

The production of nanotubes starts from an allotrope of carbon - graphite, the structure of which consists of graphene layers stacked along the c-axis in a staggered array [154]. When such a graphene sheet is rolled over, the cylindrical segment of a single wall carbon nanotube is obtained (see Figure 4.9). A single wall carbon nanotube is a hexagonal network of carbon atoms rolled up into a seamless, hollow cylinder, with each end capped with half of a fullerene molecule. Although similar in chemical composition to graphite, carbon nanotubes (CNT) are highly isotropic, and it is this topology that distinguishes them from other carbon structures and gives them their unique properties. There are many possibilities for rolling a slice of graphene into a seamless cylinder, because when rolled into a nanotube, the hexagons may spiral around the cylinder, giving rise to "chirality", a twist that determines whether the CNT behaves like a metal or a semiconductor. The diameter, chirality and form of the nanotube determine its properties. [155].

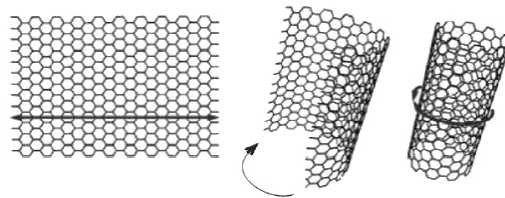


Figure 4.9: Rolling up of graphene sheet into a single wall carbon nanotube

The discovery of multi-walled carbon nanotubes produced by the arc evaporation of graphite in an atmosphere of helium by Iijima [156] has attracted scientific and technological interest worldwide.

Carbon nanotubes can be classified into single-walled nanotubes (SWNT), multi-walled nanotubes (MWNT) depending on the number of graphitic cylinders with which it is formed. SWNT with a diameter of 1 - 2 nm consists of a single graphene layer wrapped into a cylindrical shape, and hemispherical caps seal both ends of the tube. SWNT can be further divided into three classes, i.e. armchair, zigzag and chiral depending on the arrangement of hexagons in their structures.⁶¹ MWNT generally exist with diameters of 10 - 40 nm and length of a few micrometers. SWNT and MWNT can be synthesized by means of the arc discharge [157], laser ablation [158, 159] and chemical

vapor deposition (CVD) from hydrocarbons [160].

CNT prepared from the arc discharge, laser ablation and thermally activated CVD contain impurities like amorphous carbon, graphite particles and metal catalysts. Therefore, purification of CNT is needed prior to blending with polymers. CNT can be purified by oxidation, acid treatment or combined oxidation and acid treatment [161, 162].

Vapor grown carbon nanofibers (VGCF) are another important member of this class of carbon based nanofillers. They possess the graphitic structure similar to that of CNTs, with typical diameters of 50 – 200nm. The inner diameter is 30 – 90nm and the length is in the range of 50 – 100 μ m, so that the aspect ratios are in the 100 – 500 range.

4.4.6 Dispersion and distribution of fillers

The properties of rubber products are influenced decisively by the distribution of filler agglomerates in the polymer matrix. The importance of the mixing process is paramount in obtaining a homogeneous mixture of the filler and the polymer through distributive and dispersive mixing. Figure 4.10 displays a schematic view the two mixing types with the mention that in real conditions their influences occur in parallel and cannot be separated.

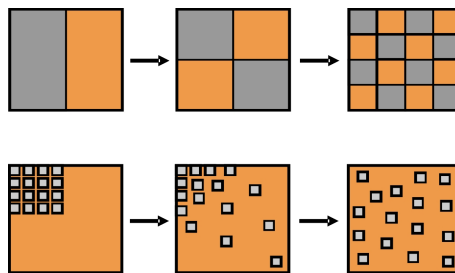


Figure 4.10: Distributive and dispersive mixing

The term dispersion is used, in this context, to describe the downsizing of filler agglomerates through the input of mechanical shearing forces to microscopical particles. This way the contact surface between the main components of the mix, polymer and filler, is increased up to a certain threshold.

The dispersion of filler agglomerates in the rubber matrix requires the fulfillment of certain energetic requirements. If the interactions between the filler and the polymer are stronger than those between the filler particles the conditions are created for a successful destruction and dispersion of the filler agglomerates. When the agglomerates have been downsized to small aggregates the interactions between the rubber chains and the filler particles are no longer enough to support a further dispersion increase, hence, continuing the mixing process would no longer bring any improvements of the

dispersion. The research conducted by Oppermann [163] into the morphology of carbon blacks in rubber systems has shown that even after long mixing times there is still a remnant of undispersed agglomerates in the mix.

Several methods exist for the dispersion state characterization like for example ASTM D 2663-87 or the later and more rapid method developed at the DIK Hannover called *Dispersion Index Analysis System - DIAS*. However accurate these methods, based on visible light microscopy, cannot give any information about the dispersion of particles smaller than this threshold. Other methods must be used such as electron microscope, small angle x-ray scattering (SAXS) or conductivity measurements.

The evaluation of the microdispersion using transmission electron microscopy (TEM) in the size range of aggregate structures is possible but very elaborate. The filler must be separated from the rubber using an adequate solvent and immersed in a solution in an ultrasound bath. Subsequently, a reasonably high amount of agglomerates are to be analyzed by TEM [145, 164, 165].

Another method for the characterization of the micro and macro dispersion is the measurement of the electrical conductivity using direct current as well as alternating current. In this case, the specific resistivity, ρ_d , or dielectric constant, ϵ_R , is a measure of the carbon black dispersion on a microscopic and macroscopic level. In case of a direct current measurement system, the electrical conductivity, k_{DC} consists of the specific resistivity, ρ_D measured by a simple resistivity check of a vulcanized sample of thickness h . The electrodes of surface A used to measure the resistivity R_D are built according to DIN 53482. The following relation applies:

$$k_{DC} = \frac{1}{\rho_D} = \frac{h}{R_D \cdot A} \quad (4.2)$$

For dielectric measurements the sample is introduced in a condenser and the frequency dependent real and imaginary components of the dielectric constant, ϵ_R , are measured. The electrical permittivity is then:

$$k_{AC} = \frac{1}{\rho} = \omega \epsilon_0 \epsilon'' \quad (4.3)$$

Such measurements cannot be applied to silica filled compounds due to their reduced conductivity.

4.5 Vulcanization of elastomers

Rubber products are characterized by high resilience following mechanical deformation: the original dimension is restored almost immediately after the load has been removed. This rubber elasticity results from a three dimensional network structure of long-chain rubber molecules that are bonded to one another at crosslinking points (crosslinks) - see Figure 4.11. Vulcanization is the chemical process by which these crosslinks between polymer chains are formed. The viscous raw rubber, characterized by irreversible Newtonian flow, is converted into an elastomer.

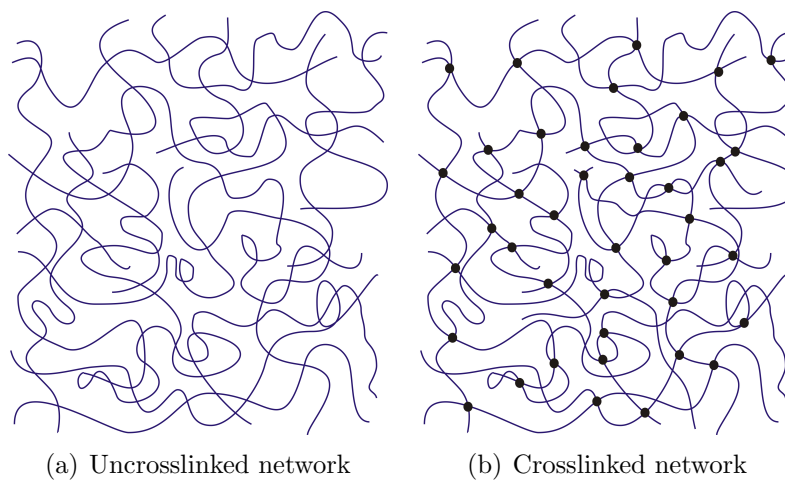


Figure 4.11: Unvulcanized and vulcanized elastomers - schematic display

Sulfur and peroxides are used mainly as curing agents; Peroxides are the most important crosslinking agents for rubber containing few or no double bonds in the chain. Examples are silicone rubber, EPDM, ethylene – vinyl acetate copolymers (EVM), and hydrogenated acrylonitrile – butadiene copolymers (HNBR). To a small extent, special crosslinking agents¹ may be employed.

The restoring force after deformation is a function of the number of network-forming polymer chains per unit volume. Increasing the number of crosslinks distributes tension over more polymer chains and thus increases the restoring force [13].

The vulcanization process can be monitored continuously by using vulcameters. The crosslinkable rubber compound is subjected to periodic deformation in a reaction chamber at a given temperature, and at the same time the force or torque necessary to produce deformation is monitored. Important industrial parameters can be determined from a plot of the crosslinking or curing isotherm as a function of reaction time (see Figure 4.12).

¹For example quinones, dioximes, polymethylolphenol resins, zinc and magnesium oxides

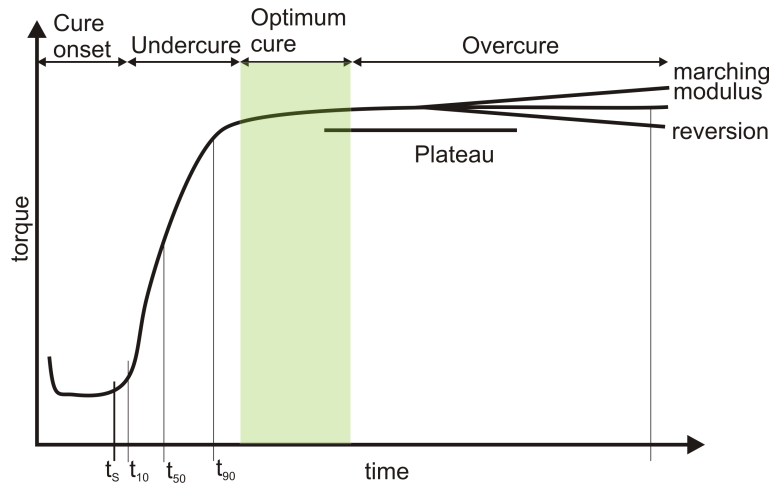


Figure 4.12: Vulcameter curve

The scorch time t_s (time taken to reach a given increase of the torque above the minimum torque) defines the beginning of the crosslinking reaction (onset of cure the end of the induction time) and gives information on the flow time and processibility of the compound at a given temperature. The minimum torque observed correlates with the compound viscosity.

Depending on the vulcanization agents chosen, the start of the crosslinking reaction can be adjusted to be rapid or delayed. For curing in molds (e.g., in tire production) a longer flow period is necessary for the rubber compound before vulcanization starts, so that the compound can fill all the cavities in the mold perfectly and trapped air can be released, hence, for the measurements carried out in this work a time $T_{90} + 1$ minute for every millimeter of thickness was calculated. In other vulcanization processes, as in steam curing or ultrahigh-frequency (UHF) vulcanization, a rapid start is desired, so that the onset of crosslinking prevents deformation of articles through the flow processes.

Too rapid an onset of cure (or scorching) is undesirable in most cases because the processing safety in compounding and molding is impaired. Scorched compounds can no longer be perfectly extruded or calendered. The steepness of the crosslinking isotherm is a measure of the rate of the crosslinking reaction. Rate constants can be calculated from the reaction times and the corresponding torque. Generally, a very rapid cure rate is preferred. In the region of optimum cure the maximum crosslink density is achieved. The ideal graph of a cross-linking isotherm is a right-angled step function. The final torque achieved is a measure of the crosslink density and often correlates with stress values (force per initial cross section required to produce a specific elongation) obtained from static stress-strain tests [166]. In the over cure region the vulcameter torque can be constant, can increase (marching modulus), or for certain rubbers (e.g.,

natural rubber and polyisoprene) can decrease (reversion) [167].

Individual physical properties reach their optimum at different vulcanization times. For example, elasticity and compression set values are optimal in the region of slight over cure, whereas tear resistance shows maximum values at slight under cure.

One of the most important factors which characterizes a network structure is the network chain density, v_e . Two techniques to estimate v_e involve the measurement of the degree of equilibrium swelling for a sample swollen in a good solvent and the estimation from the value of the plateau modulus.

All synthetic rubbers, as well as natural rubber are formed from long, flexible chain-like molecules, vulcanized to form a three dimensional network. A typical rubber of good properties contains about one crosslink to every few hundred chain atoms [168]. Even though the chemical crosslinks are the ones holding the polymer from flowing at high temperatures, it is recognized that transient crosslinks can also be formed, for example by entanglements, tiny crystallites or by strong secondary valences. If one supposes that the network was produced from infinite linear molecules by the addition of c moles of tetrafunctional vulcanizing agent per cubic centimeter of rubber than each crosslink will yield four network chains but each of these chains belongs to two crosslinks. Hence there are $2c$ moles of network chains per cubic centimeter in the crosslinked network.

$$2c = v_e = \frac{\rho}{M_c} \quad (4.4)$$

where:

- M_c - average molecular weight of the network chains
- ρ - density of the rubber
- v_e - network chain density

If the linear molecular chains before vulcanization are of finite average molecular weight the network produced by c moles of crosslinking agent per cubic centimeter of rubber will contain some terminal network chains which are ineffective in supporting stress.

After a prolonged period of time, the storage modulus (G') of a network converges towards a constant value, namely the plateau modulus while the loss modulus (G'') tends towards zero. The plateau modulus is a measure of the crosslink density and consists of two parts:

$$G_P = G_x + G_e \quad (4.5)$$

G_x characterizes the density of the bonds between chain segments that have been generated by chemical or radiation crosslinking and remain stable over time in a macroscopic network. G_e is proportional to the share of entanglements fixed by the chemical vul-

canization. Since reptation of polymer chains is impeded by the mechanically stable bonds between chain segments that form during crosslinking, entanglements can no longer come undone. They thus increase the number of crosslinks that are stable over time and lead to a plateau modulus that is increased by G_e [9].

The connection between the plateau modulus and crosslinking density is given by the formula:

$$G = 2cRT \quad (4.6)$$

The value of v_e for rubber vulcanizates can be calculated by the conventional Flory-Rehner equation [169–171] using equilibrium swelling data, since at equilibrium the chemical forces tending to dissolve the rubber in a liquid are balanced by restraining forces exerted by the rubber network.

$$v_e = \frac{\ln(1 - \phi_2) + \phi_2 + 0,4\phi_2^2}{V_0 \left(\phi_2^{\frac{1}{3}} - \frac{1}{2}\phi_2 \right)} \quad \text{and} \quad \phi_2 = \frac{m_{rubber}}{\rho_{solvent} \cdot m_{solvent} + m_{rubber}} \quad (4.7)$$

In equation 4.7 Flory assumes an affine deformation of the elastic network during swelling. The swelling process is expected to take place until the network is fully stretched, therefore, compared to the crosslinking density estimated by the plateau modulus, it is expected that this yields smaller values since it does not retain any influence of physical crosslinking [172].

5

Results and Discussion

The ongoing demand for sustainable development of new materials requires optimization of the functional and mechanical properties of multi-component systems such as polymers, blends and composites based on improvements of the morphology, interfacial adhesion and dispersion of particulate fillers. This calls for a deeper understanding of the effect that dynamic excitations in a wide range of frequencies exert on the bulk as well as the shear properties of the materials' constituents especially for such ones made by elastic and rigid components. Besides dynamic excitations at low frequencies, of a practical and scientific interest are low amplitude deformations at high frequent oscillations. For the investigation of dynamic-mechanical properties of low frequencies well established methods are available, which are described in chapter 3.2. However, the properties in the high frequency regime cannot be measured directly by commercial machinery. The mechanical properties of polymeric materials generally depend on time, i.e., on whether they are deformed rapidly or slowly. The time dependence is often remarkably large. The complete description of the mechanical properties of a polymeric material commonly requires that they be traced through several decades of time. The class of polymeric materials referred to as thermorheologically simple allows, in a theoretical approach, the use of the superposition of the effects of time and temperature in such materials as a convenient means for extending the experimental time scale [173]. One has to apply the time-temperature superposition principle and the WLF equation to harvest information concerning the high frequency regime. This requires the development of precise methods of investigation which expand the low frequency dynamic-mechanical testing methods and theoretical approximations used to extrapolate the viscoelastic properties to a broad frequency range. Such a methodological development can provide the necessary estimation of material properties in the high frequency regime which is crucial for many technical applications of rubber parts. For this reason an in house made ultrasonic spectrometer was built and further developed. The potential of the method was demonstrated for a group of homopolymers

and copolymers as well as blends and filled composites of these raw materials. The objective was to investigate and understand the effects different chain structures have on the dynamic mechanical properties in the high frequency regime in comparison to the low frequency regime.

The investigations reported in this work were carried out in a temperature range which covered the main transition of the tested materials enabled the characterization of the rubbery region. The frequency influence was characterized isochronally at 0.5 MHz using the Ultrasonic Spectrometer (US) prototype and at low frequency (and, using the time-temperature superposition temperature, on a broad temperature and frequency range) using the Dynamic-Mechanical Analyzer (DMA). The correlation that arise from using different methods to characterize the stored and the dissipated energy (ultrasound velocity, storage modulus and ultrasound attenuation and loss modulus, respectively) are discussed in terms of structural characteristics of polymers, processing parameters, blending and filler loading. The correlation of the glass transition temperature at different frequencies with the aforementioned parameters is also discussed.

The direct and practical approach involves the use of US to investigate dynamic mechanical properties at high frequencies. The immediate advantage of this method is the intrinsic ability to use it also for thermorheologically complex materials such as filled composites and polymer blends.

5.1 Method development

5.1.1 Apparatus and procedure

The measuring principle of the method used is based on wave transmission. Ultrasonic waves, emitted by an ultrasonic transducer, are propagated through a sample surrounded by a coupling medium and are received on the opposite side of the measuring system by an identical transducer. The characteristic features of the samples imply that a certain amount of the energy carried by the ultrasonic wave will be attenuated during the passage. However, attenuation consists of two components: reflection¹ and damping. The latter refers to the energy dissipated within the sample as heat, which is an important material dependent characteristic.

The apparatus used herein is a prototype based on a device proposed by Gerspacher et al. [174]. A schematic display can be seen in Figure 5.1.

The system uses two similar ultrasonic transducers located opposite from one another

¹Here the term reflection is used to cover all phenomena that imply energy loss by other means than absorption in the sample, i.e. refraction, diffraction, scattering.

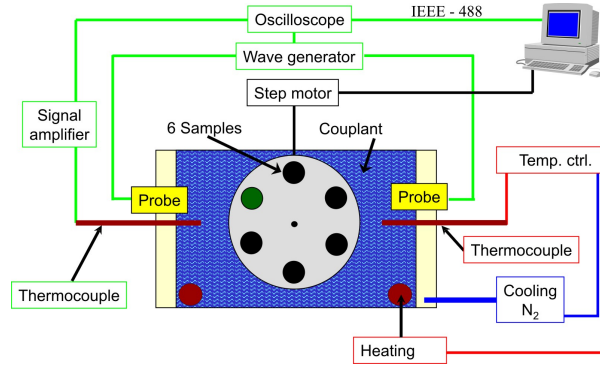


Figure 5.1: Ultrasonic spectrometer - schematic display

at approximately 30 cm. The distance between the transducers can be varied $\pm 10\text{cm}$. They are equipped with a special steel membrane to cope with the coupling fluid.

Between the transducers a sample holder wheel provides room for six samples of the same material. One place is left empty and the other five are occupied by samples of different thickness, from five to thirteen centimeters. The minimum size is related to the approximations mentioned in the theoretical chapter 3.2.2 i.e. the wavelength must be small compared to sample thickness. The different thicknesses are required in order to minimize measurement errors. The sample holder is driven on a revolver principle by a step motor controlled by the computer software which is responsible for the measurement as well.

The ultrasonic (square wave) 400 V pulse is emitted by a 5077PR impulse generator manufactured by Panametrics. The pulse causes the piezoelectric material in the transducer to oscillate sending a sound wave through the sample. The mechanical wave passes through the couplant and the sample and is subsequently converted back into an electrical impulse by the receiving transducer. The analogue electrical signal is amplified and converted into digital format by a digital oscilloscope from Tektronix with a bandwidth of 300 MHz.

Most applications where ultrasound is used require the presence of a coupling medium, as mentioned earlier in section 3.2.2. This is usually a fluid which is supposed to reduce the impedance mismatch between the sample to be measured and the space between it and the ultrasonic transducer, i.e. reduce the reflection coefficient at the boundary (see Equation 3.76). For most measurements presented in this thesis the coupling medium used was 1-propanol. Due to its melting temperature of -126°C and boiling temperature of 97°C it confers a broad window in which measurements can be carried out, without having to change the medium.

5.1.2 Requirements

A typical feature of the ultrasonic transducers is the fact that the sound wave originates from a number of points along the transducer face therefore the ultrasound intensity along the beam is affected by constructive and destructive wave interference. These are sometimes also referred to as diffraction effects. This wave interference leads to extensive fluctuations in the sound intensity near the source and is known as the near field [175]. Because of acoustic variations within a near field, it can be extremely difficult to accurately evaluate material properties when they are positioned within this area.

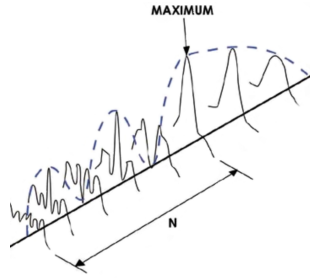


Figure 5.2: Path of sound beam

At a given distance the pressure waves combine to form a relatively uniform front at the end of the near field. The area beyond the near field where the ultrasonic beam is more uniform is called the far field. In the far field, the beam spreads out in a pattern originating from the center of the transducer. The transition between the near field and the far field occurs at a distance, N_0 , and is sometimes referred to as the "natural focus" of a flat (or unfocused) transducer. The near/far field distance, N_0 , is significant because amplitude variations that characterize the near field change to a smoothly declining amplitude at this point. The area just beyond the near field is where the sound wave is well behaved and at its maximum strength. Therefore, optimal results will be obtained when the sample is located in this area.

The distance to the far field is calculated with the following formula:

$$N_0 = \frac{D^2 f}{4c} = \frac{D^2}{4\lambda} \quad (5.1)$$

where N_0 is the length of the near field, D is the diameter of the emitting transducer and λ is the wavelength.

For the 0.5 MHz transducers which were employed in this research the values for N_0 was 4cm. Since the sample holder is placed 5 cm from the ultrasonic transducer the far field approximation is justified.

In the far field the waves originating on the transducer surface can be seen as parallel. For a spherical wave emitting transducer the integral over the emitting surface, according to far field approximations, is solved analytically into:

$$\frac{P}{P_0}(\gamma) = \frac{2J_1\left(\frac{\pi}{\lambda}D\sin\gamma\right)}{\frac{\pi}{\lambda}D\sin\gamma} \quad (5.2)$$

where J_1 is a Bessel function of the first kind [176, 177], γ is the reception angle, P_0 is the pressure maximum that occurs on the transducer axis which decreases inversely proportional to the distance z (spheric wave characteristic trait).

The chosen transducers' diameter - wavelength combination leads to a strong grouping, bundling of the sound field where the smaller wavelengths are more bundled. The proportion of shear to longitudinal pressure components, related to the pressure maximum P_0 on the transducer axis is given by:

$$\frac{r_p}{r_s} \frac{P}{P_0}(\gamma) = \tan\left(\frac{\gamma\pi}{180}\right) \frac{P}{P_0}(\gamma) \quad (5.3)$$

From here it can be concluded that for the frequency range in use, the longitudinal components clearly dominate at the contact with the sample surface and the shear components can be neglected.

5.1.3 Data treatment

The received signal is a pulse in the time domain (blue signal in Figure 5.3). Its characteristic maximum is used in the calculation of the sound velocity. In some cases the signal shows two positive peaks with amplitudes very close to one another and a minimum. In such cases the software is programmed to look for the time where the minimum appears. These issues are usually material dependent.

In order to estimate the ultrasonic attenuation the ultrasonic signal is transformed from the time domain into the frequency domain by means of Fourier transform [178–182].

The Fourier transform of the blue signal in Figure 5.3 shows a maximum at the frequency of the ultrasonic transducer, i.e. 0.5 MHz. Consequently, an integration of an area left and right of this frequency gives the intensity of the received wave.

For each pulse the software records and analyses an oscillogram or amplitude scan (blue signal in Figure 5.3) which contains all the information necessary for the determination of sound attenuation and velocity. At the end of the measurement, the data is exported into an ASCII type file which is accessible to most spreadsheet programs.

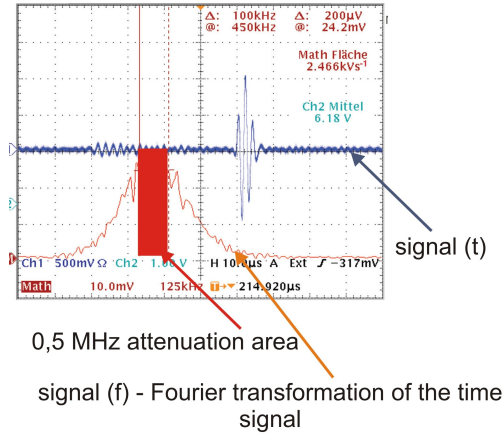


Figure 5.3: Measured signal and Fourier transform

5.1.4 Determination of the longitudinal wave attenuation, velocity and modulus

In order to determine the frequency dependent attenuation coefficients of the polymers, α_{rubber} , at a certain frequency, an analysis of the Fourier transformation over a $\pm 10\%$ range is evaluated (see Figure 5.3) and leads to a two sided spectrum in complex form that is normally considered symmetrical and only its positive half is displayed, the negative is considered redundant.

The temperature dependent signal intensities of the different samples (of different thickness) are proportional with the transmitted longitudinal pressures:

$$P_i(T) = P_0 \exp[-(\alpha_{rubber}(T) d_i + \alpha_{coupl}(T)(d - d_i))] \quad \text{where } i = 1, \dots, 6 \quad (5.4)$$

In Eq. 5.4 d represents the distance between the emitting and the receiving transducer whereas α_{rubber} and α_{coupl} the attenuation in the polymer and in the couplant, respectively. P_0 is a constant that contains any reflection effects at different interfaces.

However, ascribed to the similar surface of the samples and to the bundling (focusing) of the ultrasonic signal, the signal modifications that occur when passing from one medium to the other are eliminated when samples of different thicknesses are measured. Modifying Eq. 5.4 it follows:

$$\alpha_{rubber} = -\frac{\ln P_i - \ln P_j}{d_i - d_j}, \quad \text{where } i \neq j \quad (5.5)$$

If the intensity decrease of a wave passing through a sample is considered, equation 5.5

can be written as:

$$\alpha(f_0, T) = -\frac{\ln I_i^{f_0}(T) - \ln I_j^{f_0}(T)}{d_i - d_j} \quad (5.6)$$

$I_i^{f_0}$ represents the intensity as function of frequency that occurs when passing through a sample of thickness d_i . The value $\alpha(f_0, T)$ is the frequency and temperature dependent attenuation factor that is determined from a linear regression of several isothermal measurements. The temperature ramp was set at a temperature increase of 0.3 K/min so that enough time is given to reach the temperature equilibrium and for the wheel to bring each sample into measuring position. This way the best compromise is achieved between thermodynamic equilibrium and the practical necessity of constant temperature increase.

One of the main issues in estimating the high frequency dynamical properties using longitudinal ultrasonic waves is represented by the correct measurement of the wave velocity in the polymer. The speed at which a longitudinal wave propagates is a direct indication of the energy stored by the compound, therefore it is directly proportional to the storage modulus of the ultrasonic wave, M' .

The velocity of the ultrasonic waves is calculated from the time differences, Δt , that occur during the passage through the samples of different thickness, Δd . Knowing the wave velocity in the couplant¹, $c_{couplant}$, the velocity in rubber is:

$$c_{rubber}(T) = \frac{\Delta d}{\Delta t + \frac{\Delta d}{c_{couplant}(T)}} \quad (5.7)$$

Δt is quantified from the position of the maximum (or minimum) of the measured signal (blue in Figure 5.3). The calculation over all times is conducted via a linear regression of the function $1/c_{rubber}(T)$.

The wave velocity in the couplant is estimated during the measurement from the reference time through the empty sample holder, in function of the velocity through the couplant at 23°C. This method, in comparison to using a reference measurement of the couplant for all materials and adjusting the values through interpolation, has the advantage of taking into account any changes that might occur in the medium, from water intake to plasticizer extraction.

The determination of the ultrasonic attenuation and velocity enables one to calculate the components of the complex longitudinal wave modulus based on the wave equation of motion for harmonic oscillations as described also in section 3.2.2.

The decay of the oscillation amplitude is described by an exponential factor, $e^{-\alpha x}$,

¹i.e. 1 – *propanol*

to express the rate at which the amplitude in the material is reduced. The term α is measured directly from the rate of the emitted wave amplitude to the received amplitude after passing through the sample, see Eq. 5.6. The wave equation for viscoelastic materials becomes:

$$y = a (\sin (\omega t - kx) + i \cos (\omega t - kx)) e^{-\alpha x} \quad (5.8)$$

By substituting in Eq. 3.65, evaluating the terms M' and M'' it is possible to form two simultaneous equations which can then be solved by real and imaginary parts depending on the four measured parameters ρ , c , α and ω .

$$M' = \rho c^2 \frac{1 - \beta^2}{(1 + \beta)^2} \quad (5.9)$$

$$M' = \rho c^2 \quad \text{when} \quad \beta \ll 1 \quad (5.10)$$

$$M'' = \rho c^2 \frac{\beta}{(1 + \beta)^2} \quad (5.11)$$

$$M'' = \frac{\rho c^3 \alpha}{\omega} \quad \text{when} \quad \beta \ll 1 \quad (5.12)$$

where $\beta = \frac{\alpha c}{\omega}$.

5.1.5 Error sources in ultrasonic measurements

As any device that measures material properties, the ultrasonic spectrometer presented here is prone to error sources which have to be taken into account when evaluating the results. An assessment of these deviations is relevant for proving the viability of the method.

The reproducibility measurements were performed on the same samples using the same type of coupling fluid on different days with several other measurements performed in between. It should be noted that during one measurement the alcohol used extracts several chemicals from the samples. To avoid any interferences from these extractables the couplant is changed before each measurement. Results are given in Table 5.1.

To assess the couplant influence on the measurements performed in this work a model mixture was prepared and its attenuation coefficient was measured using different coupling fluids (see Table 5.2). The alcohols were proven to be by far the most suitable ascribed to them showing relatively constant properties through the required temperature range. A fluorinated hydrocarbon was also tried and the resulted attenuation coefficient is in the same range as the alcohols, however this fluid changes its viscosity to such an extent that over 40°C it flows right out of the measuring chamber. Fur-

Table 5.1: Measurement reproducibility.

<i>day</i>	<i>alpha</i>			
	-35°C	-15°C	+10°C	+25°C
0	0.0148	0.0182	0.0640	0.0756
15	0.0111	0.0191	0.0660	0.0806
30	0.0315	0.0210	0.0681	0.0780
σ_{\pm}	0.0108	0.0014	0.0020	0.0025

thermore, as it is insoluble in most solvents it is very difficult to clean. Water was also used but only for this test, as the low temperatures are not available.

Table 5.2: Influence of the couplant.

<i>fluid</i>	<i>alpha</i>			
	-35°C	-15°C	+10°C	+25°C
ethanol	0.0280	0.0636	0.0157	0.0077
propanol	0.0273	0.0640	0.0156	0.0085
butanol	0.0267	0.0643	0.0157	0.0076
pentanol	0.0282	0.0639	0.0163	0.0079
<i>FC</i> – 40	0.0292	0.0640	0.0158	0.0081
water	N. A.	N. A.	0.0160	0.0078
σ_{\pm}	0.0009	0.0003	0.0003	0.0003

The determination of the ultrasonic velocity, c , involves the measuring of the time of flight (TOF), i.e. the time a wave needs to travel from the emitting to the receiving transducer. In order to compensate for the presence of the coupling fluid it is necessary to measure beforehand the sound velocity in it.

The measurement of the time of flight is performed by the LabView software directly on the received signal. The time at which the highest peak occurs in Figure 5.3 is usually taken as the travel time between the two transducers. The intensity of the signal is strongly influenced by the temperature, i.e. at very low temperature the intensity is reduced and it is possible that the highest peak shifts either to the right or to the left which gives erroneous time measurements (see Figure 5.4(a)). As it can be deduced from the later development of the time curve, these points can be discarded. This is performed either by removing each point by hand and, subsequently interpolating between the remaining or by using a program written in LabView, as part of this work, which performs these operations automatically. The result is shown in Figure 5.4(b).

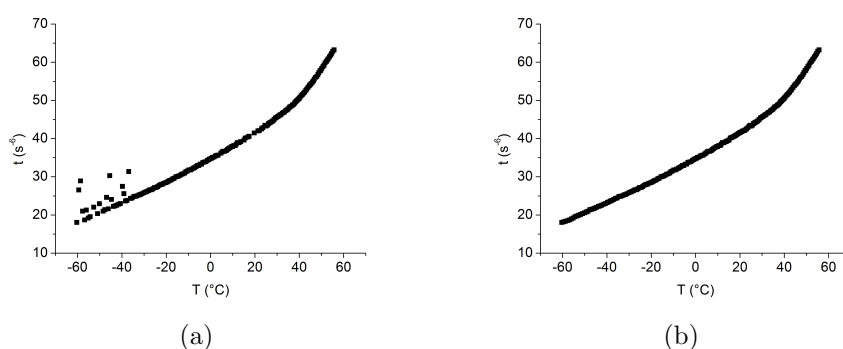


Figure 5.4: Time of flight measurements
 (a) - before correction
 (b) - after correction

5.2 Investigation of homopolymers

The elastic properties of rubber compounds are primarily determined by the structure of the macromolecules, the degree of crosslinking, the content of plasticizer and finally the type and loading of the filler. The comparison of low and high frequency dynamic properties starts with a selection of representative homopolymers. They are characterized by low glass transition temperatures, high chain mobility and specific technological relevance. The location of the glass transition temperature is related to the structure of the repeating units, i.e. to the amount of energy required for one bond to rotate in respect to its neighbor.

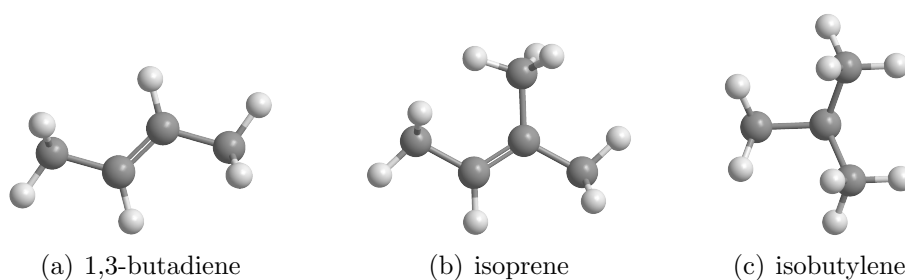


Figure 5.5: Monomer units of BR, NR and IIR.

Figure 5.5 displays the monomers used as structural basis for the homopolymers BR, NR and IIR. The methyl side groups in NR and IIR are clearly distinguishable. Their presence is responsible for a reduced chain mobility and the broadness of the glass transition regime.

Polybutadiene is composed of a sequence of cis/trans-1,4-butadiene units with a very low chain cross-section (19 \AA) which provides a highly mobile chain and a very low

T_g of -100°C due to the lack of side groups. If the polymer has a high cis or trans content it will form crystallites upon cooling due to the regularity of the macromolecular backbone.

The only naturally occurring polyisoprene is characterized by a very high molecular weight. The presence of methyl side groups in its chain set its T_g at -58°C . Natural rubber is an unsaturated aliphatic hydrocarbon of a very regular structure which enable it to crystallize under certain thermal conditions as well as under stretching.

Butyl rubber (IIR) is tested in comparison to the two above due to the unusually broad glass-to-rubber transition. Its T_g places it below NR ascribed to the symmetry of the CH_3 groups in polyisobutylene but the entire glass transition extends over a broad range of temperature.

The strongest dissipation peak of the three homopolymers, quantified by the height of the attenuation and shown by the natural rubber, can be traced back to the molecular weight difference between the three rubbers. The Rouse theory that connects energy dissipation to molecular weight and relaxation times of polymer chains [48] does not apply, strictly speaking, to the glass transition region so other influences should also be considered.

The polymers are characterized in Table 5.3¹. Their commercial description can be found in Table 7.2. The difference in their structure is characterized by the presence

Table 5.3: Homopolymers' characterization.

Polymer	Abbr.				$T_g(^\circ\text{C})$
Polybutadiene	BR	cis-1,4 > 96%	trans-1,2 2%	vinyl < 1%	-100
Poly(isobutylene-co-isoprene)	IIR	2-methyl-propene 97%	2-methyl-1,3-butadiene 3%		-62
Natural rubber	NR	cis-1,4-polyisoprene			-58

of methyl side groups, every third carbon atom on the main chain of NR and every second carbon atom on the main chain of IIR, respectively. The resulting effects on energy dissipation and chain mobility are characterized in the following in the low and high frequency domains by comparison to BR.

Ultrasonic attenuation and loss shear modulus values were used to characterize the energy dissipation at the respective frequencies. The three homopolymers, BR1, NR2 and IIR, had similar backbone but the latter two had different amounts of pendant

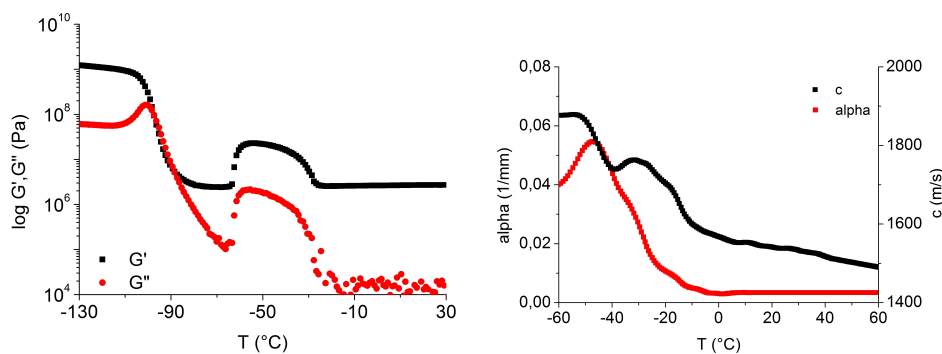
¹The glass transition temperatures (T_g) correspond to the location of the shear modulus maximum on the temperature axis as detected in a 1Hz DMA measurement.

methyl groups. The measurements show that butyl rubber has the highest energy dissipation of the three followed by NR and the highly mobile BR.

5.2.1 Butadiene Rubber (BR)

The shear modulus components displayed in Figure 5.6(a) for butadiene rubber demonstrate a low glass transition temperature defined at the maximum of the loss modulus or the inflection of the $G'(T)$ curve. This polymer shows one of the lowest T_g values in the field of polymeric materials. The storage modulus characterizes the energy elastically stored by the polymer chains and it shows a drop when passing from the glass into the rubbery state. At -60°C the storage modulus increases suddenly from 0.1 MPa to 3 MPa indicating the presence of an internal reinforcing mechanism. Around -20°C the storage modulus drops to a level characteristic of the rubbery plateau. This intermediate process is also shown in the curve of the loss modulus as a characteristic peak. The origin of this peak will be discussed in some detail below.

The evolution of α and c as a function of temperature demonstrates the same phenomena but in a specific manner.



(a) Components of the complex shear modulus for BR1 at 1 Hz. (b) Ultrasonic attenuation and velocity for BR1 at 0.5 MHz.

Figure 5.6: Dynamic mechanical characterization of BR1 at 1 Hz and at 0.5 MHz

The maximum of the ultrasonic attenuation is reached at ca. -50°C thus the T_g of BR1 is shifted by ca. 50°C when the test frequency is increased from 1 Hz to 0.5 MHz. This is considerably more than what is assumed when extrapolating via the WLF equation. The inflection point in the $c(T)$ occurs at the same point as the maximum of the attenuation coefficient. More relevant than the shoulder in the $\alpha(T)$ curve, the sound velocity shows a pronounced maximum which indicates that the intermediate process corresponds to a more compact material with higher density. Both the ultrasonic attenuation and the velocity display this secondary process which extends to -10°C . As its location appears to be in a similar range as the process noticed at 1 Hz, a DSC

measurement is performed on the BR1 sample to obtain additional information about thermal processes at temperatures above the glass transition process of this material.

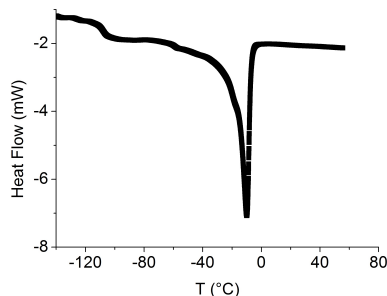


Figure 5.7: DSC scan of BR1 at $10^{\circ}\text{C}/\text{min}$ heating rate.

The thermogram of a dynamic DSC scan for BR1 is shown in Figure 5.7. The glass transition is located at -100°C . An endothermic peak localized between -80°C and -60°C indicates a reorganization of the material and the formation of a supramolecular structure i.e. cold crystallization. The proof of this is the appearance of a pronounced melting peak at -10°C (the melting enthalpy is $\Delta H = 25 \text{ J/g}$). Therefore it can be concluded that the increase in the mechanical moduli and the second maximum in c or the shoulder in α above T_g is related to the mechanical response of the crystallites formed. The most interesting fact is that by ultrasonic spectroscopy this phenomenon can be resolved.

The occurrence of crystallinity in polymers depends on the regularity of structure of the main chain. Several types of polybutadiene rubbers are known to crystallize and this phenomenon could pose difficulties to the dynamic mechanical ultrasonic measurements if their size grows over the Rayleigh scattering limit. Furthermore, such polymers are most of the times of a thermorheologically complex nature so their behavior cannot be easily evaluated at high frequency using the time-temperature superposition principle.

The significantly low value of the maximum damping, shown by the BR sample in Figure 5.6(b) can be ascribed to effects of the crystalline phase. The increase in frequency determines a shift of the glass transition temperature from approximately -100°C at 1Hz to -50°C which causes the glass transition to superimpose over the melting region of the crystallites. But as the crystallites are elastic bodies, they store a part of the energy therefore the recorded attenuation is reduced.

Crystallites are formed during the cooling process and the recrystallization stage. Typically they are composed by folded lamellae which form spherulites. The formation of spherulites is initiated at independent nuclei and then extends outwards to form spherical semi-crystalline arrays [183–185]. In absence of a thermal gradient, growth of the lamellae occurs radially, in all directions resulting in spherical aggregates (Figure 5.8).

The largest surfaces of the lamellae are terminated by molecular bends and kinks, and growth in this direction results in disordered regions. Therefore, spherulites have semi-crystalline structure where highly ordered lamellae plates are interrupted by amorphous regions. The growth rate of the spherulites, which determines their final size, has been connected by several authors [43, 186, 187] to the mobility of the chain. A high degree of branching or a large amount of side groups determine an increase of the reptation time which in turn reduces the growth rate.

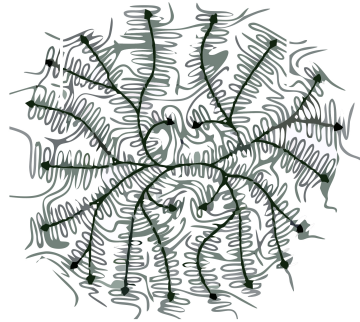


Figure 5.8: Schematic model of a spherulite.
Black arrows indicate the direction of molecular alignment.

The occurrence of spherulites in BR has been reviewed by Magill [188] and Cheng [185]. The latter investigated three BRs with different levels of long chain branching and noticed that the size of the formed spherulites depended also on the cooling rate. His results show spherulites of approximately $50\mu m$ for a BR with low branching and below $10\mu m$ for branched BR.

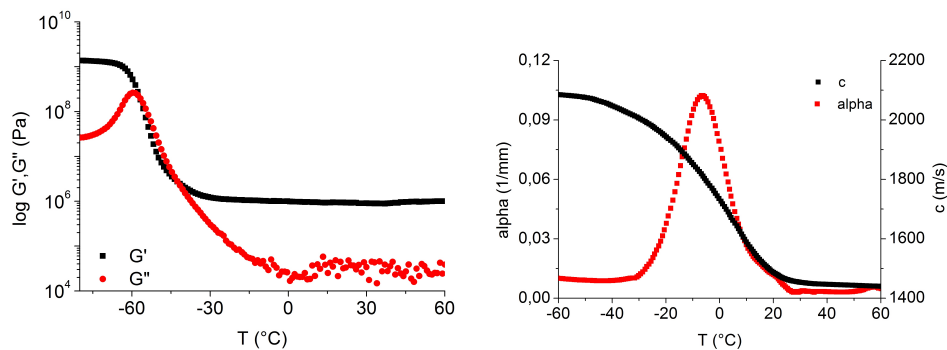
Connecting these findings to the results presented herein (Figure 5.11(d)), one can assume the size of the crystallites did not exceed $20\mu m$. If they were larger scattering of the ultrasonic wave would cause unusually high attenuation values which is not the case. A demonstration of the scattering effects is showed in section 5.9.

Furthermore, rubbers that are known to crystallize should be treated with caution when investigating properties characterized by ultrasonic wave transmission. If the size of the crystallites exceeds the Rayleigh scattering limit, the results of the attenuation cannot be interpreted in terms of energy dissipation by the polymer matrix.

5.2.2 Natural Rubber (NR)

The NR selected for this investigation is an amorphous polymer that does not exhibit thermodynamic first order processes. The behavior illustrated in Figure 5.9 is typical of an elastomer subjected to a periodic oscillation using different frequencies.

The temperature dependent energy dissipation is characterized by the red curve in both sub figures. At 1 Hz a maximum is noticed at -58°C which is associated with the glass transition temperature at this frequency. The entire glass transition process covers a wider temperature range compared to BR. Upon entering in the rubbery region the dissipation curve displays a certain noise which is a systematically occurring error of the measuring apparatus. These problems are caused by the very low values of the shear modulus above T_g which are close to the resolution threshold of the force transducer.



(a) Components of the complex shear modulus for NR2 at 1 Hz. (b) Ultrasonic attenuation and velocity for NR2 at 0.5 MHz.

Figure 5.9: Dynamic mechanical characterization of NR2 at 1 Hz and at 0.5 MHz

Correspondingly, the energy dissipation curve demonstrates a maximum around -6°C at 0.5MHz, which is located at a significantly higher temperature than the one for G'' . With 50°C the T_g shift demonstrated by NR is in the same range as the one shown by BR (55°C). The glass transition process covers a range of 60°C which is close to that observed at low frequencies.

As far as the temperature dependence of the storage modulus and the sound velocity is concerned, a narrower glass transition is observed for G' whereas c demonstrates a steady decrease in quite large temperature range.

5.2.3 Butyl Rubber (IIR)

Butyl rubber with its high concentration of small side groups demonstrates a glass transition temperatures at -62°C for the 1 Hz measurement and approximately 12°C as detected at 0.5 MHz. At low frequencies the glass transition temperature is even lower than for NR but at high frequency this process requires supplementary activation in the case of IIR and the T_g is 18°C higher.

Noticeably the entire glass transition for the IIR at 1 Hz is significantly wider than for NR. In terms of half width, the value for IIR is 13.2mm^{-1} and for NR 8.3mm^{-1} .

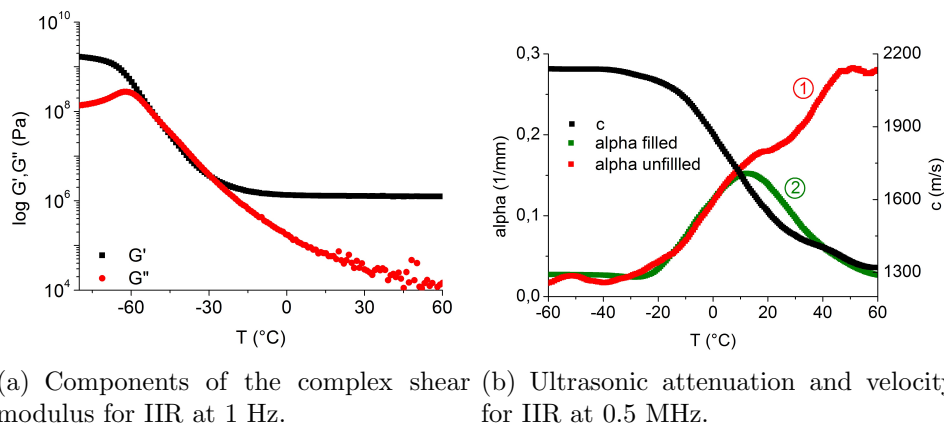


Figure 5.10: Dynamic mechanical characterization of IIR at 1 Hz and at 0.5 MHz

This is associated with the internal structure of IIR. When compared to NR for each structure unit of butyl there are two CH_3 units, located on the same carbon atom. The size of the CH_3 group and their location on the chain causes steric hindrances into a lower chain mobility also higher energy dissipation. This was also discussed by Rehner [189] in his work concerning side group effects on elastomer properties.

This type of rubber is well known for its reduced gas permeability which makes it one of the primary choices for tire innerliners, for example [104, 190]. This outstanding property has, however, its disadvantages, in that it is very difficult to get proper vulcanizates at the thickness required by the ultrasonic measurement. The outcome was that all unfilled samples presented several gas inclusions which are "seen" experimentally as high attenuation values above the glass transition region. As an example, in Figure 5.10(b) the green curve (number 2) represents the 30phr carbon black filled sample with no gas inclusions whereas the red curve (number 1) shows the high frequency behavior of the unfilled sample with gas inclusions. It is noticed that the attenuation apparently increases even beyond T_g in the unfilled sample but as it is discussed later in the section on inactive fillers 5.9, this is not generated by the polymer under consideration.

The reason for the high attenuation coefficient is the scattering of the waves at the rubber air contact surface, a phenomenon not related to damping, which cannot be separated from it.

As a result the ultrasonic attenuation values are higher (see Figure 5.10(b)) compared to NR and BR and the shape of the curve suggests the effect is stronger in the rubbery region.

5.3 Investigation of copolymers

A tailoring of the characteristics of polymers can be achieved by copolymerization. This process introduces new segment units in the polymeric chain which specifically affects chain dynamics. The main factors influencing elastomer properties, relative to the chemical structure, are the type of the side groups, their size and their concentration along the main chain. As a consequence the inter- and intramolecular interactions between the chains are also affected by, for example, the induced dipoles of the side groups.

The significance of copolymers with a random (statistical) distribution of comonomers has directed research into estimating the glass transition temperature from the composition of the copolymers (ratio of comonomers, weight fractions, volume fractions) and from the T_g of the corresponding homopolymers on the assumption that the free volume of the monomer units along the chain is additive. This is depicted in the empirical formulae derived by Fox and Flory [25] and Gordon and Taylor [26] (see chapter 3.1.5). Depending on the composition of the copolymer, these equations allow an analytical insight into the influence of monomers' concentration on T_g .

In the following the influence of three relevant side groups -vinyl, styrene and nitrile- is investigated using the aforementioned testing methods. The composition of the chosen copolymers is shown in Table 5.4.

Table 5.4: Copolymers' characterization. Concentrations are in weight %

	vinyl	styrene	acrylonitrile	cis 1,4	T_g (°C)
BR1	1			96	-100
BR2	12			37	-86
BR3	70				-5
SBR1	30	10		60	-60
SBR2	30	20		50	-50
SBR3	30	30		40	-39
SBR4	45	20		35	-38
SBR5	65	20		15	-21
SBR6	25	25		50	-42
SBR7	50	25		25	-14
NBR1			18		-44
NBR2			28		-26
NBR3			34		-22
NBR4			44		-7

The BR2 and BR3 are variations of BR1 with higher vinyl content. In the SBR assortment the variations 1 to 5 are specially synthesized copolymers to achieve an

increasing vinyl content while maintaining the styrene constant (SBR2, SBR4 and SBR5) whereas SBR1, SBR2 and SBR3 display an increasing styrene concentration at constant vinyl fraction. The NBR2 are different only in nitrile content.

5.3.1 Influence of vinyl groups

The variation of the vinyl concentration is investigated in the case of BR1, BR2 and BR3 as well as SBR2, SBR4 and SBR5. The systematic increase of the vinyl concentration was reported to result in a linear increase in T_g [191] and a decrease in chain mobility, respectively. The scope of this group of experiments was to evaluate the corresponding phenomena at high frequencies, the evaluation of the frequency dependent T_g shift and the amplitude of energy dissipation in the T_g regime.

5.3.1.1 Vinyl in BR

In Figure 5.11(a) and 5.11(b) the characteristic low frequency moduli G' and G'' show the influences induced by side groups. In the glassy state BR3 with the highest vinyl content shows the highest value for the storage modulus and the lowest for the loss modulus, respectively, followed by BR1 and BR2. The T_g determined either at the inflection point of the $G'(T)$ curve or at the maximum of the $G''(T)$ curve is shifted to higher temperatures with increasing vinyl concentration, which is a sign of reduced main chain mobility. In the rubbery region only BR1 shows a secondary process associated with the occurrence of crystalline domains, already discussed in section 5.2.1.

The loss modulus in the glassy region at 1 Hz shows the lowest values for the high vinyl BR3 (Figure 5.11(b)). Between -100°C and -50°C the modulus is characterized by a broad and discreet peak which could indicate low temperature process (see inset of Figure 5.11(b)). The peak maxima of the three BRs decrease with the vinyl concentration.

The ultrasound attenuation curve demonstrates two moderate peaks for BR1 and BR2 but a significant higher energy dissipation for BR3 which occurs as a result of the increased vinyl content. Thus the effect of the vinyl side groups becomes more pronounced in the high frequency regime (Figure 5.11(d)). It is apparent that below the glass transition temperature two dissipation processes occur (at -50°C and at -10°C , respectively) indicating a certain motion of macromolecular chain fragments. It is also likely that this process is the same as the one noticed and discussed in Figure 5.11(b) only shifted as a result of the higher excitation frequency. However, the nature of these processes could not be elucidated until now. The shoulder that appears above -40°C for BR1 and the unusual broadness of the attenuation peak of BR2 could be related to

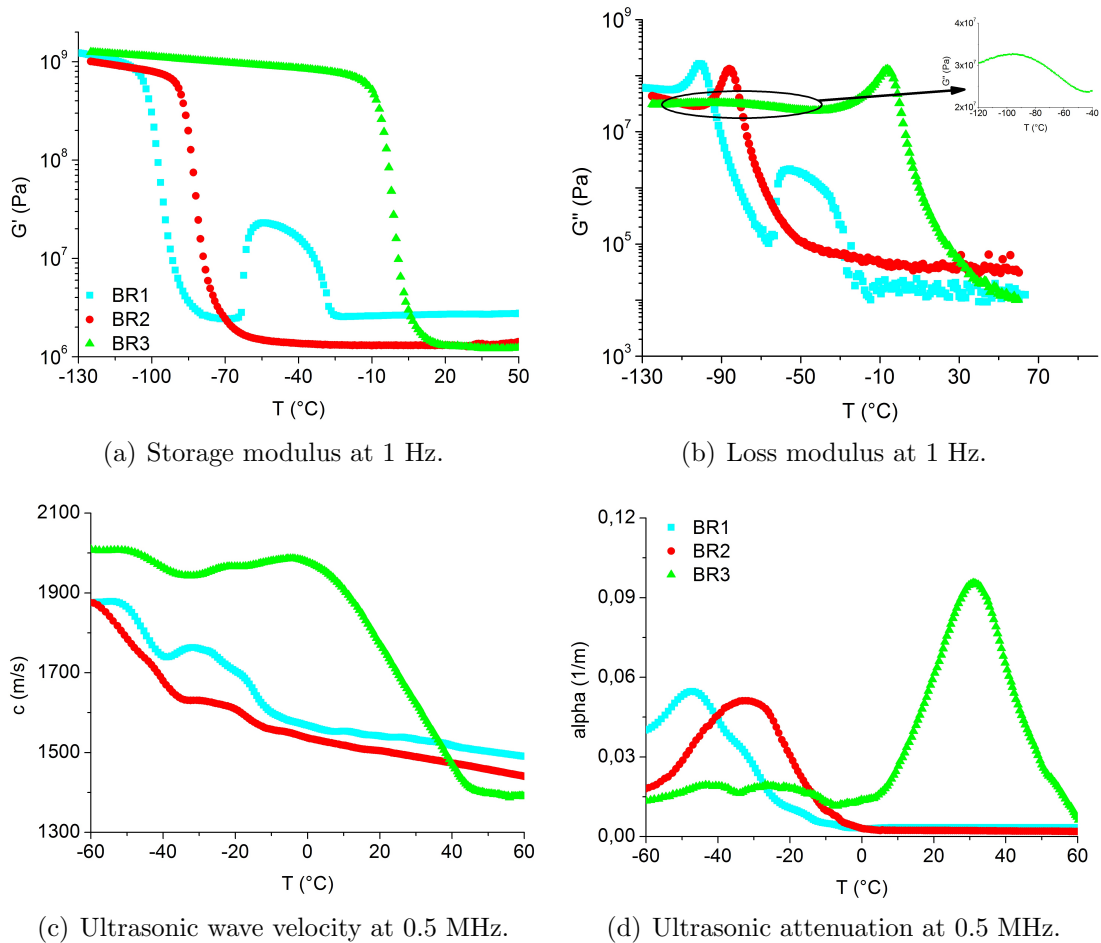


Figure 5.11: Dynamic mechanical evaluation of BRs with different vinyl content at 1 Hz and 0.5 MHz.

the occurrence of crystallites as discussed. The accuracy of these measurements was checked by a threefold repetition at different days.

As far as the crystallization influence is concerned, it can be seen that the two BRs that showed to a different extent crystallization traces (BR1 and BR2) display similarly low attenuation values of approximately 0.05 mm^{-1} whereas BR3's attenuation is twice as high (Figure 5.11(d)). It can now be concluded that due to the frequency dependent activation, the glass transition is shifted and overlaps the region where the crystallites melt.

In an approximation that makes use of a spring-dashpot combination to simulate viscoelastic behavior, a material containing crystalline regions would display a strong contribution of the spring element. As the ultrasonic attenuation is a representation of the dissipated energy at 0.5 MHz - represented by the dashpot - it is expected that it shows lower values for materials with crystalline content, especially when the

crystallization region overlaps with the glass transition.

The measured ultrasound velocity (Figure 5.11(c)) is marked by several features. Below the glass transition regime the sound velocity of BR3 is up to 400 m/s higher compared to BR2 and BR1. In the glassy region the BR3 sound velocity displays a minimum of approximately 50 m/s apparently associated with the secondary attenuation process discussed above. However, this process should not be associated with crystallites because BR3 does not show this type of supramolecular organization. The glass transition temperature is depicted by a stepwise decrease of c which corresponds to the maximum of the attenuation coefficient. The recrystallization and afterwards the melting of crystallites seems to be located several degrees to higher temperature compared to the measurements at 1Hz is not related to the higher frequency of measurement, being known that crystallization is a process which is independent of frequency, but to the different heating rates of the measuring devices, as will be shown below. Above T_g a shoulder is seen for BR2, in the same temperature region (-40°C to -20°C) as the one occurring in BR1 that can be associated with the formation of small crystallites.

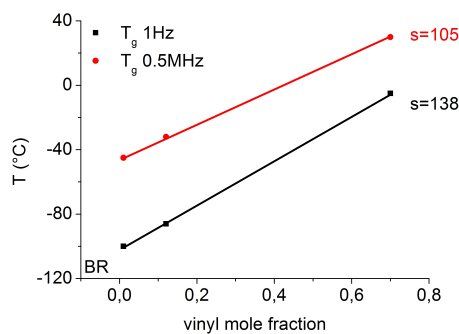


Figure 5.12: Dependence of T_g on vinyl content in BR.

Above T_g the ultrasound velocity is decreased in the sequence of the polymers density $BR1 > BR2 > BR3$.

One important conclusion that comes out from investigating this group of polymers is the specific influence of the vinyl concentration on the main chain dynamics, characterized by the change of the glass transition temperature. In the low frequency regime the T_g increases linearly with a slope of $130^{\circ}\text{C}/mole\%$ vinyl. This increase obeys qualitatively the semi-empirical relation proposed by Flory and Fox [25]. When the ultrasonic attenuation is considered, the glass transition temperature is seen to increase according to the different activations, in the high frequency regime, with a considerable lower slope (Figure 5.12). This result demonstrates that the T_g shift observed with increasing the measurement frequency is in fact not the same for this group of copolymers but it is a function of the copolymers' composition. Noteworthy is that the shift of the T_g decreases with the vinyl content from 55 degrees for BR1 with only $1mole\%$ of vinyl

groups to 35 degrees for BR3 with 70mole% of this comonomer. From this data it can be predicted that the T_g shift for a 100% 1,2-BR is 26°C.

5.3.1.2 Vinyl in SBR

The anionic copolymerization of SBR enables the manufacturing of polymers with tailored micro-structure. In the following three SBRs with constant styrene content and a variable vinyl content are investigated with respect to their dynamic-mechanical properties.

Characteristic of the increase of the mole fraction of the vinyl groups is the reduction of the capability of the polymer chain to perform positional changes or concerted rotational movements of an assembly of chain segments which translates into a higher glass transition temperature. As a matter of fact, the maxima of G'' in the low frequency regime and of α in the high frequency regime are shifted to higher temperatures if the vinyl content increases.

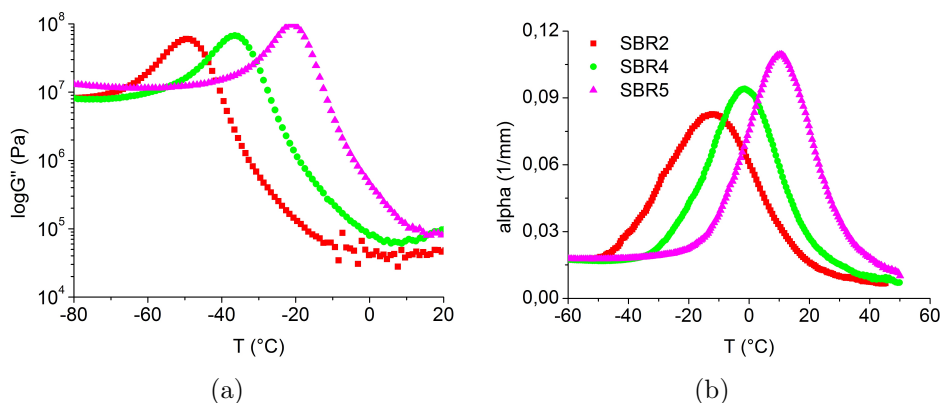


Figure 5.13: Vinyl content variation in SBR.

The increase of the vinyl content manifests itself by increases of the amount of dissipated energy clearly separating the three polymers, which is shown by both measuring techniques, but more pregnantly by the ultrasonic attenuation. In order to enter an equivalent state of chain mobility for chains with more vinyl side-groups a larger amount of mechanical energy is dissipated into heat. The attenuation increase could be related to physical interactions between the side groups that lead to increased barriers for rotational and translational displacements of the chains.

The position of the maximum of the dissipation peak on the temperature axis is shifted approximately 0.7°C for each mole of vinyl. Notably, the glass transition is shifted some 30°C to higher temperatures for the 0.5 MHz measurements.

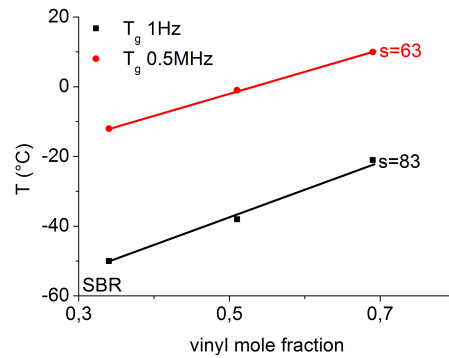


Figure 5.14: Dependence of T_g on vinyl content in SBR.

5.3.2 Effect of styrene groups

The effect of styrene monomer content variation is investigated with three SBR samples prepared by anionic polymerization where the content of butadiene monomer has been kept constant. The variation of the energy dissipation in the T_g regime can be characterized by the maxima of the loss shear modulus at 1 Hz and of the ultrasonic attenuation signal at 0.5 MHz respectively in Figure 5.15.

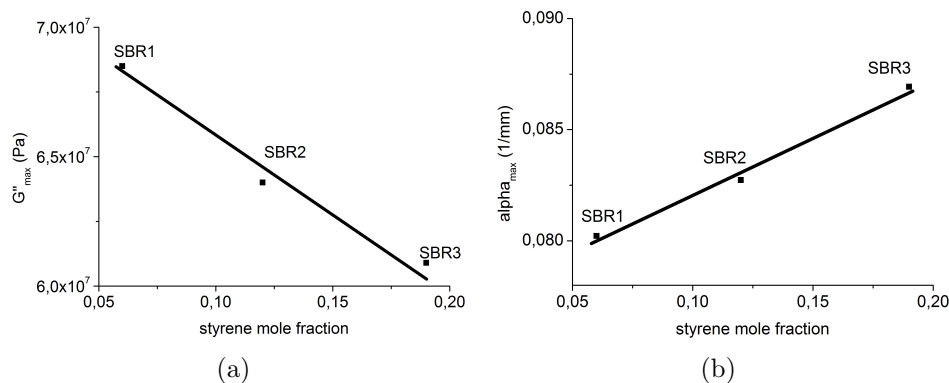


Figure 5.15: Damping maxima variation with styrene/vinyl content

The contribution of the styrene groups unveils itself differently in the two frequency ranges under consideration. At low excitation frequencies the increase of the styrene content determines a decrease of the G''_{max} , whereas at high frequencies the ultrasonic attenuation maxima increase slightly with styrene content. This striking result might be influenced by the variation of the crosslinking density in the sequence of increasing styrene content. However, it shows that the high frequency dynamics of the polymer can be overlapped by specific processes less evident and effective in the low frequency range.

Besides the amount of energy dissipated in the glass transition regime the glass tran-

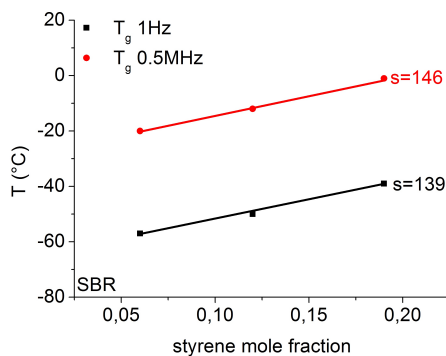


Figure 5.16: Dependence of T_g on styrene content in SBR.

sition temperature dependence on styrene monomer content becomes important. The experimental data shows a linear increase in both frequency regimes as delineated in Figure 5.16. In contrast to the group of homopolymers the slope of the T_g increase is moderately stronger (146°C/mole fraction) than the one of the low frequency range. This “parallelism” demonstrates that styrene groups are able to impair to the same degree the mobility of the chain irrespective of the excitation frequency of the polymer network.

5.3.3 Influence of SBR hydrogenation

The challenge for nowadays copolymers is to modify their structure using polymer analogue reactions. In this case it is possible, without the necessity of developing new monomers, to modify the chains of existing polymers in such manner that important properties like mobility, interactions with fillers, aging resistance, etc. can be adjusted according to application necessities.

Hydrogenation is an important option for polymer analogue modification resulting in a variety of new polymers with unique structures and properties. Hydrogenation also offers a convenient synthetic route to polymers with new monomer sequences which are inaccessible, difficult or too expensive to prepare by conventional polymerization methods. By hydrogenating butadiene copolymers to some degree, the resulting products can be considered as copolymers of ethylene, 1-butene, butadiene and styrene or acrylonitrile. However, such structures are not available starting directly from ethylene or α -olefines. In addition hydrogenated elastomers may have good resistance to oxidative and thermal degradation, improved weathering and low permeability to gases. Nonetheless, hydrogenation does not change the character of the hydrocarbon polymer. Therefore the resistance to oils and hydrocarbon fuels remains on a similar level as for the original non-hydrogenated polymer.

Several SBRs hydrogenated to different levels, were tested within this work to asses the

influence this modification has on the dynamic response in the frequency regime under consideration (1 Hz and 0.5MHz). Figures 5.17(a) and 5.17(b) show the dissipated energy at the two frequencies, characterized by the loss shear modulus and the attenuation coefficient. Interestingly in the low frequency range the hydrogenation effect translates into a systematic shift of the dissipation curve to lower temperatures and a slight reduction of the maximum amplitude.

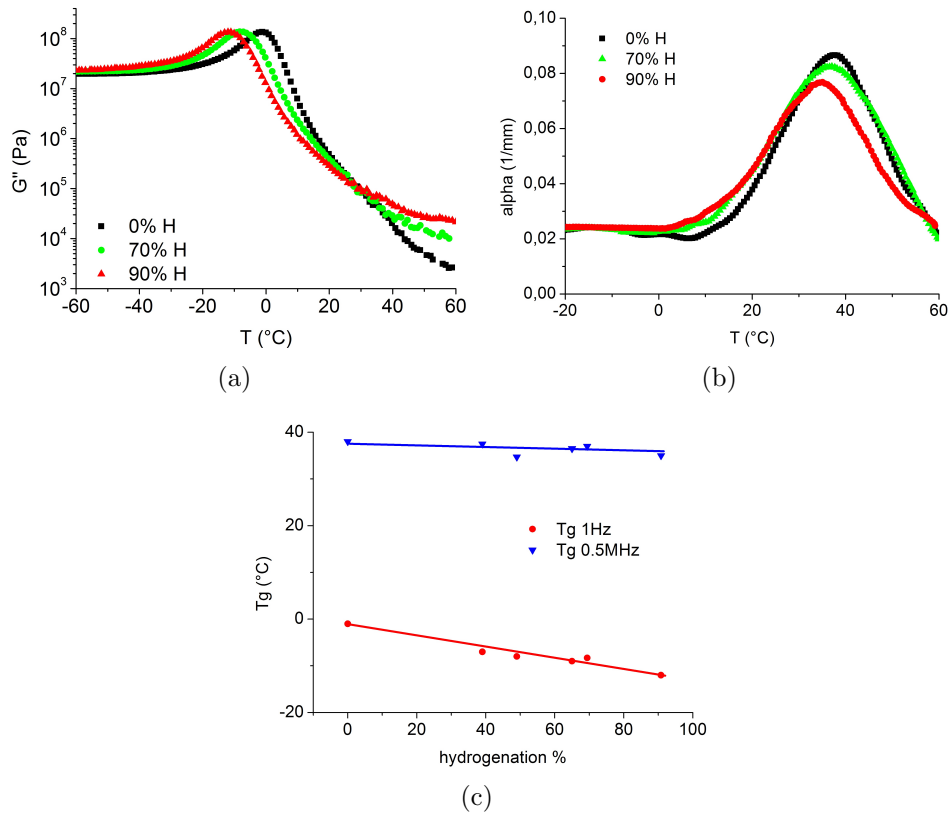


Figure 5.17: Influence of hydrogenation on SBR.

By removing 70% and 90% of the unsaturation the glass transition occurs at lower temperatures and the amplitude of the energy dissipation in the glass transition regime decreases (Figure 5.17(a)). Besides the changes in the glass transition, significant changes of the dynamic-mechanical properties in the rubbery regime become obvious. With decreasing unsaturation the flow processes that lead to energy dissipation are depressed significantly.

In the high frequency regime the consequences of the hydrogenation become even more obvious (Figure 5.17(b)).

In case of the attenuation coefficient, with increasing hydrogenation degree there is a pronounced decrease of the maximum attenuation and shift of the glass transition

temperature towards lower values. In addition the broadness of the dissipation signal becomes more narrow.

A correlation of the frequency dependent glass transition temperatures of the SBRs hydrogenated to different degrees (Figure 5.17(c)) gives a good insight into the influence of hydrogenation on chain mobility. For the low frequency range it can be said that the T_g decreases linearly with the hydrogenation degree. The reason for this experimental result is not yet clear. It was proven by auxiliary swelling experiments that there is no drop in crosslink density. It could be assumed that the high amount of ethylidene side groups which result from the hydrogenation of 1,2-butadiene units can act to increase the free volume in the system. Remarkably in the high frequency range the decrease of T_g as a function of the degree of hydrogenation is much less pronounced. Due to this fact the difference between the glass transition temperature at 1 Hz and the one at 0.5 MHz increases with the hydrogenation degree.

5.3.4 Effect of acrylonitrile groups

NBR vulcanizates are requested in various applications where good compression set, good hot air resistance, high abrasion resistance connected with high swelling resistance in oils, fats and fuels are requested. The latter property is ascribed to the polar acrylonitrile groups and it improves the more ACN is present in the chain. This melioration is directly connected with the high dipole moment of the nitrile groups and therefore the higher solubility parameter of the copolymer. The more polar the polymer matrix becomes due to its ACN content, the less (non-polar) oils fats and fuels can swell it [104, 192]. Another interesting effect of the ACN groups is connected to the frequency of the intra- and intermolecular dipole-dipole interaction in the rubber which form a physical network that affects the mechanical response such as rebound, hardness and compression set.

The dynamic response to sinusoidal excitation of four NBRs was investigated at 1 Hz and at 0,5 MHz (Figure 5.18). The low frequency measurements carried out at a strain amplitude of 0.5%, show constant increase of the dissipation maximum (G'') with the ACN content except in the case for the one containing 28% ACN. This behavior is partly explained by the increasing concentration of nitrile side groups which form a physical network and reduce the chain movement. Furthermore, ascribed to the increased stiffness, the glass transition temperature represented by the temperature of the G''_{max} , is also increased proportional with the side group concentration. The linear increase in T_g obeys the empirical relationships proposed by Flory and Fox [25]. The damping of the ultrasonic mechanical waves is affected by the increase of ACN concentration (Figure 5.18(b)). The increase of the α_{max} indicates saturation when getting over 34% ACN - another 10% raise of its concentration produces only 15%

increase of the α_{max} compared to 40% from 18% to 28% and from 28% to 34%. The exception that occurs in the case of NBR 28 at 1Hz doesn't appear in the ultrasonic measurements.

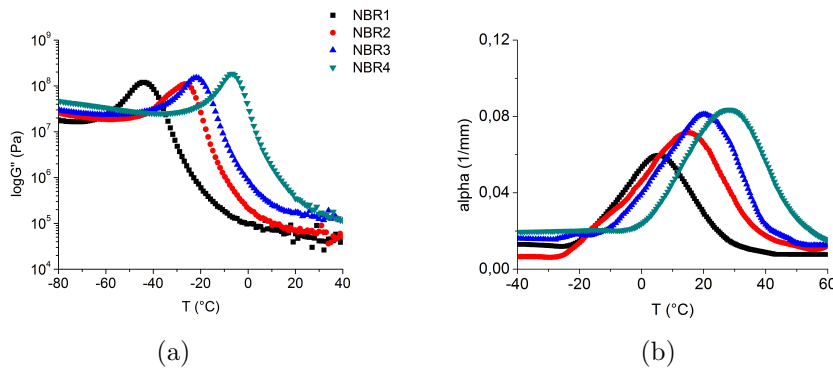


Figure 5.18: Influence of the ACN content on energy dissipation.

The integral signal increases asymmetrically in its area indicating damping processes of nitrile groups that become active at higher temperatures. It seems reasonable to assume that the strength of the physical network provided by nitrile groups is more efficient in the high frequency regime in which the strain amplitude can be considered negligible. Representing the resulted T_g s as a function of the ACN content (Figure 5.19) it becomes obvious that the polymer dynamics in NBR is affected not only by the ACN content but also by the frequency regime. The slope of the T_g vs ACN content strongly depends on ω .

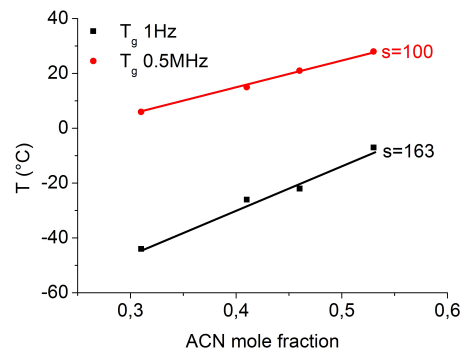


Figure 5.19: Dependence of T_g on ACN content in NBR.

If a low content of ACN is considered the high frequency glass transition temperature is shifted with approximately 50°C while at a high ACN content this shift is less than 40°C.

The comparison with the SBR discussed above shows that the dynamics of copolymers of polybutadiene with styrene and acrylonitrile are governed by the physical nature

of the comonomer unit and the content of the unit or the monomer ratio. The high dipole moment of nitrile groups leads to higher T_g s but also to another shift of T_g at higher frequencies so that the particular knowledge of the high and low frequency dynamic-mechanical properties is hence of capital importance.

It was noticed for all tested polymers that the maxima of the relaxation peaks showed a linear correlation to the co-monomer concentration, therefore it is meaningful to evaluate the effect of vinyl units, styrene units and acrylonitrile units on the slopes of the linear dependencies which are summarized in Table 5.5.

Table 5.5: Energy dissipation dependence on side group concentration in SBR and NBR.

	styrene	vinyl	ACN
$G''_{max}/\text{mole fraction}$	-0.58	0.69	3.05
$\alpha_{max}/\text{mole fraction}$	0.05	0.08	0.12

Despite having the largest volume and molar mass (104 g/mole) styrene groups produce the least increase in energy dissipation. At half of styrenes' molar mass, vinyl groups are apparently capable of producing a stronger increase of the energy dissipation that occurs as a result of the mechanical friction between the polymer chains. This effect is characterized by higher values of the slopes of the loss modulus and attenuation maxima, respectively.

The higher polarizability of the nitrogen atoms compared to the carbon atoms induces polarization effects in the CN group, which is part of the acrylonitrile (ACN) monomer. This in turn leads to the formation of dipoles between neighboring ACN units. As such, the acrylonitrile side group causes significant energy losses (the loss modulus increases four times faster than for vinyl) at every chain movement compared to vinyl, even though it has similar molar mass.

5.3.4.1 Secondary transitions

So far the discussion was concentrated on the glass transition described by the maxima of $G''(T)$ and $\alpha(T)$ respectively. It should be noted that the NBR3 attenuation curve (Figure 5.18(b)) displays a shoulder shortly before the main transition begins, with an apparent maximum around -20°C . This peak can be attributed to a secondary phase transition that takes place in NBR. It has been reported that these transitions, where the change in modulus (low frequency measurements in shear) amounts to a factor not larger than 2, have a marked effect on the mechanical behavior of some plastics [193]. For example, in the case of impact resistant polystyrene which retains its properties below the glass transition but becomes brittle once the operating temperature drops

below the β transition temperature. The importance of this process resides in that the flexibility imparted to the chain by the secondary chain motion contributes to its ability to respond to stress [8].

To demonstrate that the secondary shoulder observed in the ultrasonic attenuation curve occurs due to a secondary phase transition, low frequency measurements have been performed at 0.1Hz, 0.5Hz, 1.0Hz, 1.5Hz, 10Hz and 15Hz.

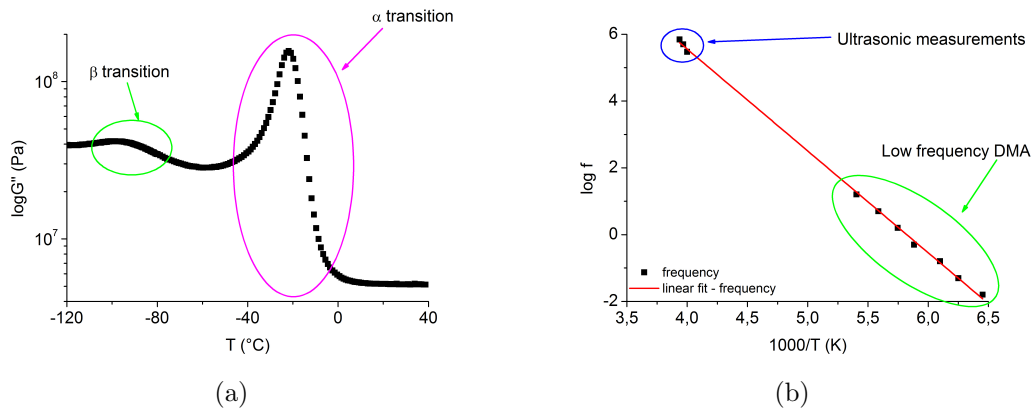


Figure 5.20: Beta transition in NBR 3

As it can be seen, the loss modulus curve at 1 Hz (Figure 5.20(a)) displays the secondary transition around -100°C . An Arrhenius plot of the β transitions at the aforementioned frequencies shows a linear temperature dependence at low frequencies. These results obtained in the low frequency range correlate well with the maxima of the high frequency measurements (Figure 5.20(b)). The values for 0.4 and 0.6 MHz were calculated by integrating the Fourier transform of the time signal in Figure 5.3 the areas to the left and to the right of the central region representing the 0.5 MHz value. The linearity of the Arrhenius plot allows for the estimation of an activation energy which is related to the remnant segmental movement. This estimation yields a value of 12 kJ/mole, which is close to the value for the activation energy for rotation about a CH–CN single bond [194].

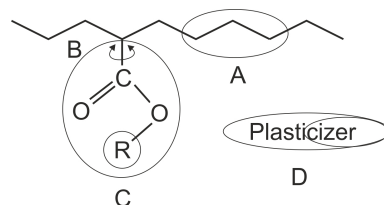


Figure 5.21: The various kinds of groups whose movements give rise to secondary mechanical loss peaks.

According to Heijboer [193] there are four main types of motion that still possible under T_g and that give rise to mechanical peaks (Figure 5.21):

- Type A: a motion still within the main polymer chain, but locally much more restricted than the motion corresponding to the glass transition. The corresponding loss peak often marks the transition from brittle to tough behavior.
- Type B: the rotation of a side group about the bond linking it to the main chain.
- Type C: this is an internal motion within the side group itself, without interaction with the main chain.
- Type D: this is a motion of, or taking place within, a small molecule, dissolved in the polymer. It can be a motion within a plasticizer molecule.

The temperature difference, ΔT , between the two phase transitions has an interesting frequency dependence. At 1 Hz $\Delta T \approx 80K$ whereas at 0.5 MHz the value is reduced to $\Delta T \approx 40K$. The explanation for this behavior resides in the different activation processes, i.e. the β transition follows an Arrhenius process whereas the α transition, or T_g , follows the WLF equation [6], therefore the secondary transition will be completely shadowed by the glass transition over 10MHz.

5.4 Frequency effects on the glass transition temperature

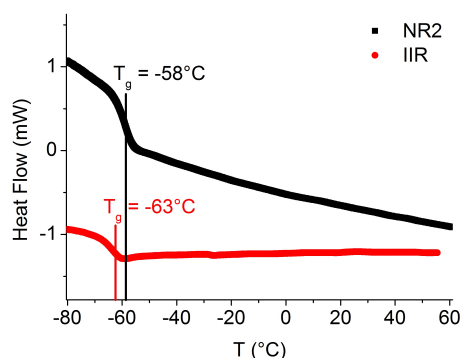
The influence of different factors on the glass transition temperature can be summed up as follows: those that increase the energy required for the onset of molecular motion increase T_g whereas those that decrease the energy requirements decrease T_g .

The influence of the higher oscillation frequency on the dynamics of polymer chains translates into a stiffer backbone which in turn determines a shift of the glass transition to higher temperatures. Theoretical models predict this shift to be 6-8 °C per decade of frequency. The results presented in this work confirm these predictions for the copolymers of polybutadiene, i.e. the SBRs and NBRs (above 26% ACN) but not for pure BR, NR and IIR.

The glass transition temperature for the homopolymers is lowest for BR1 ascribed to the lack of side groups on the main chain and followed by NR with one methyl side group per chain segment (Table 5.6). Butyl rubber, despite having more side groups attached to the polymer backbone displays lower T_g than NR2 as can be seen also in the dynamics DSC scan shown in figure 5.22.

Table 5.6: T_g dependence on frequency.

	$T_g(^{\circ}\text{C})$ 1 Hz	$T_g(^{\circ}\text{C})$ 0.5 MHz	$\Delta T_g(^{\circ}\text{C})$
NR2	-58	-8	50
IIR	-62	2	64
BR1	-100	-45	55
BR2	-86	-32	54
BR3	-5	30	35
SBR1	-57	-20	37
SBR2	-50	-12	38
SBR3	-39	-1	38
SBR4	-38	-1	37
SBR5	-21	10	31
NBR1	-44	6	50
NBR2	-26	15	41
NBR3	-22	21	43
NBR4	-7	28	35

**Figure 5.22:** DSC scan of NR2 and IIR.

This behavior of IIR can be related to the symmetrically substituted carbon atom by methyl groups which causes significant steric impediments to the neighboring bonds and less intra- and intermolecular interactions due to the minor polarizability of the methyl groups. The first effect that results is an increase of the available free volume which explains the lower T_g . A similar effect was noted by Brydson [195] in case of polar groups. One polar group attached to a chain segment contributes to an increase in T_g which is proportional to the amount of groups and their dipole moment. Two identical polar groups attached to the same atom lead to a lower T_g than in the case of only one atom. This is the case for poly(vinylidene chloride) as compared with poly(vinyl chloride). In this case, the explanation was the reduction of the dipole moment as a result of the symmetry of the substitution.

The broad transition peak of IIR should also be associated with the steric hindrance as a structural characteristic of this particular polymer.

As described in the introduction to the section on copolymers, there are several theoretical methods to estimate the glass transition temperature of copolymers based on the assumed additivity of the monomers' free volume. Figure 5.23 gives an impression of the accuracy of such empirical equations, the Gordon-Taylor and Fox-Flory equations (see Equ.3.33 and 5.23(a)) applied for SBR and NBR copolymers, considering the variation of styrene and acrylonitrile concentrations, respectively.

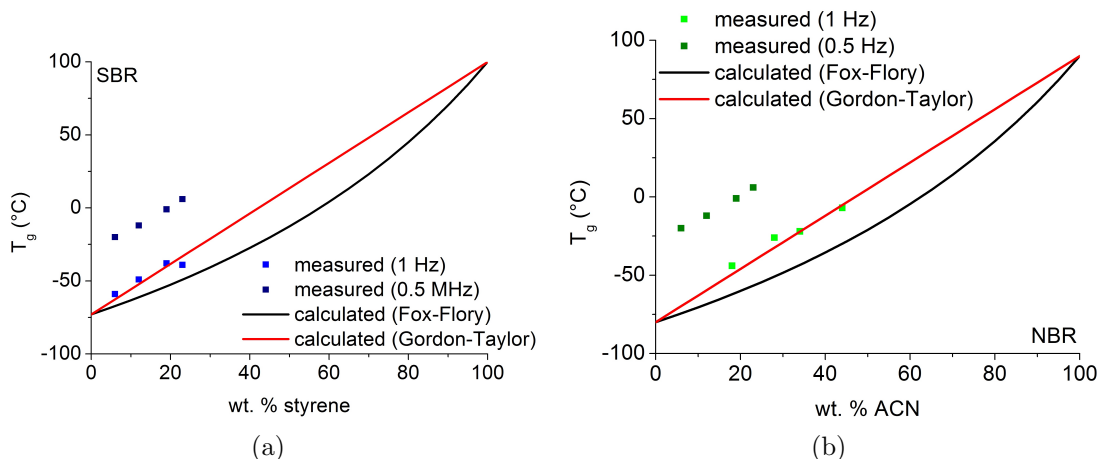


Figure 5.23: T_g of copolymers

The glass transition temperatures are taken from the maxima of the 1 Hz loss moduli and from the maxima of the ultrasonic attenuation at 0.5 MHz. In the cases discussed the low frequency T_g s of both SBR and NBR copolymers can be quantitatively estimated using the Gordon-Taylor equation. The linearity of this dependence implies the possibility of using the slope of a linear regression to characterize the side group effect on chain mobility. It can be concluded that neither of the two semi-empirical models take into account the frequency dependence of the glass transition process.

A comparative analysis of Figures 5.12 , 5.14, and 5.19 reveals striking effects on the high and low frequency T_g . When considering the ultrasonic measurements, the strongest increase is shown for the styrene variation followed by ACN and vinyl. These results suggest the glass transition temperature which describes the mobility of the main chain, is affected by geometrical characteristics induced by the size and position of the side groups more than by the electrostatic interactions between neighboring groups.

As can be deduced from the data in Table 5.6 the T_g shift is dependent on the chemical nature of the polymer. In the case of the homopolymers tested above a one notices a T_g shift between 50°C and 64°C. This values are clearly above what was assumed until now, according to the WLF model; it seems that the origin of this phenomenon cannot, for now, be traced back to any molecular characteristics of the polymers. A

clearer trend can be observed in the case of BR and NBR. With increasing co-monomer concentration (1,2-butadiene in case of BR and ACN in case of NBR) a systematical decrease of the T_g shift is noticed.

In their study of SBR/BR polymer blends, Fujimoto and Yoshimura [196] also investigated the styrene influence in SBR on several mixes with styrene contents between 8.6% and 100% - i.e. polystyrene. The tests included dynamic mechanical measurements at 100Hz, dielectric measurements as well as tensile strength, elongation and tear resistance. The dynamic loss at 100Hz showed a decrease of the maximum with increasing styrene content up to approximately 30% styrene followed by an increase up to pure polystyrene. Serious differences are seen in the glass transition temperature where the increase in styrene over 40% induces T_g s above 0°C. For similar measurements Nielsen [197] even reports glass transition temperatures between 5°C and 10°C for 60% styrene content. It is interesting to notice that their measurements confirm the behavior shown herein by the measurements at 1Hz, namely that the styrene groups determines a proportional increase of the glass transition, i.e. a decrease of the chain mobility while, at the same time, the amount of energy dissipated by the materials decreases, at least up to 30 – 40% styrene content. The dielectric loss measurements (also in [196]) show a steep decrease of the maxima connected to the styrene content increase which also fits into the main idea of the styrene increase determining a reduction of the amount of energy the compound dissipates into heat.

The contribution of the vinyl groups is manifested firstly by higher glass transition temperatures with increasing content but the temperature step up per mole percent of vinyl (0.85°C/mole percent vinyl) is lower than in the case of styrene (2°C/mole percent styrene). This effect can be connected with the actual size of the vinyl and styrene groups which, in case of the latter determine a higher increase, i.e. a stiffer backbone. Secondly, the vinyl content determines an increase of the energy loss as is quantified by the low frequency as well as the high frequency measurements. In this case additional dissipation is caused by molecular friction which occurs between the vinyl groups. It is reasonable to ascribe this effect to a typical and very important characteristic of the polymers containing high 1,2 structures.

The ACN side groups induce sterical hindrances on the main chain due to their formation of strong dipoles which act like physical crosslinks. With a value of 2.3°C/mole percent ACN the acrylonitrile groups exert the strongest influence on the T_g compared to vinyl and styrene.

The differences (ΔT_g) between the transition temperatures at 1 Hz and 0.5MHz, respectively, are strongly polymer dependent as seen in the third column of Table 5.6. Therefore, any attempts at evaluating high frequency phenomena, i.e. tire traction, based on theoretical models that assume all polymers shift similarly within a certain

temperature range per increased frequency can lead to erroneous results. This is further discussed on concrete examples in section 5.5.

5.5 Broad range frequency analysis - WLF

The investigation of the homo- and copolymers demonstrates that the frequency dependent glass transition temperature is strongly correlated to the time allotted to the experiment, becoming higher as the experiment is carried out at higher frequencies.

Because the dynamical-mechanical methods based on forced oscillations of a sample are restricted to a relatively narrow range of frequencies (10^{-2} - 10^3 Hz) the dynamic-mechanical properties in the high frequency range (MHz) are usually estimated by using the time-temperature superposition principle. Alternatively, as it is done in the present work, the investigation can be performed by applying the ultrasonic spectroscopy for direct measurements. One advantage of the ultrasonic measurement is that the resulting data are not affected by uncertainties and assumptions made by the application of the WLF equation. Especially the assumption according to which T_g increases by 5 – 6°C for each decade of frequency can be averted. Therefore the results from the ultrasonic spectroscopy can be used to evaluate the precision of the WLF extrapolation described in section 3.50.

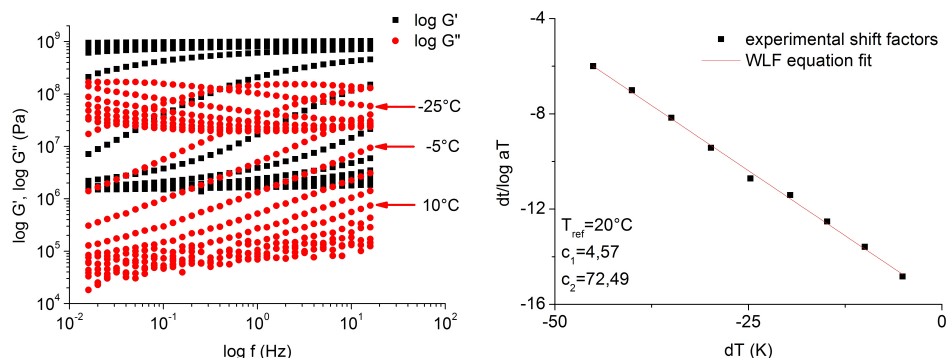
In this section the shifting procedure based on the WLF-method will be exemplary applied to two groups of polymers, which demonstrate different T_g shifts as a function of deformation frequency. The selected polymers are SBR7, NBR3 and NR2, IIR.

The broad frequency range analysis of an unfilled polymer is accomplished by isothermal scans at different temperatures (usually at a 5°C interval) of the dynamic moduli over the entire frequency range the device is capable of (in this case, 0.01Hz to 16Hz). The different scans are shown in Figure 5.24(a) in their raw, “unshifted” form. In order to consider the linear deformation range the strain deformation is kept at 0.5%. After choosing a reference temperature i.e. 25°C the isothermal scans are shifted horizontally until a master curve, such as the one in Figure 5.25(d) is obtained. The shifting factors (i.e. the logarithm of the difference between f_i - the frequency of the shifted isothermal - and the f_{ref} - the frequency of the reference isothermal) divided by the temperature difference ($\Delta T = T_i - T_{ref}$) are then plotted against ΔT , as in Figure 5.24(b) and fitted using Equation 3.50.

$$\log a_T = -\frac{C_1 \cdot (T - T_0)}{C_2 + (T - T_0)}$$

A correct shift of the dynamic data yields a linear fit which enables the calculation

of the empirical parameters $c_1 = \frac{-1}{s}$ and $c_2 = \frac{i}{s}$ where s is the slope of the linear regression and i the intercept point.



(a) Isothermal shear moduli of NBR3 at different temperatures.

(b) Shifting factors and parameters.

Figure 5.24: Typical example of a multi frequency DMA measurement.

However, the aforementioned procedure is affected by errors. One error source would be the assumption that with increasing frequency every polymer changes its properties in the same way, another one would be the subjectivity of the operator, and another is the artificial curvature of the isotherms which can be induced by the device working at its highest frequency.

An easy way to check the shifting factors at the chosen T_{ref} , c_1 and c_2 is based on the independence of Equation 3.50 of the choice of T_{ref} [6]. It involves the choosing of a second reference temperature, T_{ref1} , and performing the graphical evaluation in exactly the same way as before. This provides new parameters $c_1^{T_{ref1}}$ and $c_2^{T_{ref1}}$. Further, these new parameters can be transformed in the ones correlated to T_{ref} by $c_1^{T_{ref}} = \frac{c_1^{T_{ref1}} \cdot c_2^{T_{ref1}}}{c_2^{T_{ref1}} + T_{ref} - T_{ref1}}$ and $c_2^{T_{ref}} = c_2^{T_{ref1}} + T_{ref} - T_{ref1}$. Several such determinations can be performed in order to adjust the reference temperature but the final choice of c_1 and c_2 is, however, subjective.

The master curves (Figure 5.25) have been obtained and checked using the procedure described above (manual shifting at several other temperatures and subsequent check of the c_1 and c_2 factors). It is seen that the shape of the master curves resembles the mirror images of the dynamic temperature sweeps obtained at 1Hz displayed, for example, in Figure 5.6(a) which is a proof of the validity of the time-temperature correlation on which the WLF equation is based.

Based on the shifting procedure, the loss modulus of each polymer demonstrates a maximum which corresponds to the frequency dependent dynamic glass transition. The frequency of maximum energy dissipation for a reference temperature of 20°C are

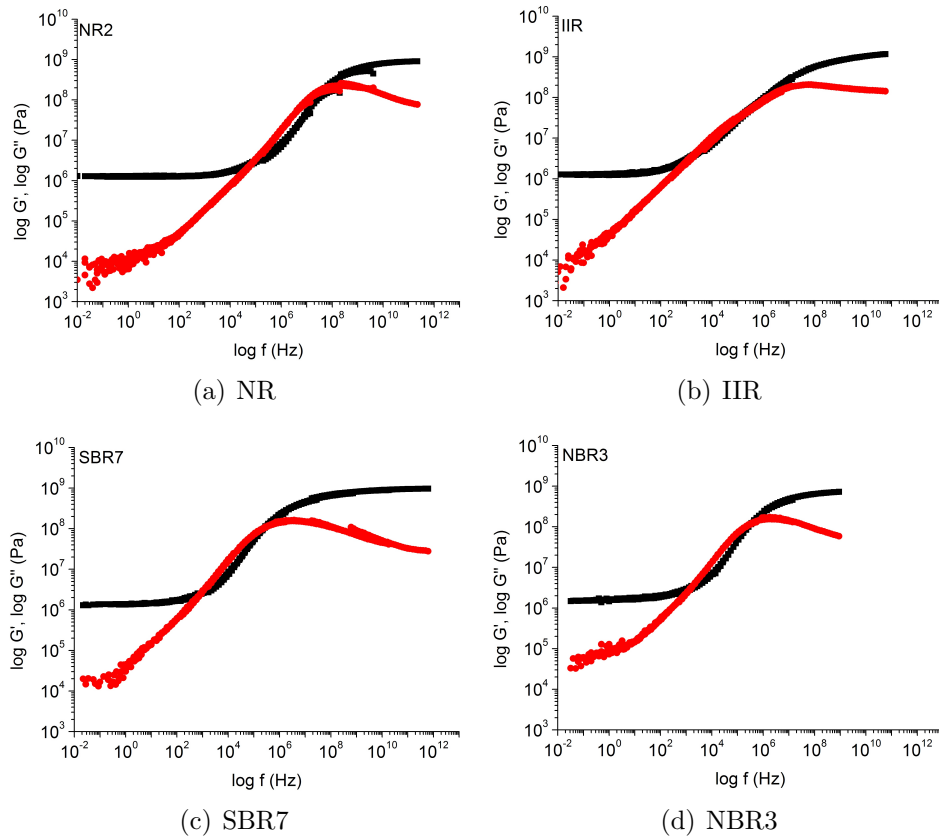


Figure 5.25: Master curves at 0.5% strain amplitude for unfilled polymers

given in Table 5.7.

Table 5.7: Frequencies of maximum dissipation.

polymer	frequency (MHz)
NBR3	1.8
SBR7	2.9
IIR	73
NR	219

This frequency is ascribed to the dynamic glass transition temperature and can be used to calculate this value.

Assuming that a shift in temperature is equivalent to a shift in frequency and vice-versa as it follows from the description of this phenomenon by the WLF equation (Equ. 3.50) than it is possible to reinterpret the entire shifting procedure either with regard to a given reference temperature or to a given reference frequency (say 0.5MHz, for

example). In the latter case from Equation 3.50 $f(T)$ it follows:

$$f(T) = f_{ref} \cdot 10^{-\frac{c_1 \cdot (T - T_{ref})}{c_2 + T - T_{ref}}} \quad (5.13)$$

This equation enables one, after a double (even triple) checked shifting procedure, to extract from the master curve a temperature sweep at literally any frequency required.

The possibility of obtaining a temperature sweep at any frequency can be useful in predicting other dynamic properties of polymers than the shear modulus, G^* . In section 3.2.2 Equation 3.73 shows the connection between the longitudinal wave modulus, the compression modulus and the shear modulus. It was stressed that a calculation of any of the modulus values requires the knowledge of the other two measured at the same frequency, preferably by different devices.

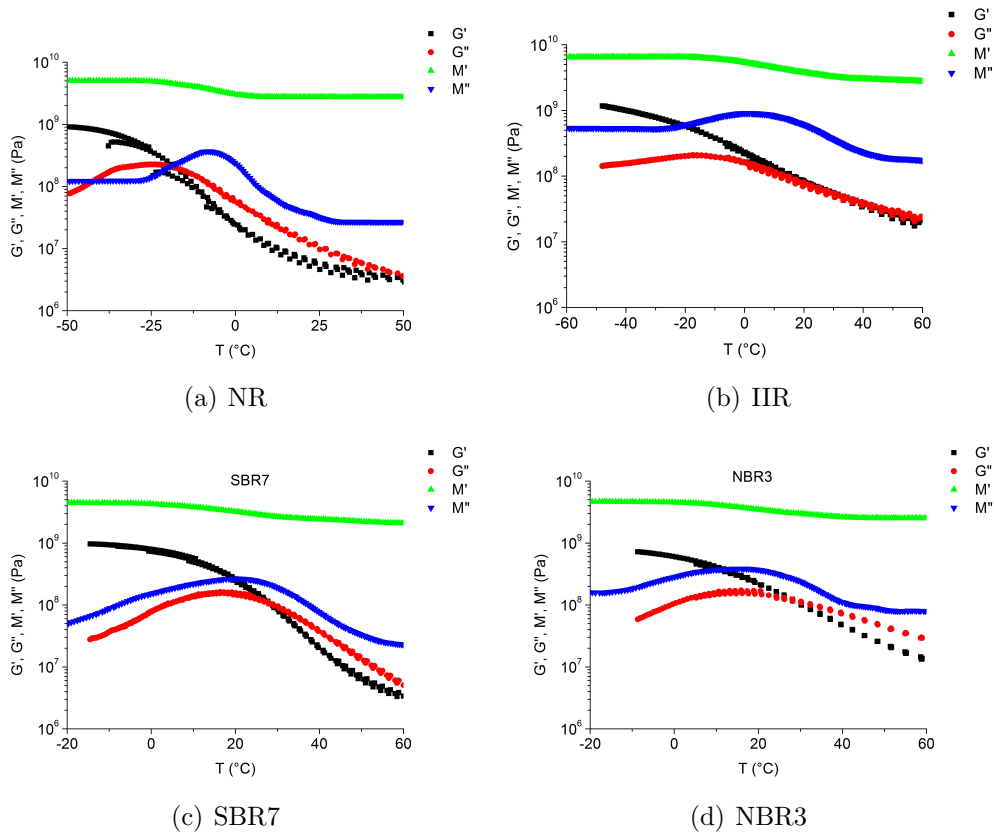


Figure 5.26: Shear and longitudinal wave moduli at 0.5MHz - WLF conversions

In Figure 5.26 an attempt is made, based on the assumed validity of the time temperature superposition principle [6, 8, 198], at combining ultrasonic measurements of the longitudinal wave modulus at 0.5MHz with shear modulus measurements at the same frequency derived from WLF-master curves with a purpose of obtaining the com-

pression modulus, K^* ¹. The knowledge of these three moduli enables the complete dynamic-mechanical characterization of a polymer. This would require that, after the shifting procedure is applied to the shear data, the recalculated curve for G'' , for example, is located beneath the M'' curve, having the maxima at the same temperature. Only then can it be assumed that the two moduli are based on the same molecular processes. As seen in the aforementioned figure, this occurs only in the case of SBR7 and NBR3 the two polymers that obey the requirements of a $5-6^\circ\text{C}$ T_g shift per decade of frequency. Other experiments not shown herein have proved that for all polymers displayed in Table 5.6 that obey the aforementioned requirements of T_g variation with frequency it is possible to perform such moduli calculations.

One interpretation of these differences could reside in the different molecular origins of the two moduli that are discussed above. It could be assumed that the shear modulus originates in long range chain movements which give rise to friction and hysteresis as they slide by one another, whereas the longitudinal wave modulus could be associated with short range, local movements. In this case it would be possible that some polymers show the same T_g s for the different moduli and in these cases it would be possible to calculate one modulus from the other.

There are several literature references where the molecular origin of the longitudinal wave and the shear moduli are thoroughly discussed.

Kono found evidence of an energy dissipating process associated with volume deformation taking place in PS and PMMA. The activation energies associated with shear deformation is different from that associated with volume deformation and the former is somewhat smaller than the latter which led him to imply that the molecular mechanism in the two types of deformation may be different [83].

Concerning the relationships between shear and bulk relaxation time or retardation time distributions, Knauss et al [199, 200] have more recently reported measurements of the bulk compliance of a PVAc (poly(vinyl acetate)) sample. The authors' comparison of these with shear compliance measurements on a different specimen of the same PVAc sample produced an indication that the breadths of the transition zones in bulk and in shear are closely similar but that the compression modulus transition is shifted to lower frequencies than the shear modulus transition.

On the other side, there are also authors [201] that have come to the conclusion that bulk and shear measurements have similar time-temperature shift factors and similar retardation spectra at short times which suggests that the molecular origin for bulk and shear responses are the same. Results from Bero and Plazek [202] as well as White and coworkers [203] come to support their findings.

¹The next section discusses the compression modulus and its estimation from pressure-volume-temperature measurements.

The results on the glass transition temperature presented in this work suggest a close connection between the WLF predictions and the copolymers of polybutadiene with styrene and acrylonitrile (in case of ACN content variation NBR1 behaves similarly to BR, IIR and NR i.e. it does not follow the WLF rule). Even if the mechanisms responsible for shear and bulk relaxations were indeed different, the implications on the applicability of the WLF assumptions are irrelevant as long as there is also a direct method, such as Ultrasonic Spectrometry, to measure the glass transition at the required frequency. As long as the T_g s correspond and the free volume considerations are correct, estimating the shear modulus at the checked frequency from low frequency data should pose no threat to the end application. If, however, the T_g s do not match, than it is possible that the predictions of the WLF equation are erroneous at this frequency and this is exactly the point where Ultrasonic Spectrometry can be of great use in estimating the correct dynamic-mechanical behavior in the MHz regime.

Clearly, in the case of the BR-copolymers the high frequency dynamic-mechanical properties predicted with the aid of the WLF equation match the direct results of the ultrasonic measurements. This correlation enables the use of equation 3.73 to simply calculate the compression modulus.

As a concluding remark it must be stated that, based on the results presented in this work and corroborated with the available literature as well as taking into consideration the wide array of polymers available, the sole use of the WLF equation to predict the dynamic-mechanical behavior of elastomer parts is bound to give erroneous results. The only possibility for a reliable interpretation of the dynamic-mechanical behavior resides with the use of at least one other comprehensive method, such as ultrasonic spectroscopy, which does give reliable information in a frequency range not available to the device used for the WLF evaluation.

5.6 Compression modulus

The correlation of WLF data with ultrasonic spectrometry measurements enables the determination of the compression modulus for several polymers, under the conditions described in the previous section. Such a determination would enable a complete dynamic-mechanical characterization of a material but it must be stated that it may be tainted by errors ascribed to the difficulties that come about when performing mathematical operations with data obtained from different measuring devices.

The compression modulus bears a different relation to the structure of an elastomer than do other elastic moduli. It is associated with short range and local structure and is only indirectly determined by longer-range polymer chain mechanics that are of central importance in determining tensile and shear properties. From a structural

standpoint, the bulk modulus may be considered to play a role that is complementary to the roles of shear and tensile moduli. Despite the importance of the compression modulus as a complement to the other elastic properties, it has been the least studied of the elastic properties of elastomeric solids. This is partly because of the practical difficulty in measuring this modulus with high accuracy [204] which resides in the necessity of applying the same constant pressure from all three spatial directions onto a rubber part.

As to the connection that exists between the different dynamic-mechanical moduli, Leaderman [205] suggested that intramolecular motions control the bulk modulus, while the shear modulus is governed by the intermolecular (intersegmental) dynamics. Bulk compression usually does not involve long-range conformational changes but rather a forcing together of the chain atoms. This is consistent with earlier findings by Roland et al [206] that the strength of the dielectric normal mode of polymers is insensitive to volume changes. They assume that the chains accommodate hydrostatic pressure by a reduction in interchain distances, with minimal change in the actual molecular (chain coil) size. Further it is suggested that the bulk modulus arises from intermolecular (inter-chain) interactions (van der Waals interactions) [207].

In Figure 5.27 the components of the complex longitudinal wave modulus at 0.5MHz and of the shear modulus at 1Hz are plotted as a function of the temperature. The former are calculated from the ultrasonic attenuation and velocity measured at 0.5MHz whereas the latter are estimated from the 1 Hz dynamic-mechanical measurements via the procedure discussed in the previous chapter.

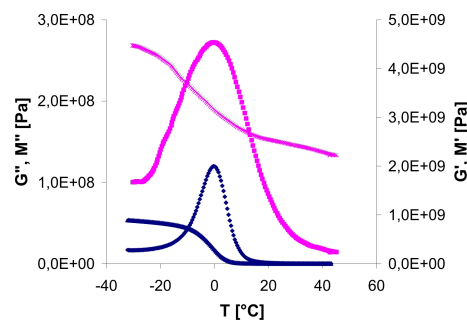


Figure 5.27: Shear (in blue) and longitudinal (pink) moduli at 0.5 MHz for SBR7

The plots show the higher values for the longitudinal wave moduli due to the presence of the compression modulus and, in the case of M'' , it can be seen that its values, especially above T_g are more than a decade higher than those of the M'' . The storage component

of the longitudinal wave modulus also contains the static compression modulus:

$$\begin{aligned} K^* &= K_{stat} + K_{dyn} \\ K_{dyn} &= K' + iK'' \\ K_{stat} &= \rho \frac{\partial P}{\partial \rho} \end{aligned} \quad (5.14)$$

A rough estimation of the static compression modulus K_{stat} yields a value of 2.2GPa at 40°C.

This modulus can also be evaluated from PVT (Pressure-Volume-Temperature) measurements. During such an evaluation the volume change of a sample is observed while the temperature is varied at three or more constant pressures. In this case the measurement was performed in a temperature range from 40°C to 100°C at three different pressures (20 MPa, 70MPa and 120MPa bar) on two SBR compounds, one unfilled and the other filled with 60 phr of carbon black. The samples were vulcanized in situ by subjecting them to 180°C and 20 MPa for 10 minutes, prior to the actual measurement.

The static compression modulus (Figure 5.28) can be calculated from these measurements by linear regression, where the negative inverse of the slope is the required value or by applying the following formula:

$$K = \Delta P \frac{V_1}{V_1 - V_2} \quad (5.15)$$

where ΔP is the pressure difference between the two measurements, V_1 is the volume at the first pressure and V_2 at the second one. In Figure 5.28 the modulus is calculated with the first method.

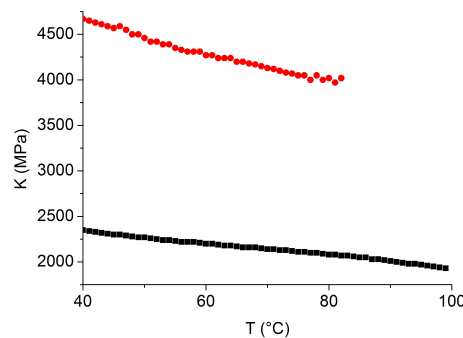


Figure 5.28: Static compression modulus
 black - unfilled
 red - filled with 60phr CB22

Physically, as the temperature is increased through the glass transition, the distance between the molecules is expected to increase. The resulting decrease in the com-

pression modulus may be attributed to the consequent decrease in the slope of the interatomic potential. This increase in volume also increases the molecular mobility, decreasing the resistance to shear. This leads to the situation where, as a glass is heated and softens, it becomes more compressible.

The static compression modulus at 40°C is 2.3 GPa which is in good agreement with the above estimation from the longitudinal wave modulus M' . The values of the static compression modulus for the unfilled polymer are in the same range as stated in the literature [208].

It is therefore possible, albeit technical issues, to give a good estimation of the compression modulus by using data obtained from two different measuring techniques both for unfilled and filled polymers. The main source of errors lies, in this case, in the estimation of the high frequency shear modulus from low frequency measurements. As it was shown in chapter 5.5, the procedure based on the time-temperature superposition principle was not always successful in estimating the glass transition temperature at 0.5MHz as measured by ultrasonic spectrometry.

5.7 Influence of processing parameters

During the mechanical processing especially during mixing some long chain polymers suffer a significant decrease of the average molecular weight. The reason for the chain break down is related to the entanglement density of the polymer melt and the self diffusion of the chains which determines the characteristic relaxation times. In case of polymers with a very high molecular weight the breakdown of chain length and reduction of viscosity facilitates the incorporation of nano-scaled fillers. Due to the very high viscosity of filled polymer melts the addition of plasticizers becomes necessary. This group of ingredients generally increases the free volume of a polymer mixture and reduces the glass transition temperature. All these mentioned processes can affect the dynamic-mechanical behavior of the resulting network. In addition the efficiency of the crosslinking process leads to a reduction of chain mobility. The influence of these overlapping processes on the polymer have never been investigated in the high frequency range.

The parameters regarded herein are the influence of molar mass, plasticizer and crosslinks on the dynamic-mechanical properties in the dynamic T_g regime and the energy dissipation. These effects are analyzed for the model polymers SBR and NR.

5.7.1 Molar mass

The dynamic response of NR masticated for an increasing sequence of time on a two roll mill which should yield a reduced average chain length is considered in this section.

According to [209, 210] the energy supplied to the extended rubber chains during mechanical deformation is sufficient to cause homolytic chain scission. The main factors responsible for this behavior are the entanglements of the polymer chains which give rise to large tensions near the central portions of the molecules [211]. It was also demonstrated that during mechanical mixing the molecular weight is reduced to the half [212].

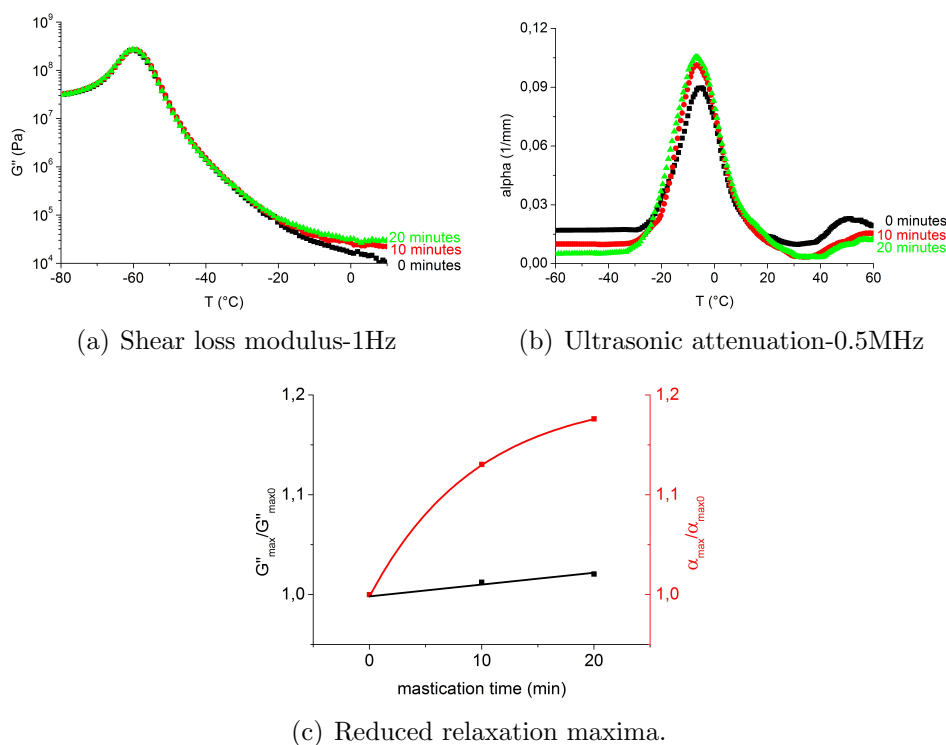


Figure 5.29: Influence on the molar mass of NR on the dynamic mechanical properties.

The masticated samples with decreasing chain length and melt viscosity were crosslinked under identical conditions. The mastication of the NR compounds shows close to no difference in the dynamic-mechanical shear modulus at temperatures in the range of the glass transition temperature (-60°C) at 1 Hz. The effect of 10 and 20 minutes of mastication decrease T_g by approximately one degree (see Figure 5.29(a)). Correspondingly the maximum of the $G''(T)$ curve is slightly shifted to lower temperatures.

In the rubbery regime, a clear ranking of the differently milled compounds can be noticed with the longest time showing the highest loss modulus. Both the G'' increase

in the rubbery region and the dissipated energy in the transition zone are related to the increase of free chain ends as a result of chain scission. Because every free end has a larger free volume than the corresponding segment in the middle of the chain, a crosslinked network with a larger number of free chain ends will have a greater free volume and can demonstrate more intensive flow processes and energy dissipation.

The effects noticed in the attenuation curves (Figure 5.29(b)) are mostly an amplification of what could be observed at low frequencies. The maximum of the attenuation is shifted 2 degrees to lower temperatures for the longest mastication time. Also the amplitude of the attenuation, which quantifies the energy dissipation at 0.5 MHz, is increased as a result of the higher content of free ends in the network which contributes to energy dissipation.

Beyond the glass transition temperature in the rubbery region the similarities with the low frequency measurements are no longer at hand. The presence of impurities or oligomeric residues play a stronger role at high frequencies and the prolonged milling apparently reduces their effect on the total attenuation which can be observed by the reduction of the peak around 50°C.

Figure 5.29(c) shows a comparison of the reduced attenuation and the reduced loss modulus maxima. The lines drawn are to be regarded as guidelines for the trend. The actual values for the attenuation coefficient seem to stabilize to a plateau.

5.7.2 Plasticizer

In order to improve the processability of rubber compounds and to increase chain flexibility in the T_g region low molecular weight substances are added to the compounds under consideration.

In a polymer the segmental motions and their temperature dependence are determined by intermolecular and intermolecular interactions which are responsible for flow properties and internal friction between different chain units. The effect of plasticizer is based on the increase of the free volume that can significantly reduce interactions between polymer chains and enables cooperative translational chain movements to an extent dictated by the plasticizer concentration and its solvating ability [213]. A technical mineral oil which is a complex mixture of hydrocarbons with paraffinic, naphtenic and aromatic species was used to investigate this effect in SBR7.

In Figure 5.30(a) the effect of plasticizer addition on mixes with SBR7 is presented. In the low frequency range the major effect of the plasticizer is the change in energy dissipation as a result of the increased free volume or reduced friction between polymer chains. The effects of these processes are macroscopically expressed by a shift of the

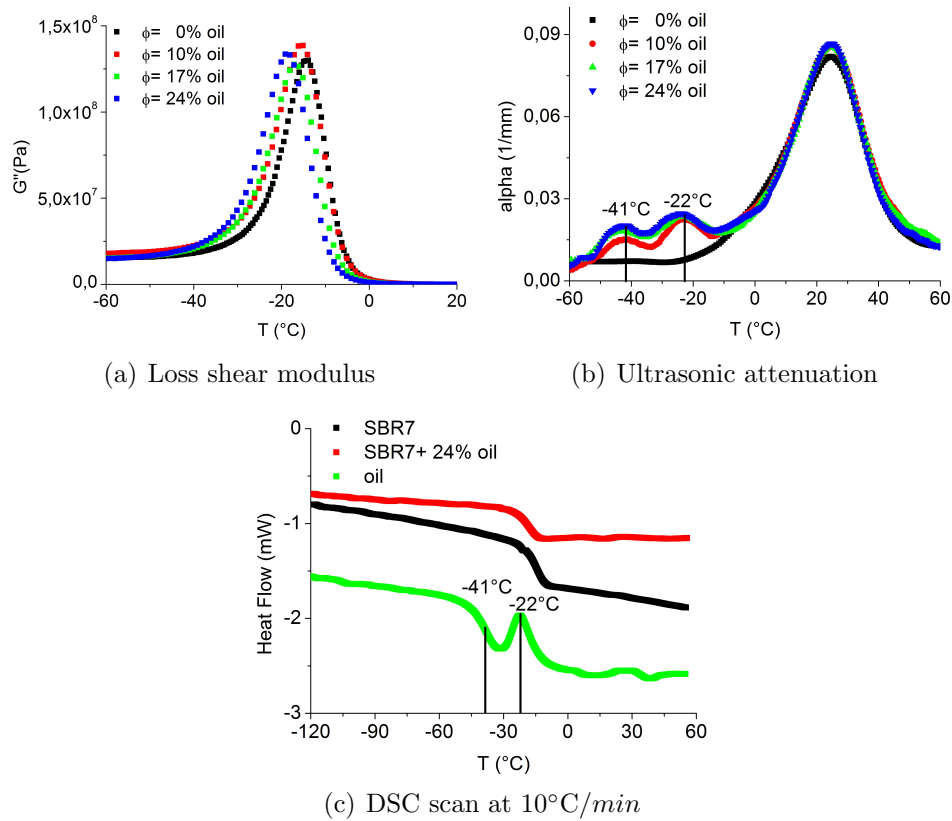


Figure 5.30: Plasticizer effect on SBR7.

relaxation peak to lower temperatures. A change in the amplitude of the loss peaks is also noted but it does not seem to vary systematically with the oil content in the low frequency curve. The change of T_g with oil addition sums up to 5 degrees for 24% oil as detected by the low frequency measurement (Figure 5.31).

Differently from the low frequency range the ultrasonic attenuation in the glass transition region shows an overall increase in the amplitude maxima with the oil addition but not further with higher concentration. Surprisingly, the shift of T_g provoked by the mineral oil is not significant ($\Delta T_g = 0.5^{\circ}\text{C}$). This result contains an important statement for the contact mechanics of SBR compounds which reads that the friction and traction properties at high frequencies are not influenced by the oil content.

The main difference that occurs in the temperature dependence of the attenuation coefficient are two well resolved peaks below the glass transition, at -41°C and at -22°C . As they do not appear in the pure material it can be assumed they are generated by the oil. The scan in Figure 5.30(c) (green curve) shows a pour point corresponding to the first peak (-42°C) followed by a second transition (-22°C). The fact that these transitions are found with both methods at the same temperature suggests the corresponding processes (similarly to the crystallization process in BR) to be generated by

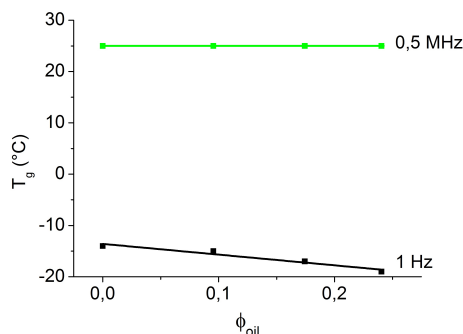


Figure 5.31: Plasticizer effect on glass transition temperature in SBR7 at 1 Hz and 0.5MHz.

phase transitions of hydrocarbons with larger π electrons interactions (i.e. aromatics). A small transition can also be seen around 30°C but in the ultrasonic measurement this would be masked by the glass transition. The fact that these transitions can not be observed in the low frequency measurements is another proof of the sensitivity and specificity of the ultrasonic method.

5.7.3 Crosslinking density

Two groups of polydiene networks (NR and SBR) produced by crosslinking with an increasing amount of sulfur were investigated. In both cases the crosslink density of the networks increases linearly with the molar concentration of sulfur.

Figure 5.32 displays the storage and loss components of the complex shear modulus as a function of the sulfur dosage used for crosslinking. Furthermore, the energy dissipation in the rubbery region (G'') which is related to the energy dissipated by the freely mobile chains and chain ends, shows a decrease with increasing the sulfur content. The storage modulus, which is a measure of the elasticity or strength of the network, shows a marked increase for both polymers. This is a clear indication that, as the sulfur content (at constant accelerator content) increases, the network chains become smaller and the chain mobility is reduced. Due to this the internal pressure of the system gets increases and the retractile forces or the modulus especially is increasing. Complementary to these effects the viscous flow is restricted and the loss modulus is decreased. However, the width of the G'' peak increases with the crosslink density. This is probably due to the presence of heterogeneous micro regions which relax over a range of temperatures; the width of such temperature interval increases with the crosslinking.

Figures 5.32(a) and 5.32(b) indicate similar effects of sulfur addition on the dynamic shear moduli at 20°C in the rubbery region, in NR and SBR.

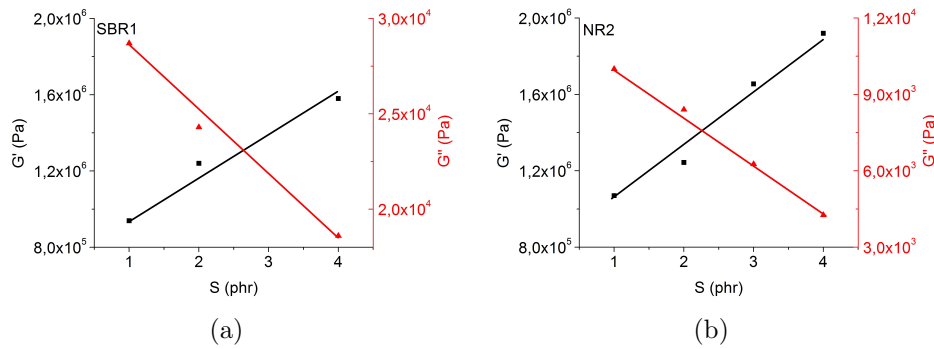


Figure 5.32: Shear modulus of SBR1 and NR2 mixes with different sulfur contents at 20°C

The ultrasonic attenuation curves, displayed in Figures 5.33, show primarily results that are consistent with the low frequency characteristics. The increase of the sulfur content induces in SBR and NR a significant shift in T_g towards higher temperatures and a decrease of the attenuation maxima.

The reduction of the attenuation maxima can be associated with the decrease of the concentration of free chain ends and consequently with a less dissipative process per unit volume. At the same time the attenuation in the rubbery region is slightly increased, at least in the temperature range available to the ultrasonic technique.

With a similarly high resolution, in the case of NR2 (Figure 5.33(b)) the attenuation maxima demonstrate the T_g shift, the decrease of the attenuation maxima and differences in the attenuation in the rubbery region. The peak at 50°C, seen also in Figure 5.29(b) is lowest at the highest sulfur to accelerator ratio suggesting an influence of the crosslinking density on the dynamic response of the oligomeric rests present in NR as well.

The ultrasonic velocity (Figure 5.33(c) 5.33(d)) which is a representation of the energy stored by the polymeric matrix at 0.5MHz, shows an increase with the sulfur content even in the glassy state, and in the rubbery state as well. This significant effect is connected with the increase of the density and the free volume of the polymeric matrix as a result of crosslinking.

Supplementary, the glass transition temperature is shifted significantly with the sulfur concentration as a direct consequence of the reduced mobility and the particular density of the matrix.

The fact that such effects are detectable by ultrasonic spectroscopy was the result of several improvements of the method and the data acquisition. Using this technical level it would be possible to develop an analytical tool for online monitoring the crosslinking density in thin sheets and membranes.

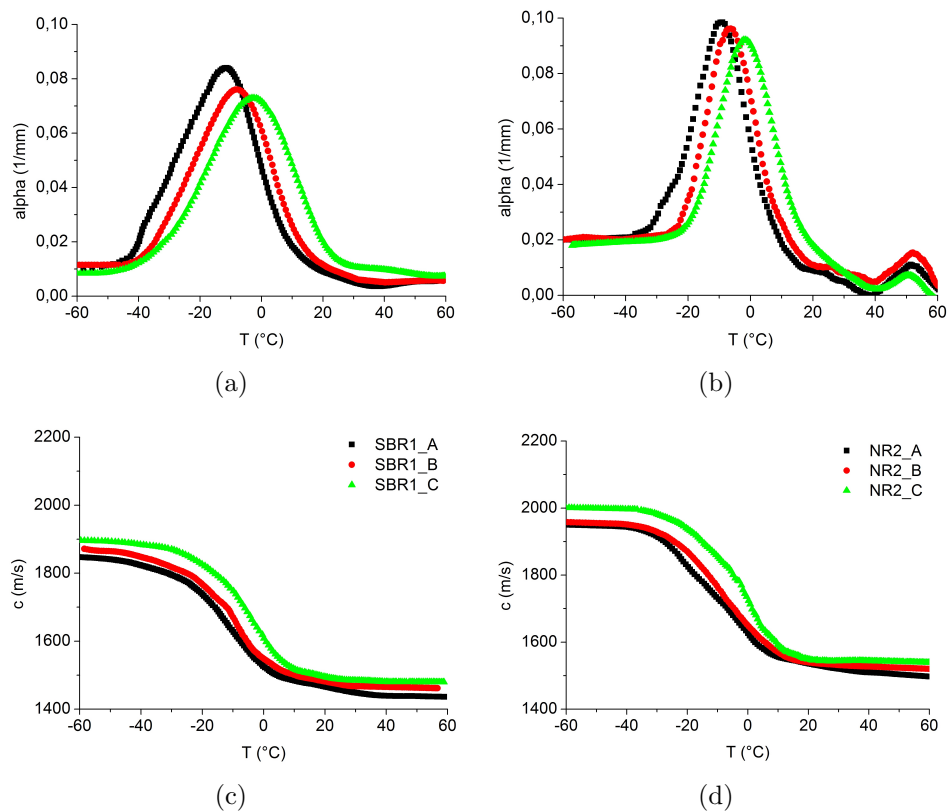


Figure 5.33: Ultrasonic measurements of SBR1 and NR2 mixes with different sulfur contents

5.8 Polymer blends

Blending of elastomers is often used to combine the properties of original polymers or to achieve new properties and, thusly, enhance the performance characteristics of rubber products. The immiscible nature of most polymers leads to a heterogeneous blend morphology with domains that demonstrate the physical properties of the polymers under consideration. Ascribed to the high chain length of the polymers the mixing entropy is small, but in any case negative. This immiscibility is a consequence of the small positive enthalpy that exceeds the limited increase in positional disorder. In the absence of any physical reactions¹ between the respective chain units the intermolecular forces are Van der Waals type interactions [214]. The prediction of miscibility is based on the combinatorial entropy and the polymer-polymer interaction parameter which describes the contribution of the mixing enthalpy. Due to the fact that the combinatorial entropy can be calculated from the blend composition and the degree of polymerization of the constituents the difficulties in the prediction of miscibility

¹e.g., hydrogen bonding, complex formation or charge transfer

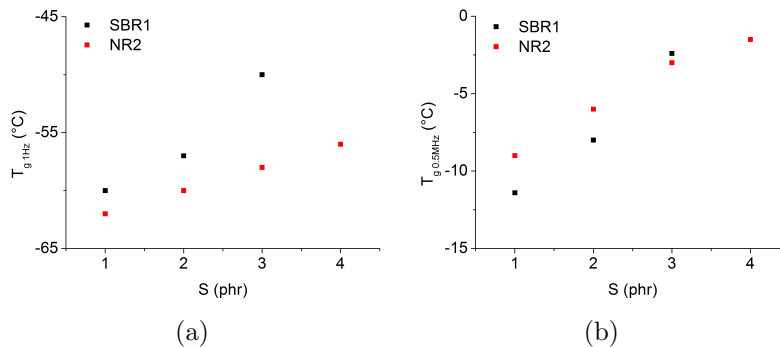


Figure 5.34: T_g variation with crosslinking density.

arises from the polymer-polymer interaction parameter which has to be determined experimentally. An estimation of it can be made based on the solubility parameter introduced by Hildebrand and Scott [215–217]. This parameter is defined as the square root of the cohesive energy density (molar energy of vaporization H_v /molar volume equation V_m 5.16).

$$\delta = \sqrt{\frac{\Delta H_v - RT}{V_m}} \quad (5.16)$$

The solubility parameter of a polymer is usually obtained experimentally, i.e. by determining the solvent which swells the polymer most or by using inverse gas chromatography. The polymer is then considered to have the same solubility parameter as that of the solvent. If data are available on the interaction parameter in several solvents for the polymer in question, the solubility parameter of the polymer may be estimated by determining the solubility parameter of the solvent for which the interaction parameter is lowest. The values of the solubility parameters for the rubbers used in this section are displayed in Table 5.8 from references [208, 218].

Table 5.8: Solubility parameters.

	BR1	NR2	SBR6	SBR7
$\delta(J/cm^3)^{\frac{1}{2}}$	17.52	16.7	17.65	17.78

According to theoretical models the interfacial tension is proportional to the square root of the interaction parameter or to the difference of the solubility parameters. Therefore the solubility parameter difference indicates the degree of incompatibility. For the polymers indicated in Table 5.8 the following sequence of increasing incompatibility is predicted:

$$\Delta\delta_{SBR7:BR1} < \Delta\delta_{SBR6:NR2} < \Delta\delta_{SBR6:NBR3}$$

It is expected that the discrete domains of the blend constituents increases in the

same order.

This section deals with the dynamic mechanical properties of several, industrially relevant, elastomer blends isochronically measured at 1Hz and at 0.5MHz. Firstly, mixes of SBR6, containing 25% vinyl groups, and natural rubber, in concentration ratios of 0/100, 20/80, 40/60, 50/50, 60/40, 80/20 and 100/0 are analyzed. The sensitivity of the two methods in detecting the separate phases are discussed.

Secondly, solution SBR is mixed with NBR (in concentration ratios of 0/100, 20/80, 40/60, 50/50, 60/40, 80/20 and 100/0) which yields blends where the interfacial tension is higher and correspondingly the interface is greatly reduced due to the polarity difference of the two rubbers.

Lastly, two rubbers typically known to be relatively compatible as the difference in solubility parameters is small, SBR7 with 50% vinyl and BR1 are blended.

The morphology of the mechanically mixed blends has been investigated by using transmission electron microscopy. In Figure 5.35 the micrographs of the SBR:NR and SBR:NBR blends are shown, demonstrating a heterogeneous phase morphology.

The micrographs underline the co-continuous phase morphology and their relatively even distribution in the composite.

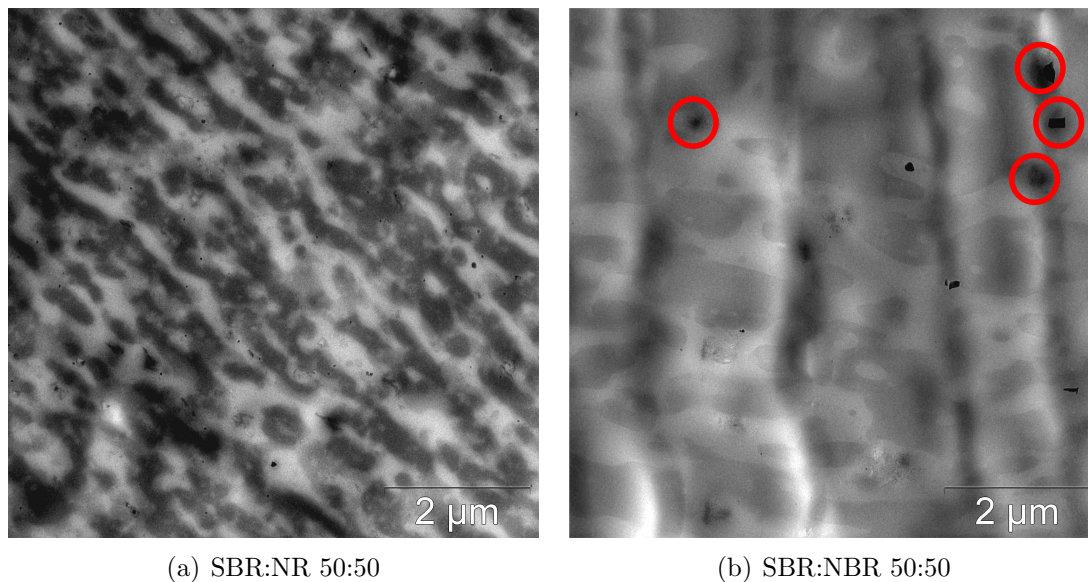


Figure 5.35: Transmission electron microscope pictures of SBR:NBR, SBR:NR blends

The dark domains in figure 5.35(a) are associated with the NR phase. The two phases are clearly distinguishable but the size of the domains is relatively small.

The differences in polarity on top of the large $\Delta\delta$ led to the occurrence of a heterogeneous morphology consisting of dark dispersed NBR regions (figure 5.35(b)) of approximately $0.5\mu\text{m}$ to $4\mu\text{m}$ in the continuous SBR matrix. The very dark spots, denoting areas of high electron density, are ascribed to ZnO crystals and the waviness of the SBR:NBR to difficulties in the process of cutting the deep cooled sample in the microtome.

The discussion sets forth with the dynamic-mechanical analysis of SBR6:NR2 blends. A first glimpse at the shear data in the low frequency range ascertains that the two polymers are immiscible but for the SBR:NR 20:80 (Figure 5.36).

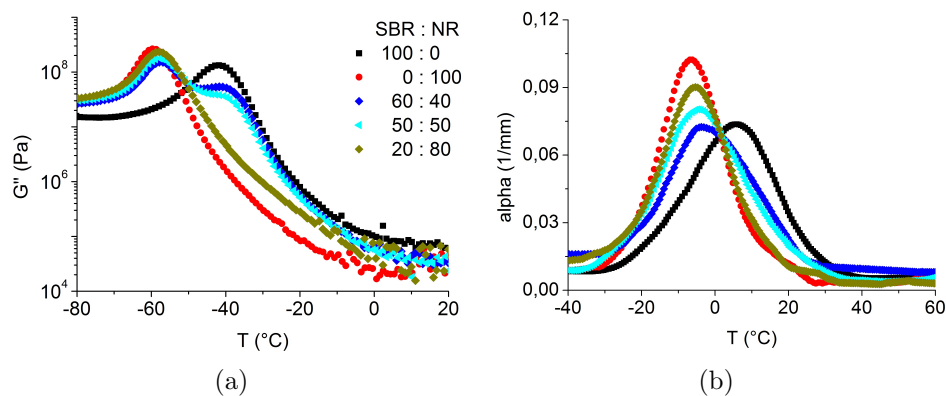


Figure 5.36: Shear modulus and ultrasonic attenuation of the SBR:NR blends.

An estimation shows that about 17 percent of the SBR is apparently soluble in the NR forming a single phase signal. However, according to the difference between the solubility parameters the two polymers should be incompatible. However, the dynamic - mechanical measurement at 1 Hz does not distinguish 2 phases below 17% of SBR because of the resolution limit of the method. The presence of a low concentration of SBR6 in the mix and the immiscibility of the two phases leads to the formation of small regions of SBR6 within the NR2 matrix. The increase of the low frequency modulus above the T_g of NR can be expected to occur due to the glassy SBR regions acting as a non-reinforcing filler, so due to hydrodynamic reinforcement. A higher concentration of SBR6 leads to the formation of a co-continuous phase “network” and a second peak is noticed.

The difference between the transition temperatures of the 2 peaks is reduced, ascribed to the different activation parameters of the involved phases, from 18°C at 1 Hz to 14°C at 0.5 MHz. The highest energy dissipation is shown by the raw NR. With the addition of SBR the height decreases while the broadness of the peaks increases slightly. The most challenging observation is the fact that in the high frequency range the bimodal damping signal does not appear at all. The increased width of the $\alpha(T)$ curves and the

shoulder indicate the heterogeneity of the blends. Phenomenologically only one glass transition temperature (due to the high frequency only one peak is seen for all mixes) is observed that does not change significantly until 80 parts of SBR are added when it shifts close to the SBR temperature at 0.5 MHz. Seen from the right to the left, the addition of 20 parts of NR into SBR determines, similar to the addition of SBR in NR, a decrease in the maximum dissipated energy and a broadening of the peak. The joining closer together and the higher broadness of the peaks is a well known effect of the increase in frequency. The macromolecular chains have less time to slide past one another as the excitation frequency increases, therefore they appear to be stiffer leading to higher T_g s and lower energy dissipation.

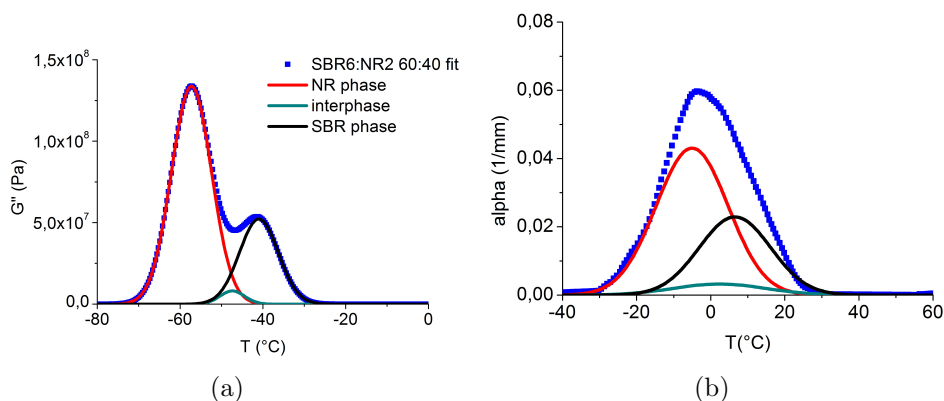


Figure 5.37: Fit of the separate polymers' contribution.

A trial was performed to evaluate the influence of the polymers in a 60 SBR6 to 40 NR2 blend by a deconvolution procedure (Figure 5.37). The resulting Gaussian peaks, obtained after a baseline was subtracted from the original and the maxima were chosen taking into account the second derivative of the original peak, show accurately the stronger influence of the NR phase as well as a relatively low third contribution which could be associated with the interface. A fit of a chosen mixture reveals approximately 4% of the total area which can only be assigned to the interphase that is formed. The fit of the blend for the 0.5MHz measurement using the same procedure was less successful due to complications that arose as a result of the different shifting of the peaks with the frequency change. Even so it is seen that the two larger peaks which can be ascribed to the two phases - SBR and NR - cannot alone account for the complete surface of the curve. The rest of the surface can therefore be ascribed to the interphase that forms between the two rubbers in the blend.

The effect of the heterogeneous phase composition on the glass transition temperature(s) is influenced by the morphological characteristics of the mix. The shift of T_g of the NR2 phase with increasing SBR concentration is more pronounced than that of its corresponding SBR6 phase, a characteristic feature which is seen both in low and high

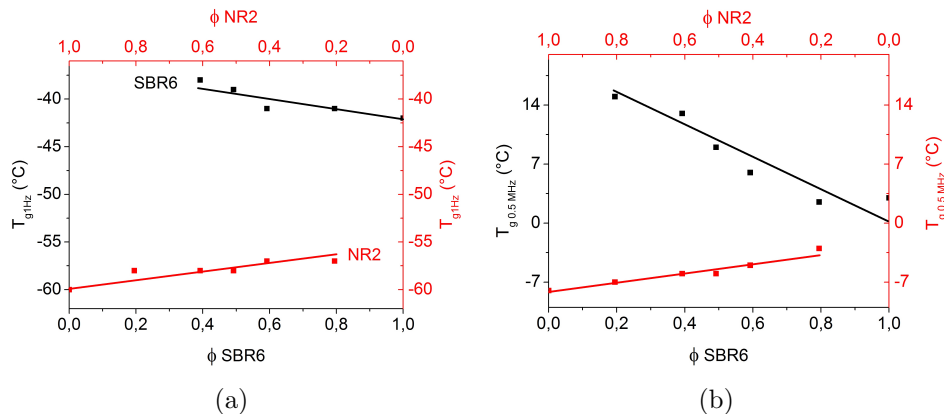


Figure 5.38: T_g shift of the individual phases.

frequency measurements (Figure 5.36 and 5.38). The phase displaying the lowest T_g begins its transition first and in most cases, the second phase is still in a glassy state acting as a filler. The increasing concentration of the second phase, on the other hand, leads to the formation of a cocontinuous morphology and finally to a phase shift. In the case of the first phase (i.e. in this case NR6) the amount of free volume available for chain movements will constantly decrease as it is taken up by glassy regions of the second phase (SBR6) leading to a shift of the T_g . This should happen regardless of phase compatibility but it must be augmented by it. From the other direction, as more NR2 is added to SBR6, the latter is “filled” with a soft, viscoelastic, phase and in the absence of phase compatibility its T_g should not be dramatically affected.

The dynamic mechanical properties of SBR6:NBR3 blends are shown in figure 5.39 at 1Hz and 0.5MHz. Compared to the SBR6:NR2 blends, the characteristic T_g shift of the individual phases towards each other is not noticed. Furthermore, ascribed to the polarity difference between the constituent polymers, the individual phases are clearly visible at both frequencies. In the high frequency range the formation of shoulders in the $\alpha(T)$ curves becomes evident.

As at the beginning of this section the miscibility dependence of two polymers on the difference between their solubility parameters was emphasized, not taking into consideration the effects crosslinking has on the actual dynamic response of the compound. While studying SBR/BR and NR/BR blends, Fujimoto [219] and Corish [220] demonstrated the development of an interphase crosslinking that occurred within the blends, which cause a merging of the dynamic-mechanical loss peaks, characteristic of the individual polymers. Separate loss peaks, which were observed in uncured blends of the polymers, combined upon progressive vulcanization to provide a pseudo single phase system, a mechanically compatible blend. A fit of the dynamic mechanical loss modulus reveals a small contribution of 1% of interphase, of the total fitted area.

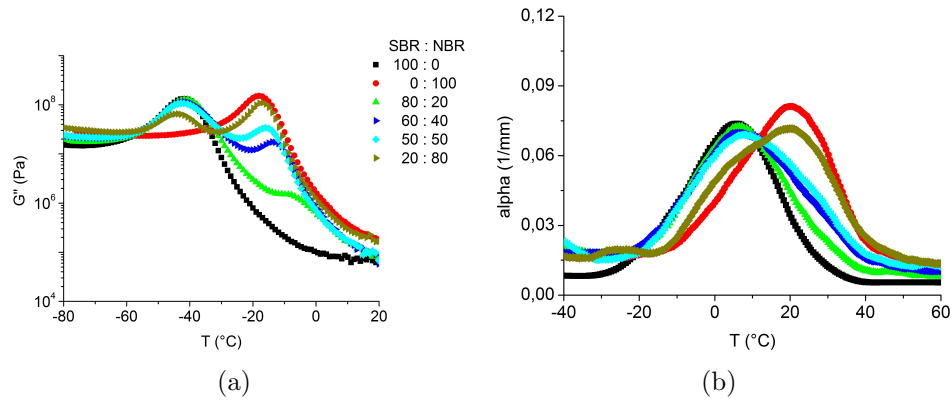


Figure 5.39: Shear modulus and ultrasonic attenuation of the SBR:NBR blends.

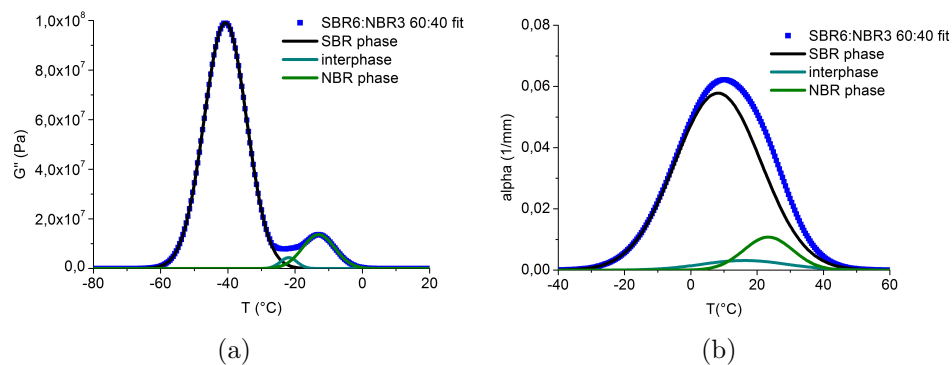


Figure 5.40: Fit of the separate polymers' contribution.

The rest of the curves also show a hint of a shoulder (due also to the low resolution of the measuring device) indicating the presence of an immiscible phase. The relatively close proximity of the The displacement of the NBR shoulder to the right, compared to the clean NBR compound (red curve), could indicate a preferential migration of the crosslinking chemicals, during the mixing process, into the NBR phase.

Differential distribution of vulcanizing agents such as sulfur, and accelerators in a sulfur cure system and peroxide as well as co-agents in a peroxide cure system is possible in elastomer blends, particularly when the two elastomers differ in the concentration of reaction sites such as degree of unsaturation and polarity. This is because sulfur, peroxide, and most accelerators are polar in nature and are likely to partition preferentially into the polar phase [221]. Gardiner [222] noticed that curatives such as sulfur, TMTD, MBTS and DOTG migrate from compounded rubbers to uncompounded ones and between compounded rubbers from those with low unsaturation to the ones with high unsaturation even if the initial concentrations are equal. Furthermore, he demonstrated that whereas sulfur distribution from NR to SBR occurs gradually, from NR to IIR is sharp at the interface. This is due to large differences of sulfur solubility

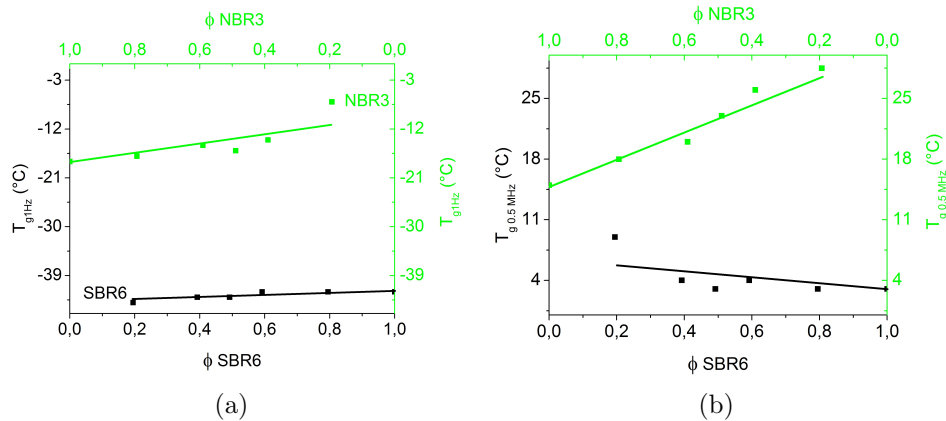


Figure 5.41: T_g shift of the individual phases.

in NR and IIR compared to that in NR and SBR. MBTS diffusion follows the same trend. However, the difference in distribution is smaller because of the smaller diffusion rate contributed by its larger molecular size. This imbalance in sulfur and accelerator concentration can lead to over and under cure of the phase and to an inhomogeneous network with respect to network density (see figure 5.42).

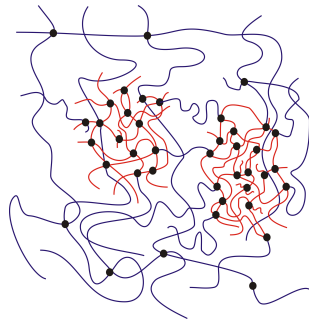


Figure 5.42: Crosslinking in two phase polymer blends
 red - polar phase
 blue - non polar phase
 black dots - crosslinking sites

The relativity of such observations is underlined by Schaper [223] who performed several calorimetric measurements on BR/SBR blends, in an uncrosslinked state, and noticed the different glass transitions ascribed to the two distinct phases. Since after vulcanization, in the same proportions, there was only one distinct peak still to be observed, he concluded that the appearance of only one peak in the vulcanized state is not to be associated with the formation of one single phase but, most likely, with the *freezing in* by crosslinks of the amount of interphase formed during mixing whose energy dissipation is higher than that of the individual phases.

The case displayed in figure 5.43(a) is that of two polymers which seem compatible

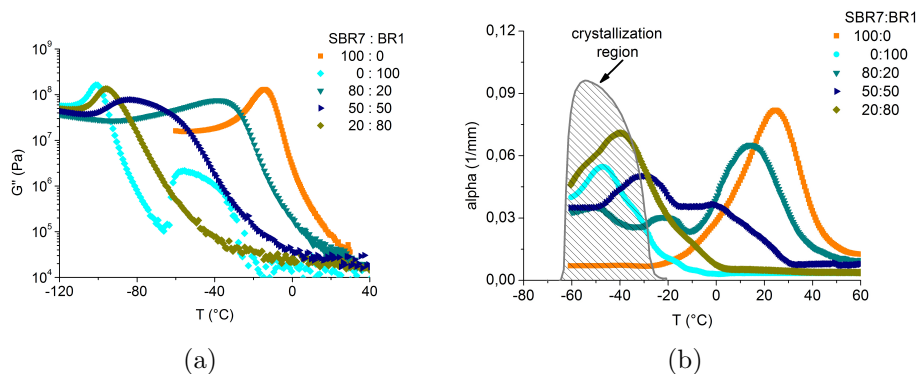


Figure 5.43: Shear modulus and ultrasonic attenuation of the SBR7:BR1 blends.

as quantified by the dynamic mechanical measurement at 1Hz. Considering also the above explanation, it is reasonable to admit that an originally fairly fine heterogeneous state that occurred upon mixing was locked in by co-crosslinking - the formation of polysulfidic bonds between the chains of different polymers. In this case, under an externally induced excitation the motion of the individual chains would interfere with each other and as a whole they would have an average motion observed as the response of a homogeneous compound.

Blends of SBR7 and BR are known to be more compatible than the other ones discussed in this work. The same conclusion can be drawn when looking at figure 5.43(a) where only one transition is seen for each concentration. It was also shown, in the same chapter, that the ultrasonic measurement at 0.5MHz can tell little about the different phases even in known incompatible blends due to the broadening of the transition peaks with increasing frequency which overlap reducing, therefore, the resolution. However, having seen that ultrasonic waves seem to be relatively sensitive to the presence of crystallites in the matrix, it is of interest to investigate this in such a blend where, due to the formation of an extensive interface, the BR peak is expected to wander more to the right leaving any remaining crystallites exposed as another transition.

The curves shown in figure 5.43(b) are representative for these blends and the rest reflect the same concept. Firstly it can be stated that both phases are clearly represented in all mixes clearly as a consequence of the large temperature difference between them.

In the case of blends in which one of the partners is able to crystallize can provide additional information on blend miscibility being known that rates of crystallization depend on the amount of diluent present in homogeneous systems [224] and on particle size in nonhomogeneous systems [225], provided the different phases can be discerned by the testing method. It is seen in figure 5.43(b) that already at 20 phr the BR phase is very present at -18°C . At 50 phr the SBR phase is represented by a pronounced shoulder around 0°C and the BR appears to be the matrix.

Perhaps the most interesting of the curves in figure 5.43(b) is the one for the 20:80 blend. The attenuation of the BR phase is clearly higher than that of the raw polymer, even if only 80phr of it were added in the mix. One can argue that this is ascribed to the presence of the BR crystallites in spherulitic form, which is causing scattering of the ultrasonic waves. On looking closer at the crystallization region depicted by the low frequency storage modulus as a hashed area, it is obvious that the crystallites are completely melted at -25°C where the attenuation is still higher than for normal BR. An explanation for this is the different heating ramps used in the DMA measurement and the ultrasonic one. It is known that the cooling and heating rate can have a strong effect on the formation and size as well as on the melting of crystallites. Collins and Chandler [226] performed extensive measurements on BR, concerning the crystallization and recrystallization processes and they noticed that with increasing heating rate the crystalline transition region became smaller. In the case presented in this work, the DMA and ultrasonic cooling rates were similar, whereas the heating rate was $1^{\circ}\text{C}/\text{min}$ for the DMA and $0.3^{\circ}\text{C}/\text{min}$ for the ultrasonic apparatus therefore it is possible that crystallites are still present in the mix and they cause the strong attenuation.

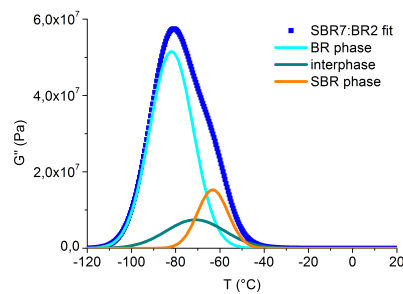


Figure 5.44: Fit of the separate polymers' contribution.

Following the same procedure as for the other blends, a fit of the individual phases known to be present in the blend was performed for the 1Hz measurement. The 0.5MHz measurement was not fitted because it is not certain to what amount the crystallites are present in the BR phase.

At 1Hz the better compatibility of these polymers is confirmed by the presence of an amount of 20% of in the 60 : 40 blend.

A further estimation of the variation of the glass transition temperature of the individual phases would be imprecise due to the good compatibility of the constituent phases.

The investigations contained in this section were centered on the dynamic-mechanical properties of rubber blends 1 Hz and at 0.5 MHz. The estimation of these properties at frequencies up to 1000 Hz is usual and poses little difficulties. The high frequency analysis is usually performed, when no devices are available that can measure in that

range, by using theoretical approximations such as the time-temperature superposition principle. This principle, however, does not apply for materials composed of two or more phases with different glass transition temperatures due to the overlapping of their activation processes. Such materials are termed *thermorheologically complex* materials. Ultrasonic spectrometry is one of the few methods which can directly measure the dynamic-mechanical properties in the MHz range.

It was shown for 3 different blends that the evaluation of the ultrasonic attenuation can reveal useful information about the energy loss at 0.5MHz and the location of the glass transition of the different phases. It was also shown that blends of materials with T_g s separated by less than 30°C are detected by ultrasound as composed of a single phase. Also if one of the components contains crystallites, as in the case of SBR:BR blend, the ultrasonic method was able to detect three different peaks, ascribed to the two rubber phases and to the crystalline regions.

5.9 Influence of inactive fillers

This section is concerned with the effects that the addition of elastic¹ inclusions, other than active fillers² has on the ultrasonic attenuation and velocity values. The goal was to investigate, without being exhaustive on the matter, the influences of inclusions that overshoot, in size, the one hundredth of a wavelength critical value beyond which Rayleigh scattering occurs (see paragraph on wave scattering in section 3.2.2).

In this section trials with SBR7 and BR1 are run to investigate the effect of elastic inclusions of known approximate size in the ultrasonic waves. To this purpose, glass spheres of two different diameters (40 microns and 180 – 220 microns) are used as fillers. As the glass spheres do not melt during the measurements, like the crystallites do, it is interesting to see how their presence affects the ultrasonic attenuation over the entire temperature range of the measurement.

It was previously said that the ultrasonic measurement is based on the absorption of energy from the longitudinal wave and its subsequent conversion into heat as a result of typical hysteresis phenomena associated with the viscoelastic response of the polymer matrix. In this case we speak of *damping*. The broader term, which signifies the actual difference between the emitted energy and the received one and which is based on several other phenomena besides viscoelastic loss, is the *attenuation*.

¹In the sense of the Maxwell or Kelvin-Voigt element, i.e. a body which does not dissipate energy, like the spring.

²Active fillers are nanosized particles which added to a polymer matrix induce reinforcement through physical and chemical filler-polymer interactions.

When the incident wavelength is sufficiently large compared to the particle radius, the viscoelastic loss dominates the overall attenuation in the composite, and the composite attenuation decreases as the particle concentration [227]. However, if the particle size exceeds a hundredth of the wavelength, the so called Rayleigh scattering occurs [76]. As a result, the attenuation will increase especially above the glass transition of the polymer. This happens because the impedance (see chapter 3.2.2) of the matrix in the glassy state resembles that of the elastic inclusions whereas in the rubbery region it changes as a result of the matrix becoming softer.

The addition of glass spheres, regarded as "inactive" fillers, would be expected to determine only minor changes in the damping, perhaps to lower values due to their elastic nature¹ as was the case for BR1 in Figure 5.11(d). The results in Figure 5.45 show an entirely different picture, as the attenuation values are clearly above those of the unfilled polymer. As the interactions with the polymer matrix are considered to be relatively weak, the only plausible explanation for the attenuation increase is scattering.

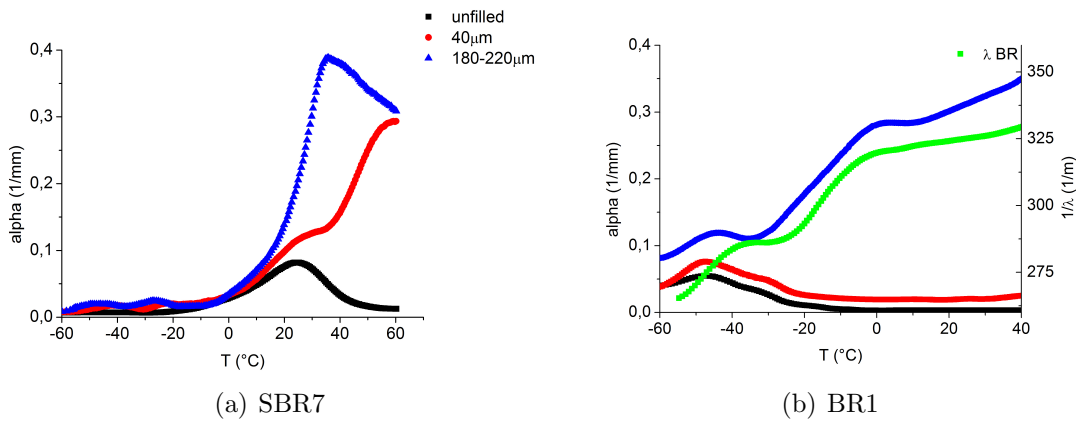


Figure 5.45: Rayleigh scattering influence on attenuation in BR1 and SBR7

The way scattering actually influences the attenuation is revealed in Figure 5.45. The first trials were conducted on SBR mixes (Figure 5.45(a)). They show that below the glass transition temperature, the influence of the glass beads is negligible, as both matrix and filler are in the glassy state, i.e. the impedances are similar. As soon as the testing temperature approaches the glass transition point, the impedance of the matrix changes as a result of softening and the attenuation increases. The measured differences between the two types of glass beads at the ultrasonic frequency are obviously due to their dissimilar sizes. The glass transition point is obvious for both filler types but scattering in the case of the beads with a diameter lower than $40\mu m$ seems to be very strong shortly after the T_g . This increase is apparently not connected to the matrix,

¹In the sense of a Maxwell or Kelvin-Voigt element again.

but to the increase of scattering effects with temperature, as will be discussed for BR. The larger glass beads begin scattering the ultrasonic waves at the first sign of matrix softening. The glass transition of the matrix can still be seen as the attenuation decreases beyond it.

As these results did not shed enough light on how much of this is a result of the matrix' transition to the rubbery state and how much of Rayleigh scattering, mixes with BR1 and the same glass beads were prepared. As BR1 has a much lower T_g (-50°C at 0.5MHz) compared to the SBR7 (25°C at 0.5MHz) it was expected that the scattering influence is better underlined. This is shown in Figure 5.45(b). Here the red curve, corresponding to the glass beads with a diameter smaller than $40\mu\text{m}$, shows a tiny shoulder after the glass transition and subsequently it enters the rubbery plateau. As its amplitude is higher than that of the original unfilled mix (black curve) and the only difference is the addition of inactive filler it can be assumed that the increase shown is a scattering effect.

For the large glass beads the effects are a bit more complicated. The glass transition peak is shown in this case as well and beyond it the attenuation increases in two steps. This increase can be ascribed to a combination of three factors. The first increase just beyond T_g is connected to scattering induced by the filler and by the crystallites present in the BR matrix (see also the blue curve in figure 5.45(b)). When the crystallites have completely melted (around 10°C , see also Figure 5.7), the attenuation increase is only due to scattering induced by the glass beads. This is clearly shown with the aid of the inverse wavelength variation with temperature (green curve in figure 5.45(b)). Since the wavelength is $\lambda = \frac{c}{f}$ where c is the sound velocity and f is the excitation frequency, it varies with the temperature. The inverse shows therefore the correlation between temperature and Rayleigh scattering which is proportional to wavelength.

It can be concluded that inclusions which have little to no interactions with the matrix determine abnormally high values of the ultrasonic attenuation which is ascribed to Rayleigh scattering. Therefore, when determining dynamic-mechanical properties of elastomers using ultrasonic waves, the presence of such inclusions should be avoided.

5.10 Investigation of carbon black filled compounds

One of the consequences of incorporating carbon black into a polymer is the creation of an interface between a rigid solid phase and a softer polymer. The amount of interface depends on filler loading, its specific area, the surface activity of the filler and the influence of mechanical mixing on filler dispersion. The interactions between polymer and filler lead to the rubber molecules being adsorbed on the filler surface

either chemically (more likely in the case of channel blacks, out of use nowadays) or physically. This leads to the restriction of segmental movements of polymer chains -bound rubber and/or the immobilized layer¹.

Bound rubber is defined as the rubber portion in an uncured compound which cannot be extracted by a good solvent due to its adsorption on the filler surface. A comprehensive review on the mechanism and factors affecting the formation of bound rubber was given by Dannenberg [228]. This immobilized layer refers to a change in the segmental mobility of the rubber molecule in the vicinity of the filler. The individual segments whose motion is affected by the presence of the filler constitute the immobilized layer, whether they are connected to the filler surface or they are located in its immediate neighborhood (Figure 5.46).

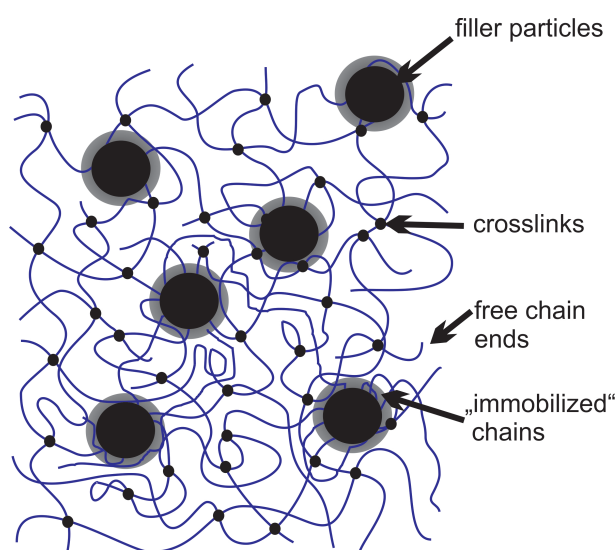


Figure 5.46: Schematic representation of polymer mobility in the vicinity of nanoscaled filler particles, i.e. carbon black.

Since the immobilized layer has its origin in the restriction of the segmental motion of chain segments near the filler surface, it should depend on temperature and the rate of strain to which the rubber is subjected. It is highly probable that at high frequencies of dynamic strain this layer reacts as if it were “harder”.

In this section the reinforcing effects and the filler networking induced by carbon black on different types of general purpose rubbers will be analyzed as a function of volume fraction and aggregate characteristics². The dynamic-mechanical properties are characterized at low frequencies (1 Hz) and, using the time-temperature superposi-

¹The word “immobilized” is not to be taken literally. It refers to a gradual reduction of mobility in the immediate vicinity of the filler

²Surface area and structure

tion principle, on a broad frequency range by DMA and at 0.5 MHz using ultrasonic longitudinal waves.

5.10.1 Variation of the volume fraction

Dynamic mechanical experiments at 1 Hz were performed on compounds filled with carbon black N347 in concentrations ranging from 4 to 25 vol%. In order to provide a clearer picture only 4 concentrations are shown for NR2 and NBR. These two were chosen for their differences in structure and polarity which is expected to induce relevant effects on the filler polymer interactions.

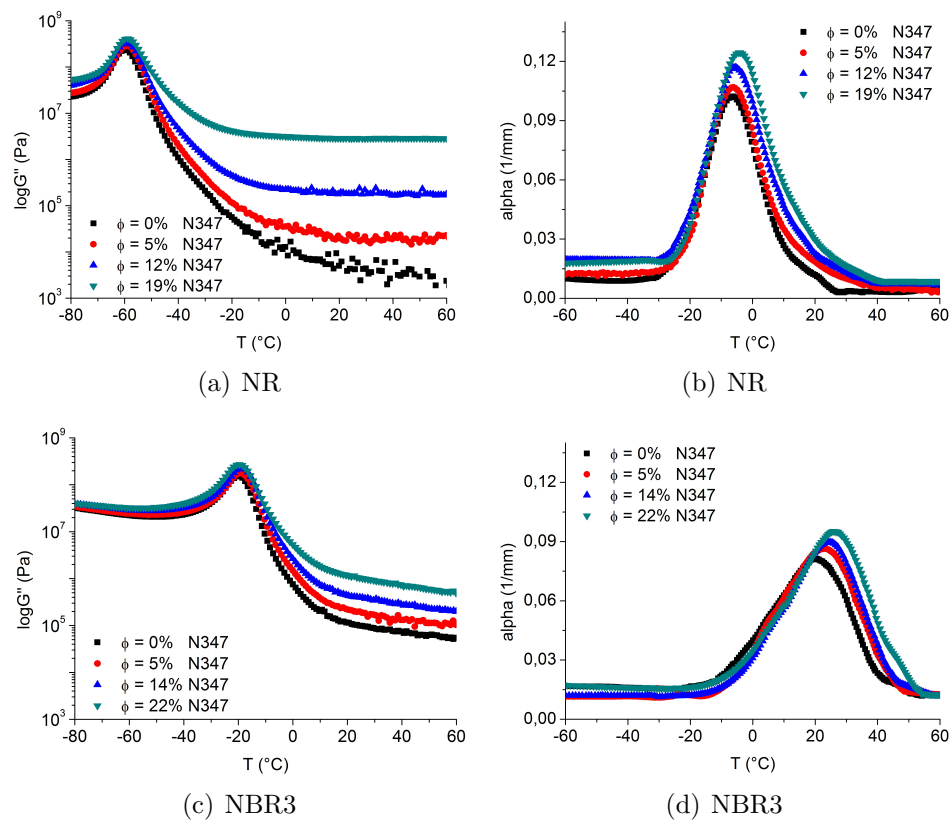


Figure 5.47: Loss modulus and attenuation coefficient for N347 filled polymers.

The measurements shown in Figure 5.47 offer a good insight on the effects of reinforcing carbon black. In the glassy state of the polymer a small increase of the loss modulus can be observed. As a function of the filler loading this reinforcement is more pronounced for NR than for NBR. As it was proven for other systems also, the presence of the filler provokes a rather insignificant shift of the T_g in the low frequency measurement. More important is the increase of the maximum of G'' in the T_g regime, which occurs for all polymers with the increase of the filler content. This was ascribed by Ziegler

[229] to an increase in the filler-polymer interaction and can be used to estimate the filler content in a discrete phase of a polymer blend. Furthermore, it is noticeable that besides the maximum increase the curves also become broader, indicating a wider relaxation time spectrum. A more clear cut influence of the filler is shown in the rubbery regime ($T > 0^\circ\text{C}$) where G'' increases exponentially with the filler loading. The increase certainly reflects the degree of the polymer-filler interaction as the comparison presented in Figure 5.48 demonstrates.

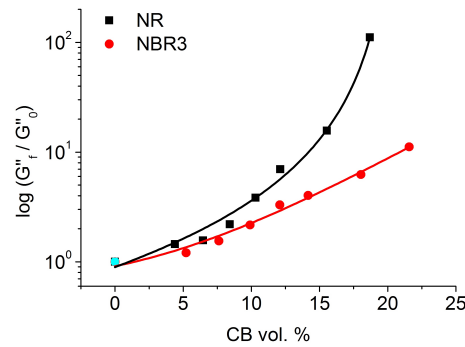


Figure 5.48: Filler influence on the reduced G'' at 30°C .

The difference between NR and NBR mixes can be attributed to the viscosity of the matrix and polymer-filler interactions.

Considering the experiments in the high frequency regime new and specific effects were observed for the two filled polymers.

Due to the strong adsorption of the polymer chains on the filler surface the interface should demonstrate a higher density than the matrix domains. It is expected that at the contact of the propagating longitudinal wave with such an interphase, the wave velocity and the amount of dissipated energy are significantly affected. Therefore the excess signals recorded in filled systems should depend on the filler loading and the extent of the interface per volume unit exposed to ultrasonic excitations.

The same interphase should provide for a coupling effect between the rubber matrix and the filler, whose impedances are different and could induce scattering at the interface as discussed in section 5.9. Perhaps a confirmation of this hypothesis are the measurements shown in Figure 5.47(b) and 5.47(d) for NR2 and NBR3. They show for a maximum of 22 vol.% of filler increase of the attenuation maximum of “only” 13% for NR and approximately 23% for NBR3. This can mean either that the dispersion of the carbon black particles was good enough so that no agglomerates larger than $20\mu\text{m}$ ¹ were formed, or, if they did, they do not induce scattering to an extent that would interfere with the measurements. In the second part of section 5.9 the glass spheres

¹The wavelength is defined as $\lambda = c/f$ and at T_g it is at least 2 mm.

whose diameter was smaller than $40\mu\text{m}$ induced a 45% increase of the attenuation maximum.

Both groups of curves demonstrate common features such as:

- a significant shift of the T_g as a function of the filler loading especially in the case of NBR3. As will be discussed later as well, the activity of the filler seems to influence the high frequency glass transition temperature directly proportional to the polarity of the polymer matrix.
- an increase of α_{max} as a consequence of the hydrodynamic reinforcement as well as of the interactions between carbon black and polymer matrix.
- a broadening of the peak towards higher temperatures while the left side of the peaks remains unchanged. This phenomenon has been associated by [230, 231] with polymer chains close to the polymer/filler interface whose mobility is restricted due to interactions with the filler surface. It seems that at high frequencies, the filler affects only the right (high temperature) side of the dissipation peak whereas on the left side there seems to be little influence on the chain dynamics. This can be related to a thermal activation of the glassy polymer layer on the filler surface.

5.10.2 Influence of the polymer structure

The influence of carbon black addition was tested further as a function of the polymer micro structure in the group of SBRs tested in the previous chapter. The carbon black used was N347. To summarize the filler effects on the low and high frequency energy dissipation it is convenient to plot the value of G''_{max} and α_{max} as a function of the filler volume fraction.

Figure 5.49 shows a nearly linear dependence of the dissipation maxima on the filler content. The numbers in the figure represent the slopes of a linear regression through the points belonging to each polymer. It is assumed that these values represent a measure, a gauge of the polymer filler interaction directly connected to the induced energy dissipation. At low frequency the $\frac{\Delta G''}{\Delta \phi}$ values are highest for the SBR containing the lowest amount of styrene. The increase of the styrene molar fraction apparently reduces the amount of energy dissipated at the glass transition temperature. At 0.5 MHz the ranking is different: the SBR with the lowest content of styrene displays the lowest values for the attenuation but its slope is the second lowest. The high styrene SBR3 has the highest values both in terms of attenuation and slope. However, the three values at 0.5 MHz are situated within a 3% interval so an interpretation of the causes that lay behind is difficult.

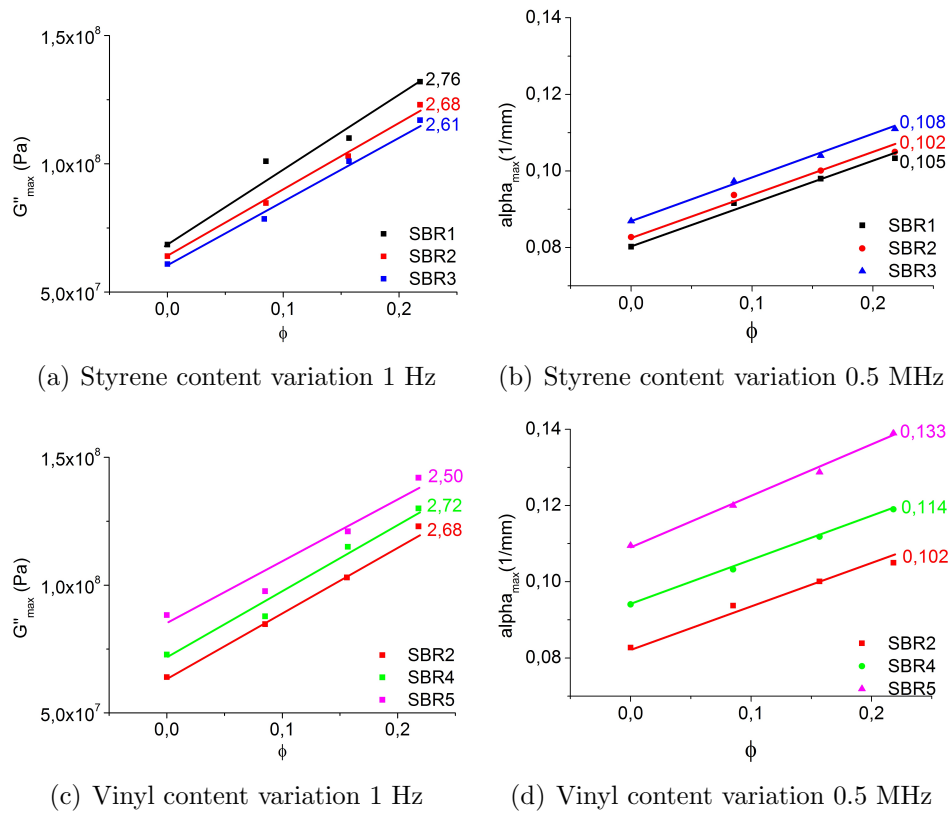


Figure 5.49: Influence of SBR microstructure on reinforcement in N347 filled polymers.

In the case of the vinyl variation at low frequency there is apparently a decreasing trend for the slope of the filler variation with increasing molar fraction of vinyl side groups. The high frequency data, on the other hand, show, similar to the case of styrene variation, an increase with the vinyl content of approximately 10%.

Generally it can be said that an interpretation of the influence side group variation in SBR has on the filler-polymer interactions based on dynamic mechanical measurements can only be made when accepting that the effects that the two methods are sensitive to have different origins. Therefore, it is possible that the ultrasonic method is more sensitive to the immobilized layer which forms on the filler surface and which is expected to increase with the amount of side groups, especially in the case of styrene. The general trend for the low frequency measurements is the opposite of the high frequency behavior. The decrease of the slope with the side group concentration is best seen in for the styrene variation whereas the vinyl values are less systematic.

5.10.3 Apparent activation energy of the CB network.

Several studies [232, 233] showed (for a model carbon black in oil mixture) that it is feasible to quantify the filler network energy by considering the variation of the temperature dependent storage shear modulus at very low strains. Extrapolating this theory to rubber filler compositions, Gerspacher et al. [234, 235] confirmed the direct proportionality that exists between the modulus and the number of filler-filler bonds N_f [236]. If one considered that the number of bonds forming the network at temperature T can be calculated from the number of bonds N_{f0} at a reference temperature T_0 then N_f can be expressed using an Arrhenius type relationship:

$$N_f = N_{f0} \cdot \exp \frac{E_A}{R} \left(\frac{1}{T} - \frac{1}{T_0} \right) \quad (5.17)$$

If the modulus of a carbon black polymer composite (G'_0) is proportional to the modulus of the filler network which, in turn, should be proportional to the number of filler bonds then the following applies:

$$G = G_0 \cdot \exp \frac{E_A}{R} \left(\frac{1}{T} - \frac{1}{T_0} \right) \quad (5.18)$$

Equation 5.18 basically suggests that by measuring G as a function of temperature and by plotting $\log G$ as a function of $1/T$ it is possible to estimate the value of E_A ascribed to a (filler) network cohesion energy. This is based on the fact that filler-filler bonds are thermally unstable and they begin to open with the increase of the temperature. The higher the temperature the more bonds will break which gives the modulus curve in the viscoelastic region a certain linearity. This feature can be used for a linear regression the slope of which is ascribed to the aforementioned E_a . The procedure is shown in Figure 5.50. It can be seen that the method is subjective as to the temperature where the curve becomes linear.

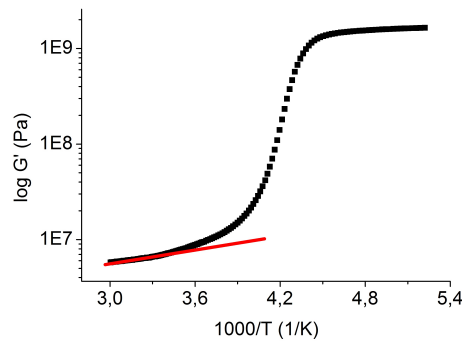


Figure 5.50: Arrhenius plot for $\log G'$ in 50 phr CB filled SBR6.

Based on this method, several determinations were performed for the polymers mentioned in this work. Some values are shown in Table 5.9 whereas others will be shown later.

Table 5.9: Activation energy.

	$E_A^{G'(T)}$ (kJ/mol)
IIR	15
NR2	15.5
SBR6	16.2
NBR3	17.1

It can be seen that the values of the activation energy depend strongly on the polymer matrix, else they should have equal values independently of the polymer. Furthermore, it is known that the carbon black aggregates are surrounded by a layer of polymer characterized by reduced mobility. The thickness of this layer is strongly dependent on the filler-polymer interactions. If it is accepted that this layer is also temperature dependent than the effects of this dependence overlap with those of the temperature dependence of the filler-filler contacts which could induce errors in the estimation of the activation energy by this method.

This topic is further discussed later in section 5.10.8 where a method is shown which separates the matrix influence from that of the filler network.

5.10.4 Investigation of filler networking

This section focuses on electric and dynamic mechanical (DMA at 1Hz) investigations of the percolation behavior of conducting carbon black¹ in elastomers by varying the amount of carbon black systematically.

One of the many interesting characteristics of carbon black reinforced elastomeric compounds is their unique electrical behavior which makes it possible to vary their electrical conductivity over a 10^{12} -fold range while maintaining their useful mechanical properties. This significant change in conductivity is brought about simply by the choice of the type and volume loading of carbon black [237].

It has been known that the electrical conductivity of insulating polymers filled with conducting particles, such as metal or carbon powder, discontinuously increases at some content of the filler. This sharp break in the relationship between the filler content and the conductivity of composites implies some sudden change in the dispersing state of conducting particles, i.e. the coagulation of particles to form networks which facilitates the electrical conduction through the composites.

A similar discontinuity is noticed for CB filled polymers in the dynamic-mechanical moduli variation with filler content above the glass transition temperature. The knowl-

¹N347

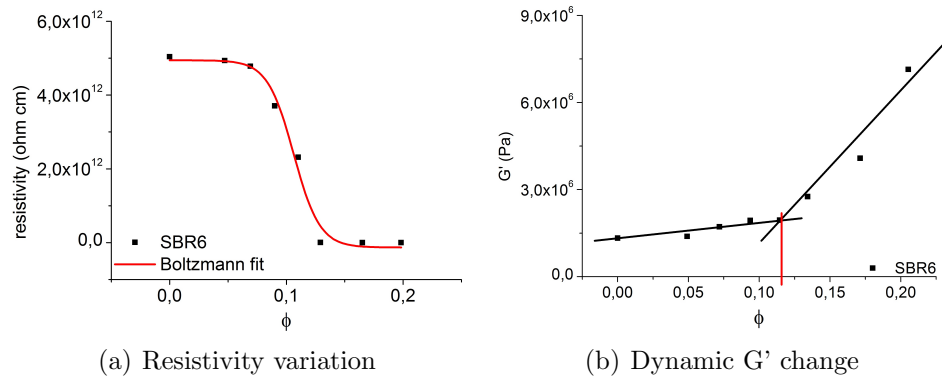


Figure 5.51: Estimation of the critical CB concentration in SBR6 mixes.

edge of the critical concentration, i.e. percolation threshold, where this sudden change occurs is relevant, for example, in applications where filled polymers are used as electrical insulators, etc. Figure 5.51 shows an example of how this concentration can be estimated from electrical resistivity measurements and dynamic-mechanical measurements. The critical concentrations are compared in Table 5.10

Table 5.10: Percolation threshold of carbon black in different polymers.

	from R^1	from G' at 20°C
IIR	0.070	0.075
NR2	0.080	0.090
SBR6	0.100	0.110
NBR3	0.120	0.120

Bueche [238] pointed out the similarities between the percolation threshold and the gel point, where the weight average molecular weight of a polymer becomes infinite and introduced the relation² $\phi_c = \phi / (f - 1)$ using Flory's [13] equation.

In trying to predict the conductivity threshold concentrations for randomly admixed conductive filler particles, Janzen [239] improved Bueche's relation and obtained the following equation which is useful in carbon black filled compounds:

$$\phi_c = \frac{1}{1 + 4\rho v} \quad (5.19)$$

where ρ is the particle density and v the specific void space of randomly close-packed filler agglomerates assumed as equal to the DBP absorption value.

The aforementioned theoretical approaches, including that of Aharoni [240] who used an averaged number of contact of conduction particles to discuss the possibility of

²where ϕ_c is the critical volume fraction, f is the coordination number and ϕ is the close packing volume fraction of a sphere

the network formation, to predict the sharp increase of the electrical conductivity at the particular carbon contents emphasize a lot the geometrical effects while the thermodynamic effects are hardly taken into consideration. This makes it difficult for their models to explain why the break in the conductivity change should depend on the species of polymer and filler as can be seen in figure¹ 5.52. Similar results were obtained by Schuster and Gerspacher (unpublished and [243]).

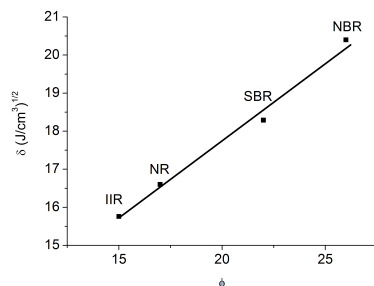


Figure 5.52: Influence of the polymer solubility parameter on the critical carbon black concentration.

Pouchelon and Vondracek [244] measured the storage modulus, the elongation at break and the conductivity on several rubber filler mixes and concluded that the percolation is strongly dependent on the level of polymer filler interaction. Reducing it results in a less significant percolation behavior i.e. the slope of the increase is less significant, but, at the same time, the critical concentration shifts to smaller values.

Miyasaka et al. [245] have shown that the critical volume fraction of carbon black which affects the electrical conductivity of the compounds is strongly dependent on the viscosity and surface tension of the polymer. The increase of the viscosity means that the shear forces during mixing will also be high which translates into a better filler dispersion. This leads to a higher percolation limit for the respective polymer.

Studies on adsorption energies of the low molecular weight analogs of elastomers, performed by Wang, Wolff and Donnet [246] generally showed that the interactions between carbon blacks and rubbers depend not only on the filler surface energies but also on the structure of the elastomers. Due to their polar functional groups, NBR and SBR (by comparison with NR or IIR) show a stronger interaction with the blacks than less polar rubbers. Similar to the results displayed above, the authors also showed that among the rubbers simulated in their work, IIR had the lowest interaction with the filler.

¹Solubility parameters are cited from references [208, 218, 241, 242]

5.10.5 Filler influence on T_g

The effect of the filler concentration on the glass transition temperature of polymers has been a debated subject of research for many years. The mutually accepted theory at the moment is that filler content has little to no influence on the temperature range where glass transition occurs [9, 16, 247].

As already mentioned the addition of active fillers to a polymer matrix leads to the formation of a nanosized layer of rubber adsorbed to the surface of the particles physically and chemically forming an insoluble interface. According to Kraus [248], this layer, ascribed to its reduced mobility, has a T_g 10K higher than that of the matrix.

The results of the low frequency measurements in Figure 5.53 summarize the effects of filler content on the glassy transition for four polymers with different structures and polarities.

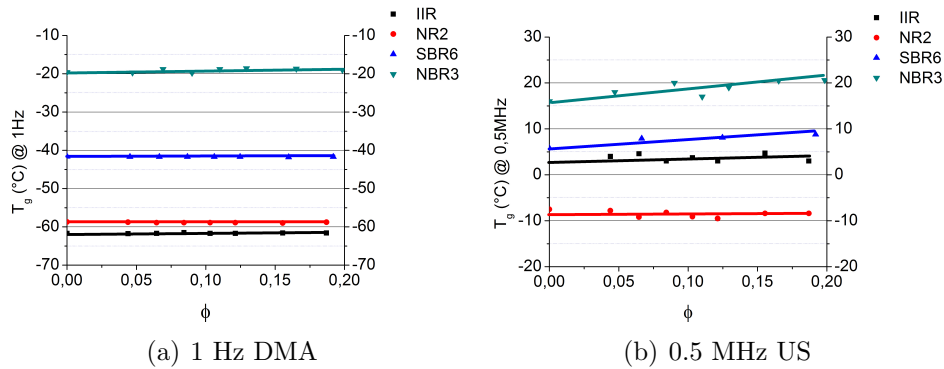


Figure 5.53: Influence of the filler volume fraction on the glass transition temperature.

The dynamic mechanical measurements at 1Hz in shear for NR2, NBR3, SBR6 and IIR show a slight increase of the T_g of almost 3°C with the increase of the volume fraction of filler up to 0.2. High frequency data concerning the filler effect on the glass transition temperature show a somewhat more pronounced effect.

Mason [249, 250] measured dynamic properties of NR compounds, filled with two types (particle sizes of 0.4 μm and 0.04 μm , respectively) of carbon black, from the velocity and attenuation of longitudinal waves at 1 kHz. His results indicate that there is no change in T_g with increasing content of carbon black up to 18% volume loading.

Baccareda [251] performed sound velocity and damping factor measurements on filled and unfilled *cis* - 1,4 - *polybutadiene* in a frequency range from 2 kHz to 20 kHz. His results indicate once more no to little influence of the filler volume fraction on T_g . However, these results might be affected by inaccuracies ascribed to the approx. 10°C difference between two consecutive measurement points.

The high frequency measurement results reported in this work confirm those of Mason in the case of NR only. The ultrasonic measurements at 0.5MHz (Figure 5.53) indicate that out of the 4 polymers in question natural rubber (NR) and butyl rubber (IIR) seem to be only to a little extent affected by the filler variation, as far as the T_g is concerned. The change of the glass transition temperature with filler is highest in the case of NBR 7°C followed closely by SBR with 5°C.

The ultrasonic measurements hint towards an influence of the amount of filler-polymer interaction on the main chain segmental mobility. These interactions seem to be more evident in the high frequency measurements and they can be regarded as a further evidence of the chemical contribution to reinforcement.

5.10.6 Effect of the carbon black surface and structure

It has been proven in several studies that the specific area and especially the shape (structure) of carbon black aggregates lead to specific properties of filled elastomers.

This section is concerned with the effect a group of carbon blacks with different surface area and structure have on the energy dissipation in the low and high frequency regime. The impact of the degree of particle-polymer interaction on the dynamic mechanical properties in the glass transition region was probed by studying carbon blacks with widely varying particle size and surface area (Figure 5.54(a)).

Table 5.11: Properties of the used blacks.

ASTM designation	STSA (m^2/g)	COAN ($ml/100g$)
N220	106	98
N326	82	69
N330	82	88
N347	90	99
N550	43	85

The carbon blacks used (compounded to 20 volume percent in SBR7) ranged from a highly reinforcing N220 with a surface area of 106 m^2/g and an aggregate diameter of 65 nm [252] to N550 with a surface area of 43 m^2/g , aggregate diameter of 139 nm which is expected to show a weaker reinforcement of the polymer matrix. Their properties are summarized in Table 5.11. The COAN¹ number gives indication of the filler structure whereas the STSA² is a measure of the filler surface.

In the glass transition region the backbone mobility is insufficiently affected by the differences in structure and particle size of the carbon blacks. It can be concluded that

¹Compressed oil absorption number - ASTM D 3493

²Statistical thickness surface area - ASTM D 6556

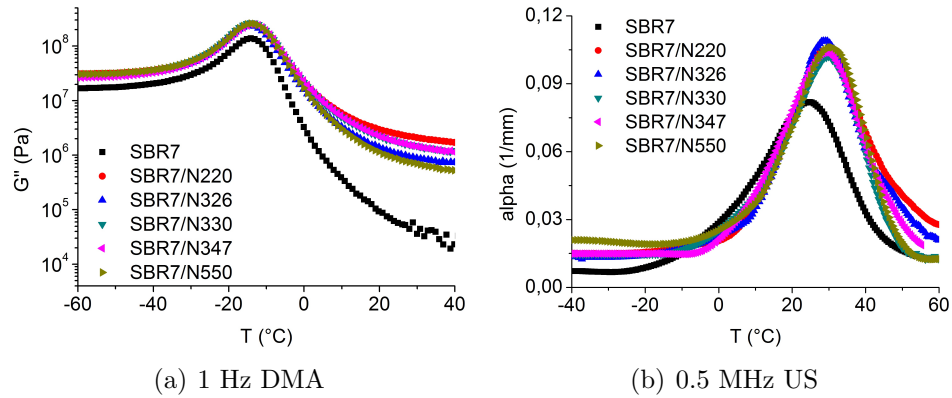


Figure 5.54: Influence of the CB type at a loading of $\phi = 0.2$ on low and high frequency energy dissipation.

in the glassy regime differences in aggregate size and structure play a less important role than the filler loading itself. While descending into the rubbery zone, the discreet influences of the different blacks go into effect. Ascribed to its high surface area the N220 filled compound shows the highest energy dissipation as a result of the strong interactions with the polymer matrix. It is followed by the compound filled with N347 which displays a lower surface area but increased agglomerate structure. The least interactions are shown in the N326 and N550 filled compounds due to their low surface area and structure.

The results of the ultrasonic measurements, shown in Figure 5.54(b), indicate that the attenuation peak, which is associated with the high frequency response of the macromolecular chains, appears not to be influenced by the particle surface area or the structure of the different carbon blacks. The compounds, which were each filled with 0,2 volume fraction of the respective black, show very similar behavior in the glass transition. Once past the transition zone the black with the smallest particle size (N220) shows the highest attenuation due to its strong interactions with the polymer matrix while N550 shows the lowest attenuation decreasing immediately to the level of the unfilled polymer ascribed to the weaker bonds formed with the surrounding polymer. N220 on the other hand, well known for the strong bonds it forms with the polymer due to its high surface activity, impairs the composites the highest attenuation in the rubbery zone. Interestingly, N326 shows attenuation characteristics which are high for it to be only due to its interaction with the filler both in the maximum and in the rubbery zone. It is expected that this behavior is partly ascribed to some scattering effects induced by the poor dispersion characteristics and comparatively low structure of this black .

These results together with the ones from the low frequency measurements (Figure 5.54(a)) are in agreement with data from Robertson and Roland [253, 254] who dealt

with the subject in an exhaustive manner. They concluded that for the materials studied (SBR, BR filled with carbon black and silica of different particle size and structure) which had varying degrees of filler-polymer interactions, the polymer segmental motion, as determined using dynamic mechanical spectroscopy, was not significantly affected by the grade of filler. Varying the particle surface area in carbon black-filled polybutadiene or changing the extent of chemical attachment of SBR chains to silica particles by varying the degree of coupling with silanes does change the shape and magnitude of the $\tan\delta$ vs temperature peak in the glass-to-rubber softening transition. However, this might be attributed to changes in the small-strain rubbery response, arising primarily from the inter particle network.

Before analyzing the behavior of the other compounds it must be stated that the propagation of the ultrasonic waves is distinctly influenced by the polymer-filler interactions, i.e. one distinguishes two important systems¹ according to the factors that govern wave attenuation. Firstly - system 1 - one can mention a system where part of the wave energy is absorbed by the matrix, i.e. a viscoelastic medium, another part is absorbed by the filler particles, considered to be viscoelastic in this case also. The second system to mention - system 2 - is similar to the first with the remark that the filler aggregates are considered elastic, therefore they will not absorb energy at all but they will scatter it instead. The theories behind the way the attenuation in filled lossy media appears have been treated elaborately in the extensive work of Biwa, Beltzer and Brauner [227, 255–257]. They applied the model to the longitudinal wave attenuation in glass-particle reinforced epoxy composite and rubber-toughened PMMA blend. The numerical results have been compared favorably with the actual measurements of the attenuation spectrum for each of the two composites, thus showing the predicting capability of the model.

When one applies the aforementioned assumptions to the systems discussed in this contribution, it can be concluded that system 1 is the one that applies to the polymers filled with active fillers ascribed to the formation of an immobilized layer, several nanometers thick, of polymer with reduced mobility [9, 258]. It is possible that this layer confers the filler particles their viscoelastic character under ultrasonic excitation. It can, thusly, be assumed that the immobilized layer acts as a couplant between the viscoelastic polymer and the elastic filler particles reducing the impedance mismatch (see theoretical chapter) therefore minimizing the scattered energy, in the same way the propanol acts to minimize the impedance mismatch between the transducer and the rubber sample.

Ascribed to the impedance mismatch the losses that come from scattering at the rubber-inactive filler interface should be much higher than those that come from the absorption in the immobilized layer, therefore, when using an inactive filler one should notice a

¹here only filled systems are regarded

stronger damping peak compared to the one shown by the active fillers.

5.10.7 Influence of the filler dispersion on ultrasonic wave velocity.

The sound velocity at the glass transition temperature is associated with the density of the system and the stored energy in the rubber-filler composite. It can be assumed that the sound velocity increased with the polymer-filler interaction and due to the interface contribution the volume fraction of interphase generated during filler dispersion and by increasing the filler loading. The experimentally proven sequence of normalized sound velocities shows interesting correlations features.

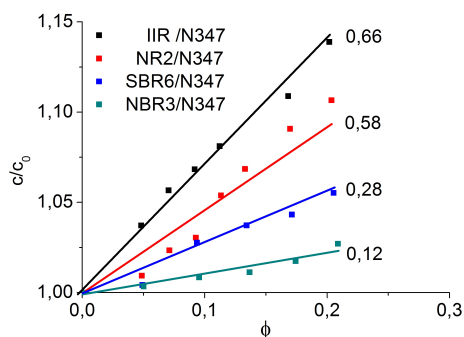


Figure 5.55: Reduced sound velocity in N347 filled polymer systems.

The four polymers in Figure 5.55 are ranked in a sequence that suggests a connection of the reduced sound velocity and the interaction of the polymer and the filler (N347). The highest values are shown by the butyl compound. As it was shown previously in this chapter, this particular type of rubber is characterized by weak interactions with carbon black which translates into poor dispersion. This, in turn, apparently causes the sound velocity to increase. The next ones in the sequence are NR2 and SBR6 and the very last is NBR3. Due to its polarity carbon black is dispersed more readily in it which induces a lower increase of the sound velocity.

Having noticed that in the previous systems the reduced sound velocity showed an increase inversely proportional to the polarity of the polymer it is interesting to observe within a polymer, such as SBR, the effects that the variation of the polar styrene groups content induce (Figure 5.56). The compound with the least amount of styrene, SBR1, induces the strongest increase of the sound velocity whereas SBR3 shows an increase comparable to the one seen for NBR in Figure 5.55. Again this appears to be related to the dispersion of the filler in the rubber matrix. The higher the amount of styrene the easier carbon black can be dispersed and the lower the sound velocity becomes.

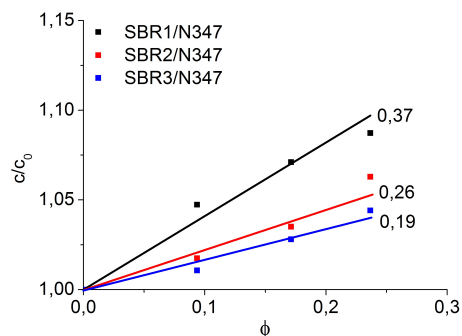


Figure 5.56: Reduced sound velocity in N347 filled SBR systems.

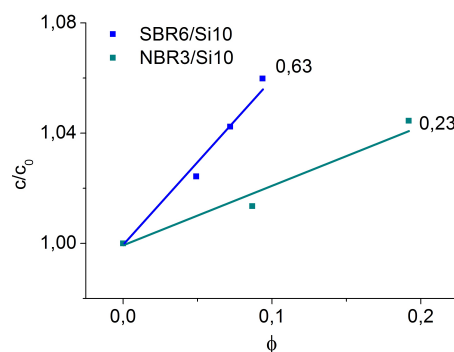


Figure 5.57: Reduced sound velocity in silica filled systems.

As the change of filler fits very well into the discussion at this point the influence of silica will be analyzed at this point. Seen in Figure 5.57 are two polymers of different polarities filled with polar silica. The sound velocity shows a mild increase for NBR3 and a nearly 3 times as high an increase for SBR6. This can be connected to the better dispersion of the silica in a polar matrix than in an only slightly polar one. It should also be noted that the increase of the sound velocity for the NBR3 composite with silica is twice as high as in the case of N347. This should be ascribed to the stronger silica-silica bonds that prevent a better dispersion.

It is known that the speed at which a longitudinal wave propagates is directly proportional to the rigidity of the matrix, i.e. the higher the density, the closer individual molecules are to each other the faster the wave will propagate. In the case of filled polymers the wave propagates through the highly elastic filler at a much higher velocity compared to the viscoelastic polymer. Following this concept, the filler influence on the ultrasonic velocity should be that of strong increase with its volume fraction, rather independently of the polymer type.

For the compounds above the same type of carbon black was used always in the same concentrations. Besides the aforementioned increase with filler volume fraction a strong effect of the polymer is noticed. The slopes of the increase $\alpha(\phi)$ are very different and

characteristic for the particular polymer-filler systems. Surprisingly the slope is highest for the systems with less good filler-polymer interaction. It seems it is not the filler-polymer interactions (its increase) that determine the different ranking of the slopes. The strongest increase is noticed for the butyl rubber compounds, a rubber which is known to have a poor interaction with carbon black and can badly disperse even coarse blacks. It seems that large filler agglomerates and non-dispersed pellet fragments increase the propagation velocity of the ultrasonic wave in the compound.

5.10.8 Broad range frequency analysis - WLF

With the introduction of fillers as reinforcing agent, the complex interactions between the filler network and the polymer matrix are at the origin of strong nonlinear effects with respect to the amplitude of deformation [236]. The influence of the filler system during the master curve construction is considered via the introduction of a temperature-dependent vertical shift factor physically interpreted as the activation energy of the regions of reduced mobility between adjacent filler particles. Figure 5.58(a) illustrates the necessity to introduce a vertical shift factor for low-frequency data, corresponding to high temperatures according to the WLF equation. Indeed, once the isothermal moduli segments are horizontally shifted with the same parameters as for the unfilled compound, the poor overlapping in the low frequency/high temperature region indicates that the filler system is influencing the dynamic behavior within this experimental range and should be associated with a thermally activated mechanism. The physical origin of the observed shifting behavior is the superposition of two relaxation processes in filled elastomers, the one of the polymer matrix and that of the filler network. The applied horizontal and vertical shifting procedures allow for a separation of both relaxation processes [259].

In more detail, the procedure required to overcome this impediment consists, firstly, of using the same horizontal shifting factors as for the unfilled polymer with the assumption that there is no change in the dynamics of the macromolecular chain with the addition of the filler. Secondly the same reference temperature is used to start a *vertical shifting* procedure until the usual master curve is obtained [259] (see Figure 5.58(b)). By using the same shifting factors for the horizontal shifting means that the two processes have been recognized and separated: the polymer dynamics and the filler-polymer influence. In the end it is important that master curve is optically sound which is, according to Ferry [6], a good indication that the compound is thermorheologically simple (i.e. the behavior of the compound is dominated by a single molecular process). It should be mentioned that inactive fillers do not give any secondary processes.

An Arrhenius plot (a display of the logarithm of frequency over the inverse temperature) of the shifting factors (both horizontal and vertical) used in the construction of the

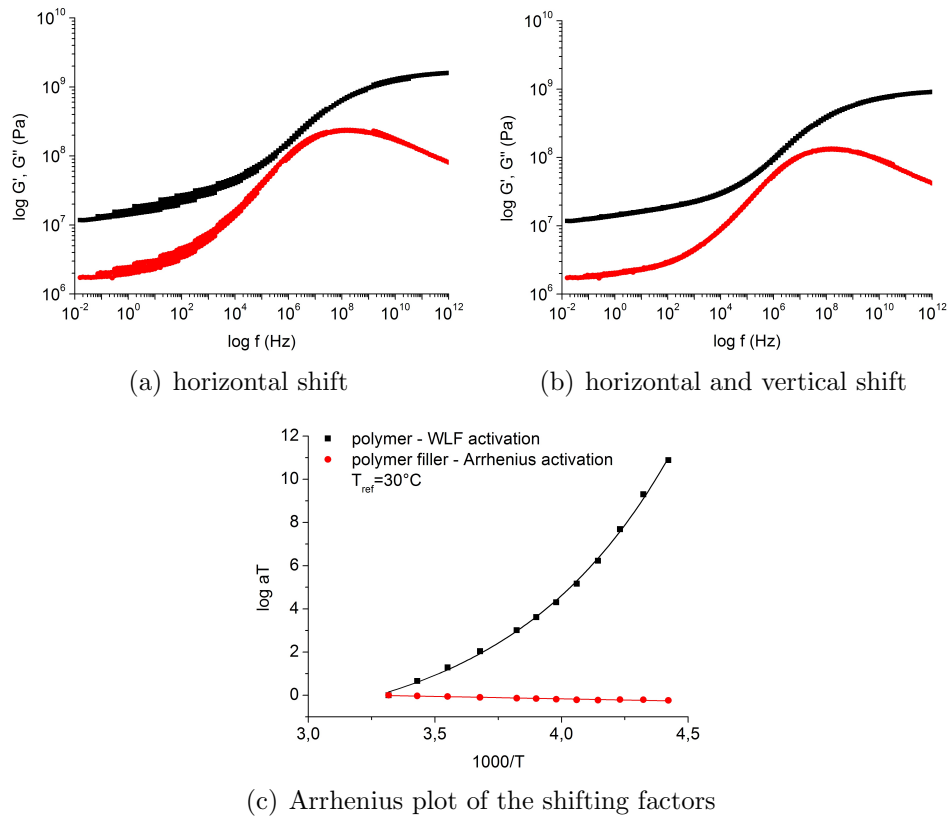


Figure 5.58: SBR3+CB22 - separation of two processes by the shifting procedure.

master curve reveals the two processes that occur in the filled SBR3 compound. As mentioned above the polymer matrix dynamics is described best by the WLF equation. In Figure 5.58(c) the black dots represent the polymer activation (horizontal shifting factors) and the red ones the filler (horizontal shifting factors) influence. Clearly the latter obeys the Arrhenius law (they are linear - characteristic of the movements of small particles or chain segments) and is therefore characterized by an apparent activation energy of the filler network. This can be interpreted as the opening of the filler-filler bonds with temperature increase.

Table 5.12: Apparent activation energies from vertical shifting (v_s) and $G'(T)$, respectively for CB22 filled SBRs in dependence of the styrene content.

styrene variation in SBR	$E_a^{v_s} (kJ/mol)$	$E_a^{G'(T)} (kJ/mol)$
SBR1 10%	3.5	16.1
SBR2 20%	4.2	16.5
SBR3 30%	5.4	16.6

The activation energies obtained from the horizontal shifting procedure are shown in Tables 5.12 and 5.12 for the five SBRs with varying styrene and vinyl content together

Table 5.13: Apparent activation energies from vertical shifting (vs) and $G'(T)$, respectively for CB22 filled SBRs in dependence of the vinyl content.

vinyl variation in SBR	$E_a^{vs}(kJ/mol)$	$E_a^{G'(T)}(kJ/mol)$
SBR2 20%	4.2	16.5
SBR4 45%	6.0	16.7
SBR5 65%	5.6	16.8

with the values that come out from the interpretation of the high temperature storage modulus as being dependent only on the filler network, as shown earlier in the low frequency section.

Interestingly the values of the apparent activation energies determined by both methods increase proportionally with the styrene content. This should be interpreted as an effect of the stronger filler polymer interactions that occur due to the increasing polarity of the polymer matrix with styrene step-up. Therefore the apparent activation energy cannot be attributed only to the filler network and is in any case also polymer dependent.

In [260] Herrmann and Niedermeier investigated SBR systems (solution SBR containing 50% vinyl and 23% styrene groups) filled with 3 carbon blacks with different surface areas, in contents from 20 to 50 phr, by dynamic-mechanical measurements and subsequent master curve construction. They notice the necessity of the vertical shifting and associate the characteristic activation energy with a network agglomeration energy. In their view this energy originates not directly from the interactions between the filler particles but it actually occurs via a so called “bridging effect” between the immobilized layers of two adjacent filler aggregates. The layer which forms by adsorption onto the filler has a reduced mobility as described earlier. By decreasing the temperature of the environment the surrounding polymer reduces its mobility due to a T_g gradient in the polymer matrix surrounding the filler. In this way it is possible that two adjacent agglomerates become connected. When the temperature increases these connections are broken as the mobility of the polymer matrix increases.

The results presented in this work support the model presented in [260] by showing that the activation energy which results from the vertical transition varies with the polymer type and with the polymer microstructure when the same filler is used. It is noticed in Table 5.12 that an increase of the styrene content of 20% induces a subsequent increase of the activation energy of approximately 2 kJ/mole. A similar increase is obtained by Herrmann and Niedermeier for a step-up of the filler surface area of 30%.

The applicability of this method resumes, however, to materials constituted of only one phase whose activation dynamics are temperature dependent, i.e. thermorheologically simple materials. It cannot be applied for polymer blends because the different temperature activation of the phases (for example when the one of the polymers is in

its rubbery state and the other one starts its transition) leads to different shapes of the isothermal moduli which cannot be optically superimposed.

5.11 Investigation of silica filled compounds

Silica used as filler for elastomers is mostly compounded after a surface modification by chemical treatments added during the processing or in the lab prior to incorporation in rubber or during the mixing process. The consequences of this treatment is a reduction of the filler-filler interactions and, at the same time, a coupling with the polymer matrix. This, in turn, modifies the reinforcement efficiency of the silica filler via a possible change of both the dispersiveness of the filler and the stiffness of the bonds at the origin of the filler network created in the composite.

5.11.1 Variation of the volume fraction

The influence of silica on filled rubbers properties is discussed in the following on SBR and NBR firstly by varying the filler concentration. Apart from the low frequency information, valuable data about the compounds energy dissipation characteristics as a function of temperature is obtained at 0.5MHz.

Figure 5.59 displays the effects of silica on the loss component of the complex shear modulus at 1 Hz for SBR2 and NBR3.

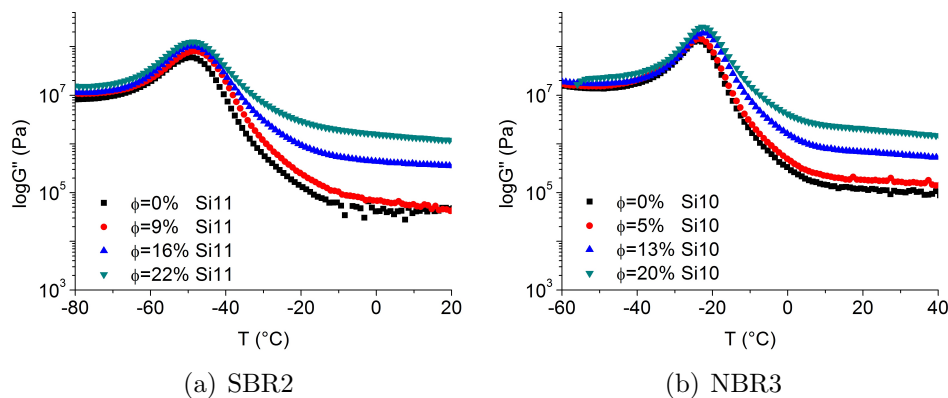


Figure 5.59: Influence of silica volume fraction on NBR and SBR.

For both rubbers the addition of silica induces an overall increase of the loss modulus. Similarly as in the case of CB filled composites, a small shift of the glass transition temperature is observed. It is noticeable that for both polymers the modulus curve becomes broader with the filler fraction.

A decrease of the modulus is noticed above T_g for all concentrations which is associated with the temperature dependence of the filler filler bonds. The gradient of this decrease (or the one of the storage modulus) is usually interpreted as the apparent activation energy of the filler network, e.g. $E_{aNBR3}^{G'(T)} = 15.4kJ/mol$ and $E_{aSBR6}^{G'(T)} = 16.3kJ/mol$. The differences that arise at high filler content hint toward a polymer dependence, which, immobilized on the filler surface, changes its dynamic properties as a function of temperature with different velocities ascribed to the strength of the interactions between the filler and the polymer. When compared to the activation energy obtained for carbon black filled compounds (Table 5.9) a higher value is noted for the carbon black filled NBR3 which hints towards a weaker interaction with the silanized silica. For the chosen polymers the attenuation of ultrasonic waves is seen to follow a similar

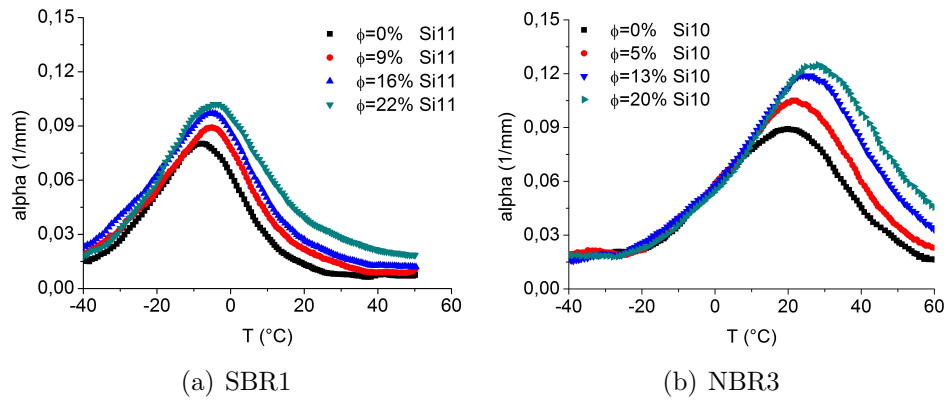


Figure 5.60: Influence of silica volume fraction on α for NBR and SBR.

pattern to the loss shear modulus (Figure 5.60). The addition of silica induces an increase of the attenuation characterized by broader peaks in both polymers. In the case of NBR3 the broadening of the curve occurs beyond the T_g whereas for SBR1 it takes place in the low temperature region as well. The asymmetry of the temperature dependent ultrasonic attenuation hints for both polymers towards a dependence of the glass transition temperature on the silica content.

Different from the low frequency measurement is the shift of the glass transition process with the volume fraction of silica. In the case of SBR2 the T_g changes 5°C for 22 vol.% whereas in the case of NBR3 the shift is 10°C for 20 vol.%. This change is related to the stronger influence of the immobilized layer in the low amplitude high frequency measurements.

5.11.2 Influence of the polymer structure in silica filled compounds

The influence of the SBR microstructure on the G''_{max} and ultrasonic attenuation maxima of silica filled composites is shown in figure 5.61.

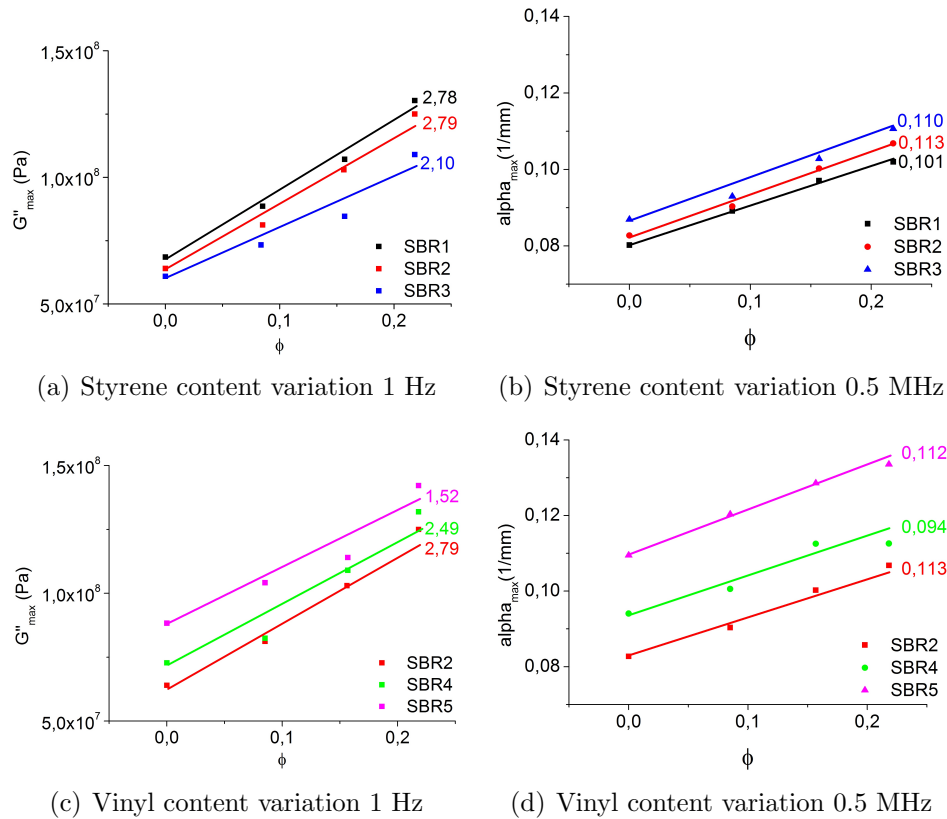


Figure 5.61: Influence of SBR microstructure on reinforcement in Si11 filled polymers.

The results in Figure 5.61 are a measure of the intensity of the filler-polymer interactions in the glass transition region. In [261] Wang et al. used inverse gas-solid chromatography operated at infinite dilution to assess the surface energies of silica and estimated the interactions that take place between the rubber matrix and silicas from the absorption of low molecular weight analogs of elastomers. The free energies and enthalpies indicate that the interactions of the functional groups with the fillers decrease following the sequence nitrile, phenyle ring, double bond. So in the case shown in Figure 5.61(b) the ultrasonic attenuation gives input on the strength of the silica SBR interaction.

Corroborated with Figure 5.59 and 5.60 the results in Figure 5.61 confirm that the loading effects at different temperature regions are governed by different mechanisms. It seems that at temperatures near the dissipation peak in the transition zone, the

presence of silica gives a lower increase of the energy dissipation for a given energy input than in the rubbery region. This may be interpreted in terms of a reduction in polymer fraction in the composite as the polymer would be responsible for the high portion of energy dissipation and individual solid filler particles in the polymer matrix may not absorb energy significantly.

The immobilized layer is, as in the case of carbon black, strongly dependent on the polymer type (macro and micro structure).

If the case of SBRs where the styrene content was varied is taken it can be seen that an increase of polarity ascribed to higher phenyl content determines induces no systematic influence on the slopes variation ascribed to the surface treatment of silica. The highest value both at 1Hz and 0.5MHz belongs to the SBR2 containing 20% styrene. The reversed ranking in case of the G''_{max} and α_{max} values is maintained as seen in the case of carbon black which hints on the polymer being the cause rather than the filler.

5.11.3 Broad range frequency analysis - WLF

The time-temperature superposition principle was applied for the silica filled systems in the same way as described for carbon black filled compounds. Due to the strong reinforcing effect of the filler network, it was necessary to further adjust the master-curve by vertical shifting. The resulting shifting factors were subsequently fitted using an Arrhenius equation and the apparent activation energy of the filler network was deduced.

Table 5.14: Apparent activation energies from vertical shifting (vs) and $G'(T)$, respectively for Si11 filled SBRs.

styrene variation in SBR	$E_a^{vs}(kJ/mol)$	$E_a^{G'(T)}(kJ/mol)$
SBR1 (10%)	4.6	15.7
SBR2 (20%)	5.0	16.1
SBR3 (30%)	5.9	17.1

Table 5.15: Apparent activation energies from vertical shifting (vs) and $G'(T)$, respectively for Si11 filled SBRs.

vinyl variation in SBR	$E_a^{vs}(kJ/mol)$	$E_a^{G'(T)}(kJ/mol)$
SBR2 (20%)	5.0	16.1
SBR4 (45%)	6.9	16.3
SBR5 (65%)	5.2	16.3

The apparent activation energies (E_a^{vs}) calculated for the silica filled SBR systems are

generally higher than the ones for the CB filled systems (Tables 5.12 and 5.13). This denotes the stronger filler-filler network that occurs for silica filled compounds.

It can be noticed that the increase of the matrix polarity induced by the styrene content determines higher activation energies, an effect that was observed for the CB systems as well. The results obtained by Wang et al [261] while performing inverse gas chromatography to investigate rubber silica interactions showed that the intensity of these interactions was reduced directly proportional to the content of functional groups and degree of unsaturation in SBR. The results on the styrene influence in silica-SBR interactions is related to the electron density of the conjugated π -bond system in the styrene phenyl rings elevating the polarity of the compound.

5.11.4 Influence of silica surface treatment

The dispersion of a filler in a rubber matrix depends on the polarity difference between the polymer and the filler. This difference is significantly larger in a silica-filled system compared to a carbon black filled rubber, due to the concentration of silanol groups on the silica surface. In order to decrease this polarity that supports inter-aggregate interactions and facilitate mixing, the silica surface is chemically modified by coupling monofunctional silanes onto the particles. With chemical modification, the filler surface can be changed in such a way that it is tailored to its application. For the filler used in rubber products, two types of chemicals have been used for surface modification: grafts of chemical groups on the filler surface to change the surface characteristics and grafts that may react with polymer. The latter are frequently called coupling agents or bifunctional coupling agents as they provide chemical linkages between the filler surface and polymer molecules. The former is sometimes referred to as monofunctional coupling agents even though no chemical reaction with the polymer takes place with these grafts.

These coupling agents preferably react with the silanol groups on the silica surface during the mixing operation, and create a chemical bond between the silane-coated silica and the rubber polymer during the vulcanization operation [262]. In spite of the silanization, the silica particles still interact with each other and form a strong filler-filler network. And even though this network is broken during mixing, the filler tends to re-agglomerate afterwards.

In the following the effects of silica surface treatment are shown for NBR3 composites filled with 20 vol.% silica with unmodified surface and silanized.

The DMA measurements at 1 Hz are shown in Figure 5.62(a) for NBR3 composites. The filler addition induces an increase of the loss modulus due to hydrodynamic reinforcement and polymer-filler interactions. The temperature of the glass transition is

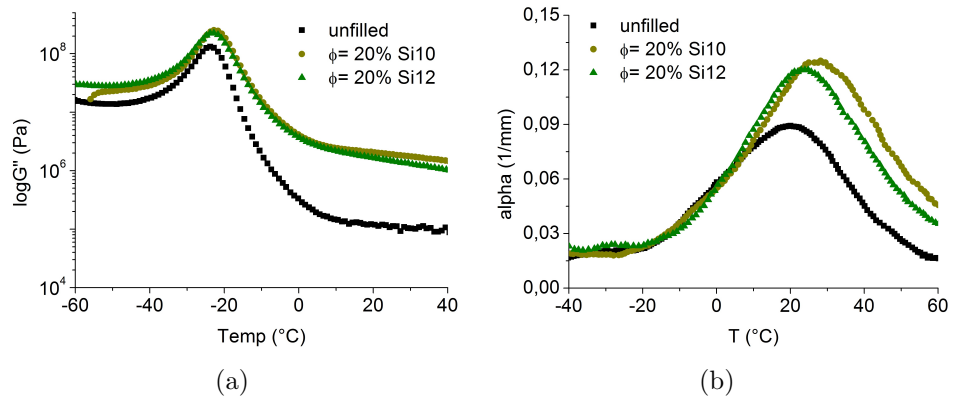


Figure 5.62: Influence of the silica surface treatment in NBR3 composites.

shifted 2°C to higher temperatures. As a result of the silanization the glass transition temperature is shifted 1°C towards lower values. This should be attributed to the reduction in the NBR-silica interactions as a result of the polarity decrease which occurs after the surface treatment.

The loss component of the complex shear modulus is visibly affected by the silica surface treatment. Most effects of the changes occurring in the filler-polymer interactions are seen in the high temperature region. As a result of the reduced polarity filler surface the interactions became weaker and the the high temperature modulus decreased.

The addition of unmodified silica to NBR determined an increase of the dissipated energy, characterized by higher α . Secondly, it determined the shifting of the glass transition temperature by some 10°C to higher temperatures. This is associated for high frequency measurements with changes in the local chain dynamics as a result of the strong filler polymer bonds determined by chain adsorption on the filler surface and polar bonds between the OH groups on the silica surface and CN side groups in NBR.

The modification of the silica surface with a monofunctional silane determines a change in the filler polarity which translates into a lower glass transition temperature. The decrease in filler polymer bond determines also a reduction of the attenuation.

Although modification of silica by monofunctional chemicals may greatly improve the micro dispersion of the filler and provide low hysteresis materials, the lack of polymer filler interactions would result in a lower static modulus and poorer failure properties particularly abrasion or wear resistance.

5.12 Investigation of novel fillers

This last part of the section on the effect of active fillers on dynamic mechanical properties of elastomers deals with novel compounds with very promising reinforcing characteristics. The results of ultrasonic and DMA tests and comparisons with the effects noticed for carbon black and silica are thoroughly discussed with regard to global reinforcing effects of active fillers.

Besides the expected increase in the modulus due to the inclusion of rigid filler particles in the soft matrix, another contribution arises from filler-rubber interactions leading to additional cross-links¹ in the network structure. A further consequence of the incorporation of filler in an elastomer is the significant change in the dynamic properties of the rubber. This phenomenon, of great importance in the rubber industry, has attracted a great deal of interest. Filler networking, formed by filler-filler interactions or via a model of immobilized elastomeric layer on the filler surface, seems to be one of the main parameters which governs the dynamic response.

Compared with carbon black, obtained via the furnace process, whose surface consists of a certain portion of unorganized carbon but mainly graphitic basal planes, the silica surface consists of siloxane and silanol groups. In the sense of surface physical chemistry, based on the adsorption investigation of different chemicals by means of IGC, it has been found that carbon black possesses a high dispersive component of surface energy, γ_s^d , while silica is low. By contrast, the specific or polar component of the surface energy, estimated from the specific interaction between filler surface and polar chemicals, is much higher for silica than for carbon black [261, 263]. With regard to the polymer-filler and filler-filler interaction, Wang et al [263, 264] were able to differentiate these two fillers by means of adsorption energies of model compounds which are related to different components of their surface energies. In principle, as cited earlier, while fillers have polar surfaces the hydrocarbon rubbers are generally non- (or very low-) polar materials. A higher population of silanol on the silica surface would lead to strong hydrogen bonding between silica aggregates and a stronger filler network in comparison with its carbon black counterpart. In addition, the lower filler-polymer interaction of silica with hydrocarbon rubber would also result in a lower level of bound rubber in the compound [265] which would facilitate filler flocculation. Consequently, the filler network of silica should be more developed and much stronger in hydrocarbon rubber. In fact, with a silica and carbon black having the similar surface area and structure, Wolff et al [265, 266] have demonstrated in NR that the Payne effect of a silica compound is much higher than for carbon black.

Owing to their unique mechanical properties, carbon nanotubes are considered to be

¹of a physical or chemical nature

ideal candidates for polymer reinforcement. However, a large amount of work must be invested especially in the mixing process (to achieve proper dispersion) in order to realize their full potential. Effective processing of nanotubes and polymers to fabricate innovative composite materials is still a great challenge. The key point is to transfer the potential mechanical, thermal and electrical properties of the CNTs to the polymer composite. In this context, two main issues have to be solved to effectively improve the material properties of polymers by adding carbon nanotubes as filler. These issues are the interfacial bonding and especially the proper dispersion of the individual CNTs in the polymeric matrix. Investigations focussing on the interfacial bonding have been performed by Wagner and co-workers [267, 268]. They performed pull-out experiments of individual carbon nanotubes embedded in a polymer matrix with a specially developed test in order to evaluate the interfacial shear strength of the nanotube polymer system. The interfacial adhesion to the polymer can be enhanced by chemical functionalisation of the nanotube surface. Molecular dynamics simulations by Frankland et al. [269] predicted an influence of chemical bonding between the nanotubes and the matrix on the interfacial adhesion. The dispersion of the CNTs in the matrix system is another challenge to overcome for nanotube-reinforced polymers. Nano-scaled particles exhibit a comparatively high surface area being several orders of magnitude larger than the surface of conventional fillers. This surface area acts as interface for stress transfer, but is also responsible for the strong tendency of the CNTs to form agglomerates. An efficient exploitation of their properties in polymers is therefore related to their homogeneous dispersion in the matrix, a break-up of the agglomerates and a good wetting with the polymer.

Among layered silicates, montmorillonite (MMT) is particularly attractive as reinforcement for the polymer clay because it is environmentally friendly, readily available in large quantities with relatively low cost and its intercalation chemistry is reasonably well understood. This type of clay has a layered structure. Each layer is constructed from tetrahedrally coordinated Si atoms fused into an octahedral plane of either $\text{Al}(\text{OH})_3$ or $\text{Mg}(\text{OH})_2$. According to the nature of the bonding between these atoms, the layers should exhibit excellent mechanical properties parallel to the layer direction. The layers have a high aspect ratio and each one is approximately 1 nm thick, while the diameter may vary from 30 nm to several microns or larger. Many such layers are stacked together with weak van der Waals forces to form a clay particle [270]. The principle used in clay/polymer nanocomposites is to separate individual silicate layers in a polymer. By doing this, the excellent mechanical properties of the individual clay layers can function effectively, while the number of reinforcing components also increases dramatically because each clay particle contains hundreds or thousands of layers.

Products obtained from renewable resources are gaining more and more interests due

to the discussion of sustainability. A great emphasis in this area lies on fiber polymer composites where the fibers, the polymer matrix or both can be of natural origin. With increasing oil prices the natural or naturally based materials like cellulose demonstrate an interesting potential as substitutes to some conventional petroleum based materials. For example, semi crystalline cellulose fibers which are cheap, chemically and physically stable in a large temperature range can have mechanical properties similar to those of glass fibers. The breakthrough in the successful use of cellulose in the reinforcement of rubber composites was a recently developed process of dynamical co-coagulation (CDLC) [271, 272], which can be applied to a large variety of rubber emulsions and/ or polyelectrolytes. It was shown that properties of composites obtained from this process are superior or at least similar to those of conventionally filled elastomers.

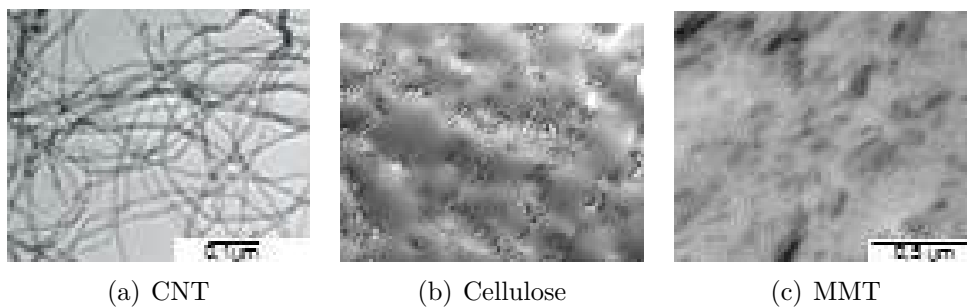


Figure 5.63: TEM micrographs of novel fillers.

Low frequency DMA measurements performed on three different rubbers filled with carbon black, silica, cellulose, MMT and CNTs (Figure 5.64) give an insight into the comparative reinforcing effects of the alternative fillers in comparison with carbon black and silica. In Figure 5.64(a) the reinforcing effect of cellulose, characterized by the reduced shear modulus, is more reduced than that of CB and silica but it is relatively close. As the cellulose surface is covered with polar groups it is expected that the interactions with the non-polar SBR are relatively low, from that respect the results are better than expected.

The layered silicate (MMT) added to the NBR matrix shows the highest increase of reinforcement of all the fillers used followed by CNT.

The mechanical performance of polymer-filler composites depends greatly on the types of nanofillers and polymeric matrices used. Overall, MMT provides the largest modulus enhancement in the tested polymer systems at a fixed filler loading compared to cellulose, CNTs, carbon black and silicas.

The investigation of the alternative fillers' influence on ultrasonic dynamic mechanical properties is carried out on NR2, SBR and NBR composites.

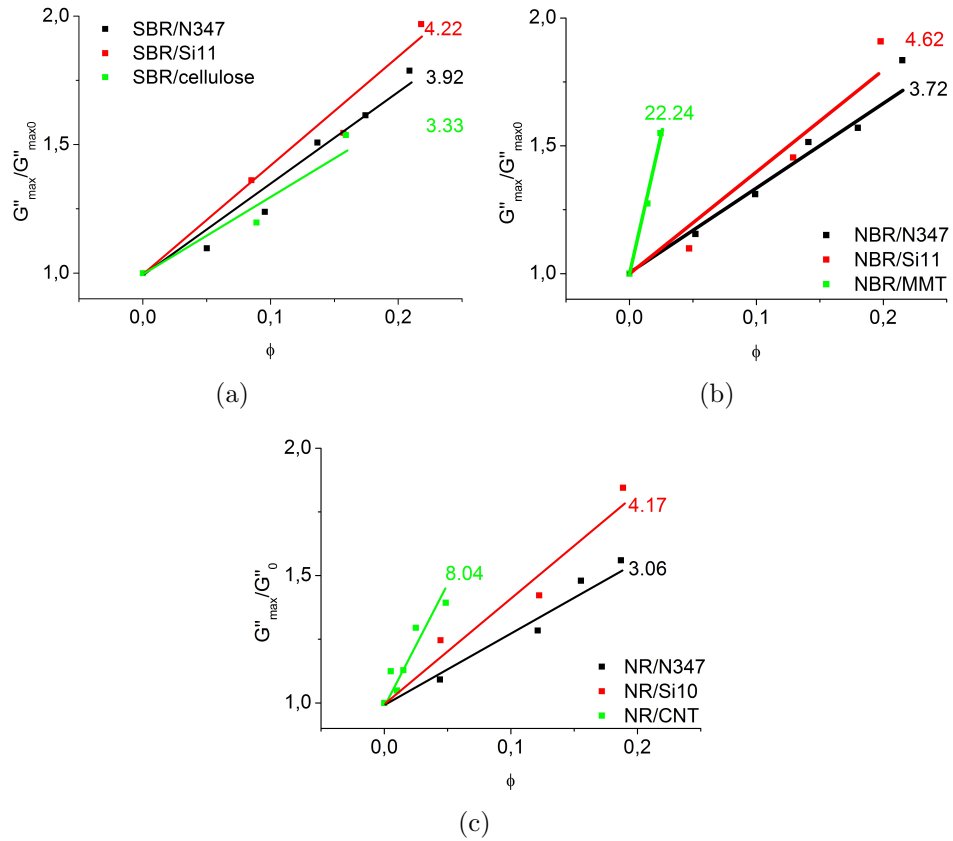


Figure 5.64: Comparative effects of used fillers at 1 Hz.

Due to the new CDLC technique the dispersion degree, as well as the aspect ratio are quite high. TEM pictures reveal that cellulose fibers with a diameter of 10 – 20nm and fiber length of 200 – 250nm are surrounded by a rubber shell and therefore not agglomerated and well dispersed. Similarly graded is the dispersion of the MMT into fan-like platelets with aspect ratio of 90. These fillers have small enough particle sizes and adequate surface compatibility to effectively play a role in reinforcing elastomers. It was proven that both cellulose nano fibers and MMT increase the shear storage modulus and significantly the Youngs modulus, tensile strength at lower volume fractions than carbon black or silica.

The reduced attenuation coefficient α/α_0 shown in Figure 5.65, indicates a significantly lower slope than for the two conventional fillers taken as reference. This special behavior can be traced back to the fact that on the surface of the cellulose fibers there are remaining xanthate groups after the rapid co-coagulation of the cellulose during the CDLC process. These groups can form chemical links to the rubber matrix. As a result of this “chemical pinning” of the fibers the attenuation becomes less pronounced. If the reduced area of the attenuation curves, which includes the entire attenuation process is considered the attenuation effects caused by the pinned nano fibers become close

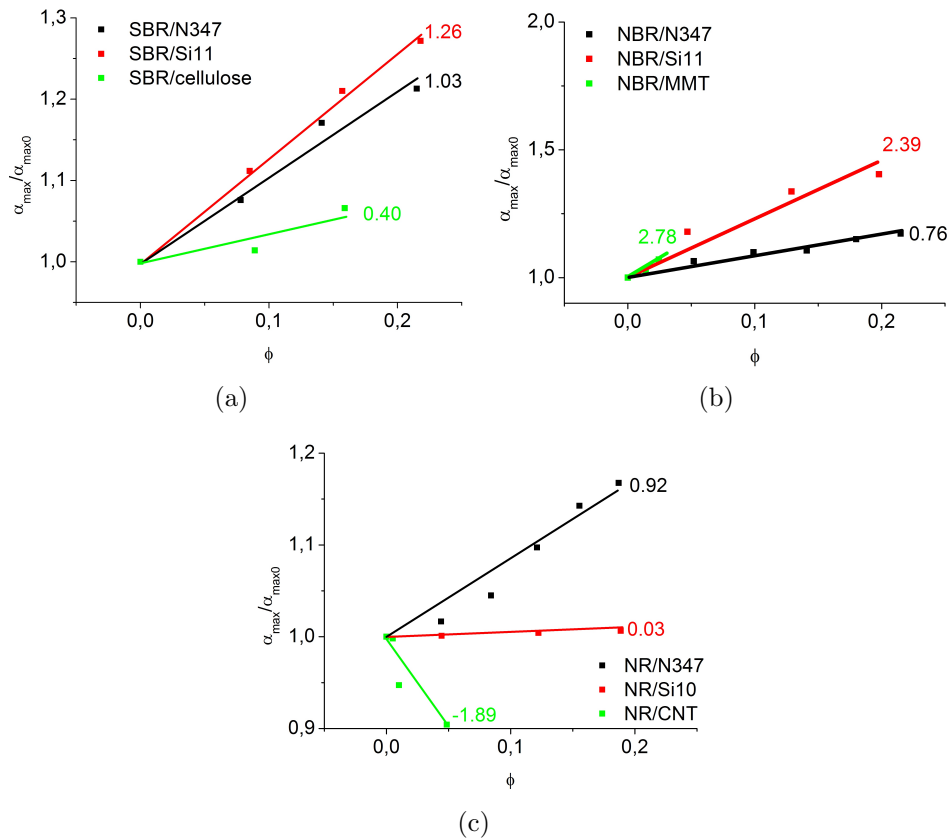


Figure 5.65: Comparative effects of used fillers at 0.5 MHz.

to the carbon black and silica filled ones because the contribution to attenuation at higher temperatures are also taken into account.

If the attenuation effect of the dispersed MMT in NBR is considered, it can be seen that this nanofiller is superior to carbon black or silica. The results for the reduced attenuation maxima show very high values for the layered silicate, ascribable mostly to good dispersion and the strong filler-polymer interactions even if there are good reasons to consider the contribution of strong scattering effects.

The use of novel fillers such as the ones presented in this section are under current investigation for use both as replacement for the classic active fillers, such as carbon black and silica, and as completely new filler systems which impart improved properties to nanocomposites. The main issue which is still being dealt with is represented by the difficulties that occur in obtaining a good dispersion in the rubber matrix. The fillers used in the present work were dispersed using newly developed methods and it was shown that, by comparison with CB or silica, rather small quantities of filler induced reinforcing effects which were comparable or even better than those shown by the typical fillers.

6

Conclusions

The dynamic mechanical properties of filled and unfilled systems were investigated using an improved (better temperature control, increased precision of the data acquisition, more accurate data evaluation procedure) prototype Ultrasonic Spectrometer, at 0.5 MHz, and a classical Dynamic-Mechanical Analyzer at 1 Hz.

It was shown by performing measurements on several different polymers, i.e. NR, IIR, BR (with different vinyl content), SBR (with different styrene and vinyl content), NBR (with different acrylonitrile content) that the changes that occur in the dynamic response of macromolecular chains by increasing the measuring frequency depend strongly on the polymer structure. For the homopolymers NR, BR and IIR the shift of the T_g amounts to ca. 55°C. The energy dissipation, characterized at 0.5 MHz by the ultrasonic attenuation coefficient, α , and at 1 Hz by the loss modulus, G'' is highest for IIR due to its unique structural characteristics. In case of copolymers SBR and NBR the glass transition temperature shift, ΔT_g , is strongly connected to the micro structure. When the vinyl content is increased in SBR and the acrylonitrile content is increased in NBR ΔT_g is found to decrease. It is shown that the energy dissipation, at both measured frequencies, increases with the side group content for all measured polymers. In case of SBR copolymers it was noticed that the increase of the vinyl concentration has a stronger effect on the energy dissipation than the styrene content increase. It has been proven by the aforementioned measurements that the influences of the measurement frequency on the polymer dynamics are not always reliably described by theoretical approaches, even when one stays in the linear deformations region where the materials tested demonstrate thermorheological simplicity. The T_g shift that takes place when changing from 1Hz to 0.5MHz is demonstrated to be strongly dependent on the polymer macro and micro structure.

The sensitivity of the ultrasonic method is proved in the characterization of discrete micro structural variations in BR copolymers as well as in the detection and charac-

terization of crystallization in BR and SBR:BR blends, as well as the investigation of secondary transitions determined by movements of short chain segments or side-groups. Relevant processing parameters such as the molar mass, the crosslinking density and the plasticizer effect were investigated as well. It was shown that the molar mass has a stronger influence on the high frequency chain dynamics than on the low frequency G'' . The increasing sulfur content is shown by both methods to increase the T_g . The plasticizer induces only an insignificant increase of the attenuation maximum at 0.5 MHz but no change of the T_g . Insoluble fractions of the plasticizer are detectable at lower temperature only in the ultrasonic measurements.

For polymer blends the ultrasonic spectrometer can give valuable information concerning the influence of crystallization and the general dynamic mechanical behavior concerning the different shift of the glass transition temperature with frequency, information that is not available to other testing methods. Due to this different shift of the constituent phases of a blend on the temperature axis, at 0.5 MHz it is seen that for SBR:NR and SBR:NBR blends there is one dissipation peak with a shoulder hinting to the presence of an insoluble phase.

The presence of elastic inclusions (non-reinforcing fillers) with particles sizes larger than a hundredth of the wavelength should be regarded as a potential error source for ultrasonic measurements because the attenuation that results from scattering and reflection does not describe the viscoelastic losses induced by the polymer matrix. The results presented herein imply that active fillers that are dispersed in a suitable way will not pose any scattering problems possibly due to a coupling effect induced by the immobilized layer of polymer adsorbed on their surface. The difficulties are usually in the case of crystallites where it is rather difficult to know exactly their size and number that exist at a certain temperature during the ultrasonic testing.

It was noticed, in the ultrasonic measurements, for polymers filled with active fillers that a certain dependence of the glass transition temperature on filler content does exist especially for SBR and NBR. This should be ascribed to the influence of the immobilized layer present on the surface of the filler particles which shows a stronger influence in the low amplitude high frequency measurements. Further, it was demonstrated that the evaluation of the ultrasound velocity as a function of the filler volume fraction can give insight into the state of dispersion of carbon black and silica.

The wide range of tests performed on a group of filled and unfilled polymers in the course of this work using ultrasonic spectroscopy have shown its reliability and the wealth of information it can provide by itself or in combination with other dynamic mechanical measurement techniques.

Its limitations ascribed to the relatively low temperature and frequency range are the main topics where further research is needed. Even so it is thinkable that a further

development of the method should aim at incorporating in the same device specially designed ultrasonic transducers capable of measuring the shear modulus. Once this is achieved the full spectrum of dynamic-mechanical characterization will be available and the frequencies will be only restricted by the ability of the manufacturers to come up with the proper transducers.

7

Experimental

7.1 Sample preparation

7.1.1 Unfilled samples

The unfilled composites were prepared by mixing in an internal mixer (Haake Rheomix 3000) with Banbury type rotors. The speed of the rotor was set at 50 rpm and the temperature of the mixing chamber at 40°C. At first the raw polymer was introduced in the mixing chamber and masticated for 2 minutes. Next stearic acid, zinc oxide and antioxidants were added and mixed for another 2 minutes. The last stage consisted of the addition of the vulcanization chemicals i.e. sulfur and TBBS. Afterwards, the mixing procedure was continued on the two roll mill (Berstorff 150 350RR) for one minute, mostly for practical purposes. A typical mixing recipe is detailed in table 7.1 which is applicable to all composites used in this work with the exceptions detailed at their occurrence.

In the case of polymer blends, the two polymers were added together in the first mixing stage which was also extended to 3 minutes.

7.1.2 Filled samples

The filled samples were prepared in a similar way as the unfilled as far as the rotor velocity and starting temperature are concerned. After the polymer addition and its subsequent 2 minutes mastication the filler was added in one or more stages. Usually quantities up to 20 phr were added in one stage. Once the filler inclusion stage was completed, antioxidants, zinc oxide and stearic acid were added. If, at this point, the temperature of the mixing chamber was higher than 110°C the rotor velocity was

Table 7.1: Typical mixing recipe.

Component	phr
Polymer	100
Filler	0-50
6PPD	2
TMQ	2
Stearic acid	1
Zinc oxide	3
Sulfur	2
TBBS	2

reduced to 20 rpm. Subsequently the crosslinking chemicals were added. The mix was then dumped from the internal mixer and put on the two roll mill. The rolls were cooled and the mixing proceeded for another 5 minutes to improve the filler dispersion.

7.1.3 Vulcanization

The crosslinking behavior was checked for all composites using a moving die rheometer manufactured by Alpha Technologies type MDR 2000 E at 160°C. The vulcanization time was calculated by adding to the time at which 90% of the maximum torque, i.e. t_{90} , was achieved one minute for every centimeter of required sample thickness. The measurements were carried out according to DIN 53529 at a frequency of 1.67Hz and an amplitude of $\pm 0.5^\circ$. The samples were covered with two sheets -one PA and one PET- on each side.

The data evaluation was performed using a software (Alpha 2000 R) produced by Scarabaeus.

According to their calculated vulcanization time the samples were subsequently compression molded at 160°C and 250 bar using a Wickert & Soehne WLP 63/3.5/3 vulcanization press.

7.2 Testing methods

7.2.1 Ultrasonic spectrometry

The system uses two similar ultrasonic transducers located opposite from one another. Between the transducers a sample holder wheel, driven on a revolver principle by a step motor, provides room for six samples of the same material. The samples have different

thicknesses (5, 7, 9, 11, 13 mm) to reduce propagation errors. One position on the wheel is left empty as reference in the calculation of the attenuation, α . The position of the holder wheel ensures a propagation of the ultrasonic waves perpendicular to the sample.

The entire measurement process is controlled by a computer running the LabView software from National Instruments. This enables the stepper motor to be controlled at the same time with the data acquisition. The exact sequence is as follows:

1. the impulse generator emits five identical 90ms pulses
2. the stepper motor turns the sample holder wheel so that the next sample takes position between the transducers
3. the system waits for 20 seconds for the measuring environment to reach thermodynamical equilibrium
4. the impulse generator emits another five pulses

This results in a measuring time for one complete rotation of 165 seconds.

The temperature control is not integrated herein, but it is performed by an external PID controller manufactured by Omega. The heating ramp is configured so that it achieves a $0.3^{\circ}\text{C}/\text{min}$ heating rate (200seconds for 1°C), so that the influence of temperature variation is irrelevant during one wheel turn. Cooling is done by liquid nitrogen and heating by electrical heating elements. As mentioned before, the transducers have their own temperature control system which ensures they operate at approximately 25°C . Temperature sensors are located next to the sample being measured and the temperature is recorded for each pulse after which a mean value is calculated.

For each pulse the software records and analyses an oscillogram or amplitude scan - blue signal in Figure 5.3 which contains all the information necessary for modulus determination. At the end of the measurement, the data is exported into a .txt file which is easily accessible to most spreadsheet programs.

For most measurements presented in this thesis the coupling medium used was 1 – *propanol*. Due to its melting temperature of -126°C and boiling temperature of 97°C it confers a broad window in which measurements can be carried out, without having to change the medium.

7.2.2 Dynamic Mechanical Analyzer

The low frequency dynamic mechanical analysis was carried out on a RDA II device manufactured by Rheometrics Scientific (see 7.1) on thin strips (approx. 2 mm thick, 10 mm wide and 35 mm long).

Isochronal measurements were performed between -80°C and $+80^{\circ}\text{C}$ using a 1 degree per minute heating rate, at 1 Hz and 0.5% amplitude.

Frequency and temperature dependent measurements were carried out between -80°C and $+80^{\circ}\text{C}$. For each defined temperature a frequency sweep was performed in the range $f \in [0.015, 16]\text{Hz}$ at an amplitude of 0.5%. The temperature was varied in 5 degrees steps.

The principle is based on a clamped strip specimen which undergoes a sinusoidal excitation under torsion at a constant deformation. The resultant torque (between 200 gcm and 2000 gcm) and the angle between imposed stress and corresponding strain are measured by the device. This enables the calculation of both the storage (G') and loss (G'') moduli. As long as the deformation remains small compared to the specimen' height, torsion can be assimilated to shear deformation. The frequency range of the device lies between $f \in [0.001, 16]\text{Hz}$ while the deformation range goes from $\epsilon \in [0.5, 3.5]\%$. A static pre-tension of 100g is applied on the specimen to ensure proper conditioning over the entire temperature range. Lastly, the experimental setup also includes a temperature chamber which enables the user to perform the dynamic mechanical measurements from -150°C to $+500^{\circ}\text{C}$.

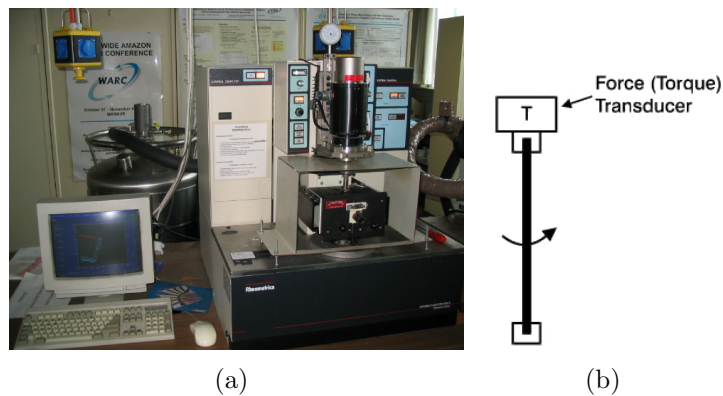


Figure 7.1: Experimental setup of the RDA II dynamic mechanical spectrometer

Dynamic mechanical tests are usually made in the linear viscoelastic region of the material where the dynamic moduli are function only of temperature and frequency. In such a measurement, the computer makes a digital cross-correlation of strain and torque by comparing the amplitude and phase-shift between the imposed motion (strain) and the force (stress).

For the geometry displayed in Figure 7.1 stress and strain are calculated as follows:

- dynamic strain

$$K_\gamma = \frac{T}{L} \left(1 - 0,378 \left(\frac{T}{W} \right)^2 \right)$$

$$\gamma = K_\gamma \cdot \theta \quad (7.1)$$

- T - thickness in mm
- W - width in mm
- L - length in mm
- K_γ - strain constant
- θ - actuator angular displacement in rad
- γ - strain

- dynamic stress

$$K_\tau = 1000 \cdot \left(\frac{3 + 1,8 \frac{T}{W}}{WT^2} \right) \cdot G_c$$

$$\tau = K_\tau \cdot M \quad (7.2)$$

- T - thickness in mm
- W - width in mm
- M - transducer torque in gm-cm
- K_τ - stress constant
- $G_c = 98,7$ Pa
- τ - stress

Dividing the stress by the strain produces the complex modulus, G^* , which indicates the total energy required to deform the material. Multiplying G^* by the cosine of the phase angle yields the in-phase component of the stress, G' , which is proportional to the energy stored elastically. Multiplying G^* by the sine of the phase angle gives the out of phase component of the stress, G'' , which is proportional to the amount of energy lost to viscous dissipation.

7.2.3 Transmission Electron Microscopy

Ultrathin cuts (70nm) obtained with the aid of an UltraCut FC4 (Reichert Jung) microtome were investigated using electron spectroscopy imaging on a transmission electron microscope (Zeiss EM 902). No chemically staining procedures were used for contrast, as the outblending of inelastically scattered electrons using filters was enough to produce high quality pictures. In this case, the phase with the higher electron density appears as the darkest.

7.3 Polymers and chemical aids

Table 7.2: Polymers.

Label	Trade name	Producer
SBR1	SBR1027	Dow Olefinverbund GmbH
SBR2	SBR2127	Dow Olefinverbund GmbH
SBR3	SBR3027	Dow Olefinverbund GmbH
SBR4	SBR2145	Dow Olefinverbund GmbH
SBR5	SBR2163	Dow Olefinverbund GmbH
SBR6	Buna VSL2525	Lanxess Deutschland GmbH
SBR7	Buna VSL5025	Lanxess Deutschland GmbH
NBR1	Perbunan1846	Lanxess Deutschland GmbH
NBR2	Perbunan2845	Lanxess Deutschland GmbH
NBR3	Perbunan3470	Lanxess Deutschland GmbH
NBR4	Perbunan4456	Lanxess Deutschland GmbH
BR1	Buna CB25	Lanxess Deutschland GmbH
BR2	PB5800	Dow Olefinverbund GmbH
BR3	PBR4005	Lanxess Deutschland GmbH
NR1	SMR CV50	
NR2	SMR CV60	
NR3	RSS1	
IIR	Lanxess Butyl 301	Lanxess Deutschland GmbH

Three variations of SBR6 were also prepared with different sulfur contents. SBR6_A contains 1 phr of sulfur whereas SBR6_B contains 2 phr sulfur and SBR6_C contains 4phr sulfur.

Table 7.3: Fillers.

Label	Trade name	Producer
	N220	Evonik Degussa
	N326	Evonik Degussa
	N330	Evonik Degussa
	N347	Evonik Degussa
	N550	Evonik Degussa
Si10	Ultrasil 7000GR	Evonik Degussa
Si11	Ultrasil 7000GR + Si69	Evonik Degussa
Si20	Ultrasil VN2	Evonik Degussa

Table 7.4: Crosslinking chemicals and antioxidants.

Chemical	Trade name	technical data, producer
Sulphur		99.5%, Solvay Barium Strontium GmbH,
Stearic acid	Edenor ST 4A	activator, mixture of palmitic and stearic oil, Henkel KG
Zinc Oxide (ZnO)		activator, 99.6%, Grillo Zinkoxid GmbH
N-tertbutyl-benzothiazole sulfenamide (TBBS)	Vulkacit NZ/EG-C	accelerator, Lanxess Deutschland GmbH
2, 2, 4-trimethyl-1, 2-dihydroquinoline (TMQ)	Vulkanox HS/LG	antioxidant, Lanxess Deutschland GmbH
N-(1, 3-dimethylbutyl)-N'-phenyl-p-phenylenediamine (6PPD)	Vulkanox 4020/LG	antioxidant, Lanxess Deutschland GmbH

References

- [1] S. D. Gehman, *Rubber Chemistry and Technology*, **30**, 1202, 1957.
- [2] J. H. Dillon and S. D. Gehman, *India Rubber World*, **115**, 61, 1946.
- [3] A. W. Nolle and S. Mowry, *Journal of the Acoustical Society of America*, **20**, 432, 1948.
- [4] A. W. Nolle, *Journal of Applied Physics*, **19**, 753, 1948.
- [5] J. D. Ferry, *Journal of Colloid Science*, **8**, 244, 1953.
- [6] J. D. Ferry, *Viscoelastic Properties of Polymers*, Wiley, New York, 1980.
- [7] J. McHugh, Ultrasound Technique for the Dynamic Mechanical Analysis of Polymers, Ph.D. thesis, Bundesanstalt für Materialforschung und -prüfung, 2008.
- [8] L. H. Sperling, *Introduction to Physical Polymer Science*, John Wiley & Sons, Inc., Hoboken, New Jersey, 2006.
- [9] C. Wrana, *Introduction to Polymer Physics*, Lanxess AG, Leverkusen, 2009.
- [10] J. H. Gibbs and E. A. DiMarzio, *Journal of Polymer Science*, **1**, 1417, 1963.
- [11] J. H. Gibbs and G. Adam, *Journal of Chemical Physics*, **43**, 139, 1965.
- [12] J. H. Gibbs and E. A. DiMarzio, *Macromolecules*, **9**, 763, 1976.
- [13] P. J. Flory, *Principles of Polymer Chemistry*, Cornell University Press, Ithaca and London, 1953.
- [14] L. R. G. Treloar, *The Physics of Rubber Elasticity*, Clarendon Press, 1975.
- [15] L. Nielsen, *Mechanical Properties of Polymers and Composites*, Marcel Dekker, New York, 3rd edn., 1994.
- [16] U. Eisele, *Introduction to Polymer Physics*, Springer-Verlag Berlin Heidelberg, 1990.
- [17] J. F. Nye, *Physical Properties of Crystals*, Clarendon Press, Oxford, 1985.
- [18] E. Riande, R. Diaz-Calleja, M. G. Prolongo, R. M. Masegosa and C. Salom, *Polymer Viscoelasticity*, Marcel Dekker Inc., New York, 2000.
- [19] K. Deutsch, E. A. W. Hoff and W. Reddish, *Journal of Polymer Science*, **40**, 121, 1959.

- [20] A. Eisenberg, *The Glassy State*, in Physical Properties of Polymers, American Chemical Society, Washington DC, 1984.
- [21] D. J. Williams, *Polymer Science and Engineering*, Englewood Cliffs, New Jersey Prentice-Hall, 1971.
- [22] E. Donth, *The Glass Transition - Relaxation Dynamics in Liquids and Disordered Materials*, Springer-Verlag Berlin Heidelberg, 2001.
- [23] W. Kauzmann, *Chemical Reviews*, **43**, 219, 1948.
- [24] G. Jaeger, *Archive for History of Exact Sciences*, **53**, 51, 1998.
- [25] T. G. Fox and P. J. Flory, *Journal of Applied Physics*, **21**, 581, 1949.
- [26] M. Gordon and J. S. Taylor, *Journal of Applied Chemistry*, **2**, 493, 1952.
- [27] A. K. Doolittle, *Journal of Applied Physics*, **22**, 1471, 1951.
- [28] M. L. Williams, R. F. Landel and J. D. Ferry, *Journal of the American Chemical Society*, **77**, 3701, 1955.
- [29] D. Turnbull and M. H. Cohen, *Journal of Chemical Physics*, **31**, 1164, 1959.
- [30] F. Bueche, *Journal of Chemical Physics*, **21**, 1850, 1953.
- [31] F. Bueche, *Journal of Chemical Physics*, **30**, 748, 1959.
- [32] E. H. Andrews, *Fracture in Polymers*, American Elsevier, New York, 1968.
- [33] A. Kaye, R. F. T. Stepto, W. J. Work, J. V. Alemán and A. Y. Malkin, *Pure and Applied Chemistry*, **70**, 701, 1998.
- [34] T. Horino, Y. Ogawa, T. Soen and H. Kawai, *Journal of Applied Polymer Science*, **9**, 2261, 1965.
- [35] R. E. Cohen and N. W. Tschoegl, *International Journal of Polymeric Materials*, **2**, 205, 1973.
- [36] D. Kaplan and N. W. Tschoegl, *Polymer Engineering and Science*, **14**, 43, 1974.
- [37] M. Takayanagi and S. Uemura, *Journal of Applied Polymer Science*, **10**, 113, 1966.
- [38] M. Rubinstein and R. H. Colby, *Polymer Physics*, Oxford University Press, 2003.
- [39] M. Doi and S. F. Edwards, *The Theory of Polymer Dynamics*, Oxford University Press Inc. New York, 1986.
- [40] M. Doi, *Introduction to Polymer Physics*, Clarendon Press, Oxford, 1996.
- [41] P. G. de Gennes, *Journal of Chemical Physics*, **55**, 572, 1971.
- [42] J. Klein, *Encyclopedia of Polymer Science and Engineering*, vol. 9, Wiley & Sons, New York, 2nd edn., 1987.

- [43] P. G. de Gennes, *Scaling Concepts in Polymer Physics*, Cornell University Press, Ithaca, New York, 1979.
- [44] S. F. Edwards, *Proceedings of the Physical Society*, **92**, 9, 1967.
- [45] S. F. Edwards, *Polymer*, **9**, 140, 1977.
- [46] S. F. Edwards and R. T. Deam, *Philosophical Transactions of the Royal Society*, **280**, 317, 1967.
- [47] M. Gottlieb and R. J. Gaylord, *Polymer*, **24**, 1644, 1983.
- [48] S. F. Edwards and M. Doi, *Journal of the Chemical Society*, **74**, 1789, 1978.
- [49] S. F. Edwards and M. Doi, *Journal of the Chemical Society*, **74**, 1802, 1978.
- [50] S. F. Edwards and M. Doi, *Journal of the Chemical Society*, **74**, 1818, 1978.
- [51] S. F. Edwards and M. Doi, *Journal of the Chemical Society*, **75**, 38, 1979.
- [52] R. H. Colby, *Macromolecules*, **20**, 2226, 1987.
- [53] M. Mooney, *Journal of Applied Physics*, **19**, 434, 1948.
- [54] R. S. Rivlin, *Transactions of the Royal Society*, **240**, 459, 1948.
- [55] H. G. Kilian, *Kautschuk Gummi Kunststoffe*, **36**, 959, 1983.
- [56] J. H. Poynting, *Proceedings of the Royal Society A*, **82**, 546, 1909.
- [57] E. T. Lessig, *Industrial Engineering and Chemistry*, **9**, 592, 1937.
- [58] H. Roelig, *Rubber Chemistry and Technology*, **18**, 62, 1945.
- [59] M. Takayanagi, *Proceedings of the 4th international Congress of Rheology*, **161**, 187, 1965.
- [60] J. Gillham and J. Enns, *Trends in Polymer Science*, **2**, 406, 1994.
- [61] C. Makosko and J. Starita, *SPE Journal*, **27**, 38, 1971.
- [62] A. W. Nolle and A. Q. Hutton, *Journal of Applied Physics*, **25**, 350, 1954.
- [63] K. Schmieder and K. Wolf, *Kolloid Zeitschrift*, **134**, 149, 1953.
- [64] A. Nolle, *Journal of Polymer Science*, **5**, 1, 1950.
- [65] W. Philippoff, *Journal of Applied Physics*, **25**, 1102, 1954.
- [66] R. B. Blizard, *Journal of Applied Physics*, **22**, 730, 1951.
- [67] W. P. Fletcher, A. N. Gent and R. I. Wood, *Rubber Chemistry and Technology*, **30**, 652, 1957.
- [68] L. E. Nielsen, *Review of Scientific Instruments*, **22**, 690, 1951.

- [69] R. Brown, ed., *Handbook of Polymer Testing - Physical Methods*, Marcel Dekker Inc., New York, 1999.
- [70] T. E. Morrison, L. J. Zapas and T. W. DeWitt, *Review Scientific Instruments*, **26**, 357, 1955.
- [71] H. Kolsky, *Stress Waves in Solids*, Dover Publications, New York, 1963.
- [72] R. H. Bolt and T. F. Hueter, *Sonics: Techniques for the use of Sound and Ultrasound in Engineering and Science*, John Wiley & Sons, Inc., 1955.
- [73] H. J. Pain, *The Physics of Vibrations and Waves*, Wiley & Sons, New York, 1993.
- [74] H. J. McSkimin, *Ultrasonic methods for measuring the mechanical properties of liquids and solids*, vol. 1 of *Physical Acoustics*, New York: Academic, 1964.
- [75] A. E. H. Love, *Mathematical Theory of Elasticity*, Cambridge University Press, London, 1927.
- [76] A. P. Cracknell, *Ultrasonics*, Wykeham Publications, 1980.
- [77] Y. C. Angel and J. D. Achenbach, *Journal of Applied Mechanics*, **52**, 53, 1985.
- [78] B. Drinkwater, R. Dwyer-Joyce and P. Cawley, *Journal of the Acoustical Society of America*, **101**, 970, 1997.
- [79] A. W. Nolle and P. W. Sieck, *Journal of Applied Physics*, **23**, 888, 1952.
- [80] J. R. Cunningham and D. G. Ivey, *Journal of Applied Physics*, **27**, 967, 1956.
- [81] D. G. Ivey, B. A. Mrowca and E. Guth, *Journal of Applied Physics*, **20**, 486, 1949.
- [82] R. S. Witte, B. A. Mrowca and E. Guth, *Journal of Applied Physics*, **20**, 481, 1949.
- [83] R. Kono, *Journal of the Physical Society of Japan*, **15**, 718, 1960.
- [84] A. F. Yee and M. T. Takemori, *Journal of Polymer Science*, **20**, 205, 1982.
- [85] R. Kono, *Journal of the Physical Society of Japan*, **16**, 1793, 1961.
- [86] H. A. Waterman, *Kolloid Zeitschrift und Zeitschrift für Polymere*, **192**, 1, 1963.
- [87] H. A. Waterman, *Rheologica Acta*, **16**, 31, 1977.
- [88] J. Kroll, T. Alshuth and R. H. Schuster, *Kautschuk Gummi Kunststoffe*, **59**, 33, 2006.
- [89] C. Oprisoni, T. Alshuth and R. H. Schuster, *Kautschuk Gummi Kunststoffe*, **61**, 301, 2008.
- [90] R. E. Challis, R. P. Cocker, D. L. Chadwick, D. J. Dare, C. Martin, A. Mahendrasingam and W. Fuller, *Plastics, Rubber and Composites*, **29**, 110, 2000.
- [91] F. Lionetto, R. Rizzo, V. A. M. Luprano and A. Maffezzoli, *Materials Science and Engineering*, **370**, 284, 2004.

- [92] Y. Maeda, *Journal of Polymer Science*, **18**, 87, 1955.
- [93] S. Eckert-Kastner, T. Alshuth and R. H. Schuster, *Kautschuk Gummi Kunststoffe*, **57**, 423, 2004.
- [94] Y. P. Singh, S. Das and R. P. Singh, *Journal of Pure and Applied Ultrasonics*, **3**, 1, 1981.
- [95] Y. P. Singh and R. P. Singh, *European Polymer Journal*, **19**, 529, 1983.
- [96] Y. P. Singh and R. P. Singh, *European Polymer Journal*, **20**, 201, 1984.
- [97] N. S. A. El-All and A. A. Yehia, *Journal of Pure and Applied Ultrasonic*, **16**, 103, 1994.
- [98] M. A. Sidkey, A. A. Yehia, N. A. A. E. Malak and M. S. Gaafar, *Materials Chemistry and Physics*, **74**, 23, 2002.
- [99] M. A. Sidkey, A. M. A. E. Fattalh, Z. A. Aziz, A. Z. Mohamed and N. S. A. E. All, *Journal of Pure and Applied Ultrasonics*, **15**, 1, 1993.
- [100] H.-H. Greve, *Rubber 1. Survey in Ullmann's Encyclopedia of Industrial Chemistry 7th Edition*, VCH-Wiley Weinheim, 2005.
- [101] J. A. Brydson, *Rubber Chemistry*, Applied Science Publishers, 1978.
- [102] D. C. Blakely, *Emulsion Polymerization*, Wiley and Sons, New York, 1975.
- [103] E. W. Duck, *Emulsion Polymerization in Encyclopedia of Polymer Science and Technology vol. 5*, Wiley and Sons, New York, 1966.
- [104] H. D. Brandt and W. Nentwig, *Rubber 3. Synthetic Rubber*, in Ullmann's Encyclopedia of Industrial Chemistry, VCH-Wiley Weinheim, 7 edn., 2006.
- [105] IUPAC, *IUPAC Compendium of Chemical Terminology 2nd Edition*, 1997.
- [106] A. E. Hamielec and H. Tobita, *Polymerization Processes*, in Ullmann's Encyclopedia of Industrial Chemistry, VCH-Wiley Weinheim, 2002.
- [107] G. A. Olah, *Journal of the American Chemical Society*, **94**, 808, 1972.
- [108] G. Odian, *Principles of Polymerization*, Wiley-Interscience, New York, 1981.
- [109] R. M. Thomas, *Rubber Chemistry and Technology*, **42**, G9011, 1969.
- [110] J. L. White, T. D. Schaffer, C. J. Ruff and J. P. Cross, *Macromolecules*, **28**, 329, 1995.
- [111] B. Rodgers, ed., *Rubber compounding: chemistry and applications*, CRC Press, 2004.
- [112] G. W. Marwede, B. Stollfuß and A. J. M. Sumner, *Kautschuk Gummi Kunststoffe*, **46**, 380, 1993.
- [113] R. Zelinski and C. W. Childers, *Rubber Chemistry and Technology*, **41**, 161, 1968.

- [114] S. Bywater, *Anionic Polymerization*, in Encyclopedia of Polymer Science and Engineering, vol. 2, Wiley-Interscience, New York, 1985.
- [115] M. Morton, *Anionic Polymerization: Principles and Practice*, Academic Press Inc, 1983.
- [116] D. H. Richards, *Anionic Polymerization*, in Development in Polymerisation, Applied Science Publishers, Essex, 1979.
- [117] M. Szwarc, M. Levy and R. Milkovich, *Journal of the American Chemical Society*, **78**, 2656, 1956.
- [118] M. Szwarc, *Living Polymers*, in Encyclopedia of Polymer Science and Technology, vol. 8, Wiley-Interscience, New York, 1968.
- [119] A. D. Jenkins and A. Ledwith, eds., *Reactivity, Mechanism and Structure in Polymer Chemistry*, John Wiley & Sons, 1974.
- [120] J. Boor, *Macromolecular Review*, **2**, 115, 1967.
- [121] J. Boor, *Ziegler – Natta Catalysts and Polymerizations*, Academic Press, New York, 1979.
- [122] R. P. Burford, *Journal of Macromolecular Science, Part A*, **17**, 123, 1982.
- [123] A. K. Bhowmick and H. L. Stevens, *Handbook of Elastomers, New Developments and Technology*, Marcel Dekker, New York 1988, 1988.
- [124] H. Staudinger and J. Fritschi, *Helvetica Chimica Acta*, **5**, 785, 1922.
- [125] R. Pummerer and P. A. Burkard, *Chemische Berichte*, **55**, 3458, 1922.
- [126] H. Staudinger and R. Nodzn, *Helvetica Chimica Acta*, **13**, 1324, 1930.
- [127] C. M. Cowley and J. G. King, *Rubber Chemistry and Technology*, **8**, 360, 1935.
- [128] J. Loadman, *Tears of the tree: the story of rubber-a modern marvel*, Oxford University Press, 2005.
- [129] F. Röthemeyer and F. Sommer, eds., *Kautschuktechnologie*, Hanser-Verlag, 2001.
- [130] H.-H. Greve, *Rubber 2. Natural Rubber in Ullmann' Encyclopedia of Industrial Chemistry 7th Edition*, VCH-Wiley Weinheim, 2005.
- [131] R. H. Schuster, *Angewandte Makromolekulare Chemie*, **202**, 159, 1992.
- [132] B. D. Favis, *Canadian Journal of Chemical Engineering*, **69**, 619, 1991.
- [133] D. Braun, H. Cherdron, M. Rehahn, H. Ritter and B. Voit, *Polymer Synthesis: Theory and Practice*, Springer-Verlag Berlin Heidelberg, 2005.
- [134] R. L. Scott, *Journal of Chemical Physics*, **17**, 279, 1949.
- [135] L. Bohn, *Rubber Chemistry and Technology*, **41**, 495, 1968.

- [136] P. J. Flory, R. A. Orwall and A. Vrij, *Journal of the American Chemical Society*, **86**, 3515, 1964.
- [137] I. C. Sanchez and R. H. Lacombe, *Journal of Physical Chemistry*, **80**, 2352, 1976.
- [138] I. C. Sanchez and R. H. Lacombe, *Journal of Polymer Science: Polymer Letters Edition*, **15**, 71, 1977.
- [139] D. R. Paul and S. Newman, eds., *Polmer Blends*, Academic Press Inc, 1978.
- [140] P. A. Ciullo, ed., *Industrial minerals and their uses: a handbook and formulary*, Noyes Publications, 1996.
- [141] M. Maiti, M. Bhattacharya and A. K. Bhowmick, *Rubber Chemistry and Technology*, **81**, 384, 2008.
- [142] W. B. Wiegand, *Indian Rubber Journal*, **60**, 397, 1920.
- [143] J.-B. Donnet, *Rubber Chemistry and Technology*, **71**, 323, 1998.
- [144] J.-B. Donnet, R. C. Bansal and M.-J. Wang, eds., *Carbon Black Science and Technology*, Marcel Dekker Inc., New York, 1993.
- [145] W. M. Hess, L. L. Ban and G. C. McDonald, *Rubber Chemistry and Technology*, **47**, 1209, 1969.
- [146] C. E. Hall, *Journal of Applied Physics*, **19**, 271, 1948.
- [147] F. A. Heckman and D. F. Harling, *Rubber Chemistry and Technology*, **39**, 1, 1966.
- [148] W. M. Hess, L. L. Ban and F. J. Eckert, *Rubber Chemistry and Technology*, **41**, 356, 1968.
- [149] O. W. Flörke, *Silica*, Ullmann's Encyclopedia of Industrial Chemistry, Wiley-VCH, Weinheim, 7 edn., 2007.
- [150] W. Brindley and G. Brown, *Crystal Structures of Clay Minerals and Their X-Ray Identification*, Mineralogical Society, London, 1980.
- [151] N. Hasegawa, M. Kawasumi, M. Kato, A. Usuki and A. Okada, *Journal of Applied Polymer Science*, **67**, 87, 1998.
- [152] J. Zhu and C. A. Wilike, *Chemistry of Materials*, **13**, 4649, 2003.
- [153] R. D. Kroshefsky, J. L. Price and D. Mangaraj, *Rubber Chemistry and Technology*, **82**, 340, 2009.
- [154] M. S. Dresselhaus, *Graphite Fibers and Filaments*, Springer-Verlag, London, UK, 1988.
- [155] M. S. Dresselhaus, Y. M. Lin, O. Rabin, A. Jorio, A. G. Filho, M. A. Pimenta, R. Saito, G. G. Samsonidze and G. Dresselhaus, *Material Science and Engineering*, **C23**, 129, 2003.

- [156] S. Iijima, *Nature*, **354**, 56, 1991.
- [157] H. Park and S. C. Jana, *Polymer*, **44**, 2091, 2003.
- [158] A. G. Rinzler, J. Liu, H. Dai, P. Nikolaev, C. B. Huffman and F. J. Rodriguez-Macias, *Applied Physics Letters A*, **67**, 29, 1998.
- [159] P. C. Eklund, B. K. Pradhan, U. J. Kim, Q. Xiong, J. E. Fischer, A. D. Friedman, B. C. Holloway, K. Jordan and M. W. Smith, *Nano Letters*, **2**, 561, 2002.
- [160] G. G. Tibbetts, *Journal of Crystal Growth*, **66**, 632, 1984.
- [161] W. Ebbesen, P. M. Ajayan, H. Hiura and K. Tanigaki, *Nature*, **367**, 519, 1994.
- [162] Y. Zhang, Z. Shi, Z. Gu and S. Iijima, *Carbon*, **38**, 2055, 2000.
- [163] B. Oppermann, Einfluß der Rußdispersion auf die elektrische Leitfähigkeit von Kautschukmischungen, Ph.D. thesis, Universität Hannover, Fakultät für Maschinenwesen, 1994.
- [164] W. M. Hess, V. E. Chirico and K. A. Burgess, *Rubber Chemistry and Technology*, **26**, 344, 1973.
- [165] W. M. Hess, *Rubber Chemistry and Technology*, **64**, 387, 1991.
- [166] D. G. Lloyd, *Journal of the Rubber Research Institute of Malaysia*, **22**, 399, 1969.
- [167] H. W. Engels, *Rubber, 4. Chemicals and Additives*, in Ullmann's Encyclopedia of Industrial Chemistry, VCH-Wiley Weinheim, 7 edn., 2007.
- [168] A. V. Tobolsky, *Properties and Structures of Polymers*, John Wiley & Sons, 1960.
- [169] P. J. Flory and J. Rehner, *Journal of Chemical Physics*, **11**, 512, 1943.
- [170] P. J. Flory and J. Rehner, *Journal of Chemical Physics*, **11**, 521, 1943.
- [171] P. J. Flory and B. Erman, *Macromolecules*, **15**, 800, 1982.
- [172] L. E. Nielsen, *Journal of Applied Polymer Science*, **8**, 511, 1964.
- [173] N. W. Tschoegl, W. G. Knauss and I. Emri, *Mechanics of Time-Dependent Materials*, **6**, 53, 2002.
- [174] M. Gerspacher, C. P. O'Farrell, L. Nikiel and H. H. Yang, *Rubber Chemistry and Technology*, **69**, 786, 1996.
- [175] J. Krautkrämer and H. Krautkrämer, *Werkstoffprüfung mit Ultraschall*, Springer Verlag, Berlin, 1986.
- [176] F. Bessel, *Untersuchung des Theils der planetarischen Störungen*, Berlin Abhandlungen, article 14, 1824.
- [177] M. Abramowitz and I. Stegun, eds., *Handbook of mathematical functions*, National Bureau of Standards, Applied Mathematics Series - 55, 1972.

- [178] J. Fourier, *Nouveau Bulletin des sciences par la Société philomatique de Paris*, **1**, 112, 1808.
- [179] J. Fourier, *Theorie Analytique de la Chaleur*, Firmin Didot (reissued by Cambridge University Press, 2009), 1822.
- [180] G. Campbell and R. Foster, *Fourier Integrals for Practical Applications*, D. Van Nostrand Company, Inc., New York, 1948.
- [181] G. Kaiser, *A Friendly Guide to Wavelets*, Birkhäuser, 1994.
- [182] D. Kammler, *A First Course in Fourier Analysis*, Prentice Hall, 2000.
- [183] E. H. Andrews, *Rubber Chemistry and Technology*, **38**, 33, 1965.
- [184] C. W. Bunn and T. C. Alcock, *Transactions of the Faraday Society*, **41**, 317, 1945.
- [185] T. L. Cheng and A. C. Su, *Macromolecules*, **26**, 7161, 1993.
- [186] L. C. Lopez, G. L. Wilkes and J. F. Geibel, *Polymer*, **30**, 147, 1989.
- [187] J. D. Hoffman, *Polymer*, **23**, 656, 1982.
- [188] J. H. Magill, *Rubber Chemistry and Technology*, **40**, 341, 1967.
- [189] J. Rehner, *Journal of Polymer Science*, **2**, 263, 1947.
- [190] E. H. Waddell, S. W. Botfeld, C. Napier, D. F. Rouckhout and D. S. Tracey, *Rubber World*, **23**, 33, 2006.
- [191] K. H. Nordsieck and K. K. Kiert, *Kautschuk Gummi Kunststoffe*, **33**, 251, 1980.
- [192] Z. Szentivany, H. Magg, F. Leibbrandt and J. Wassen, *Kautschuk Gummi Kunststoffe*, **41**, 1118, 1988.
- [193] J. Heijboer, *International Journal of Polymeric Materials*, **6**, 11, 1977.
- [194] V. M. Timin, D. K. Kritskaya and V. I. Petinov, *Zhurnal Stmkturnoi Khimii*, **12**, 541, 1971.
- [195] J. A. Brydson, *Plastics Materials*, Butterworth-Heinemann, 1999.
- [196] K. Fujimoto and N. Yoshimura, *Rubber Chemistry and Technology*, **41**, 1109, 1968.
- [197] L. E. Nielsen, R. Buchdahl and G. C. Claver, *Rubber Chemistry and Technology*, **24**, 574, 1951.
- [198] R. M. Guedes, ed., *Creep and fatigue in polymer matrix composites*, Woodhead Publishing Ltd., 2010.
- [199] W. G. Knauss and S. Sane, *Mech. Time-Dependent Mater.*, **5**, 293, 2001.
- [200] W. Knauss and T. H. Deng, *Mech. Time-Dependent Mater.*, **1**, 33, 1997.

- [201] Y. Meng and S. Simon, *Journal of Polymer Science, Part B: Polymer Physics*, **45**, 3375, 2007.
- [202] C. A. Bero and D. J. Plazek, *Journal of Polymer Science, Part B: Polymer Physics*, **29**, 39, 1991.
- [203] D. J. O'Brien, N. R. Sottos and S. White, *Experimental Mechanics*, **47**, 237, 2007.
- [204] J. Burns, P. S. Dubbelday and R. Y. Ting, *Journal of Polymer Science, Part B: Polymer Physics*, **28**, 1187, 1990.
- [205] H. Leaderman, *Rheology: Theory and Applications*, vol. 2, Academic Press: New York, 1958.
- [206] R. Casalini and C. Roland, *Macromolecules*, **38**, 1779, 2005.
- [207] D. Tabor, *Polymer*, **35**, 2759, 1994.
- [208] J. Brandrup and E. H. Immergut, *Polymer Handbook*, Wiley&Sons, New York, 1975.
- [209] M. Pike and W. F. Watson, *Journal of Polymer Science*, **9**, 229, 1952.
- [210] G. Ayrey, C. G. Moore and W. F. Watson, *Journal of Polymer Science*, **19**, 1, 1956.
- [211] F. Bueche, *Rubber Chemistry and Technology*, **34**, 466, 1961.
- [212] H. Bartels, Der Abbau von Naturkautschuk in der Lösung durch Ultraschall, Ph.D. thesis, Universität Hannover, 1990.
- [213] L. Breitman, *Rubber Chemistry and Technology*, **29**, 492, 1956.
- [214] C. M. Roland, *Rubber Chemistry and Technology*, **61**, 866, 1988.
- [215] A. Beerbower, D. A. Pattinson and G. D. Staffin, *Transactions of the American Society for Lubrication Engineering*, **6**, 80, 1963.
- [216] J. A. Brydson, *Plastics*, **26**, 107, 1961.
- [217] P. A. Small, *Journal of Applied Chemistry*, **3**, 71, 1953.
- [218] H. M. Issel, Thermodynamische und Rheologische Steuerung der Materialeigenschaften von Elastomeren durch trans-Poly(octenylen), Ph.D. thesis, Universität Hannover, 1993.
- [219] N. Yoshimura and K. Fujimoto, *Rubber Chemistry and Technology*, **42**, 1009, 1969.
- [220] P. J. Corish, *Rubber Chemistry and Technology*, **40**, 324, 1967.
- [221] D. Mangaraj, *Rubber Chemistry and Technology*, **75**, 365, 2002.
- [222] J. B. Gardiner, *Rubber Chemistry and Technology*, **41**, 1312, 1968.

- [223] J. Schaper, Auswirkungen von Phasengrenzflächen auf Mischungs- und Vulkanisateigenschaften ungefüllter und gefüllter Kautschukverschnitte, Ph.D. thesis, Universität Hannover, 1997.
- [224] L. Mandelkern, *Rubber Chemistry and Technology*, **32**, 1392, 1959.
- [225] R. L. Cormia, F. P. Price and D. Turnbull, *Journal of Chemical Physics*, **37**, 1333, 1962.
- [226] E. A. Collins and L. A. Chandler, *Rubber Chemistry and Technology*, **39**, 193, 1966.
- [227] S. Biwa, Y. Watanabe, S. Motogi and N. Ohno, *Ultrasonics*, **43**, 5, 2004.
- [228] E. M. Dannenberg, *Rubber Chemistry and Technology*, **59**, 512, 1986.
- [229] J. Ziegler, Beeinflussung der Polymer-Füllstoff-Wechselwirkung durch Oberflächenmodifizierung von Füllstoffen, Ph.D. thesis, Leibniz Universität, Hannover, 2004.
- [230] D. Fragiadakis, P. Pissis and L. Bokobza, *Polymer*, **46**, 6001, 2005.
- [231] C. J. T. Landry, B. K. Coltrain, M. R. Landry, J. J. Fitzgerald and V. K. Long, *Macromolecules*, **26**, 3702, 1993.
- [232] E. Fitzgerald, *Rubber Chemistry and Technology*, **55**, 1547, 1982.
- [233] E. Fitzgerald and J. Ferry, *Rubber Chemistry and Technology*, **55**, 1569, 1982.
- [234] J. B. Donnet and M. Gerspacher, May, 1989.
- [235] M. Gerspacher and C. M. Lansinger, April, 1989.
- [236] A. R. Payne, *J. Appl. Polym. Sci.*, **6**, 57, 1962.
- [237] A. I. Medalia, *Rubber Chemistry and Technology*, **59**, 432, 1986.
- [238] F. Bueche, *Journal of Applied Physics*, **43**, 4837, 1972.
- [239] J. Janzen, *Journal of Applied Physics*, **46**, 966, 1975.
- [240] S. M. Aharoni, *Journal of Applied Physics*, **43**, 2463, 1972.
- [241] R. H. Schuster, H. M. Issel and V. Peterseim, *Rubber Chemistry and Technology*, **69**, 769, 1996.
- [242] A. F. M. Barton, *CRC handbook of polymer-liquid interaction parameters and solubility parameters*, CRC Press, 1990.
- [243] L. Nikiel, M. Gerspacher, H. Yang and C. P. O'Farrell, *Rubber Chemistry and Technology*, **74**, 249, 2001.
- [244] A. Pouchelon and P. Vondracek, *Rubber Chemistry and Technology*, **62**, 788, 1989.
- [245] K. Miyasaka, K. Watanabe, E. Jojima, H. Aida, M. Sumita and K. Ishikawa, *Journal of Materials Science*, **17**, 1610, 1982.

- [246] S. Wolff, M.-J. Wang and J. B. Donnet, *Rubber Chemistry and Technology*, **64**, 714, 1991.
- [247] A. R. Payne, *The Rheology of Elastomers*, Pergamon Press, London, 1958.
- [248] G. Kraus and J. Gruver, *Journal of Polymer Science A*, **2 8**, 571, 1970.
- [249] P. Mason, *Transactions of the Faraday Society*, **55**, 1461, 1959.
- [250] P. Mason, *Journal of Applied Polymer Science*, **4**, 212, 1960.
- [251] M. Baccareda and E. Butta, *Journal of Polymer Science*, **57**, 617, 1962.
- [252] W. M. Hess and C. G. McDonald, *Rubber Chemistry and Technology*, **56**, 892, 1983.
- [253] C. G. Robertson, C. J. Lin, M. Rackaitis and C. M. Roland, *Macromolecules*, **41**, 2727, 2008.
- [254] C. G. Robertson and C. M. Roland, *Rubber Chemistry and Technology*, **81**, 506, 2008.
- [255] S. Biwa, N. Ito and N. Ohno, *Mechanics of Materials*, **33**, 717, 2001.
- [256] A. I. Beltzer and N. Brauner, *Journal of Applied Physics*, **60**, 538, 1986.
- [257] N. Brauner and A. I. Beltzer, *Mechanics of Materials*, **6**, 337, 1987.
- [258] J. Berriot, H. Montes, F. Lequeux, D. Long and P. Sotta, *Macromolecules*, **35**, 9756, 2002.
- [259] M. Klüppel, *Journal of Physics: Condensed Matter*, **21**, 1, 2009.
- [260] V. Herrmann and W. Niedermeier, *Kautschuk Gummi Kunststoffe*, **63**, 559, 2010.
- [261] M. J. Wang, S. Wolff and J. B. Donnet, *Rubber Chemistry and Technology*, **64**, 559, 1991.
- [262] J. W. M. Noordermeer and W. K. Dierkes, *Silica-Filled Rubber Compounds*, vol. 2 of *Rubber Technologist's Handbook*, iSmithers Rapra Technology Ltd., Shawbury (UK), 2009.
- [263] M. J. Wang, S. Wolff and J. B. Donnet, *Rubber Chemistry and Technology*, **64**, 714, 1991.
- [264] M. J. Wang, *Rubber Chemistry and Technology*, **71**, 520, 1998.
- [265] S. Wolff and M.-J. Wang, *Rubber Chemistry and Technology*, **65**, 329, 1991.
- [266] S. Wolff, M.-J. Wang and E. H. Tan, *Kautschuk Gummi Kunststoffe*, **47**, 873, 1994.
- [267] C. A. Cooper, S. R. Cohen, A. H. Barber and H. D. Wagner, *Applied Physics Letters*, **81**, 3873, 2002.
- [268] A. H. Barber, S. R. Cohen and H. D. Wagner, *Applied Physics Letters*, **82**, 4140, 2003.

- [269] S. J. V. Frankland, A. Caglar, D. Brenner and M. Griebel, *Journal of Physical Chemistry B*, **106**, 3046, 2002.
- [270] S. S. Ray and M. Okamoto, *Progress in Polymer Science*, **28**, 1539, 2003.
- [271] K. Brandt, R. Schuster and R.C.R.Nunes, *Kautschuk Gummi Kunststoffe*, **59**, 511, 2006.
- [272] K. Brandt and R. H. Schuster, *Kautschuk Gummi Kunststoffe*, **61**, 250, 2008.

Glossary

α	ultrasonic attenuation coefficient	$\tilde{\rho}$	reduced density
α_f	free volume expansion coefficient	\tilde{G}	the Gibbs energy
$\bar{\bar{c}}$	elastic constant tensor	\tilde{P}	reduced pressure
$\bar{\gamma}$	stress tensor	\tilde{V}	reduced volume
ΔC_p	heat capacity	ζ	friction coefficient
ΔE_a	activation energy	A	work
ΔG_{mix}	mixing energy	a	acceleration
ΔH_f	heat of fusion	a_l	length of a chain segment
ΔH_{mix}	mixing enthalpy	a_T	shift factor
ΔL	deformation	BR	Butadiene Rubber
Δp	pressure variation	c	ultrasonic wave velocity
ΔS_{mix}	mixing entropy	CNT	carbon nanotubes
$\dot{\gamma}(t)$	time dependent deformation	CVD	chemical vapor deposition
ϵ	normal deformation	D	diameter of the emitting transducer
ϵ_L	longitudinal elongation	DBP	dibutyl phtalate
ϵ_Q	transverse elongation	$DIAS$	dispersion index analysis system
ϵ_R	dielectric constant	DMA	Dynamic Mechanic Analysis
η	viscosity	E	Young's modulus
γ	deformation	F	free energy
$\gamma(t)$	total deformation	f	force
γ_0	shear amplitude	f_e	force energy component
λ	wavelength	f_f	fractional free volume
ν	Poisson' ratio	f_s	force entropy component
ω	angular frequency	FFT	fast Fourier transform
ρ	density	G	shear modulus
ρ_d	specific resistivity	G'	storage shear modulus
σ	stress	G''	loss shear modulus
τ	periodic stress	G^*	complex shear modulus
τ_R	Maxwell model relaxation time	G_P	plateau modulus
τ_{rep}	reptation time	IIR	Butyl Rubber
θ	phase lag	$IUPAC$	International Union of Pure and Applied Chemistry
		K	compression modulus
		K'	storage compression modulus
		K''	loss compression modulus
		K^*	complex compression modulus
		k_{DC}	electrical conductivity
		L	initial length
		$LCST$	lower critical solution temperature
		$LVDT$	linear variable differential transducer
		M	longitudinal wave modulus
		m	mass

M'	storage longitudinal wave modulus	$SWCNT$	single-walled nanotubes
M''	loss longitudinal wave modulus	T	temperature
M^*	complex longitudinal wave modulus	T_g	glass transition temperature
M_e	mean molecular weight	T_{90}	time until 90% of the maximum torque is achieved
$MWCNT$	multi-walled nanotubes	$\tan\delta$	damping coefficient
N	Newton	TEM	transmission electron microscope
N_0	length of the near field	TOF	time of flight
n_c	critical number of mers	U	internal energy
N_e	number of segments between entanglements	$UCST$	upper critical solution temperature
N_S	number of segments in a chain	V	volume
NBR	Acrylonitrile Rubber	V^*	minimum volume necessary for a site exchange process
NR	Natural Rubber	V_f	free volume
p	pressure	V_g	free volume at T_g
Pa	Pascal	V_m	molecular volume
phr	per hundred rubber	W	work
Q	induced heat	Z	impedance
R^2	intensity of the reflected wave	ZN	Ziegler-Natta
S	entropy	I	sound intensity
SA	surface area	R	gas constant
$SAXS$	small angle x-ray scattering		
SBR	Styrene Butadiene Rubber		

Parts of this work were presented on different occasions:

Posters

- C. Oprisoni, T. Alshuth, R. H. Schuster, High frequency investigation of elastomer properties using ultrasonic spectrometry, Kautschuk Herbst Kolloquium, November 2006.
- C. Oprisoni, T. Alshuth, R. H. Schuster, High Frequency Properties of SSBR Depending on Vinyl/Styrene and Filler Content, 11th International Seminar on Elastomers, 23 – 27.09.2007 Freiburg.
- C. Oprisoni, T. Alshuth, R. H. Schuster, High Frequency Properties of SSBR Vinyl/Styrene and Filler Content, Elastomery 2007, 14-16.11.2007 Warsaw.
- C. Oprisoni, T. Alshuth, R. H. Schuster, Effect of Nanofillers on High Frequency Polymer Dynamics, 12th International Macromolecular Colloquium and 7th International Symposium on Natural Polymers and Composites, 7-10.09.2010, Gramado, Brazil.
- C. Oprisoni, T. Alshuth, R. H. Schuster, Ultrasonic Dynamic – Mechanical Evaluation Of Nanofilled Elastomers, Kautschuk Herbst Kolloquium, November 2010.

Presentations

- C. Oprisoni, T. Alshuth, R. H. Schuster, An Investigation of Rubber Properties Using Ultrasonic Spectrometry, Symposium on Functional Polymer Based Materials, 03 - 04.04.2007 Jena.
- C. Oprisoni, T. Alshuth, R. H. Schuster, Investigation of the Elastomer Properties Using Ultrasonic Spectrometry, 11th International Seminar on Elastomers, 23 – 27.09.2007 Freiburg.
- C. Oprisoni, J. Fritzsche, L. Klafke, K. Brandt, R. H. Schuster, High Frequency Investigation of Elastomer Properties, Elastomery 2007, 14-16.11.2007 Warsaw.
- C. Oprisoni, T. Alshuth, R. H. Schuster, Investigation of polymer dynamics in high frequency range depending on the rubber structure, DKG Research Projects Presentation, 12.02.2008 Fulda.

- C. Oprisoni, T. Alshuth, R. H. Schuster, Ultrasound analysis of high frequency polymer dynamics, ZFM – Festkörper Nachmittag, 04.07.2008, Hannover.
- C. Oprisoni, T. Alshuth, R. H. Schuster, Dynamic – mechanical evaluation of polymer blends at high frequencies using ultrasound , Kautschuk Herbst Kolloquium , 28.11.2008, Hannover.
- C. Oprisoni, T. Alshuth, R. H. Schuster, Investigation of High Frequency Dynamics of Polymers and Polymer Blends, PMA Slovak Rubber Conference, 21-23.04.2009, Bratislava.
- C. Oprisoni, T. Alshuth, R. H. Schuster, High Frequency Characterization of Elastomers by Ultrasound Spectroscopy, 7. Veranstaltung der Bezirksgruppe Nord der DKG, 17.10.2009, Hannover.
- S. Kajari-Schröder, U. Eitner, C. Oprisoni, T. Alshuth, M. Köntges and R. Brendel Modeling the Curing Dynamics of Ethylene-Vinyl Acetate, 25th European Photovoltaic Solar Energy Conference, 6-10.09.2010, Valencia, Spain.
- C. Oprisoni, T. Alshuth, R. H. Schuster, Progress in Ultrasonic Spectroscopy to Characterize Dynamic-Mechanical Properties of Nanostructured Elastomers in the High Frequency Regime, Paper 108A, Fall 178th Technical Meeting of the Rubber Division of the American Chemical Society, Inc., 12- 14.10.2009, Milwaukee, USA.

Publications

- C. Oprisoni, T. Alshuth, R. H. Schuster, High Frequency Investigation Of Unfilled and Filled Solution SBR Systems, Kautschuk Gummi Kunststoffe, 61 (2008), 301

Resume

Name: Cristian Oprisoni
Birth date/place: 23.08.1981 in Timisoara, Romania
Address: Halmhuberstr 4, 68219 Mannheim

Education

09/1988 - 06/2000 School in Timisoara
Final degree: Abitur
11/2000 - 06/2005 Studied Chemical Engineering (Dipl. Ing.)
„Politehnica“ University, Timisoara
01/2006 - 05/2011 PhD, Leibniz University, Hannover

Experience

07/2004 - 08/2004 Practical training
Deutsches Institut für Kautschuktechnologie e.V., Hannover
03/2005 - 07/2005 Diploma work
Deutsches Institut für Kautschuktechnologie e.V., Hannover
11/2005 - 03/2011 Researcher
Deutsches Institut für Kautschuktechnologie e.V., Hannover
04/2011 - present Researcher - Applications Technology
LANXESS AG - BU Rhein Chemie, Mannheim

Erklärung zur Dissertation

gemäß §6(1) der Promotionsordnung der Naturwissenschaftlichen Fakultät der Gottfried Wilhelm Leibniz Universität Hannover für die Promotion zum Dr. rer. nat.

Hierdurch erkläre ich, dass ich meine Dissertation mit dem Titel

Investigation of the High Frequency Dynamic-Mechanical Properties of Polymer Systems Using Ultrasonic Longitudinal Waves

selbständig verfasst und die benutzten Hilfsmittel und Quellen sowie gegebenenfalls die zu Hilfeleistungen herangezogenen Institutionen vollständig angegeben habe.

Die Dissertation wurde nicht schon als Masterarbeit, Diplomarbeit oder andere Prüfungsarbeit verwendet.

Hannover, 12. Mai 2011



Cristian Oprisoni